Abstract

This work was carried out in collaboration and support from Huber+Suhner AG, Fehraltorf, Switzerland.

An attempt was made to manufacture and characterise a nouvell composite material. The material is based on continuous carbon fibre reinforcement, bonded by a fluoropolymeric (PFA) matrix. In order to wet the fibre with the matrix an aqueous dispersion was used. To consolidate the material a high temperature press at 340 °C was applied. The quality of the manufactured specimens was confirmed using optical microscopy. Generally, the carbon fibre / PFA composite was of high quality, with low void content. But the pressure and dwell time applied had an influence on the fibre distribution. Mechanical tests reviled that there was little difference between different fibre sizing. The theoretical Young's modulus calculated by the rule of mixtures was not obtained. Also the failure strain was very low, indicating that failure originated at the interface in the interlaminar region.

In the thermal analysis no distinctive glass transition temperature could be distinguished. Dynamic mechanical analysis reviled a secondary phase transition at 90 °C. Furthermore it showed that the elastic moduli decreases linearly with increasing temperature. Thermographimetric analysis was used to determine the fibre volume fraction, which was directly correlated to the pressure applied during manufacturing.

During this project it has been shown that it is possible to produce an aligned continuous carbon fibre / PFA matrix composite of high quality and fibre volume fraction. But it's characteristics are determined by antiadhesive property of the PFA. This is where a large margin lies to improve this material.

Acknowledgements

Special thanks go to Elmar Biller for providing me with the opportunity and resources to conduct my master thesis at the composite unit of Huber + Suhner. I'm very grateful to the entire work force of the unit for all the support I received during the project, including Gerald Bize and Dr. René Koeppel for their support in the physics and chemistry laboratories.

For provision of materials I'm much obliged to Dr. Michael Dadalas at Dyneon, Ernst Braches at Toho Tenax, and Gerhard Mader at Hexcel. I'm thankful to Thomas Heinrich for the use of the heated press at ETH Zürich, and Hanspeter Eigenmann for his support during manufacturing.

For their help during testing I like to thank Dr. Toni Schneider at ZHAW during XPS; Anja Weber at PSI during SEM; Jon Wingborg at Lamera during 4-point bending; Henrik Persson at Chalmers University during tensile testing; and Mr. Meister at Huntsman for the DMA.

I'm appreciative for the useful information obtained from Ulrich Rennet at Richter Chemiepumpen, Mr. Folsche at CP Pumpen, and Alexander Starsky at Toho Tenax. For the proof reading I thank Dr. Sebastian Rider

Last but by no means least I thank Dr. Prof. Rodney Rychwalski at Chalmers University for his moral support and for being the project evaluator.

Contents

1. Introduction 1

1.1 Background 1

1.2 Literature Review 2

1.3 Aims 5

2. Materials and Manufacturing 7

2.1 Materials 7

2.2 Manufacturing 7

3. Carbon Fibre Surface Characterisation of as-received Fibres 13

3.1 XPS 13

3.2 Surface Composition of the Carbon Fibre 14

3.3 Scanning Electron Microscopy 17

3.4 Optical Analysis of the Fibre Surface Topography 18

4. Quality Assurance of Carbon Fibre/PFA Composites using Optical Microscopy 21

4.1 Sample Preparation 21

4.2 Experimental Procedure 22

4.3 Results and Discussion 22

5. Mechanical Testing 27

5.1 Preliminary Tests 27

5.1.1 4-Point Bend Testing 27

5.1.2 Tensile Test 30

5.2 Interlaminar Shear Strength 32

2.1 Short Beam Shear Test Experimental Setup 33

5.2.2 Results and Discussion 34

5.3 3-Point Bend Testing 36

5.3.1 3-Point Bending Testing Experimental Setup 37

5.3.2 Results and Discussion 39

6. Fibre Content 45

6.1 Chemical Resin Digestion 45

6.2 Resin Burn-off 46

6.2.1 Resin Burn-off Experimental Setup 46

6.2.2 Observations During the Experiment *47*
6.2.3 Results and Discussion *47*

7. Thermal Analysis **51**
7.1 Differential Scanning Calorimetry 51
7.1.1 DSC Experimental Setup *52*
7.1.2 Results and Discussion *52*
7.2 Thermomechanical Analysis 53
7.2.1 TMA Experimental Setup *54*
7.2.2 Results and Discussion *54*
7.3 Thermographimetric Analysis 55
7.3.1 TGA Experimental Setup *56*
7.3.2 Results and Discussion *56*
7.4 Dynamic Mechanical Analysis 60
7.4.1 DMA Experimental Setup *60*
7.4.2 Results and Discussion *61*

8. Final Discussion and Conclusions **65**

9. Recommendation for Further Research **67**

10. References **69**

11. Appendices **73**
Appendix A 73
Appendix B 75
Appendix C 76
Appendix D 77
Appendix E 78
Appendix F 79
Appendix G 80
Appendix H 137
Appendix J 152
Appendix K 153
Appendix L 164

List of Figures

Figure 1 *(Fluorocarbon (PTFE))* *2*
Figure 2 *(Chemical structure of PFA)* *3*
Figure 3 *(Influence of F/C ratio on ILSS)* *4*
Figure 4 *(Carbon fibre rovings used: Hexcel (left) Toho Tenax (right))* *8*
Figure 5 *(PFA dispersion)* *8*
Figure 6 *(Primed Tooling ready for filament winding)* *9*
Figure 7 *(Wetting of the fibres using a brush)* *10*
Figure 8 *(Impregnated rovings after drying of dispersion)* *11*
Figure 9 *(Fontijne TP400 two plate press)* *12*
Figure 10 *(Plates after consolidation in the Press)* *12*
Figure 11 *(XPS machine)* *13*
Figure 12 *(XPS of Hextow AS4 Fibre)* *15*
Figure 13 *(XPS of Toho Tenax HTS40 Fibre)* *15*
Figure 14 *(C1s peak of Toho Tenax HST40 fibre)* *16*
Figure 15 *(Zeiss, Supra 55VP SEM) Source: www.zeiss.de* *17*
Figure 16 *(SEM overview of Hextow AS4 fibres)* *18*
Figure 17 *(SEM overview of Toho Tenax HTS40 fibres)* *19*
Figure 18 *(Close-up of Hextow AS4 fibres)* *19*
Figure 19 *(Close-up of Toho Tenax HTS40 fibres)* *20*
Figure 20 *(Samples in clips and silicon moulds)* *21*
Figure 21 *(Prepared sample for optical analysis)* *22*
Figure 22 *(Overview 2 Hexcel flat)* *33*
Figure 23 *(Overview 4 Toho 1mm)* *24*
Figure 24 *(Overview cross section 3 Toho flat)* *24*
Figure 25 *(Unconsolidated area)* *35*
Figure 26 *(Cavities in composite)* *25*
Figure 27 *(Mecmesin (MultiTest 1))* *28*
Figure 28 *(Nominal dimensions of specimens)* *29*
Figure 29 *(Coupon dimension for tensile testing. All dimensions given in mm)* *31*
Figure 30 *(Specimens with ends enwrapped in sandpaper & clamping mechanism)* *32*
Figure 31 *(Peeled of carbon fibres on sandpaper)* *32*
Figure 32 *(Test setup applied for ILSS)* *34*
Figure 33 *(Average distribution of ILSS)* *35*
Figure 34 *(Typical ILSS graph obtained from PFA)* *36*
Figure 35 *(Nominal dimension of the three point bending specimen)* *36*
Figure 36 *(Setup for 3-point-testing)* *38*
Figure 37 *(3-point bending; graph showing force vs. crosshead distance travelled)* *40*
Figure 38 *(SEM image of crack surface showing fibres enwrapped in PFA matrix)* *42*
Figure 39 *(SEM image of PFA attached to the fibre and pulled away during fracture)* *42*

Figure 40 *(SEM image of root-like on fibres originating from PFA)*.....*43*
Figure 41 *(SEM image showing the root-like shapes remaining when the PFA was pulled away)* *43*
Figure 42 *(Weighing of the resin burn-off samples)*.....*47*
Figure 43 *(Coloration of crucibles during resin burn-off)*.....*47*
Figure 44 *(Importance of the components on the performance of a composite)* *51*
Figure 45 *(DSC thermogram of a carbon/PFA composite)*.....*53*
Figure 46 *(TMA testing machine)*.....*54*
Figure 47 *(TMA thermogram of carbon/PFA composite)* *55*
Figure 48 *(Typical TGA thermogram of carbon/PFA composites)* *57*
Figure 49 *(TGA thermogram of Toho Tenax and Hexcel fibres)*.....*58*
Figure 50 *(TGA thermogram of dried PFA dispersion)* *58*
Figure 51 *(DMA plot of Hexcel fibre/PFA composite)*.....*61*
Figure 52 *(DMA plot of Toho fibre/PFA composite)*.....*62*

List of Tables

Table I *(Chemical surface composition of fibres)* *14*
Table II *(Void content of samples)* *23*
Table III *(Results of preliminary 4-point bend testing)* *30*
Table IV *(Results of ILSS test)* *34*
Table V *(Average result of the 3-point-bend test)* *39*
Table VI *(Measurements and results of resin burn-off)* *48*
Table VII *(Fibre fraction determination by TGA method)* *59*

Nomenclature

b	Width of specimens
d	Difflection
DMA	Dynamical mechcanical analysis
DSC	Differential scanning calorimetry
E_f	Flexural modulus
G’	Shear modulus
G’’	Loss modulus
h	Thickness of specimens
ILSS	Interlaminar shear stress
L_1	Span distance
m_F	Mass fibre
M_M	Mass matris
PFA	Tetrafluoroethylene-perfluoroalkoxyvinylether-copolymer
P_R	Maximal load
PTFE	Polytetrafluorethylene
SEM	Scanning electron microscopy
T_g	Glass transition temperature
TGA	Thermographimetric analysis
T_m	Melting temperature
TMA	Thermomecanical analyis
V_f	Fibre volume fraction
wt%	Weight percent
XPS	X-ray photoelectron spectroscopy
ε	Strain
σ	Stress
F/C ratio	Fluorine/Carbon ratio

1. Introduction

1.1 Background

Composite materials have been applied in a variety of fields and industries. Due to it's properties, such as low weight, robustness, high strength composites have become the material of choice in the aeronautic industry, high end automobile industries and for use in various sporting goods (Gay and Hoa, 2007). Composite materials have several possible applications in the chemical industry, including pump housings, tubing, fittings, controls, tanks, or valves. Such that their full potential may be realised, it is crucial they can withstand highly fluctuating temperatures and pressures in addition to providing exceptional chemical resistance (Wang, 2006; Drobny, 2009; Nesbitt, 2006). Traditionally mainly thermosets, such as epoxies, polyester, phenolic, and vinyl ester resins have been used as matrix materials for advanced composites. This is because they are easy to process, show high mechanical properties, and manufacturing temperature is only slightly above the maximum use temperature. Furthermore, thermosetting polymers usually show good adhesion between reinforcement and resin (Summerscales, 2007). Bonding is crucial for the performance of fibre-reinforced composites in order to transfer load and stress from the matrix to the fibres. If a fibre to matrix interaction is weak, it will result first of all in environmental load susceptibility like water intake, and/or in poor mechanical composite properties (Potter, 1999). A good fibre to matrix interface is made possible by adhesion and/or compatibility. Load transfer is achieved by mechanical means such as interlocking and/or chemical bonding (Isaac and Ori, 2006; Aström, 1997). Rychwalski (2009) further mentioned molecular entanglement following interfusion, electrostatic attraction, and attraction between anionic groups at the end of the molecules and cationic surfaces as ways of forming interfacial bonds. However, due to their limited chemical resistance and rather brittle properties they are unsuitable for application in both the chemical and the oil and gas industries (Kruijer et al., 2005). When chemical resistance was required in addition to strength and toughness, thermoplastic in-liner materials have been applied to fibre reinforced thermoset casing materials. The sole use of in-liner materials (mainly PTFE and

PFA) without reinforcements was found insufficient, as the mechanical properties of these materials showed a vast decrease when exposed to elevated temperatures.

1.2 Literature Review

In recent years thermoplastic materials have been sought which could be used as matrix materials for carbon fibre reinforced plastics. The most mentioned materials emerging form this research are the high performance fibre reinforced thermoplastic composites. These are fibre-reinforced derivates from polyetherketone known as PEK, PEEK, or most recently PEKK. These materials show the benefits of thermosetting composites, light weight and excellent mechanical properties, yet additionally show improved chemical and thermal resistance (Mitschang et al., 2003; Fujihara et al., 2004). The drawbacks of using these matrix materials are their rather large costs and difficulty in processing. In their work, Fujihara et al. (2004) mention five possible fabrication methods of continuous fibre thermoplastic composites. He was also attempting a sixth manufacturing method based on PEEK. The quality of this method is determined by testing the resulting mechanical properties.

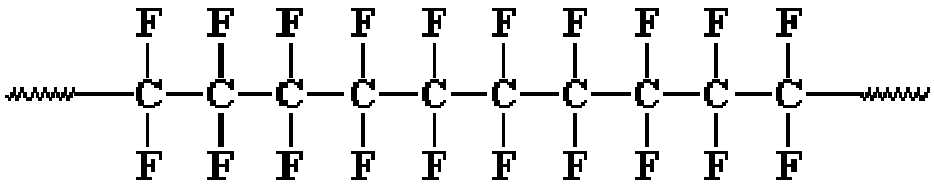

Figure 1 *(Fluorocarbon (PTFE)) Source: www.pslc.ws/macrog/ptfe.htm*

Fluorine containing polymers in their simplest form are polymers of hydrocarbons in which all or some hydrogen atoms have been replaced by fluorine atoms. One group of fluorocarbon polymers are perfluorinated fluorocarbon polymers. These have a main chain consisting of carbon and fluorine only (*Fig. 1*). Known members of this group are PTFE, FEP and PFA. According to Drobny (2001), fluoropolymers offer outstanding chemical, weather and UV resistance, and high service temperature in addition to a low coefficient of friction. Even un-reinforced they exhibit good mechanical properties when compared to other polymers. These properties are due to presence of fluorine to carbon bonds, which are stronger than hydrogen to carbon bonds. The polymer chains arrange themselves into a spiral due to the size of fluorine atom. Such a chemical structure allows the

fluorine atoms to protect the carbon-to-carbon bond wrapped within it (Toyoko, 2003). The best-known fluoropolymer is polytetrafluoroethylene (PTFE). Most of its properties have been established (Cardona et al., 2001). Nevertheless it has the disadvantage of not being meltable, plastically formable and generally difficult to process in its raw state (Karlovitz, 1995). Cardona et al. (2001) states that PTFE has a high melting temperature and an extremely high melt viscosity (10^{10} - 10^{12} Pa s). As a consequense the processing of PTFE requires advanced techniques. This led to the development of fluoropolymers that may be processed by melting, which exhibit similar properties to PTFE. The one most commonly used in the chemical industry is tetrafluoroethylene-perfluoroalkoxyvinylether-copolymer (PFA) (Drobny, 2009). In the polymer handbook (Brandrup et al., 1999) PFA is defined as perfluoralkoxy resin, copolymer of tetrafluorethylene and perfluorinated alkoxyl vinyl ethers. Other than its thermoplastic properties, the advantages of PFA over PTFE in processing, include a higher stability under load at temperatures up to 260°C and a generally higher pressure resistance and Young's modulus (Saechtlin, 1989). Another benefit of PFA, which can be beneficial for its application in this project, is its hot-melt adhesive properties (Karlovitz, 1995). The aforementioned beneficial properties of PFA result from the substitution of 5% of perfluoralkoxylvinylether with a fluorine atom (*Fig. 2*). These benefits are a trade-off for a lower maximal service temperature and lower dimensional stability under heat. Although PFA was first synthesized in the mid 1970s (Cardona et al., 2001), some of its thermal properties are yet to be recorded and studies are scarce. In addition manufacturers of this material do not readily supply the properties for all their products. Generally, Bismarck et al. (2008) based on Park (2003), mention that fluoropolymers are extremely hydrophobic in nature and that good adhesion to reinforcing fibres, or to any filler material, is difficult to achieve.

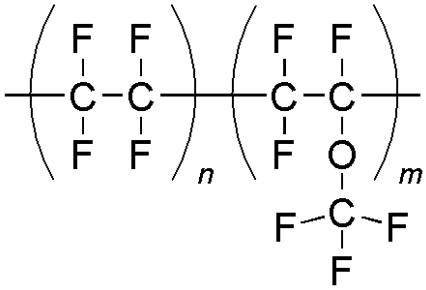

Figure 2 *(Chemical structure of PFA) Source: http://image.absoluteastronomy.com*

Findings published by Bismarck at al. (2008) contradict those by Morgan (2005). Oxidative surface treatment by providing sites for chemical interaction and mechanical interlocking did not improve the interaction between the reinforcing fibres and the matrix as assumed by Morgan (2005). Fibre pullout tests performed by Bismarck et al. (2008) did not yield higher interfacial shear strength for fibres oxidized to a higher level, but did show a decrease in interfacial shear strength. This property was used as a measurement of the adhesion between the fibre and the matrix. The findings were supported by the observation that the contact angle of the wetting agent to the surface did not change when the oxidation level was changed.

In studies based on their work performed in 1997, Bismarck et al. (2007, 2007, 2008) investigated the suitability of fluorinated carbon fibres as reinforcement for fluoropolymers, particularly poly (vinylidene fluoride) (PVDF). The contact angles of PVDF melt droplets on fluorinated carbon fibres were measured and accordingly single fibre pullout tests were performed. It was observed that the contact angle decreased simultaneously as the interfacial shear strength increased as the surface fluorine content of the F/C ratio was increased. Surprisingly, this effect reversed to values lower than the starting value when the F/C ratio surpassed a certain point (*Fig. 3*). It was concluded that there is an influence of the degree of fluorination of carbon fibres on the interaction at the fibre/fluoropolymer interface. The practical adhesion strength between fluorinated carbon fibres and fluoropolymers was found to be at an optimum when the ratio between matrix and fibre fluorine content was 9:1.

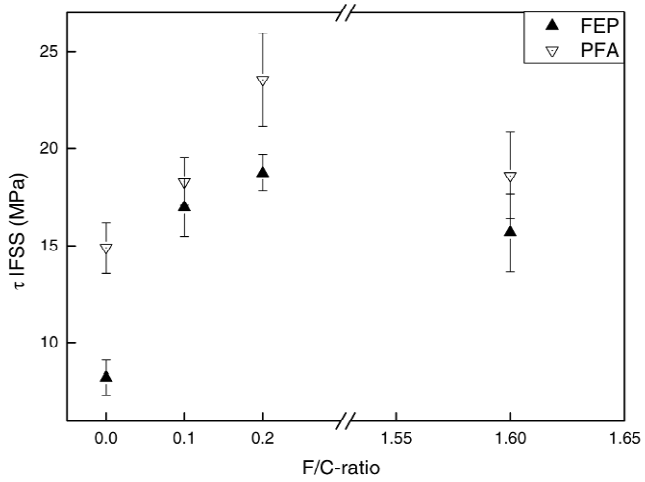

Figure 3 *(Influence of F/C ratio on ILSS) Source: Bismarck et al. 2007*

The manner in which chlorine influences the performance is still to be understood. All previously mentioned tests were conducted on single fibres. Fluorination of entire filaments or even weaves and laminates has not yet been attempted. For commercial applications, fluorination of single fibres is not feasible and different approaches need to be assessed. An approach to fabricate carbon fibre reinforced fluoropolymer composites was used by Oshima et al. (2001). It was demonstrated how PTFE could be used to manufacture a composite, using an aqueous dispersion for wetting the fibres and an electron beam cross linking treatment to connect the molecular chains of the polymer. The resulting composite showed increased one ply sheet properties compared to non-reinforced PTFE. Multi sheet laminates however, showed properties similar to non-crosslinked PTFE composites. These findings lead to the assumption that the electron beam was unable to penetrate the polymer entirely. The idea to use an aqueous fluoropolymere dispersion to impregnate reinforcing material was initially introduced by Logothetis (1993). His research was carried out at DuPont. In a complicated process reinforcing fibres were clumped together to a randomly orientated chopped strand mat. The resultant specimens had a rather low fibre volume content and the void content obtained was not mentioned. Further information about his research were not to be found, but would have been interesting for comparison purposes.

In the aforementioned studies, either only the interfacial shear strength at single fibres was determined, or the research concentrated on PTFE reinforced with one kind of fibre. However, PTFE has no functional groups that could be used for an interaction with any matrix material - PFA has one site, which can potentially have the ability for such an interaction. Consequently, research in this direction could be of more interest. Whilst the characterisation of single fibres is necessary, a method to obtain optimised properties in an industrially useful form is still to be found.

1.3 Aims

The aim of this project is to develop a viable method to produce a composite material of aligned continuous carbon fibres embedded in a PFA matrix. The resulting composite produced will have its thermal and mechanical properties determined.

2. Materials and Manufacturing

2.1 Materials

Hextow AS4 carbon fibre (*Appendix A*), supplied by Hexcel (Parla, Spain), and Tenax – E HTS40 X011 12K carbon fibre (*Appendix B*), supplied by Toho Tenax (Wuppertal, Germany), were used as reinforcement materials. Both are PAN-based carbon fibres. Hextow AS4 was a commercially available un-sized, industrially oxidised carbon fibre. Tenax – E HTS40 X011 is not yet commercially available but still under development. The sizing currently remains confidential and consequently is denoted by X in its product name. However, the company reported it to be thermoplastic sizing suitable for the application with high temperature thermoplastics.

PFA (Dyneon PFA 6900GZ) in form of an aqueous fluorothermoplast dispersion was kindly supplied by Dyneon 3M (Burgkirchen, Germany) *(Appendix C)*. Dyneon PFA 6900GZ is a 50 wt% solid fluoroplastic dispersion. PFA is a melt-processible copolymer of tetrafluorethylene and perfluorinated co-monomers, with a melt viscosity several times lower than that of PTFE.

2.2 Manufacturing

Test specimens were manufactured from dry Carbon rovings (*Fig. 4*) and an aqueous PFA dispersion (*Fig. 5*) by filament winding the fibres on a rectangular core followed by high temperature compression to consolidate the thermoplastic matrix material. To obtain a specified thickness a groove was machined into the core limiting the amount of compression. The core had a length of 130 mm; a thickness of 170 mm; and a depth of 25 mm, enabling several test specimens to be obtained per winding and pressing process.

Figure 4 *(Carbon fibre rovings used: Hexcel (left) Toho Tenax (right))*

Individual rovings spread to 4 mm (Hextow AS4) and 4.5 mm (Tenax – E HTS40 X011 12K) when being wound on the mandrel. Six layers of roving were needed to reach a thickness larger than 1 mm. Due to the high temperature required for the process, and the abundance of a suitable thermoplastic sizing agent, the first mentioned fibres were without sizing. Second fibres were with a new sizing agent, developed for high temperature thermoplastic applications. All fibre and dispersion property data were given by the manufacturer. The assumption was made that no 'wet out' occurred and the fibres were able to retain all added PFA dispersion.

Figure 5 *(PFA dispersion)*

The steel core was wrapped with Thermalimide^{TM}, an ultra high temperature antiadhesive bagging film (*Fig. 6*) (*Appendix D*). This prevented any oxidative

contamination of the specimens and ensured their removal. In addition the bagging film protected against corrosion of the core. Furthermore the core was treated with the release agent Mold Wiz F–57 NC. The roll of loose fibres was put into the filament-winding machine. The dry fibre roving was fed from the roll to the tool without passing through a dispersion-containing bath. The tension of the rovings was kept as small as possible to obtain a higher degree of wetting and to ensure that the dispersion is not pushed out from the inner layers once the other layers are laid on - thus keeping the inner layers dry. The filaments were wound on with a 0.5 mm overlap ensuring that the core was completely covered leaving no gap - this ensured the production of uniformly consistent specimens. The filament winding was carried out on a CNC winding machine (Baer, Germany, S/N WSE–V No. 1), which ensured all rovings were placed on the prepared tooling in a replicable way (*Fig. 6*).

Figure 6 *(Primed Tooling ready for filament winding)*

The exact amount of dispersion was decanted using a Mettler PM 34 Delta range medium precision scale (S/N J28086) and a syringe. The dispersion decanted accounted for the amount of matrix required per layer to obtain a fibre volume fraction of 40%. It would therefore not be possible to obtain specimens with a fibre volume fraction of less than 40%. Once a layer was wound on, the winding machine was stopped and the dispersion was applied to the dry fibres using a short bristled brush (*Fig. 7*). All the decanted dispersion had to be used per layer. Care had to be taken to ensure that the dispersion was distributed equally over the entire layer and no dry spots remained. This procedure was repeated for every layer. On the core,

each of the two fibres was used. Therefore, four plates manufactured under exactly the same conditions in one run. Hand, eye and lung protection were worn throughout the entire manufacturing process to prevent any contamination of the specimens, avoid any human contact with hazardous materials, and to comply with required safety and COSHH procedures.

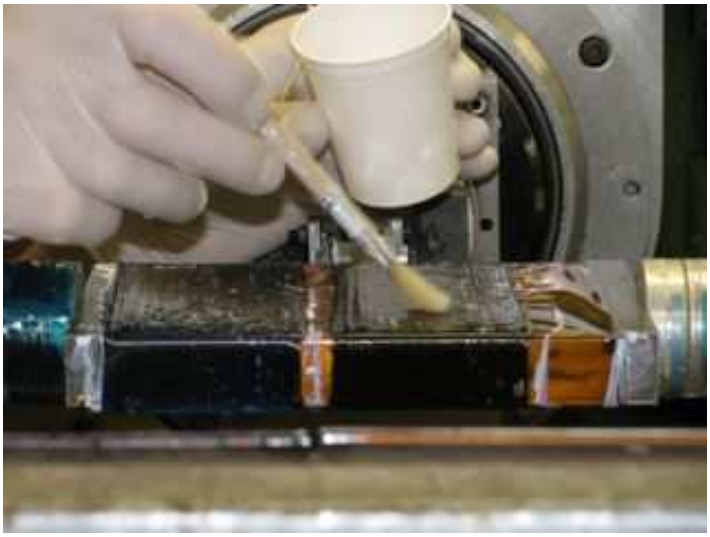

Figure 7 *(Wetting of the fibres using a brush)*

Following winding, the core was placed in an oven (Binder APT. line FD (E2), S/N 08–47682). The temperature was continuously increased to 105 °C and kept constant for 30 min to ensure all aqueous parts of the dispersions had evaporated. To remove any other solvents, the temperature was further increased steadily to 290 °C, and kept at this temperature for 30 min. Following this, the core was cooled to room temperature such that it may be handled and transported. The appearance of the fibres after the drying of the dispersion can be seen in *Fig. 8*.

Figure 8 *(Impregnated rovings after drying of dispersion)*

To ensure good consolidation and to melt the PFA particles together, high temperature and pressure were required. A Fontijne (Holland, TP 400, S/N 00026.566 – 12.92/TPB 289) two-plate press was used (For further details about the press see *Appendix E*) (*Fig. 9*). The pressing temperature was performed at 340 °C, the nominal process temperature of PFA according to the manufacturer datasheet (*Appendix C*). Once the tooling had reached 340 °C the press was closed and the plates compressed with a defined pressure for a defined amount of time. To allow for a reasonably slow cooling, no cooling system was used when the tooling was cooled to room temperature. *Figure 10* shows the plates still on the tooling just after having undergone the high temperature/cooling process. The consolidated plates were removed from the tooling. For the removal of the winding, the part was cut along small sides of the tool. The Thermalimide™ foil facilitated the removal. As the produced material was U-shaped, the vertical ends were cut off using a stencil-knife in order to process the material further. The obtained plates were then cut to the size required for the testing of the specimens needed to characterise the material. For the cutting of the test-specimens a Bossard (Switzerland) diamond disc saw with an integrated measuring scale was used. To remove any potential spurs or irregularities, the specimens were treated with P800 grit size sandpaper and the cleaning was done with acetone.

Figure 9 *(Fontijne TP400 two plate press)*

Figure 10 *(Plates after consolidation in the Press)*

3. Carbon Fibre Surface Characterisation of as-received Fibres

This chapter is a short summary of the importance of the fibre surface for the strength of a composite and is based upon the information provided by Rychwalski (pers. communication, spring 2009). In a composite there is a large interface area. This implies that the reinforcement matrix interaction is of immense importance. Rychwalski further went on to explain that a fibre achieves it's restraining ability on the matrix entirely via the fibre matrix interface. The chemical fibre surface composition determines the contact angle between a liquid (matrix) and a solid (reinforcement) and therefore, is important for the strength of the bonding between the two. Different interfacial bonds were also explained. The bonding can be enhanced by surface treatment. Sizings are often used as coupling agents. They can be used to establish a chemical link between reinforcement and the matrix particularly in thermosets. However, this mechanism may also take place, or increase the surface tension, in thermoplastics, which leads to a more integrated composite of higher quality. If good wetting has occurred surface roughness can contribute to the strength of the interface.

3.1 XPS

The fibre surfaces were characterised by X-ray photoelectron spectroscopy (XPS, SPECTRA, Phoibos 150 MCD-9, S/N 030–05.05c, ZHAW, Winterthur, Switzerland) (*Fig. 11*) to determine the composition of the surface and possible functionalisation of the fibres (Toho Tenax).

Figure 11 *(XPS machine)*

Previous to the experiment, the fibres were placed under vacuum at 80 °C ensuring the used fibres were completely dry. To obtain a measurable sample, the fibres were chopped with cleaned scissors to prevent any contamination. The chopped fibres were placed in a Petri dish and compressed in order to obtain a relatively solid sample, preventing any surrounding to be measured accidentally. A high-resolution scan was performed for each fibre sample. In addition a previous survey scans from 100 eV to 1000 eV were carried out to determine detectable elements. As an excitation source Al 202 W (1486.6 eV), a slit width of 2 x 6 mm and a take off angle of 45° were applied. The vacuum obtained was always higher than 5 x 10^{-4} MPa. For all the tests the X-ray photoelectron spectrum was referenced to the C 1s peak of carbon (284.5 eV). Data processing and analysis was performed using the CasaXPS software.

3.2 Surface Composition of the Carbon Fibre

To some extent carbon fibre surface chemistry influences the properties of the composite material either improving or reducing the interfacial adhesion between reinforcement and matrix by providing sites for interaction. XPS is a method to identify the composition of the carbon fibre surface in addition to determine possible functional groups generated by surface treatment. *Table 1* shows the chemical composition of the surface of the different carbon fibres.

Table I *(Chemical surface composition of fibres)*

Fibre	Fibre diameter (μm)	C 1s (at.%)	O 1s (at.%)	N 1s (at %)
Hextow AS4	7.1	91.4	5.9	2.7
Toho Tenax	7	84.0	14.8	1.2

The XPS-analysis the Hextow AS4 fibre (*Fig. 12*) showed an increase in the values for carbon and nitrogen content whilst the oxygen content is severely reduced compared to the Tenax – E HTS40 fibre (*Fig. 13*).

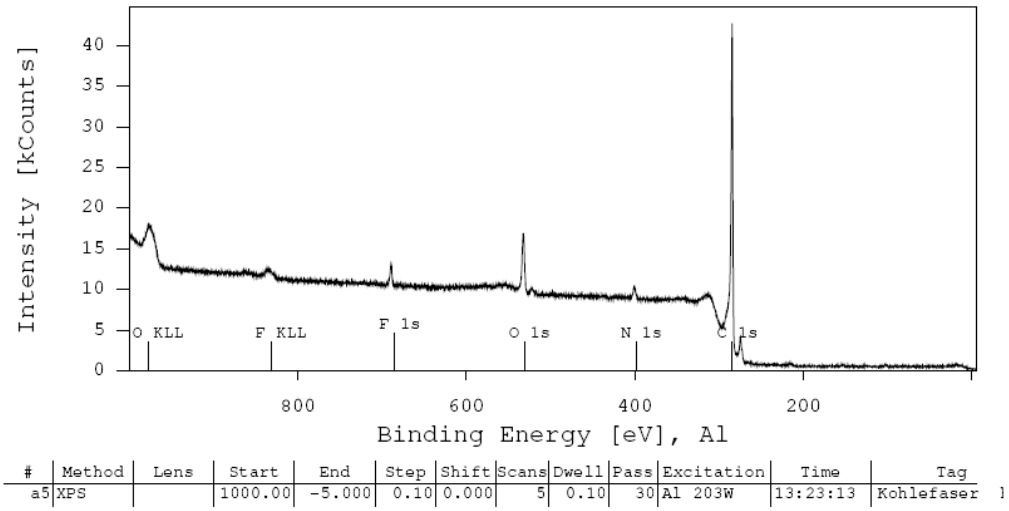

#	Method	Lens	Start	End	Step	Shift	Scans	Dwell	Pass	Excitation	Time	Tag
a5	XPS		1000.00	-5.000	0.10	0.000	5	0.10	30	Al 203W	13:23:13	Kohlefaser

Figure 12 *(XPS of Hextow AS4 Fibre)*

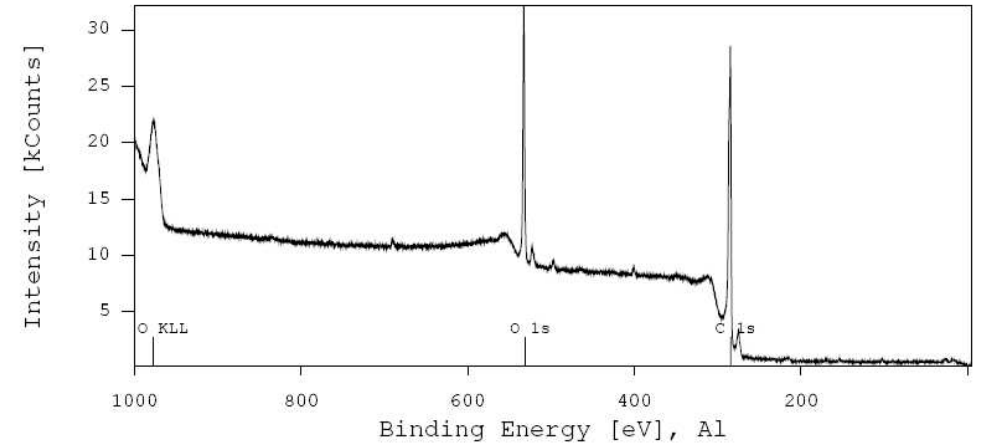

#	Method	Lens	Start	End	Step	Shift	Scans	Dwell	Pass	Excitation	Time	Tag
a2	XPS		1000.00	-5.000	0.10	0.000	5	0.10	30	Al 202W	10:28:10	Kohlefaser

Figure 13 *(XPS of Toho Tenax HTS40 Fibre)*

The nitrogen residues on the fibres can be attributed to PAN precursors. The fluorine peaks in the XPS spectra are atypical for the fibres and can be assumed to be contaminations originating from the production of test specimens when the rolls of fibres were stored in close proximity to the fluorine being handled. According to Hexcel the AS4 fibre had a surface treated with electrochemical oxidation. When the peaks of the major elements were examined the spectra of the AS4 fibre showed nice peaks without any distinctive shoulders. The C 1s peak of the Tenax – E HTS40 showed a clear shoulder (*Fig. 14*). The deconvolution of this peak in the high-resolution spectra provided information about the chemical environment of this element on the surface. However, as the binding energies of relating to carbon – nitrogen and carbon – oxygen coincide (*Appendix F*) a distinct allocation of the chemical environment is made impossible due to the similarities between carbon –

oxygen and carbon – nitrogen bonds (Biniak et. al., 1997). When this peak is compared to the figures presented by Biniak et al. (1997) the shoulder can be allocated to the binding energies of C–OH, C–O–C, C–N. The main peak in *Fig. 14* can clearly be allocated to graphitic carbon at BE = 284.6 – 285.1 eV.

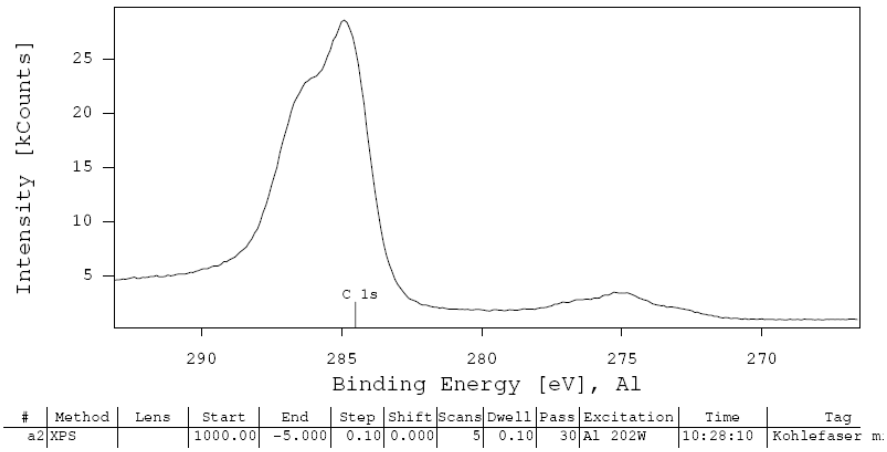

#	Method	Lens	Start	End	Step	Shift	Scans	Dwell	Pass	Excitation	Time	Tag
a2	XPS		1000.00	-5.000	0.10	0.000	5	0.10	30	Al 202W	10:28:10	Kohlefaser m.

Figure 14 *(C1s peak of Toho Tenax HST40 fibre)*

According to Biniak et al. (1997) the carbon between BE = 286.3 – 287.0 eV is present in the form of alcohol or ether groups. C=O and C–N binding energies were barely present as the binding energy is vastly declining after the shoulder dropped at 286.4 eV. All other peaks did not show any shoulder but nice pointy peaks at 400.4 eV. At this position the binding energy of C–N is located. The O 1s peak is located at 530 eV. However, the peak present in the Tenax fibre spectra was slightly higher and close to 532.6 eV. This is the position where C–OH, C–O–C, C=O have their binding energy located (Paynter, 2005). From this it could be derived that the chemical environment on the surface of the Tenax – E HTS40 fibre consists of graphitic carbon, C–OH, C–O–C as well as some C–N. As the distinctive shoulder at the C 1s peak was missing in XPS spectra of the Hextow AS4 fibre, it has to be assumed that the chemical groups on the surface were mainly C–N and C=O. That could be confirmed, as there was a shoulder low down on and further away from the main graphitic carbon peak. From *Fig. 14* it could be assumed that the apex of the shoulder was at 288 eV, the binding energy of C=O. There might also have been some CNO present, but this could not be confirmed as any further dispartment of the obtained spectra was not possible with the resources available. The small peaks in the spectra immediately following the larger peaks originate from the non-

monochromativity of the X-ray spectroscope used and were created by satellite lines in the X-ray spectrum (Paynter, 2005).

3.3 Scanning Electron Microscopy

To determine the topography of the fibre surfaces and to confirm the nominal fibre diameters given in the data sheet provided by the supplier, Scanning Electron Microscopy (SEM, Zeiss, Supra 55VP SEM, PSI, Villigen, Switzerland) was applied (*Fig. 15*) with SmartSEM® control software. As it was of utmost importance that the fibres were completely dry, the samples were placed in a vacuum chamber at 80 °C for 180 min. Prior to the experiment a small amount of fibres were placed under the microscope to confirm that the conductivity of the fibres was sufficient and thus gold sputtering of the samples to provide the sample with conductivity was unnecessary. Following the confirmation sample fibre strands were attached securely to the testing tray enduring no loose fibre could interrupt the testing by touching the electron source or damage the machinery in any other way. As there was no danger of damaging the samples, as high as possible vacuum was applied during testing so high quality images could be expected. The acceleration voltage was set to 3.00 kV. The testing always followed the same procedure. First a general overview of the sample at relatively small magnification was taken. Potential areas of interest were localised and magnified. Desired micrographs were taken allowing the surface to be investigated and analysed.

Figure 15 *(Zeiss, Supra 55VP SEM)* *Source: www.zeiss.de*

3.4 Optical Analysis of the Fibre Surface Topography

As mentioned before, mechanical interlocking is one mechanism providing interfacial strength. It is generally acknowledged (Bismarck et al., 2007) that the higher the amount of irregularities the higher the possibility mechanical adhesion can take place. These irregularities can originate from the manufacturing process of the fibre or any surface treatment that might have followed. Bismarck et al. (2007) mentioned that the higher the amount of oxidation, the higher the amount of surface irregularities**.** Therefore, it could have been expected the interfacial strength would increase accordingly. However, Bismarck et al. (2007) vitiated this assumption by showing that the strength decreases with an increasing amount of oxidation. *Figure 16* and *Fig. 17* respectively show the overview of the fibres used for this study.

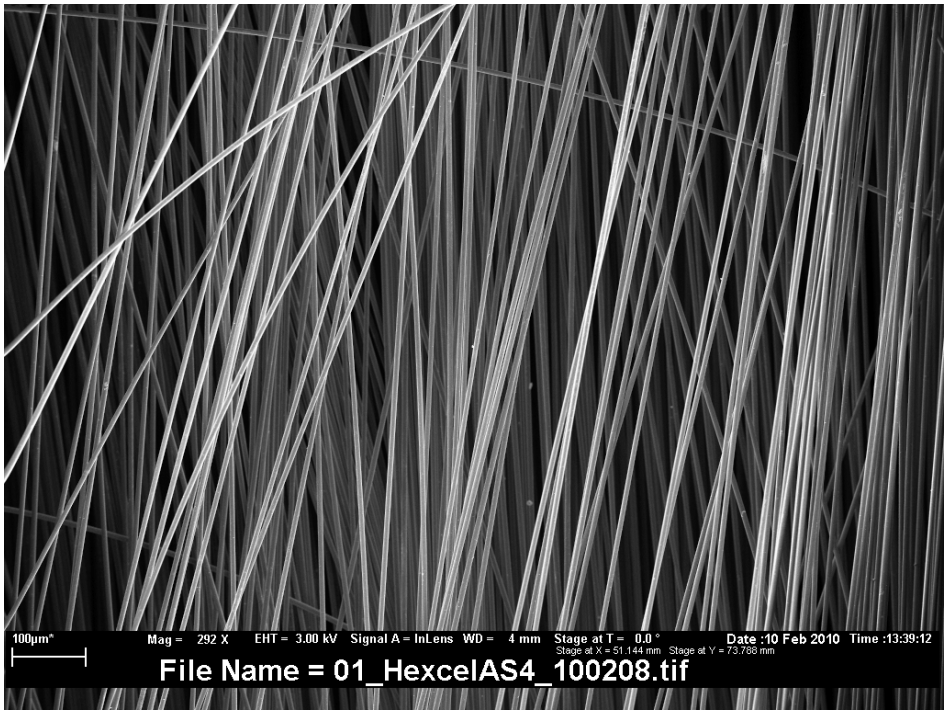

Figure 16 *(SEM overview of Hextow AS4 fibres)*

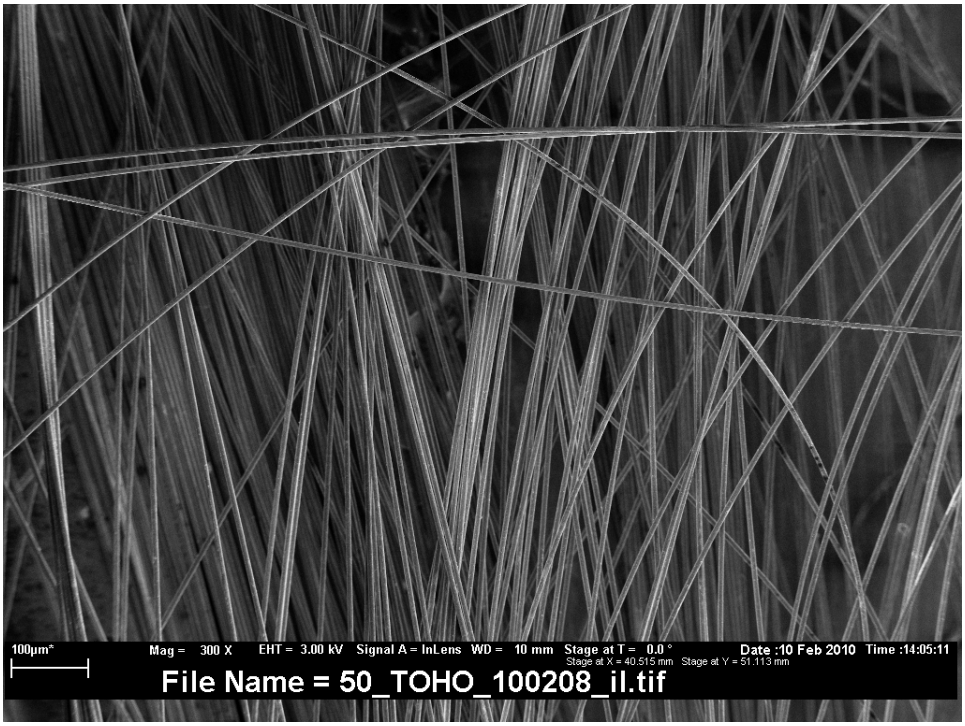

Figure 17 *(SEM overview of Toho Tenax HTS40 fibres)*

No difference between the two fibres could be observed in the overview images of similar magnification (≈300x). The obvious difference in orientation could be attributed to the areas chosen and could be neglected. At higher magnification it could be observed that the fibre texture showed some obvious differences between the two fibres (*Fig. 18 and Fig. 19*).

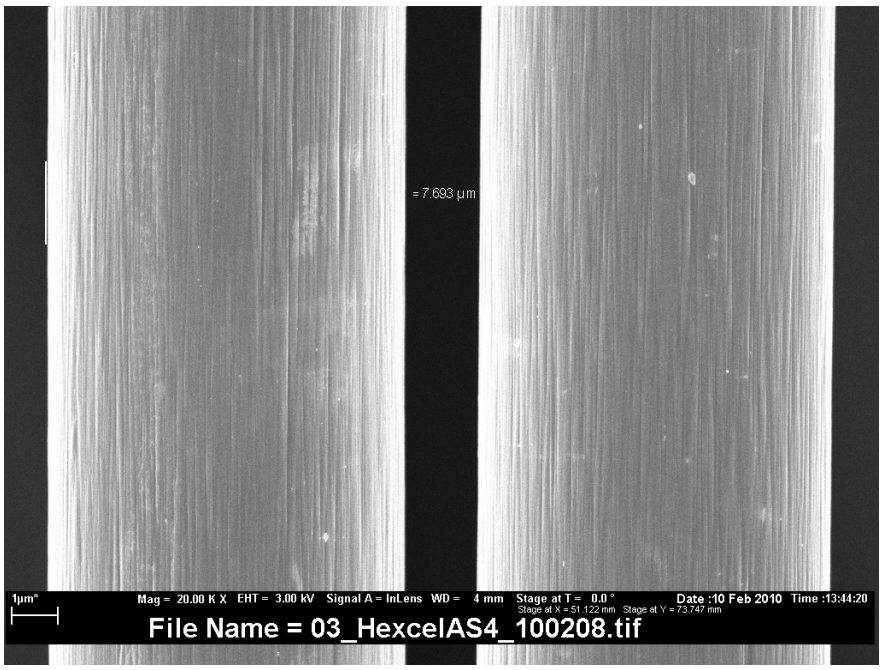

Figure 18 *(Close-up of Hextow AS4 fibres)*

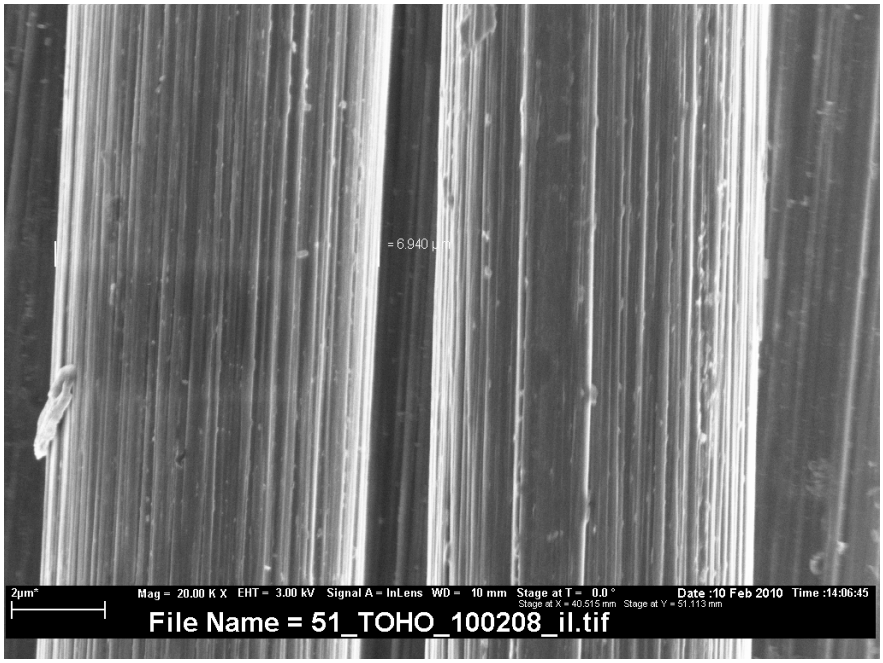

Figure 19 *(Close-up of Toho Tenax HTS40 fibres)*

Both fibres showed a lamellar structure typical for PAN fibres, due to the haphazard folding of the fibre sheets making up the carbon fibre (Xiaosong, 2009). However, in the Toho fibre these lamellas were much more prominent than could be observed in the Hexcel fibre. Also, whilst in the Hexcel fibres the lamellas were discontinuous in a random pattern, the lamellas of the Toho fibre were more continuous in what seems to be a repeating pattern. On the surface of the Toho fibres small particles could be distinguished. As these particles seemed to be a regular occurrence, it was assumed that they belonged to the fibres rather than being contaminates. Particles of this kind were also seen on the Hexcel fibre but with much less regularity. Considering the difference in chemical surface composition discussed in previous chapter these particles could be responsible for the higher oxygen content found on the Toho fibre. Measuring the diameter of the fibres under the SEM revealed that the Toho fibre was corresponding to the nominal fibre diameter given by manufacturer. The Hexcel fibres however, showed a larger diameter than supplied by the manufacturer. The fibre diameter has an influence on the interface area. Considering that the fibre matrix interface is the weakest part of a composite it resulted in more area and possibilities for interfacial failure to occur.

4. Quality Assurance of Carbon Fibre/PFA Composites using Optical Microscopy

The purpose of carrying out an analysis of the composite cross section was to investigate the quality of the composites. Properties that could be investigated with this method were concerning the homogeneity of the fibre packing of the material and potential defects. Those included voids, microcracks, and adhesion of the layers, in addition to resin rich areas and dry spots.

4.1 Sample Preparation

From each manufactured plate (*Chapter 2.2*) a sample was cut using the Bossard AG diamond disc saw. The samples had the dimension of 15 mm x 20 mm. The samples were placed with the fibres in the vertical direction in clips to keep them upright. Four samples were kept in position by each clip. The clips were then placed in silicon moulds (*Fig. 20*).

Figure 20 *(Samples in clips and silicon moulds)*

Resin (Araldit D/ curing agent) was poured into the mould to enclose the samples. The filled moulds were placed in a vacuum oven at room temperature at 125 mbar for 10 min. Following this, the oven was aired and the resin was cured for 12 hours before the cured resin blocks were demoulded. To obtain a level and smooth surface without scratches, the samples were placed in a levelling machine (Struers, Uniforce). For the preparation of the surface the samples were place in a Struers (Pedemax-2) sand and polishing machine. Water was used as a cooling and

lubrication agent. Starting with coarse sandpaper, the grain-size was reduced until no more scratches were visible on the surface of the samples. The resulting samples can be seen in *Fig. 21*.

Figure 21 *(Prepared sample for optical analysis)*

4.2 Experimental Procedure

For the analysis an optical light microscope (Olympus BH-2) was used in conjunction with a Leica microscope camera. The images were analysed with DFC320R2 image processing software with an integrated colour recognition tool. This tool was applied to determine the void percentage at the cross-sections of the samples. From each sample an overview at 100x magnification was taken. Based on the overview three images were taken at a magnification of 500x. The images were taken at the left, in the middle and at the right of the sample. The images were used to determine the void content via image processing. Furthermore, measurements to confirm the thickness of the samples were undertaken.

4.3 Results and Discussion

From the results presented in *Table 2* it can be seen that the plates, independent of the manufacturing parameters, showed very low void content. The entire results and the micrographs can be found in *Appendix G*.

Table II *(Void content of samples)*

Sample	Average (%)	Sample	Average (%)
1 Toho 1mm	0.242	**1 Toho flat**	0.147
1 Hexcel 1mm	1.297	**1 Hexcel flat**	0.484
3 Toho 1mm	0.404	**3 Toho flat**	0.179
3 Hexcel 1mm	0.344	**3 Hexcel flat**	0.483
2 Toho 1mm	0.144	**2 Toho flat**	0.150
2 Hexcel 1mm	0.097	**2 Hexcel flat**	0.170
4 Toho 1mm	0.111	**4 Toho flat**	0.100
4 Hexcel 1mm	0.097	**4 Hexcel flat**	0.046
5 Toho 1mm	0.077	**5 Toho flat**	0.084
5 Hexcel 1mm	0.068	**5 Hexcel flat**	0.080

The analysis of the cross section areas of the samples yielded some interesting observations. Based on the results presented in *Table 2* it can be stated, that the void content of the material after the heated pressing process was very low. The averages range between 0.046% and 1.297%. For advanced composite material, depending on the manufacturing process, a void content of 1% is generally accepted (Summerscales, 2007). With increasing pressure and increasing time the samples were held at processing temperature, the average void content was reduced. In the samples of the first batch a direct correlation between the kind of fibre used and the void content could be assumed as both Hexcel samples had a void content nearly four times as high as the corresponding Toho sample. One reason might have been that the Toho fibre absorbed the dispersion better than the Hexcel one, on which it was required to force the dispersion into it in order to wet it out. Also, the overall average void content of batch 1 was higher than the other batches. Reasons must have included the amount of pressure applied and the time exposed to elevated temperature. It was safe to assume that before the pressing process was commenced, the amount and the distribution of the dry dispersion were similar. The higher the pressure applied the closer the PFA particles were to be. Therefore, there was less chance for any air being entrapped in the material. When the melting temperature was reached at nominally 310 °C and increased further to the processing temperature (340 °C) the pressure was kept constant. During this process the molten polymer being forced into the cavities filled any voids still existing. The entrapped air was pressed to the sides. The longer the polymer remained in a molten state the longer the time for cavities being filled and air removed.

When inspecting the micrographs further differences between the Hexcel/PFA composites and the Toho/PFA composites could be observed.

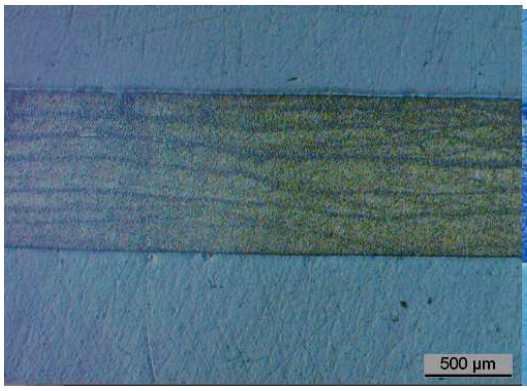

Figure 22 *(Overview 2 Hexcel flat)*

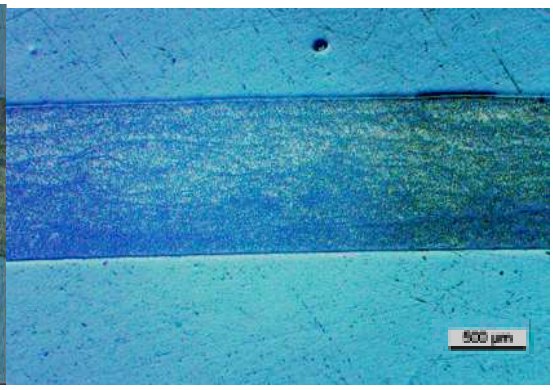

Figure 23 *(Overview 4 Toho 1mm)*

In all the Hexcel plates independent of pressure and dwell time at high temperature the individual layers and rovings could clearly be distinguished by prominent resin rich lines (*Fig. 22*). These lines could also be observed in the Toho samples, but were much less frequent and less prominent (*Fig. 23*). Another observation made on several samples was a difference in fibre packing through the cross section (*Fig. 24*).

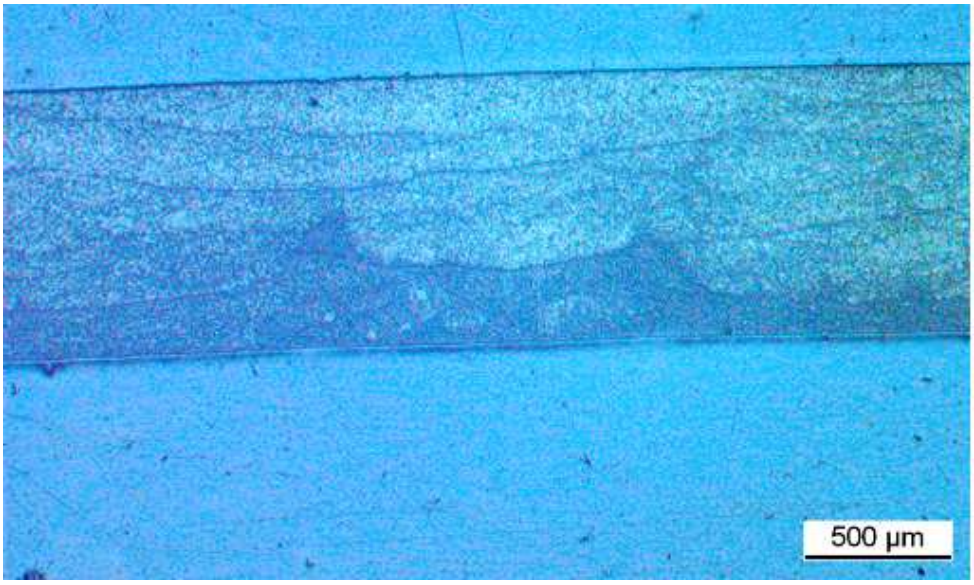

Figure 24 *(Overview cross section 3 Toho flat)*

In *Fig. 24* the lower side of the cross section was the one facing away from the mandrel and the one seen in *Fig. 8.* In the filament winding process excessive resin was pressed to the outside by the tension and pressure applied by the upper layers of rovings. Due to the low viscosity of the PFA dispersion the amount pressed out was

higher than likely if epoxy resin is used. As the dispersion dried very quickly it did not drip off but remained on the surface (clearly visible in *Fig. 8*). Since PFA in its molten state has a high melt viscosity (Ebnesajjad, 2002) it pressed the fibres towards the mandrel, causing shown inhomogeneities. Batches produced at lower pressure did not show such inhomogeneities (*Appendix G*). However, at lower pressure complete consolidation could not be guaranteed. *Figure 25* shows a line in the centre of the cross section area at which the PFA had not melted completely. Cavities were also found in low-pressure batches to which no matrix material had yet advanced, and therefore were not closed (*Fig. 26*).

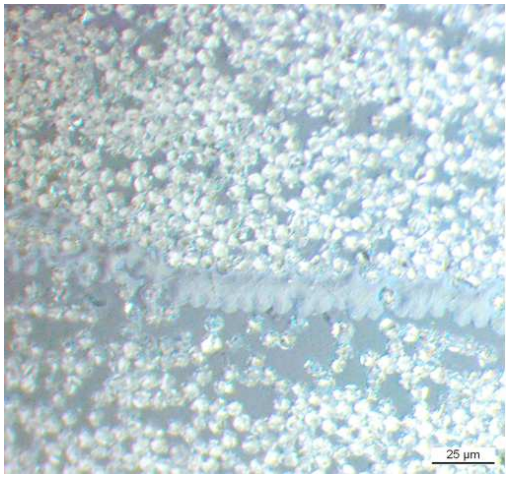

Figure 25 *(Unconsolidated area)*

Figure 26 *(Cavities in composite)*

5. Mechanical Testing

Mechanical testing is essential to evaluate the performance of a material, where stiffness, strength and toughness play a role. Physical property data was necessary to correlate with the calculated stresses, the expected environment, etc. (Brown, 2002). According to Brown (2002) without such data one would be reduced to inspired guesses with its uncertainty of possible failure, or gross over-design with its accompanying wastage. Testing has been proven to aid improved design or quality control procedures. The obtained data also helped to determine if the material could be used for certain applications and the way it compares to other materials.

There were several test methods available. Depending on the method applied results could differ significantly. It may occur that due to different reasons, a test cannot be carried out. Therefore, it was important that the right method for a given material was chosen. It was important that the test conditions and fabrication details with all possibilities that could have caused deviations were stated. Brown (2002) also mentioned that it frequently is unknown if a sample was representative of the bulk material.

The naming of the specimens always followed the same pattern: Batch number (1 – 5); type of fibre (T = Toho Tenax or H = Hexcel); side of the mandrel (F = flat and 1 = 1 mm groove)

5.1 Preliminary Tests

As it was unknown if a manufactured composite (*Chapter 2.2*) was worth continuous interest, or should be discontinued, simple preliminary tests were carried out. The results of these tests had to be considered with caution as the test environment could be described as experimental, not strictly corresponding to real service conditions.

5.1.1 4-Point Bend Testing

As tensile testing can be difficult, flexural characteristics are often measured as an alternative (Hodkinson, 2000). Also, most components are subjected to a mixture of loading modes. The advantage of flexural tests over tensile tests was the

ease of production of the specimens and the abundance of any gripping problems (Brown, 2002).

In 4-Point bending the force is applied at four points. It has the advantage over 3-point bend testing that the stress is distributed equally between the two inner forces.

Experimental Setup

The test was carried out using a Mecmesin (MultiTest 1) testing machine (*Fig. 27*). A four point bending fixture with a span of 100 mm was used. The loads were introduced 25 mm each side of the centre. The fixtures had a radius of 1mm and the testing speed of the machine was set to 2 mm/min. The introduced load was recorded over time and measured electronically. To measure the displacement a Mitutoyo – 543-390B – Digital Dial Indicator Absolute attached to the load fixings was used and the values at crucial points were recorded manually

Figure 27 *(Mecmesin (MultiTest 1))*

To obtain and control the results two specimens of each manufactured sample were tested. Due to the difficulties of cutting the specimens to given dimensions, some small deviation occurred, which had to be taken into account during the calculations.

The calculations were based on the beam bending theory and according to ASTM D 790. The flexural modulus (E_F) is given by equation [1]

$$E_F = 0.17 \times \frac{\Delta F}{\Delta d} \times \frac{L^3}{bh^3} \quad [1]$$

For the ultimate flexural stress and the corresponding strain equation [2] and [3] are used.

$$\sigma_F = \frac{3FL}{4bh^2} \quad [2]$$

$$\varepsilon_F = \frac{4.36hd}{L^2} \quad [3]$$

Where L_1 is the span between the support fixings; *F* describes the applied force; *b* the breath of the specimen; *h* the specimen thickness; and *d* stands for the distance travelled by the crosshead.

Specimen Dimensions

The nominal dimensions of the preliminary samples are shown in *Fig. 28*.

Figure 28 *(Nominal dimensions of specimens)*

Results and Discussion

In *Table III* the values obtained in the initial 4-point bend test are presented. The obtained flexural modulus was promising. The stiffness of the composite was of a value that would allow it to be used as a structural, load bearing material. However, there is a large deviation between the specimens originating from the same plate. There is the possibility that this deviation originated from the difference in the dimensions of the specimens. Based on obtained $E_{f,}$ it was decided to continue producing the specimens the same way as described in *Chapter 2.2* as reasonable values were achieved.

Table III *(Results of preliminary 4-point bend testing)*

Flat						
Fibre	**at 30N (mm)**	**at 40N (mm)**	**Initial cracking (mm)**	**width (mm)**	**thickness (mm)**	**E_f (GPa)**
	1.3	2	4	8.5	1.45	94
Hexcel	1.4	2.1	4.6	9	1.45	89
	1.3	1.9	4.6	9.5	1.45	98
Toho	1.2	1.8	4.4	10.8	1.45	86
1mm						
Fibre	**at 30N (mm)**	**at 40N (mm)**	**Initial cracking (mm)**	**width (mm)**	**thickness (mm)**	**E_f**
	1.4	1.9	3.7	11	1.5	92
Hexcel	1.4	2	4.4	10.1	1.45	92
	1.1	1.8	3.6	9.8	1.4	90
Toho	1.3	2.1	3.9	7.5	1.45	93

All the specimens failed in exactly the same manner. At a deflection between 3.5 – 4.4mm initial cracking noises could be heard. In the load vs. time graphs (*Fig. 29*) this cracking could not be observed, leading to the assumption the cracking took place on a small scale. As the load was increased further all specimens without exception failed underneath one of the loading supports. The failure was accompanied by a distinctive cracking noise. From the loading point outward an interlaminar crack could be distinguished. The failure underneath the supports would much rather have been expected for a 3-point bend test, this is the reason a 4-point bend test was attempted. Therefore, it was decided that in the future a 3-point bend test would be sufficient.

5.1.2 Tensile Test

In a tensile test a specimen is exposed to pure tension. Depending on the material, different shapes of specimens may be required. Due to the gripping force, damage of the specimens can occur that lead to invalid test results.

Tensile Test Experimental Setup

Originally a tensile test was thought about and also attempted. In order to realise fracture resulting at a loading a standard tensile testing machine can handle the dimensions recommended by DIN EN ISO 527 Part 1 and Part 4 (*Fig. 29*) were reduced to the dimensions shown in *Fig. 28.*

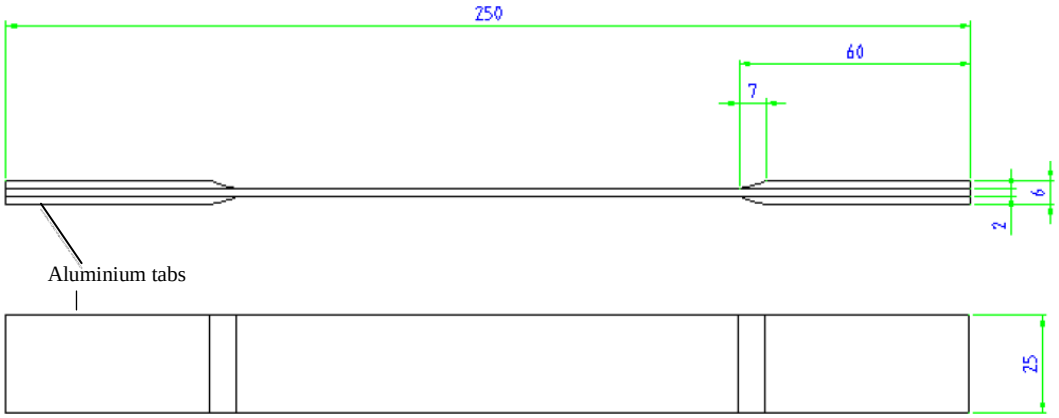

Figure 29 *(Coupon dimension for tensile testing. All dimensions given in mm)*

However, whilst preparing for testing, the following circumstances made it impossible to perform a tensile test with the composite material produced. PFA is one of the most anti-adhesive materials so as a consequence no adhesive could be found. Several adhesive manufacturers, the supplier of the PFA and testing institutes were unable to name a solution that would suffice for the required application. The solution named by one supplier, to treat the surface with LOCTITE® Prism 770 primer and to use LOCTITE® prism 406, a universal general-purpose instant adhesive, to bond the end tabs to the specimens was dismissed after it was attempted but the bonding was insufficient. The adhesive would have been necessary to bond aluminium end tabs to the specimens. The aluminium tabs would have been used to prevent damage to the composite material at the grips, causing premature failure and to ensure a good force introduction (Cattell, 2000). Thus, end tabs could not be used.

Observation and Discussion

The attempt was made to directly clamp the specimens into the testing rig and realise fracture without aforementioned end tabs. Unfortunately the force applied to the specimens by the hydraulic closing mechanism crushed the ends of the specimens severely. Afterwards the idea was brought up to cover the clamp surface using fine-grained sandpaper (*Fig. 30*). This was done in order to increase the friction between the specimen and the clamp as well as to protect the specimen against the irregularities in the clamp.

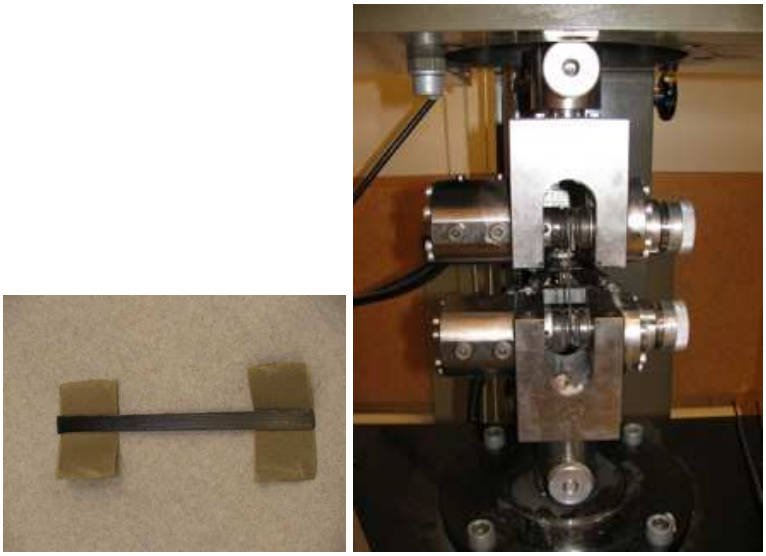

Figure 30 *(Specimens with ends enwrapped in sandpaper & clamping mechanism)*

This attempt resulted in the peeling off of single carbon fibres layers (*Fig. 31*). The peeled off fibres were not an entire roving, but were only the very surface fibres. It was observed, that the fibres that peeled off were only the ones where the matrix was punctured by the sandpaper. This can generally be attributed to the low hardness of the PFA. The matrix material in this case is unable to protect the reinforcement against puncturing environmental influences. From the fibres that were pulled off, it also became obvious that the bonding between the matrix and the reinforcing materials is a crucial weakness of the manufactured material.

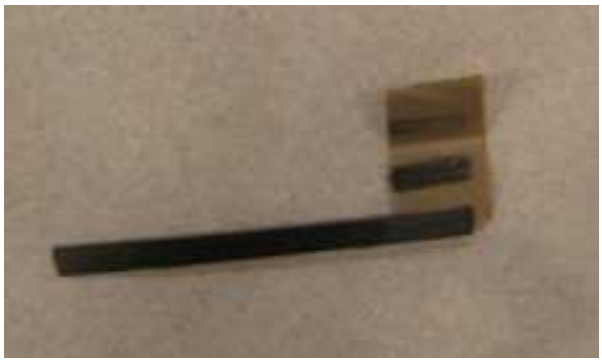

Figure 31 *(Peeled of carbon fibres on sandpaper)*

5.2 Interlaminar Shear Strength

According to Thielicke and Soltesz (1992) interlaminar shear strength (ILSS) is one of the most important properties of laminated fibre-reinforced materials. It significantly influences all other physical values and the overall shear behaviour. It intended as a measurement of the strength of the fibre/matrix bond. Interlaminar

shear testing of composite materials has proven to be one of the most difficult areas of mechanical property testing. Anon (approx. 2005) states that the presence of edges, material coupling, non-pure shear loading, non-linear behaviour, imperfect stress distributions, or the presence of normal stresses makes shear strength determination questionable. Currently there are no test methods available without their inaccuracies. The most commonly used test method, particularly in industry, is the short beam test. ILSS is based on a 3-point bending test. As the specimens should be relatively thick, short, and flat, the test is carried out with a very short span. This is meant to minimise the flexural stresses and to maximise the in-plane shear stresses (Anon, ca. 2005). Although the test is designed to measure interlaminar shear strength, it can be difficult to relate data obtained to actual fibre matrix interface properties (Rychwalski, 2009). Rosselli and Santare (1997) added that this method has been widely criticised because a pure shear stress state is not induced anywhere within the test specimen, and the material can fail in either compression or tension rather than shear. Pull-out testing is also used. The disadvantage is the use of single fibres, instead of realistic composites (Rychwalski, 2009)

2.1 Short Beam Shear Test Experimental Setup

The testing of the apparent interlaminar shear strength was based upon on the DIN EN 2563:1997 standard. It specifies the method for determination of the apparent interlaminar shear strength of carbon fibre reinforced plastics in the form of unidirectional laminates by means of a flexural test[1]. The method used can be applied to all kind of materials. However, the results obtained by the *Equation [4]* can only be used to make comparisons of laminates produced in similar ways. The result of the derivations from the norm chosen deliberately is that a direct comparison has to be considered with caution as different material may require different dimension in order for interlaminar failure to occur. The fixings used were manufactured at H+S and built to comply with aforementioned standard (*Fig. 32*). The entire testing was carried out on a Zwick 1445 testing frame using a 500N load cell with a crosshead speed of 1mm/min. The point of failure was interpreted as the point at which loading peaked the first time. For the load nose apparatus used in the

[1] DIN EN 2563:1997, (1997), 'Kohlenstoffaserverstärkte Kunststoffe; unidirektionale Laminate; Bestimmung der scheinbaren Interlaminaren Scherfestigkeit', Beuth Verlag GmbH: Berlin

tests, the support roller diameter and the loading nose diameter (both 4 mm) were larger than recommended by the standard. The testing was carried out in a controlled environment with a relative humidity of 50% at 21°C. *Figure 32* shows the test setup applied.

Figure 32 *(Test setup applied for ILSS)*

To calculate the apparent ILSS following equation was applied,

$$\tau^* = \frac{3F}{4bh} \qquad [4]$$

Where τ^* represents the apparent ILSS; F is the maximal load at the moment of first failure; b and h stand for the breadth and the thickness respectively of the measured specimens.

5.2.2 Results and Discussion

Table IV *(Results of ILSS test)*

Specimen	width (mm)	thickness (mm)	Force (N)	ILSS (MPa)
2H1	9.73	1.2	344	22
2HF	9.89	1.13	313	21
2T1	9.68	1.24	284	18
2TF	9.64	1.22	294	19
5H1	9.59	0.93	207	17
5HF	9.34	0.89	196	18
5T1	9.71	0.87	176	16
5TF	9.72	0.89	184	16

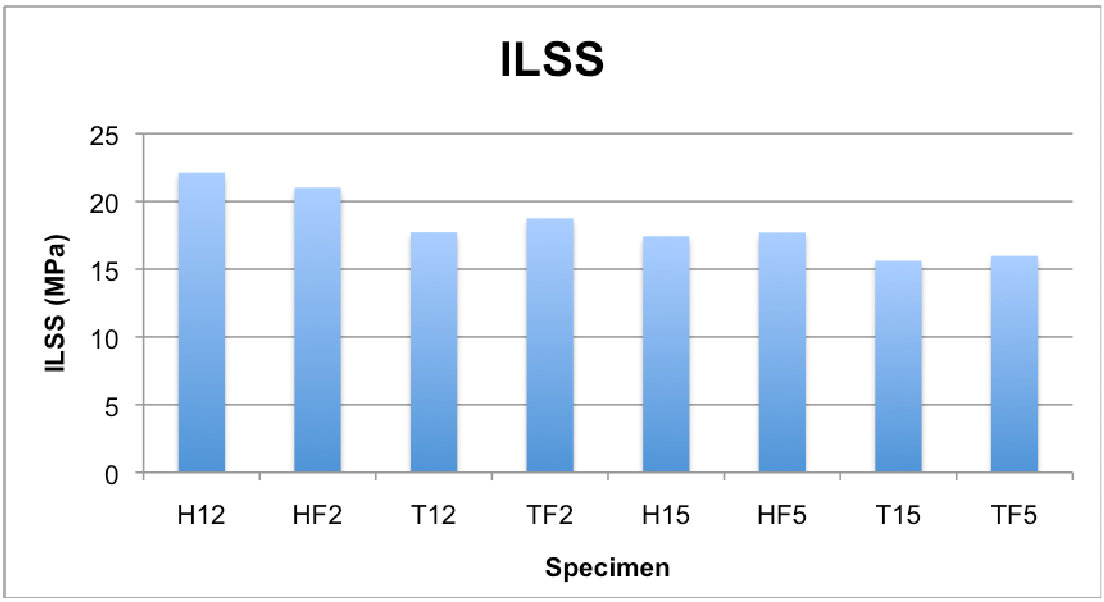

Figure 33 *(Average distribution of ILSS)*

The specimen only differed in thickness. It is stated in previous literature (Rychwalski, 2009; DIN EN 2563:1997) that the span to thickness ratio has to be 4 to 5. However, due to the small thickness of the specimens, it was hard to find a fixture of that small size and a ratio of 10 had to be opted for. Due to this the failure occurred by what was stated in the standard as plastic deformation. *Figure 34* shows typical graphs obtained. It can be seen that no distinctive peak occurred. Therefore, the failure could not be attributed to single or multiple shear failure. If a specimen fails in this mode the result obtained by *Equation [4]* is according to the standard not a true shear stress at failure. Therefore, the result could only be used for comparison with those from a series of tests related to a same material. Based on this it is still possible to compare the results obtained between specimens. In the results the specimens produced with Hexcel AS4 fibre showed better performance than the ones made from Toho Tenax HTS40. However, due to the occurring failure mode it had to be doubted if the results were representative.

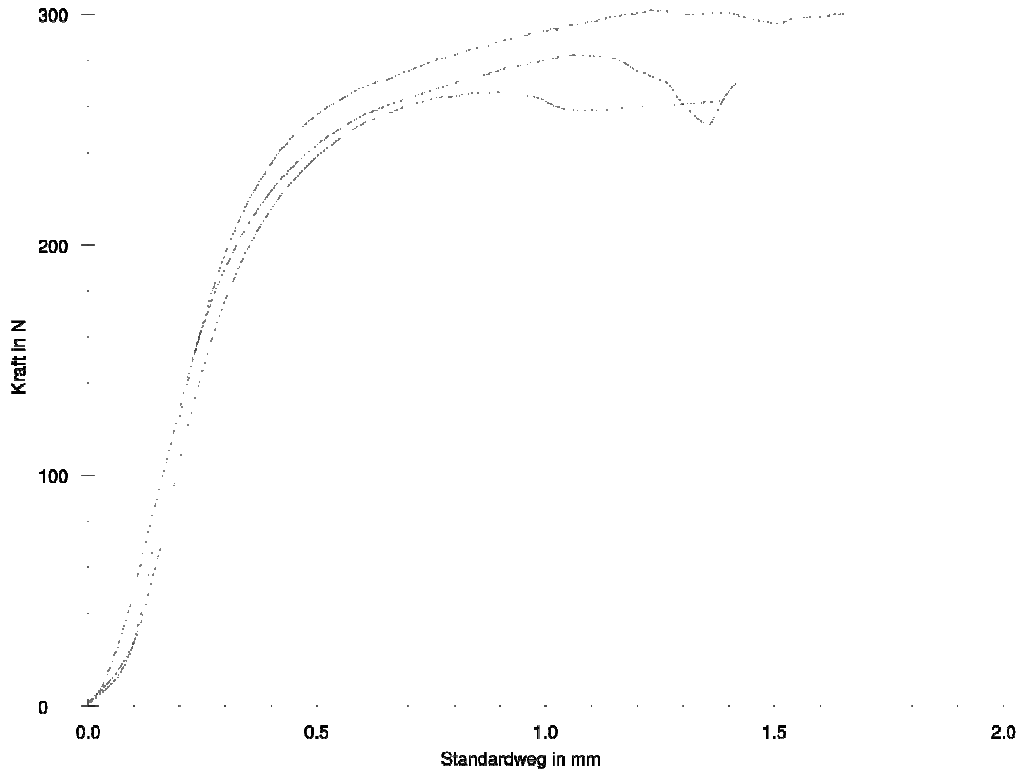

Figure 34 *(Typical ILSS graph obtained from PFA)*

5.3 3-Point Bend Testing

In *Chapter 5 section 1.2* it was shown and discussed that tensile testing could not be used for Carbon/PFA composites. Therefore, 3-point bending was applied as an alternative. 3-point bending is a rather simple test, in which a force is applied to a specimen at three points, wherein the central loading point is equidistant from the outer two supporting spans (*Fig. 35*) (Brown, 2002). The maximum stress is at the central loading point - consequently failure often occurs at that point.

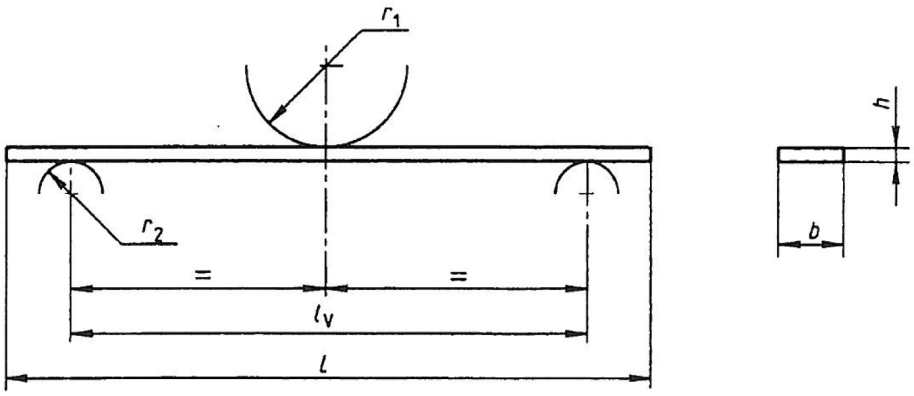

Figure 35 *(Nominal dimension of the three point bending specimen)*

As was seen in *Chapter 5 section 1.1*, failure in 4-point bend testing also took place at the points of load introduction. This was the reason a 3-point bend test instead of a 4-point bend test was opted for. In flexural tests there is potential for three modes of failure; compressive; tensile; or interlaminar shear failure (Cattell and Kibble, 2001). It is a known fact that compressive behaviour of composites is inferior to its tensile behaviour (Kim and Castro, 1994). Therefore, failure occurring during the test is likely to originate from the side of the beam that is under compression. Carbajal and Mujika (2008), based on Chaterjee et al. (1994), state that tests measuring compressive strength are conditioned by difficult to control factors and are notoriously hard to carry out. Schneider (2007) confirmed this by observing considerable amount of scatter when identical specimens were tested according to the same standard at different laboratories. Therefore, certain differences can be expected when carrying out 3-point-bend testing on specimens described above.

5.3.1 3-Point Bending Testing Experimental Setup

3-Point bend testing was carried out based upon EN ISO 178:2003. The test was performed to determine the flexural properties of materials manufactured as described in *Chapter 2.2*. The dimensions of the specimens were chosen so that different tests could have been performed.

The tests allowed determining the bending behaviour of the specimens; the bending stiffness; the flexural modulus. For this test a freely supported beam is loaded beam loaded halfway of the supporting span. The test setup is shown in *Fig. 36.* The test was undertaken on a Zwick 1445 testing frame using a 500N load cell with a crosshead speed of 1mm/min. E-modulus was determined between 0.05% - 0.25% strain. Testing was carried out under controlled environment at 25 °C and 50% relative humidity.

Figure 36 *(Setup for 3-point-testing)*

Failure occurred at the point at which the load started to decrease. For each material four specimens were tested. To calculate the flexural stress *Equation [5]* was used. Flexural strain was given by *Equation [6].*

$$\sigma_F = \frac{3FL}{2bh^2} \qquad [5]$$

$$\varepsilon_F = \frac{6hd}{L^2} \qquad [6]$$

σ_F represents the flexural stress; *F* the force applied in Newton; *L* distance of supporting span; *b* the width of the specimen; *h* the thickness of the specimen; ε_f the flexural strain; s the deflection.

The flexural modulus was determined by *Equation [7]*

$$E_F = \frac{\Delta F}{\Delta d} \times \frac{L^3}{4bh^3} \qquad [7]$$

The tensile modulus is usually slightly higher than the flexural modulus. The theoretical Young's modulus can be calculated by the rule of mixture (ROM) (*Equation [8]*).

$$E_{tot} = V_f E_f + (1 - V_f) E_m \quad [8]$$

Where E_{tot} is the overall Young's modulus of the composite; E_f and E_m stand for the Young's modulus of the reinforcement and the matrix respectively; V_f the is fibre volume fraction.

5.3.2 Results and Discussion

The data obtained by 3-point-bend testing were calculated using equations stated above and the results shown below in *Table V*.

Table V *(Average result of the 3-point-bend test)*

Specimen	E_f (GPa)	σ_{fmax} (MPa)	ε_{fmax} (%)	$E_{f\ theoretical}$ (GPa)
4H1	70	479	0.66	148
4HF	69	417	0.57	147
4T1	70	446	0.59	144
4TF	72	490	0.64	146
3H1	75	439	0.58	154
3HF	75	515	0.67	153
3T1	66	365	0.54	154
3TF	72	431	0.59	152

These results originated from graphs representatively shown in *Fig.37* and found in *Appendix H*. The force increased steadily over the crosshead distance moved. This increase occurred in a linear fashion. Undamaged specimens showed an instant decreasing steep once the maximum force was reached. Specimens not showing this decrease were often of inferior quality and where therefore not taken into account for the calculation of the results. Failure occurred suddenly with an audible cracking noise. Specimens invariably failed at the point of maximum stress described in *Chapter 5.3.* Interlaminar cracking visible with bare eye was the most common failure mode. But was mostly accompanied by folding of the fibres at the side which was under compression. No sign of damage could be observed on the side under

tension

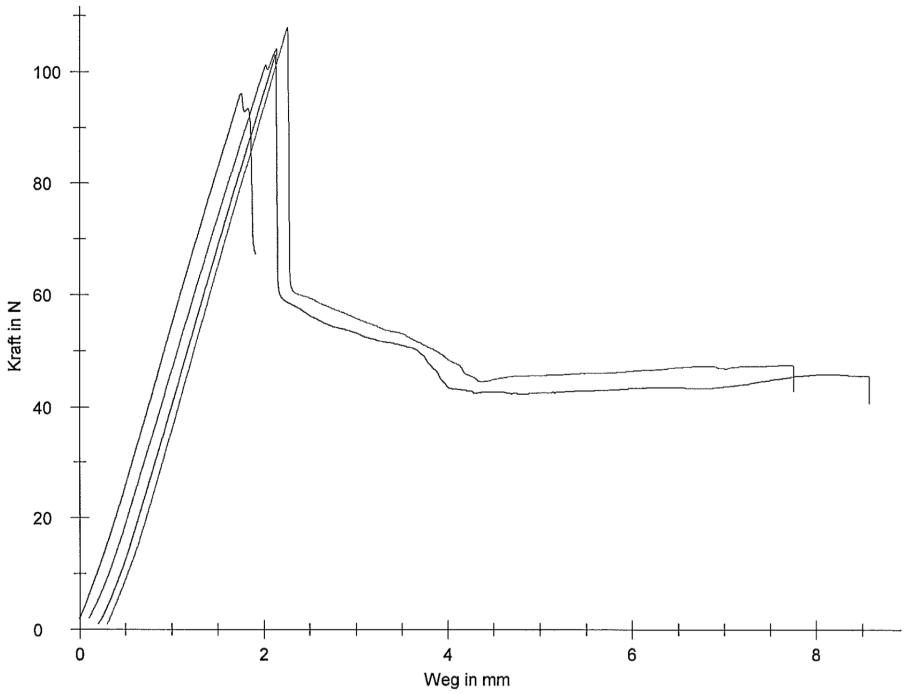

Figure 37 *(3-point bending; graph showing force vs. crosshead distance travelled)*

The results obtained (*Table V*) can be considered to be in direct correlation to the fibre volume fraction obtained and described in *Chapter 7 section 3.* As expected, the higher the fibre volume content, the higher the E-modulus. However, the E-modulus obtained does not approach the theoretical values calculated using the rule of mixture. Furthermore, the ε_{max} is lower than the maximal strain of either constituent. This led to the conclusion that the properties of this composite are determined by the interface, so any improvement of the material properties has to start at the interface.

Comparing the results of the four point bending test versus the three point bending test the resulting flexural modulus is ≈ 20 GPa lower. The specimens in both tests failed in a similar fashion, leading to the assumption that the failure mode was equivalent. However, the difference at which it occurred could be attributed to the testing methods. Failure always occurred at the point load was introduced. This is also the point at which the highest stress occurred. In three point bending all load was introduced at a single point leading to a peaked stress. In four point bending the load is distributed between two points so there is no such stress concentration.

In the 5th column of *Table V* the theoretical Young's modulus calculated using ROM is presented. The ROM assumes that there is perfect bonding between the constituents and interfacial characteristics are not taken into account. This further supported the conclusion that the mechanical properties of this composite were heavily determined by the interface.

To investigate the crack surface a cracked specimen was split along the crack and placed under the SEM described in *Chapter 3 section 3*. Inspecting received micrographs reviled some interesting observations. *Figure 38* clearly shows fibres wrapped in PFA-matrix. Due to the nonconductive properties of PFA it was charged electrostatic under the SEM. Therefore, it could not be depicted as focused as the fibre. In *Fig. 38* and more prominently in *Fig. 39* it shows the way PFA was ripped apart. In the top left corner of *Fig. 38* one can distinguish some PFA on top of the fibre that remained attached to it when the other side was pulled off. Focusing in further on the area shown in *Fig. 38* root-like shapes appear at the point where PFA is attached to the fibre (*Fig. 40*). These shapes remained visible on the fibre even after the PFA was pulled away (*Fig.41*). This showed that the PFA was attached to the fibre to a certain degree, but the bonding was not strong enough to yield higher strain properties.

Comparing obtained results of the carbon fibre/PFA composite to other carbon reinforcement composites (*Appendix A*) it shows approximately half the E-modulus of an UD carbon/epoxy composite. But as mentioned before the strain and also the maximum stress are very low.

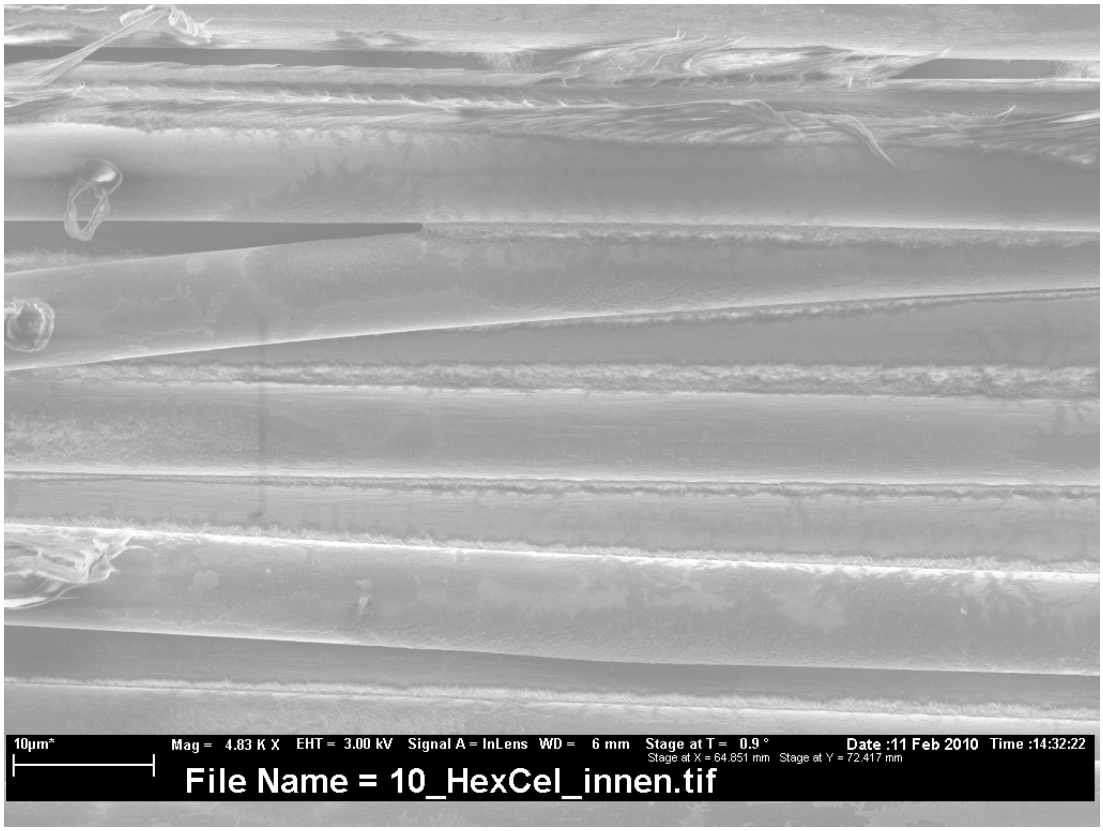

Figure 38 *(SEM image of crack surface showing fibres enwrapped in PFA matrix)*

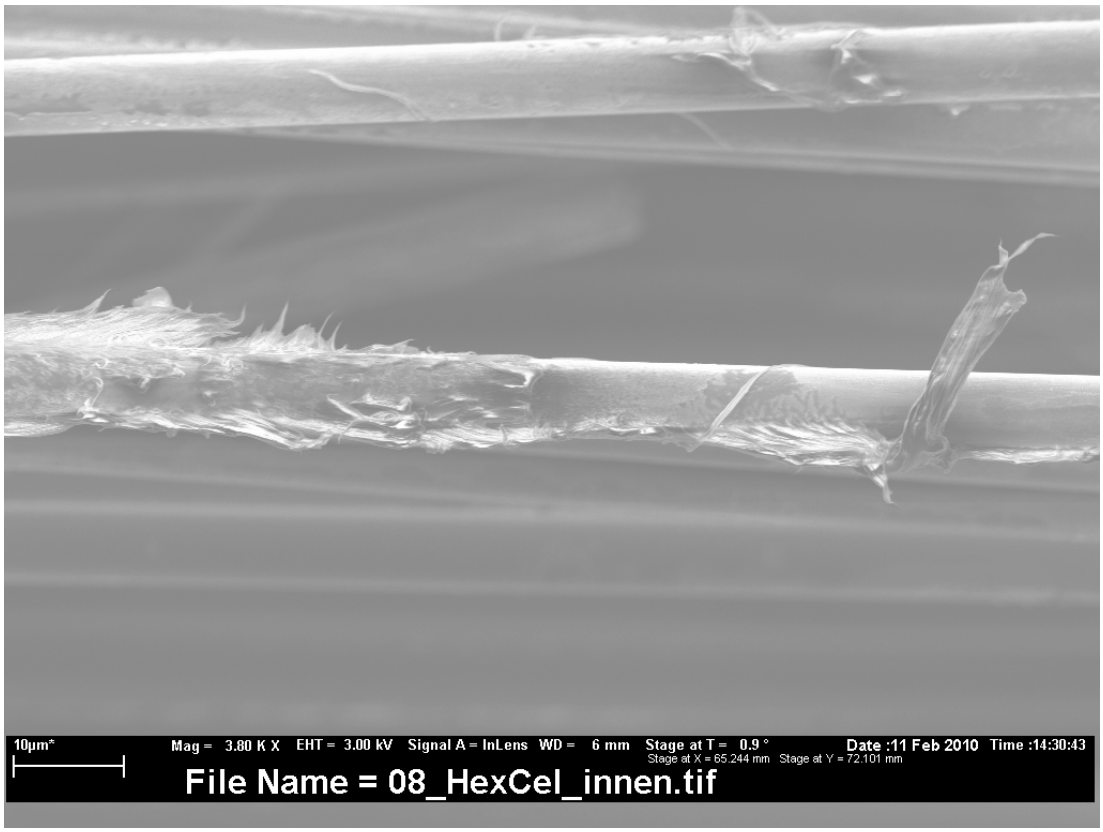

Figure 39 *(SEM image of PFA attached to the fibre and pulled away during fracture)*

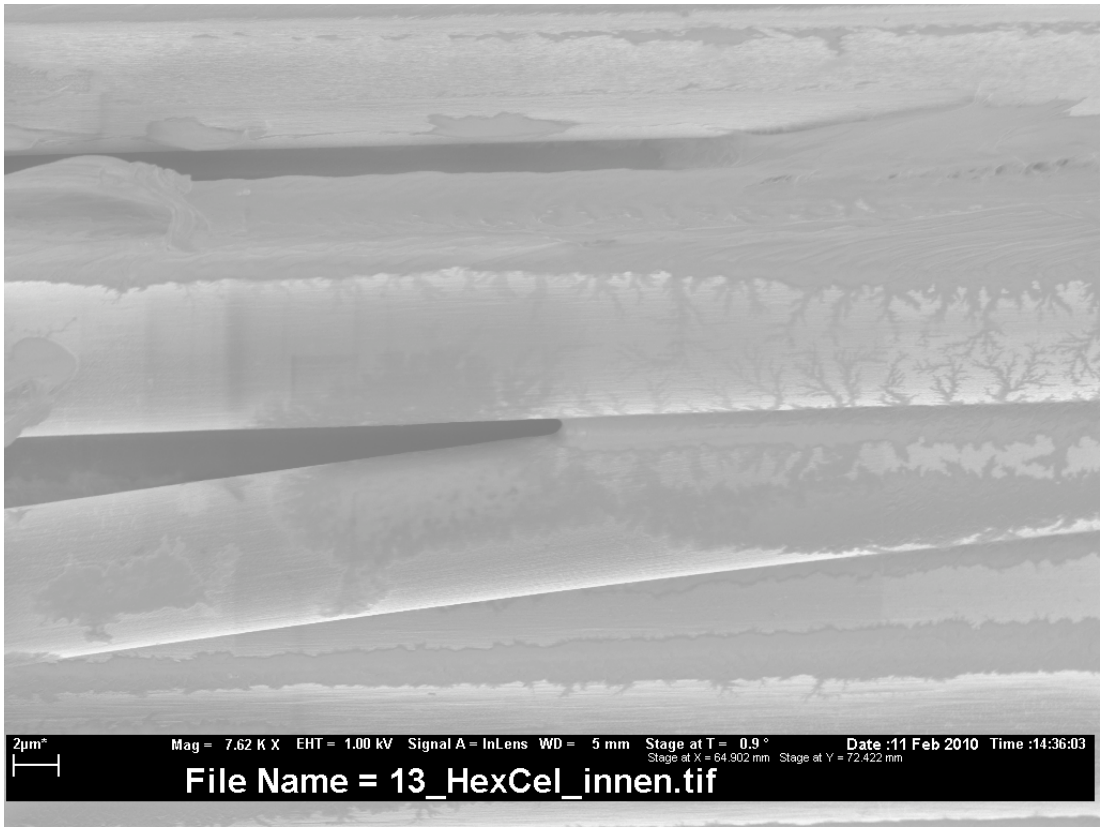

Figure 40 *(SEM image of root-like on fibres originating from PFA)*

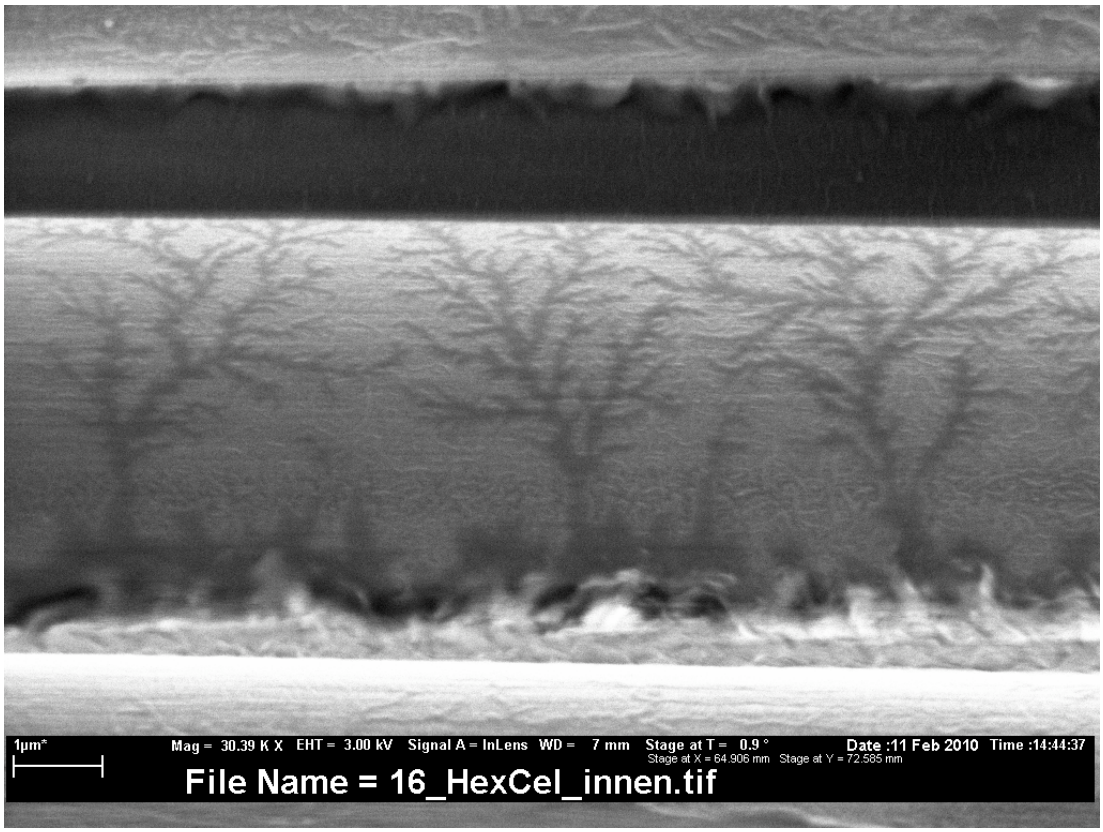

Figure 41 *(SEM image showing the root-like shapes remaining when the PFA was pulled away)*

6. Fibre Content

To determine the fibre weight fraction respectively the fibre volume fraction the fibre and the resin composing the specimens needed to be separated. To obtain the fibre weight fraction and the fibre volume fraction from the measured masses, *Equation [9]* and *Equation [10]* were applied respectively. $wt\%_f$ stands for the fibre weight fraction; V_f for the fibre volume fraction; m_f for the mass of the fibres; m_m the mass of the matrix; and ρ for the corresponding densities.

There are two different methods to attain the required values (described in *Chapter 6 section 1 and 2*). An optical microscope in combination with automatical colour recognition software might yield a close assumption, but is heavily dependent on the resolution and lighting system applied. Furthermore, the fibre fraction obtained is specific to a very limited area. The average had to be obtained by analysing several different spots on each sample. This method would be too time consuming in relation to the reliability of the results obtained.

$$wt\% = \frac{m_f}{\left(m_f + m_m\right)} \qquad [9]$$

$$V_F = \frac{\frac{m_F}{\rho_F}}{\left(\frac{m_F}{\rho_F} - \frac{m_M}{\rho_M}\right)} \qquad [10]$$

6.1 Chemical Resin Digestion

Chemical resin digestion is the most common and usually the most accurate method of determining the fibre content. It is based on the requirement that the fibres are more chemically inert than the surrounding matrix. Using a suitable chemical the resin is digested under a predetermined environment and for a given time. However, due to the chemical characteristics of the PFA matrix the aforementioned approach was unsuitable. PFA, being closely related to PTFE, was developed to be universally chemically inert. Not even nitrohydrochloric acid (aqua regina) and hydrofluoric acid are known to have any effect on PFA (pers. communication, M. Dadalas: 18.01.2010). Consequently, if a carbon/PFA specimen was to be immersed in a digesting chemical, it would be the fibres that would react rather than the PFA. As

described by Ermanni (2007) the chemical characteristics of composite materials are determined by the matrix. Therefore, the chemical behaviour of the specimen can be expected to be similar to the one of pure PFA. Due to the inertness of the matrix material, the use chemical digestion to determine the fibre content was abandoned.

6.2 Resin Burn-off

The other method, thermal degradation or resin burn off, is somewhat less accurate due to various parameters. These parameters include the oxidation of the fibre at a certain temperature and residues of the matrix remaining in the fibres. Nevertheless, it is the most accurate method available to determine the fibre content of this particular composite. The method employed for this experiment was based on the method used and described by Yee and Stephens (1996). Previous studies (Ebnesajjad, et al. 2005; Drobny, 2009) and the thermogravimetric analysis (TGA) as reported in *Chapter 7*, the thermal degradation temperature was set to 450 – 500 °C. Therefore, the furnace temperature was decided to be between 520 – 530 °C.

6.2.1 Resin Burn-off Experimental Setup

To carry out the experiment the tare weights of all crucibles were measured using a Mettler AT200 high-precision scale. From each plate produced, a sample was taken, placed in a ceramic crucible, and its weight was recorded (*Fig. 41*). The furnace used for the experiment was from Nabertherm (Model: L5/11/06; S/N: 156414). It was preheated to 250 °C. A set of ten randomly chosen samples was placed in the furnace. This was then heated up to 520 °C at a rate of 10 °C/min. The temperature was kept at the aforementioned temperature for 120 min. The crucibles were removed from the furnace and cooled to room temperature. After the cooling process the remaining fibres were weighed again and the obtained data was recorded.

Figure 42 *(Weighing of the resin burn-off samples)*

6.2.2 Observations During the Experiment

During the experiment a large amount of smoke developed at a temperature of 470 °C. To get rid of it the ventilation system was used for a short time allowing fresh air to enter the furnace. After 30 min at final temperature the furnace was opened and the samples inspected. At this point the PFA matrix has already been degraded and only loose fibres could be seen in the crucibles. To ensure that all matrix had been burned-off, it was decided for the samples to remain in the furnace for an additional 90 min. By the time the samples were removed a heavy orange coloration of the porcelain crucibles had taken place (*Fig. 42*). This coloration could only be removed by boiling hot water, an aluminium cloth, and significant effort.

Figure 43 *(Coloration of crucibles during resin burn-off)*

6.2.3 Results and Discussion

The weights of the crucibles and of the fibre samples can be found in *Table VI* shown bellow.

Table VI *(Measurements and results of resin burn-off)*

Plate	Crucible (g)	Sample (g)	Burn-off weight (g)	Calc. Fibre weight (g)	meas. Fibre weight (g)	Resin weight (g)	Fibre volume fraction (%)
4HF	23.9806	1.5716	23.9902	0.0096	0.126	1.4456	10
4TF	29.0977	1.4507	29.3185	0.2208	0.3417	1.109	28
5TF	23.6435	1.1625	23.9604	0.3169	0.4031	0.7594	40
5HF	23.9271	1.0601	24.1493	0.2222	0.3065	0.7536	33
4T1	25.1244	1.4007	25.2887	0.1643	0.2803	1.1204	24
5T1	14.1287	1.3572	14.3303	0.2016	0.3218	1.0354	28
4H1	14.0286	1.3437	14.2571	0.2285	0.3371	1.0066	29
5H1	14.0581	1.074	14.1095	0.0514	0.1578	0.9162	18
2T1	13.6413	1.1398	13.6762	0.0349	0.1471	0.9927	16
2TF	14.5155	1.3391	14.7964	0.2809	0.4085	0.9306	35
2HF	23.9839	1.165					
2H1	14.0289	1.3278					
3T1	21.6189	1.1718					
3TF	14.2209	1.3514					
3H1	14.3722	1.2957					
3HF	14.8581	1.0856					
1H1	22.0881	1.4279					
1HF	14.5544	1.4533					
1T1	13.9484	1.4328					
1TF	15.4948	1.3913					

Looking at the results in *Table VI* several observations could be made. The most prominent ones were; the weight of the fibres when measured in the original crucible was significantly less than when the fibres were measured without the crucible; the calculated fibre volume fractions showed a large deviation and were in no correlation to each other; the fibre volume fractions obtained were impossible.

First one implies that the crucibles lost weight during thermal treatment of the Carbon/PFA composite. When PFA is heated above 450 °C (nominal temperature of decomposition provided by the supplier) it decomposes into hydrofluoric acid. Hydrofluoric acid is one of most highly corrosive substances known. In this highly corrosive environment in addition to the elevated temperature also the carbon fibres corroded although its thermal decomposition temperature was not reached. On the chemical resistance data sheet provided by Toho hydrofluoric acid is not mentioned and could therefore be added. The degradation of the carbon fibres led to fibre volume fractions (*Table VI*) that were impossible. The dispersion used had a PFA content of 50 wt%. The amount used to wet out the fibres could optimally result in a composite of a fibre volume content of 40%. However, as some of the dispersion

dripped off during the application of the PFA to the fibre one could expect the fibre volume content to be higher.

Based on these findings it was decided not to carry out the resin burn-off of the second batch of the samples as the obtained results could be considered irrelevant. As fibre volume fraction received by TGA was more plausible, it appeared to be best option to carry out the determination of fibre volume content using TGA.

7. Thermal Analysis

The thermal characteristics of composite materials are mainly determined by the properties of the matrix material (Ermanni, 2007) (*Fig. 44*). There are several different methods available and necessary to obtain an understanding of how these materials behave under elevated temperatures. The tests that are established for these kind of analysis include TGA, differential scanning calorimetry (DSC), thermomechanical analysis (TMA), and dynamic mechanical analysis (DMA). The last three are recognised as key instrumentation in testing of the glass transition temperature (T_g). This property is crucial when it comes to designing for any fibre-reinforced product, as the strength of the material at this point shows a vast decrease.

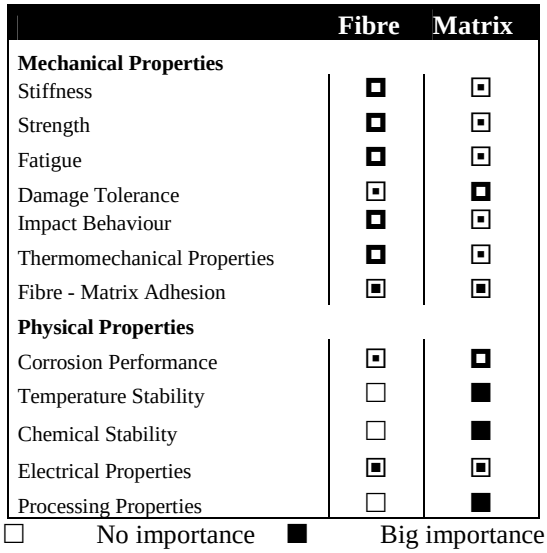

Figure 44 *(Importance of the components on the performance of a composite) Source: Ermanni, (2007)*

7.1 Differential Scanning Calorimetry

Differential scanning calorimetry (DSC) is based on the measurement of the heat flow to or from a specimen within a temperature-controlled environment (Parker. 2001). The heat flow is measured according to *Equation [11].*

$$dQ/dt = \Delta T / R_D \qquad [11]$$

dQ/dt represent the heat flow; *ΔT* the temperature difference between reference and sample crucible; R_D is the resistance of the constantan disk. The data measured is the power required to maintain the sample temperature at the same level as the reference. DSC enables the investigation of thermal transitions in materials (glass transition point; melting point; crystallisation; polymerisation; etc.) with respect to temperature and time. The advantage of DSC is that only small amounts of sample are required for an analysis and that rapid experimentation is possible. It is used as a primary material characterisation technique. For further in depth description of DSC see Parker (2001).

7.1.1 DSC Experimental Setup

The DSC measurements were obtained using a Mettler Tolledo DSC 882^e equipped with a STAR^e SW 9.20 thermal software. For all the tests a temperature increase (scanning rate) of 10 °C/min was used. The samples had a weight of 12±1 mg and were tested in a nitrogen (N_2) atmosphere. The nitrogen was induced at 50ml/min. As possible reference temperatures for T_g were of sources that could not be traced, a large temperature range was scanned, starting from 25 °C and going to 400 °C. Heats of transition were calculated from the area of the peaks by a standard software program. According to the manual the uncertainty can be up to ±0.05 Jg^{-1}. Obtaining the T_g and the T_m in the same run was attempted under the environment described above.

7.1.2 Results and Discussion

Figure 45 shows a typical thermogram as obtained from the DSC. At two locations the line is agitated and shows endothermic peaks. The more prominent peak is at 313.36 °C. This temperature corresponds closely to the melting and beginning of the processing temperature given by Dyneon and which is in accordance to the temperature provided by DuPont. The peak is asymmetric sloping towards the lower temperatures. Cardona et al. (2001) also observed this dissymmetry (*Appendix I*). It originates from different crystalline fractions that are contributing to the peak. The crystallinity of PFA is dependant on the cooling rate during manufacturing of the composite. It is generally agreed (Cardona et al., 2001; Parlevliet et al, 2008) that crystallinity has an influence on the properties of polymers and therefore is likely to influence the performance of a composite.

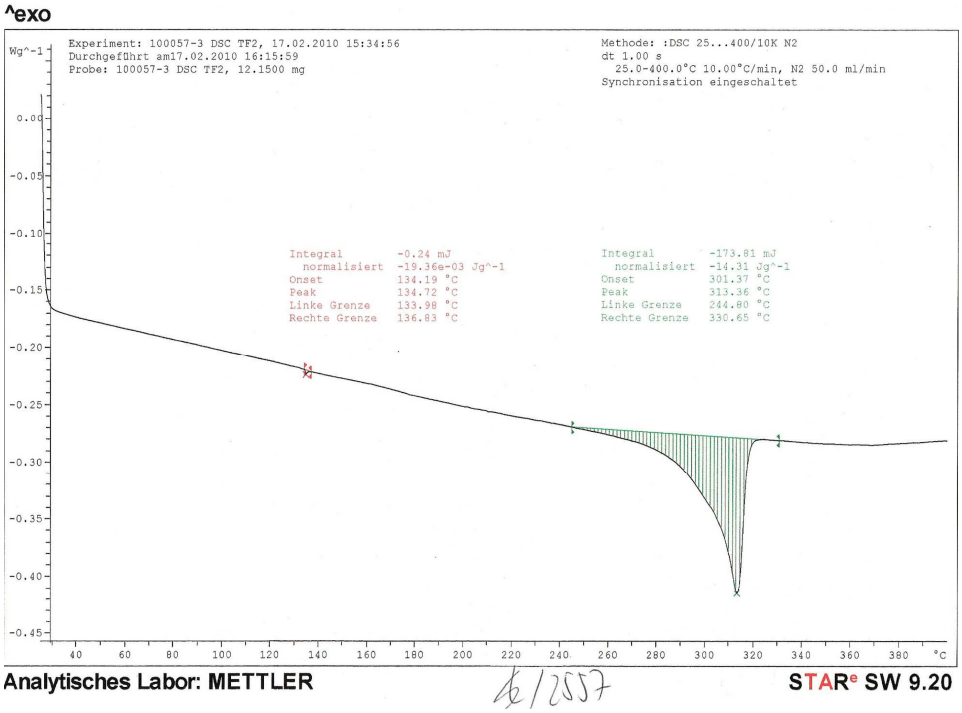

Figure 45 *(DSC thermogram of a carbon/PFA composite)*

For most polymers, DSC shows a clearly distinguishable T_g manifested by a step in the thermograph. For the PFA tested no such step could be distinguished. Also a second DSC (*Appendix J)* did not show any signs of a T_g. There is a small peak at 134.72 °C. When compared to other findings (Ebnesajjad et al., 2005, Cardona et al., 2001) this peak was found 30 – 40 °C higher than the T_g of PFA. It is therefore doubted, if this peak has anything to do with any transition in PFA. In the second scan (*Appendix J*) no such peak was found. This doubt is founded on observations made by Cardona et al. (2001) and Scheirs (1997) who found no T_g when carrying out DSC on un-grafted PFA. According to Scheirs (1997) this may be due to the extremely high stiffness characteristic of the molecular chains of the PTFE sequences in the copolymers.

7.2 Thermomechanical Analysis

TMA can be used to determine the coefficient of thermal expansion (CTE) and also the T_g. Dimensional stability is critical for composites as poor dimensional stability can cause changes in shape during service (Cheng et al., 2009). This change in shape is expressed with aforementioned CTE. The theoretical CTE can be obtained using ROM (*Equation [12]*).

$$\alpha_{tot} = V_f \alpha_f + (1 - V_f)\alpha_m \qquad [12]$$

Where α_{tot} is the thermal expansion coefficient of the composite; α_f and α_m are the thermal expansion coefficient of the reinforcement and the matrix material; V_f again stands for the fibre volume fraction.

TMA can be carried out with either a small static force or a sinusoidal oscillating force. In the second case the amplitude of the oscillation is measured. T_g is considered at the point at which a significant and instant increase in amplitude can be observed.

7.2.1 TMA Experimental Setup

The TMA was carried out in a Mettler Tolledo TMA/SDTA 840 testing machine (*Fig. 46*) equipped with a STAR^e SW 9.20 thermal software. The temperature scanning rate was set to 10 °C/min and the temperature range was from 25 °C to 400 °C. The sample had a thickness of 1.0767 mm. The force was oscillating between 0.1 N and 0.5 N at a periodic cycle time of 10 s Testing took place in an N_2 atmosphere supplied at 50 ml/min.

Figure 46 *(TMA testing machine)*

7.2.2 Results and Discussion

Figure 47 shows a thermograph obtained from the TMA scan over the entire temperature range. In the temperature range at which T_g can be assumed no change in amplitude can be noticed. However, a certain amount of thermal expansion can be observed. There is a clear increase in amplitude at approx. 280 °C. At 310 °C a sudden drop occurs. This coincides with the T_m received from literature (*Appendix C*; Drobny, 2009; Ebnasajjad et al, 2005). The curve flattens off at 340 °C. At this

temperature the entire matrix as melted and remaining 20% of the thickness is made up by the fibres.

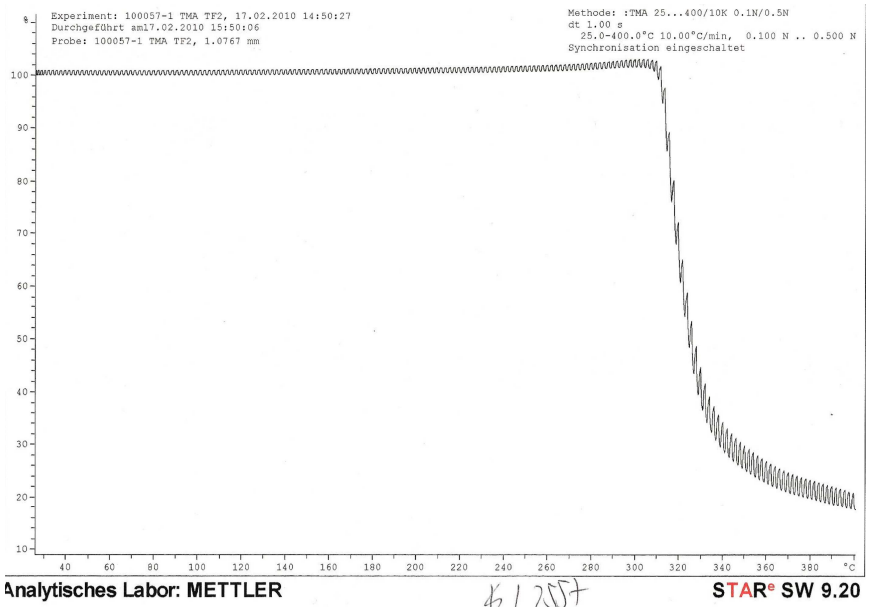

Figure 47 *(TMA thermogram of carbon/PFA composite)*

7.3 Thermographimetric Analysis

Thermographimetric analysis (TGA) is the technique that has received most attention when it comes to monitoring weight loss of a specimen under increasing temperature due to thermal degradation. TGA is easy to perform and can be considered low cost (Parker, 2001). It allows specification at which temperature thermal degradation of a material commences. Furthermore, it is possible to link TGA with mass spectroscopy to determine break down products. Thus allowing to identify products in component if they are previously unknown. Skontorp et al. (1995) showed that thermal degradation of fibre-reinforced composite materials is dependent on the laminate configuration. Based on this it can be concluded that obtained results may only be used for comparison with specimens from a series of tests related to the same material or with specimens of the same configuration. TGA has also developed to a tool to establish the weight fraction of the constituents of composite materials. The fibre weight fraction can be calculated using *Equation [8].* In order to convert the weight fraction to the volume fraction *Equation [9]* needs to be applied.

7.3.1 TGA Experimental Setup

The thermal degradation measurements were performed using a Mettler Tolledo TGA/STTA 851^e equipped with a STAR^e SW 9.20 thermal software. The samples were cut from manufactured panels described in *Chapter 2.2*. The heating program consisted of continuous heating from room temperature (25 °C) to 600 °C. The heating rate was set to 30 °C/min. The experiment took place in an oxygen environment (50 ml/min). Any occurring fumes and gases were lead from the heating compartment. All temperature and weight measurements were carried out by the testing machined and were processed with the aforementioned software. The weight of the samples was based on the experience of the laboratory staff and literature (Yee and Stephens, 1994). Each specimen was 19±2 mg. Due to the experiences that occurred during resin burn-off (*Chapter 6.2*) no dwell time was applied; consequently no chemical degradation of the crucibles or the fibres could take place.

7.3.2 Results and Discussion

Assumptions

From these experiments the following assumptions were made:

a) The carbon fibres did not undergo any thermal degradation at 600 °C. Therefore they did not lose any weight when subjected to the heating program. All weight loss came from the degradation of the resin only. This assumption was based on observations shown in *Fig. 49.*
b) There was no residual weight from the resin. All resin had completely degraded. This was supported by the thermograph shown in *Fig. 50.*
c) The fibres did not affect the degradation kinetics of the resin. Therefore, the measured weight loss is proportional to the weight loss of the resin.
d) Due to the low void content measured (described in *Chapter 4.3*), the void content was assumed to be zero and could therefore be neglected.

Thermal Stability

As described above two properties were investigated using TGA. First one was the thermal stability of the constituents of the carbon/PFA composite. Second one was the weight and volume fraction of these constituents. When it came to thermal degradation all samples tested showed identical behaviour. The thermograph shown in *Fig. 48* is representative for all others obtained (*Appendix K*).

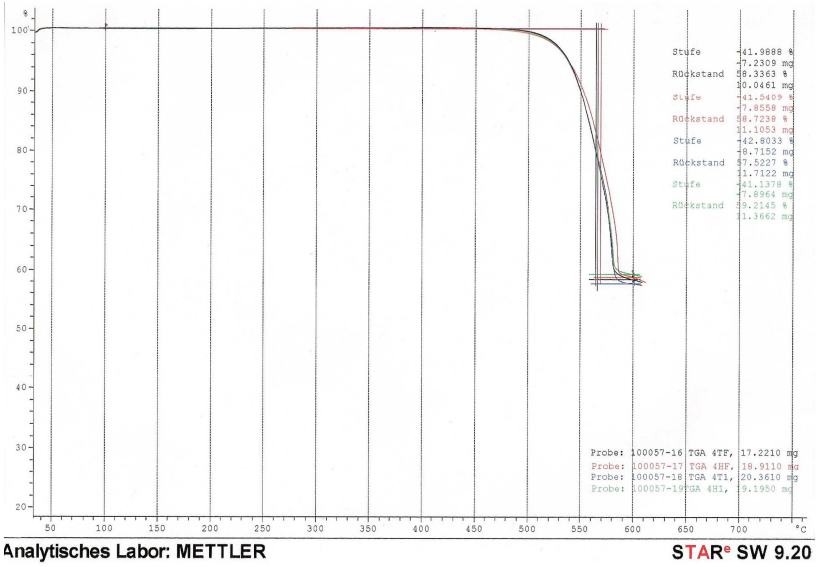

Figure 48 *(Typical TGA thermogram of carbon/PFA composites)*

No degradation/ weight loss took place before ≈ 475 °C. Implicating that any solvents present in the PFA dispersion had been removed completely during manufacturing. For comparison the thermograph of dried PFA dispersion is shown in *Fig. 50.* It can be observed that at 170 °C degradation of the solvents took place. The weight loss was ≈5 wt%. At 450 °C PFA started to degrade. The degradation of PFA ended at 540 °C when 0 mg of PFA remained. According to *Fig. 49* the degradation of the fibres commenced at 570 °C and remained slow up to 625 °C. Before that point no degradation of the fibres took place even though they were placed in an oxygen environment. Thus, there was a narrow gap in which the degradation of PFA had finished and the degradation of the fibres had not fully commenced yet. Due to the toxicity of PFA it is therefore of utmost importance that this material is never exposed to temperatures exceeding 475 °C.

Figure 49 *(TGA thermogram of Toho Tenax and Hexcel fibres)*

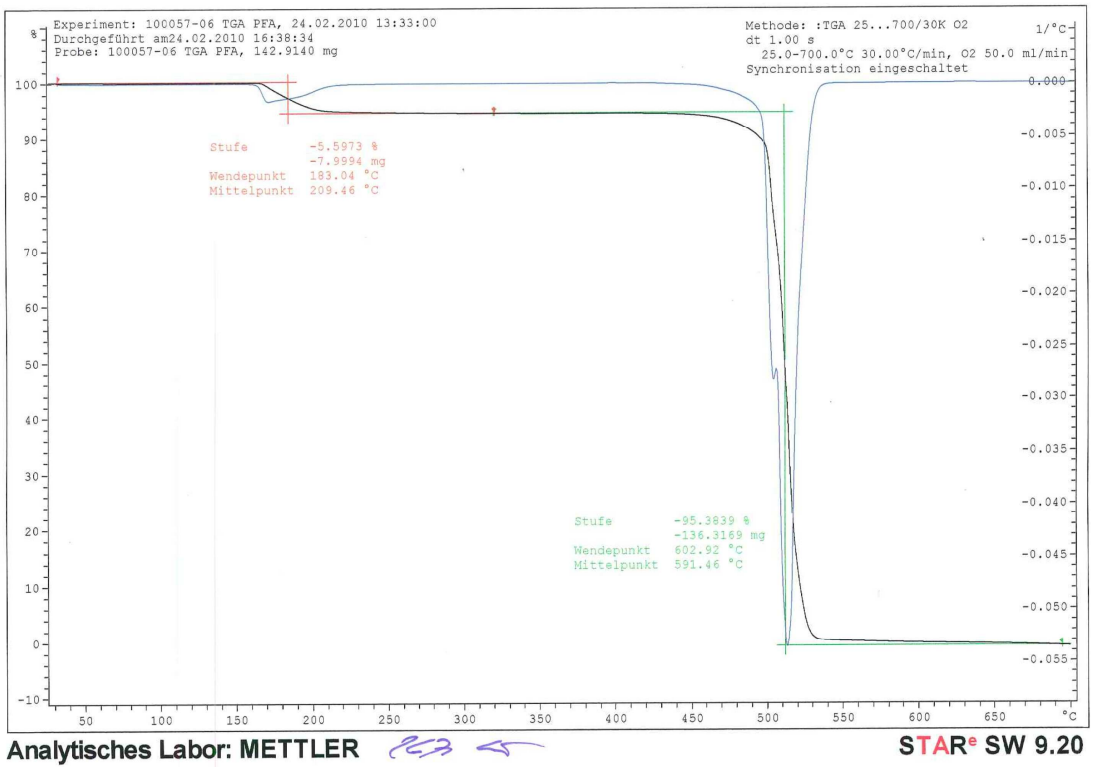

Figure 50 *(TGA thermogram of dried PFA dispersion)*

Weight Percentage Fibre Determination using TGA

As there was no residue present when the pure PFA was heated (*Fig. 50*), it did not have to be determined in order to obtain the fibre weight fraction. *Figure 48*, showing the curves of batch 4, represents typical thermographs required for the determination of weight/volume fraction. Based on the initial weight and the weight loss at a 600 °C using *Equation [8]* and *Equation [9]* respectively, the weight/volume fractions were calculated (*Table VII*). As stated in the assumption, due do the low void occurrence, any void content was neglected in the calculations. The density required for the calculations was taken from the manufacturer data sheets presented in *Appendix A, Appendix B, and Appendix C.*

Table VII *(Fibre fraction determination by TGA method)*

Sample	Initial weight (mg)	Residue fibre (mg)	wt%	V_f (%)
2T1	20.353	11.998	59	63.6
2H1	19.871	11.4481	58	62.3
2TF	13.069	7.9507	61	65.4
2HF	17.283	10.7885	62	66.9
3T1	17.263	10.7242	62	66.6
3H1	17.884	11.1023	62	66.5
3TF	17.704	10.8359	61	65.7
3HF	18.961	11.7109	62	66.2
4T1	20.361	11.7208	58	62.2
4H1	19.195	11.3662	59	63.8
4TF	17.221	10.0461	58	63.0
4HF	18.911	11.1053	59	63.3

The obtained fibre fractions (column 3 and 4; *Table VII*) showed low scattering for batch 3 and batch 4. In batch two a larger variance is present, having a difference in fibre volume content of 4.6%, compared to 0.9% / 1.1% respectively for the other two batches. Therefore, a combination of lower pressure and shorter dwell time during manufacturing could have been responsible for inconsistent fibre content. High pressure with a short dwell time, and long dwell time with low pressure resulted in a consistent fibre volume content. The difference in the fibre content between batch 3 and batch 4 can be attributed to the difference in manufacturing pressure. The higher the pressure, the more resin was being pressed out of the fibres. However, no influence of the type of fibre used on the fibre content could be

observed. The small differences in fibre content between the fibres were completely random. For batch 3 and 4 there also was not noticeable difference in fibre content between specimens produced on the flat side of the tool and the grooved side. However, in batch 2 there was a difference. The flat specimens had slightly higher fibre content than the ones produced on the grooved side. Due to the variance between the individual specimens of batch two it could be doubted if this difference was of random occurrence or not.

7.4 Dynamic Mechanical Analysis

Dynamic Mechanical Analysis (DMA) is a test at which a small sinusoidal stress or strain is applied to a specimen under increasing temperature. The resulting strain or stress response is measured and recorded. The measurements are transferred into the recoverable stored energy (storage modulus) and the dissipated energy in the form of loss modulus or phase lag (Bashaimoldu et al., 2004). It is used to study and characterise the mechanical and thermal properties of composites. These include the CTE, the T_g and the elastic modulus. Depending on the test equipment loading can be applied in different manners. Loading is applied in torsion, bending, compression or tensile. DMA has been shown to be more sensitive than other thermal analysis equipment such as DSC in detecting subtle transition like T_g (Lee et al., 1993). The temperature dependence of the elastic modulus of composite materials is one of the most important material properties when it comes to material characterisation (Shiqiang et al., 2007). According to Lee-Sulliven and Dykemann., (2000) the T_g can be measured reasonably accurately. However, the elastic modulus often shows large discrepancies between the values measured by DMA and those obtained from mechanical testing methods. Parker (2001) offers a more detailed description of the theory and the according standards behind DMA.

7.4.1 DMA Experimental setup

The test specimens had a length of 60 mm, width of 10 mm and a thickness of 0.85 mm and 0.86 mm, respectively. The span distance in the testing machine was 33 mm The DMA was carried out under torsional loading. Therefore, the resulting storage modulus measured is G'; the shear modulus. The testing was performed using a DMA Q800 (TAinstruments) testing machine. As there are no available reference temperatures, a large testing range was chosen. The testing started at 0 °C

and went to 350 °C and carried out in an air environment. To detect any transition a low heating rate of 2 °C/min was chosen. The oscillation force is applied at a frequency of 1 Hz at a strain of 0.15%. The parameters measured were storage modulus G', the loss modulus G'', and the loss tangent tan δ defined by G''/G'.

7.4.2 Results and discussion

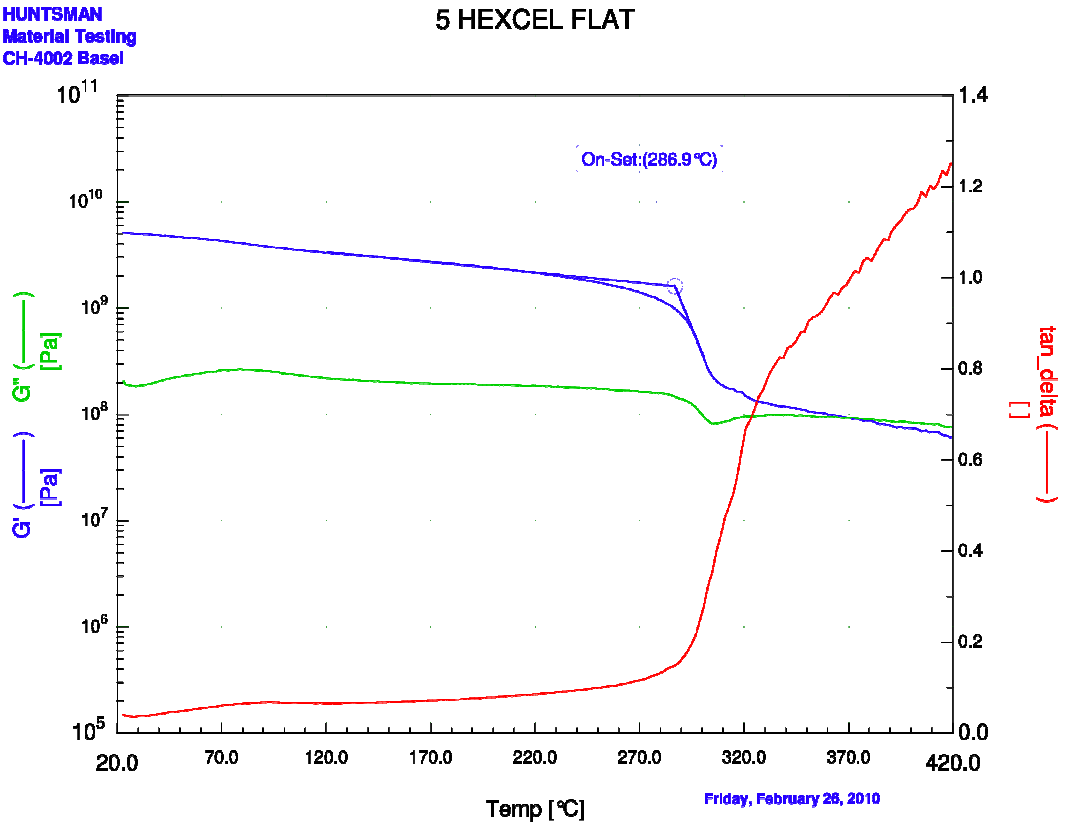

Figure 51 *(DMA plot of Hexcel fibre/PFA composite)*

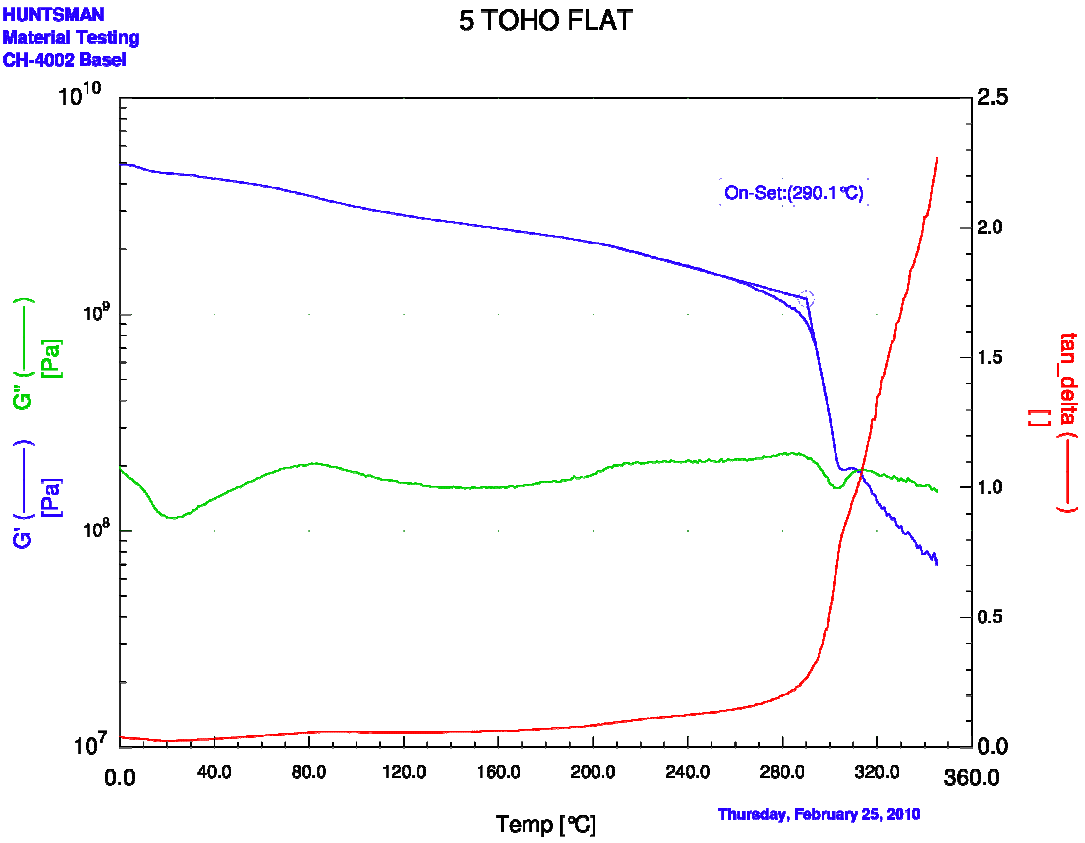

Figure 52 *(DMA plot of Toho fibre/PFA composite)*

Figure 51 and *Fig. 52* represent DMA plots of the shear storage modulus, the shear loss modulus and tan δ against the scan temperature. In both specimens tested the storage modulus (G') decreased continuously up to a temperature of ≈260 °C. At this point G' drops, as the polymer matrix goes through a transition temperature. This transition is not the T_g, which was investigated with this experiment. The onset temperatures (T_{on}) of 290.1 °C and 286.9 °C, respectively coincide rather well with the melting temperature (T_m) found with TMA and DSC described above and the T_m values of PFA obtained from literature (Ebnesajjad et al, 2005; Drobny, 2009; Scheirs, 1997; Karlovitz, 1995; Saechtlin, 1989). Furthermore, it was found that the tan δ line did not show a clear peak at which the T_g could be investigated at any point. From T_{on} onwards tan δ exhibits a continuous increase till the end of the experiment. This implies that at that point a temperature is reached at which the system is not stabilised anymore. Knowing that at this point T_m was reached it confirms that the viscosity of PFA is increasing steadily once T_m is surpassed. These results confirmed the observations made by Scheirs (1997) and explained by Ebnesajjad et al., (2005) that in fluoropolymers a distinctive T_g was often not found. Later stated that fluoropolymers often do not show glass transition in the

conventional sense during which all crystalline structures are converted to the amorphous. Glass transition of fluoropolymers is molecular relaxation that takes place in the amorphous phase of the polymer (second order transformation). Ebnesajjad et al. (2005) gives these transitions at -80 °C (γ), -2 °C (β) and 90 °C (α). Based on this information a small peak between 40 – 110 °C in the G'' and the tan δ line can be made out. Investigating the data *Appendix L* it was found that the tan δ line peaked at 90.97 °C and 92.93 °C, respectively. It can therefore be assumed that the T_g of the PFA matrix material is at ≈ 90 °C. The reasons the peak was very small were that the transition was minor and the amount of PFA in relation to the carbon is very small. This led to the conclusion that the matrix has only a small influence on the overall strength of this composite.

Considering the shear modulus of the two composites at room temperature, G' of the Hexcel/PFA composite is with 5.05 GPa ≈10% higher than G' of the Toho/PFA composite with 4.46 GPa. As the tests were only carried out on one specimen of each composite these values cannot taken to be representative. Nevertheless, both specimens showed a linear decrease of G' up to the onset of T_m. The obtained shear moduli were compared to values of carbon / epoxy composites provided by MIL – HDBK – 17 – 2E. These values correspond very closely and can therefore be assumed to be reasonable.

Whilst G' of the Toho/PFA composite decreases at 12.8 MPa/°C, the Hexcel/PFA composite decreases at a rate of 14.8 MPa/°C. Calculating the decrease in percentage, the decrease of both specimens coincides at 0.29 %/°C. As G''/G' = E''/E' where E' is the flexural modulus (Parker, 2001) one can assume that E' decreases in a similar fashion. Therefore, if this composite is investigated as a structural material this decrease in stiffness with increasing temperature needs to be considered. Any component needs to be laid out to withstand expected forces at maximal assumed temperature.

8. Final Discussion and Conclusions

In this study a process was introduced that allowed the production of a continuous carbon fibre reinforced/fluoropolymer matrix composite of high fibre content. Due to the high melt viscosity of fluoropolymers alternative ways to integrate matrix into the fibres had to be found. The low viscosity and the small particle solid particle size of the dispersion allowed excellent wetting of the fibres. But working with an aqueous dispersion made it hard to predict an achievable fibre content and the amount of dispersion required for achieving it. Because of the low viscosity, once the fibres were completely wetted out any surplus of dispersion dripped off as the tooling was turned. Furthermore, the pressure applied by the overlaying layers forced more dispersion out of the fibres. Therefore, even though a calculated amount of dispersion was applied it was impossible to predict how much of it did not end up in the composite.

The drying of the dispersion and the compressing of the matrix required additional steps, making the manufacturing process very time consuming. Due to the high process temperatures a long time was required for the heating and an even longer time for the cooling of the tooling. The pressing process further influenced the final fibre content. The higher the pressure, the larger the amount of molten PFA being pressed out of the fibres towards the sides. It can be concluded that the high pressure and a long dwell time at high temperature are required to produce composites of consistent fibre content. Initially the fibre content is determined by the mass percentage of solid in the dispersion; thus determining how much PFA would end up in the composite. Pressure not only ensured the consolidation, but also defines the final content. All these parameters made it impossible to predict fibre content in advance. But it had to be determined experimentally. Although a large part of the dispersion evaporated it was possible to produce composites of low void content. As the composite was produced on a flat panel, this was relatively simple. It would have to be investigated if the same composite quality could be obtained for a more complex shape. However, an optimal pressure needs to be found. Since the higher the pressure the more inhomogeneous the composite had become. Consequently the

balance will be between consistent fibre fraction and the homogeneity of the composite.

The XPS analysis showed different surface composition of the carbon fibres used for the manufacturing of the composites. The difference was due to a high temperature sizing applied to the fibre by one of the fibre suppliers. This sizing made the fibre easier to handle and less prone to damage during manufacturing. In addition although there was also a difference in the surface structure of the fibre, the results of the mechanical and thermal testing showed no difference that could have been attributed to the fibre surface. The only difference between the fibres was found during the TGA. The Toho Tenax fibre showed a much less rapid thermal degradation than the compared Hexcel AS4 fibre. The ILLS test yielded no representative results. This can be attributed to dimensions of the test setup, but also to the hardness of the matrix material. The 3-point-bend testing gave flexural moduli that were in correlation to the fibre content. However, the values of the moduli were 55 – 58% lower than the ones of UD carbon/epoxy composites of similar fibre volume content. Failure of the carbon/PFA composite always occurred in an interlaminar fashion. Due to the length of the specimens one cannot determine if the failure resulted form interlaminar shear or other forms of bending stresses. Nevertheless, it showed that the fibre/matrix adhesion is the property determining the weakness of the material. DMA presented that the modulus is highly dependent on temperature. Although there is no instantaneous decrease up to very high temperature (≈270 °C) a continuous linear decrease of 0.2 %/°C was shown. As a consequence care has to be taken when designing with this material. Further thermal analysis revealed no distinctive T_g. The only transition temperature clearly distinguishable is the T_m, taking place at approximately 310 °C. Overall it can be stated that PFA is a complex material to work with. The high process temperatures, the high viscosity, in addition to the high toxicity require enormous caution when handling the material. Its chemical inertness leads to limited amount of techniques applicable for determining material properties.

9. Recommendation for Further Research

The most prominent point for further research is the adhesion between fibres and matrix. If this can be improved so can the properties of the composite. A functionalisation of the fibre needs to be looked into which can interact with the O-atom in PFA. Furthermore it needs to be investigated if the single laminate produced in project can be added up to form laminates of several layers. It is also worth determining if more complex shapes are producible.

10. References

Alström, B. T., (1997), '*Manufacturing of polymer composites*', Chapman and Hall: London

Anon, (ca. 2000), '*PTFE, FEP, and PFA Specification*', [online], available at: www.boedeker.com/feppfa_p.htm, [date accessed: 22/09/2009]

Anon, (ca. 2005), 'In-plane and interlaminar shear properties', [online], available at: www. Netcomposites.com/vircon/4_1_4.asp, [date accessed: 12/02/2010]

Bashaimoldu, A. B. et al., (2004), 'Application of Dynamic Mechanical Analysis (DMA) to the determination of the mechanical properties of coated pellets', International journal of pharmaceutics, Vol. 274, pp. 53 – 63

Biniak, S. et al., (1997), 'The characterization of activated carbons with oxygen and nitrogen surface groups', *Carbon*, Vol. 35, No.12, 1997, pp.1799 – 1810

Bismarck, A. et al., (1997), 'Influence of fluorination on the properties of carbon fibres', *Journal of Fluorine Chemistry*, Vol. 84, 1997, pp. 127 – 134

Bismarck, A. et al., (2007), 'Flourinated carbon fibres and their suitablility as reinforcement for fluoropolymers', *Composites Science and Technology*, Vol. 67, 2007, pp. 2699 – 2706

Bismarck, A. et al., (2007), 'Interfacial behaviour between atmospheric-plasmafluorinated carbon fibers and poly(vinylidene fluoride)', *Journal of Colloid and Interface Science*, Vol. 313, 2007, pp. 476 – 484

Bismarck, A. et al., (2008), 'Carbon fibre reinforced poly(vinylidene fluoride): Impact of matrix modification on fibre/polymer adhesion', *Composites Science and Technology*, Vol. 68, 2008, pp. 1766 – 1776

Brandrup, J. et al., (1999), 'Polymer handbook', 4th edition, John Wiley and Sons: Chichester

Brown, R.P., (2002), '*Handbook of Polymer Testing: Short-Term Mechanical Tests*', Smithers Rapra: Shawbury

Carbajal, N. Mujika, F., (2008), 'Determination of compressive strength of unidirectional composites by three-point bending tests', Polymer Testing, Vol. 26, pp. 150 – 156

Cardona, F. et al., (2001), 'Thermal characterization of copolymers obtained by radiation grafting of styrene onto poly(tetrafluoroethylene-perfluoropropylvinylether) substrates: thermal decomposition, melting behavior and low-temperature transitions', *Polymer Degradation and Stability*, Vol. 74, No. 2, 2001, pp. 219-227

Carbon fibre reinforced plastics - Unidirectional laminates; determination of apparent interlaminar shear strength; German version EN 2563:1997

Cattell, M.K. Kibble, K. A., (2001), 'Determination of the relationship between strength and test method for glass fibre epoxy composite coupons using Weibull analysis', *Materials and Design*, Vol. 22, 2001, pp. 245 – 250

Cheng, S. et al., (2009), 'Mechanical and thermal properties of chicken feather fibre/PLA green composites', *Composites: Part B*, Vol. 40, (2009), pp. 650 – 654

Clarke, D., (2009), 'Common industry myths about magnetic drive pumps', *World pumps*, Vol. 455, Aug. 2004, pp. 20–23

Drobny, J.G. (2001), 'Blends and Composites Based on Fluoropolymers', *Macromelecular Symosium*, Vol. 170, 2001, pp. 149 – 156

Drobny, J.G. (2009), `*Technology of Fluoropolymers*', 2nd Edition, CRC Press: Boca Ratan

Determination of flexural properties , EN ISO 178. 2003

Determination of tensile properties, DIN EN ISO 527-Part 1 & 4 1996

Ebnesajjad, S., (2002), '*Fluoroplastics: Melt Processible Fluoropolymers: The Definitive User Guide*', Plastic Design Library: Norwich

Ebnesajjad, S. et al., (2005), 'Fluoropolymers applications in chemical processing industries: the devinitive user's guide and databook', Plastic design Library: Norwich

Ermanni, P., (2007), '*Composites technologien*', Skript zur ETH-Vorlesung, ETH Zürich

Flexural Properties of Unreinforced and Reinforced Plastics and Electrical Insulating Materials, ASTM designation D 790. 2005

Fujihara, K. et al. (2004), 'Influence of processing condition on bending property of continuous carbon fibre reinforced PEEK composites', *Composite Science and Technology*, Vol. 64, 2004, pp. 2525 – 2534

Gay, D. Hoa, S.V. (2006), '*Composite Materials: Design and Applications'*, Second Edition, CRC Press: London

Hodkinson, J.M., (2000), '*Mechanical testing of advanced composite fibres'*, Woodhead Publishing Ldt.: Cambridge

Isaac, D. M., & Ori, I. (2006), '*Engineering Mechanics of Composite Materials'*, Oxford University Press: Oxford

Karlovitz, B., (1995), *'Kunstsrofftabellen'*, 4th Edition, Hanser: München

Kim, R.Y. Crasto, A.S., (1994), 'Longitudinal compression strength of glass fibre-reinforced composites', Journal of Composite Materials, Vol. 13, pp. 326 – 338

Kruijer, M. P. et al., (2005), 'Analysis of the mechanical properties of a reinforced thermoplastic pipe (RTP)', *Composite Part A*, Vol. 36, 2005, pp. 291 – 300

Lee, J. et al., (2005), 'Surface characterisation and adhesion of carbon fibres to epoxy and polycarbonate', *International Journal of Adhesion and Adhesives*, Vol. 25, 2005, pp. 389 – 394

Lee, T. H. et al., (1993), 'Characterisation of a fibre-reinforced PPS composite by dynamic mechanical analysis: Effects of aspect ratio and static stress', *Composite Science and Technology*, Vol. 49, 1993, pp. 217 - 223

Lee-Sullivan, P. Dykeman, D., (2000), 'Guide lines for performing storage modulus measurements using the TA Instruments DMA 2980 three point bend mode. I. Amplitude effects,' Polymer Testing, Vol. 19, pp. 155 – 164

Logothetis, A., (1993), 'Process for making fluoropolymer composites' , [online] available at: http://www.freepatentsonline.com/5194484.html, [date accessed: 23/10/2009]

MIL HDBK – 17 – 2E, (1999), Department of Defense Handbook Composite Materials Handbook, Vol.2, *'Polymer Matrix Composite Materials Properties'*

Mitschang, P. et al., (2003), 'Processing technologies for continuous fibre reinforced thermoplastics with novel polymere blends', *Composite Science and Technology*, Vol. 63, 2003, pp. 2099 – 2110

Morgan, P., (2005), 'Carbon fibres and their composites', Taylor and Francis Group: CRC Press: Boca Raton

Nesbitt, B., (2006), '*Handbook of pumps and Pumping: Pumping manual international'*, Elsevier: Oxford

Oshima, A. et al., (2001), 'Radiation processing for carbon fibre-reinforced polytertafluoroethylene composite material', *Radiation Physics and Chemistry*, Vol. 60, 2001, pp. 95 – 100

Oshima, A. et al., (2001), ' Application of radiation-crosslinked polytetrafluoroethylene fo fibre-reinforced composite material', *Radiation Physics and Chemistry*, Vol. 60, 2001, pp. 467 – 471

Oshima, A. et al., (2001), 'Fabrication of polytetrafluoroethylene/carbon fibre composites using radiation crosslinking', *Radiation Physics and Chemistry*, Vol. 62, 2001, pp. 77 – 81

Potter, K. (1999), '*Introduction to Composite Products'*, London: Chapman and Hall

Park, S-J., (2003), 'Studies on mechanical interfacial properties of oxy-flourinated carbon fibre-reinforced composites', *Material Science & Engineering A*, Vol. 356, 2003, pp. 219 – 226

Parker, M. J., (2000), 'Test Methods for Physical Properties', Comprehensive Composite Materials, Vol. 5, BAE Systems: Lancashire (UK), pp. 183–226)

Parlevliet, P.P. et al., (2008), 'Thermal effects on microstructural matrix variations in thick-walled composites', Composite Science and Technology, Vol. 68, No. 3-4, 2008, pp. 896–907

Paynter, R., (2005), 'XPS Theory', [online], available at: http://csacs.mcgill.ca/francais/docs/CHEM634/XPS_Paynter_t.pdf, [date accessed: 16/02/2010]

Rosselli, F. Santare, M. H., (1997), 'Comparison of the short beam shear (SBS) and interlaminar shear device (ISD) tests', Composite Part A, Vol. 28A, pp. 587 – 594

Rychwalski, R., (2009), 'Composite and Nanocomposite Materials', 4th Edition, Compendium, Chalmers University: Göteborg

Saechtlin, H., (1989), '*Kunststofftaschenbuch*', 24th edition, Hanser: München

Scheirs, J., (1997), 'Modern fluoropolymers: High performance polymers for diverse applications', John Wiley and Sons Ltd: Chichester

Scheirs, J., (2001), `*Fluoropolymers – Technology*, *Market and Trends*', Rapra Technology: Shawbury

Schneider, K., (2007), 'Determination of compressive properties of fibre composites in the in-plane direction according to ISO 14126. Part 1: a round robin test', Applied Composite Materials, Vol. 14, pp. 1 – 15

Shiqiang, D. et al., (2007), 'Temperature-dependent elastic moduli od epoxiea measured by DMA and their correlations to mechanical testing data', Polymer Testing, Vol. 27, pp. 803 – 813

Skontorp, A. et al., (1995), 'High-temperature anisotropic oxidation of carbon fibre reinforced polyimide composites: Theory and Experiment', Proceedings of the tenth international conference on composite materials (ICCM – 10), Street, K. and Poursartip, A., August (1995) Vancouver, Canada, Vol. 4, 1995, pp. 375 – 384

Summerscales, J., (2007), 'Interfaces; Interphases; Voids; Meso-mechanics (clustering)', Lecture notes MATS 324, University of Plymouth

Thielicke, B. Soltesz, U., (1992), 'The interlaminar shear strength of carbon fibre-reinforced carbon-CFC- differences between various experimental methods', European Association for Composite Materials: Composite Testing and Standardisation, Woodhead Publishing Ldt: Cambridge

Toyoko, I., (2003), 'Fluorinated polymers', *Current Opinion in Colloid and Interface Science*, Vol. 8, 2003, pp. 307–314

Wang, S. S., (2006), 'Composites key to deep water oil and gas', *High Performance Composites,* Vol. 13,

Xiaosong, H., (2009), 'Fabrication and Properties of Carbon Fibres', *Materials*, Vol 2, pp. 2369 – 2403

Yee, R.Y. Stephens, T. S., (1994), 'A TGA technique for determining graphite fibre content in epoxy composites', Thermochimica Acta, Vol. 272, pp. 191 – 199

Bibliography

McElhinney, D. M. et al., (1969), 'The Use of Carbon Fibre Reinforced Plastics', *Aircraft Engineering and Airspace Technology*, Vol. 41, No.10, pp. 22 – 25

Zhou, G. et al., (1995), ' In-Plane and interlaminar shear properties of carbon/epoxy laminates', *Composite Science and Technology*, Vol. 55, (1995), pp. 187 – 193

Park, S-J. et al., (2003), ' Relationship between surface characteristics and interlaminar shea strength of oxyfluorinated carbon fibres in a composite system', *Journal of Colloid and Interface Science*, Vol. 268, (2003), pp. 127 – 132

Ramachandran, V. S., et al., (2002), 'Handbook of Thermal Analysis of Construction Materials', Noyes Publications/ William Andrew Publishing

Parker, M. J., (2000), 'Test Methods for Physical Properties', Comprehensive Composite Materials, Vol. 5, BAE Systems: Lancashire (UK), pp. 183–226

Sichina, W.J., (2000), 'DSC as Problem Solving Tool: Characterization of Consistency of PFA Resins', [online], available at: http://las.perkinelmer.com/content/applicationnotes/app_thermalconsistencyofpfaresins.pdf, date accessed: 20/02/2010

Lebrun, G. Denault, J., (2010), 'Effect of annealing on the thermal expansion and residual stresses of bidirectional thermoplastic composite laminates', Composite part A: Applied Science and Manufacturing, Vol. 41, Issue 1, January 2010, pp. 101–107

Vecellio, M., (2000), 'Opportunities and developments in fluoropolymeric coatings', Progress in Organic Coatings, Vol. 40, No. 1 – 4. Dec. 2000, pp. 225 – 242

Ye, B. J. et al., (1995), 'Mass and volume fraction properties of pultruded glass fibre – reinforced composites', Composites, Vol. 26, 1995, pp. 725 – 731

Ratna, D., (2008), 'Toughened FRP composites reinforced with glass and carbon fibre', Composites Part A: Applied Science and Manufacturing, Vol. 39, No. 3, March 2008, pp. 462 – 469

11. Appendices

Appendix A

HexTow® AS4
Carbon Fiber
Product Data

HexTow® AS4 carbon fiber is a continuous, high strength, high strain, PAN based fiber available in 3,000 (3K), 6,000 (6K) and 12,000 (12K) filament count tows. This fiber has been surface treated and can be sized to improve its interlaminar shear properties, handling characteristics, and structural properties, and is suggested for use in weaving, prepregging, filament winding, braiding, and pultrusion.

Typical Fiber Properties	U.S. Units	SI Units
Tensile Strength	643 ksi	4,433 MPa
Tensile Modulus (Chord 6000-1000)	33.5 Msi	231 GPa
Ultimate Elongation at Failure	1.8%	1.8%
Density	0.0647 lb/in^3	1.79 g/cm^3
Weight/Length		
3K	11.8 x 10^{-6} lb/in	0.210 g/m
6K	23.9 x 10^{-6} lb/in	0.427 g/m
12K	48.0 x 10^{-6} lb/in	0.858 g/m
Approximate Yield		
3K	7,086 ft/lb	4.76 m/g
6K	3,485 ft/lb	2.34 m/g
12K	1,734 ft/lb	1.17 m/g
Tow Cross-Sectional Area		
3K	1.82 x 10^{-4} in^2	0.12 mm^2
6K	3.70 x 10^{-4} in^2	0.24 mm^2
12K	7.43 x 10^{-4} in^2	0.48 mm^2
Filament Diameter	0.280 mil	7.1 microns
Carbon Content	94.0%	94.0%
Twist	Never Twisted	Never Twisted

Typical 350°F Epoxy Composite Properties (at Room Temperature)	U.S. Units	SI Units
0° Tensile Strength	320 ksi	2,205 MPa
0° Tensile Modulus	20.5 ksi	141 GPa
0° Tensile Strain	1.55%	1.55%
0° Flexural Strength	274 ksi	1,889 MPa
0° Flexural Modulus	18.4 Msi	127 GPa
0° Short Beam Shear Strength	18.5 ksi	128 MPa
0° Compressive Strength	222 ksi	1,530 MPa
0° Compressive Modulus	18.6 Msi	128 GPa
90° Tensile Strength	11.7 ksi	81 MPa
Fiber volume	60%	60%

HEXCEL

HexTow® AS4 *Product Data*

Yarn/Tow Characteristics	U.S. Units	SI Units
Specific Heat	0.279 Btu/lb-°F	0.27 cal/g-°C
Electrical Resistivity	5.6 x 10^{-5} ohm-ft	1.7 x 10^{-3} ohm-cm
Coefficient of Thermal Expansion	-0.35 ppm/°F	-0.63 ppm/°C
Thermal Conductivity	3.95 Btu/hr-ft-°F	6.83 W/m-°K

Carbon Fiber Certification

This carbon fiber is manufactured to Hexcel aerospace specification HS-CP-5000. A copy of this specification is available upon request. A Certification of Analysis will be provided with each shipment.

Available Sizing

Sizing compatible with various resin systems, based on application are available to improve handling characteristics and structural properties. Please see additional information on available sizes on our website or contact our technical team for additional information.

Packaging

Standard packaging of HexTow® AS4 is as follows:

Filament Count	Nominal Weight (lb)	Nominal Weight (kg)	Nominal Length (ft)	Nominal Length (m)
3K	4.0	1.8	28,340	8,640
6K	4.0	1.8	13,940	4,250
12K	8.0	3.6	13,870	4,230

Other package sizes may be available on request. The fiber is wound on a 3-inch ID by 11-inch long cardboard tube and overwrapped with plastic film.

Safety Information

Obtain, read, and understand the Material Safety Data Sheet (MSDS) before use of this product.

Important

Hexcel Corporation believes, in good faith, that the technical data and other information provided herein is materially accurate as of the date this document is prepared. Hexcel reserves the right to modify such information at any time. The performance values in this data sheet are considered representative but do not and should not constitute specification minima. The only obligations of Hexcel, including warranties, if any, will be set forth in a contract signed by Hexcel or in Hexcel's then current standard Terms and Conditions of Sale as set forth on the back of Hexcel's Order Acknowledgement.

For more information

Hexcel is a leading worldwide supplier of composite materials to aerospace and other demanding industries. Our comprehensive product range includes:

- Carbon Fiber
- RTM Materials
- Honeycomb Cores
- Carbon, Glass, Aramid and Hybrid Prepregs
- Structural Film Adhesives
- Honeycomb Sandwich Panels
- Special Process Honeycombs
- Reinforcement Fabrics

For US quotes, orders and product information call toll-free 1-866-566-2662 and 1-800-688-7734. For other worldwide sales office telephone numbers and a full address list, please click here: http://www.hexcel.com/contact/salesoffice

September 2009

Appendix B

TohoTenax

TEIJIN

Produktprogramm und Eigenschaften für Tenax® HTA / HTS Filamentgarn

Markenname		**Tenax®**	**Tenax®**	**Tenax®**	**Tenax®**	**Tenax®**
Produktionsstandort		**J**	**J / E**	**J / E**	**E**	**E**
Faserfamilie & Zugeigenschaften		**HTA40**	**HTA40**	**HTA40**	**HTS40**	**HTS40**
Präparationseigenschaften		H15 / F15	E13	E13	F13	F13
Filamentanzahl		1K	3K	6K	12K	24K
Garnfeinheit [1]	[tex]	67	200	400	800	1600
Garndrehung	[t/m]	15S	0/15Z	0/10Z	0/10Z	0/5Z
Lauflänge je kg	[m/kg]	15000	5000	2500	1250	625
Spulengewicht, netto	[kg]	0,5	1/2	2/4	2/4/6	2/4/6/8

1) ohne Präparationsauftrag

Eigenschaften (Richtwerte)		**HTA**	**HTS**
Filamentdurchmesser	[µm]	7	7
Dichte	[g/cm^3]	1,76	1,77
Zugfestigkeit	[MPa]	3950	4300
Zug-E-Modul	[GPa]	238	240
Bruchdehnung	[%]	1,7	1,8
Spezifische Wärmekapazität	[J/kgK]	710	710
Wärmeleitzahl	[W/mK]	17	17
Wärmeausdehnungskoeffizient	[10^{-6}/K]	-0,1	-0,1
Spez. elektrischer Widerstand	[Ω cm]	1,6 x 10^{-3}	1,6 x 10^{-3}

Präparationseigenschaften für Faserfamilie HTA / HTS

HTA und HTS sind die klassischen Tenax® Hochleistungskohlenstofffaser-Typen. Diese „High Tenacity" (HT) Fasern liefern exzellente und ausgewogene mechanische Laminateigenschaften.

E13 = Type mit ca. 1,3 % Präparationsauftrag auf Basis Epoxidharz
F13 = Type mit ca. 1,0 % Präparationsauftrag auf Basis Polyurethan
F15 = Type mit ca. 2,5 % Präparationsauftrag auf Basis Polyurethan
H15 = Type mit ca. 2,5 % Präparationsauftrag auf Basis Epoxidharz

Zur optimalen Typenauswahl steht Ihnen unser Verkauf gerne zur Verfügung. Die angegebenen Werte sind Richtwerte. Für die Auslegung von Bauteilen fordern Sie bitte über unseren Verkauf eine Spezifikation an.

Bitte geben Sie auf Ihrer Bestellung den Anwendungsbereich (Luftfahrt oder Industrie & Sport) an.

Die Ausfuhr oder Verbringung von Kohlenstofffasern kann genehmigungspflichtig sein, abhängig von den Eigenschaften, der Endbestimmung und der Endverwendung.

Toho Tenax Europe GmbH Kasinostraße 19-21 42103 Wuppertal, Deutschland
Tel.: +49 202 32 - 2339 Fax: +49 202 32 - 2360
www.tohotenax-eu.com sales@tohotenax-eu.com
(04/2008)

Appendix C

Vorläufige Technische Information

dyneon
a 3M company

3M

Dyneon™

PFA 6900G Z

Fluorthermoplast Dispersion

Merkmale

- Gut thermoplastisch verarbeitbar
- Ausgezeichnete Antihaft-Eigenschaften
- Gute UV-Beständigkeit
- Gute mechanische Eigenschaften
- Hohe Chemikalienbeständigkeit
- usgezeichnete dielektrische Eigenschaften

New Emulsifier Technology by Dyneon

Typische Eigenschaften*

Eigenschaften	Testmethode	Einheit	Wert
Feststoffgehalt	DIN EN ISO 12086	% (m/m)	50
Emulgator			nicht ionisch
Emulgatorgehalt (bezogen auf PFA)	Dyneon intern	% (m/m)	7.5
Teilchengröße	DIN ISO 13321	nm	200
pH	DIN ISO 976		> 9
Viskosität	DIN EN ISO 3219	mPa	9
Schmelzpunkt	DIN EN ISO 12086	°C	310

* Mittelwerte

Verarbeitung
Dyneon™ PFA 6900G Z Fluorthermoplast Dispersion eignet sich hervorragend zur Formulierung von Antihaftbeschichtungssystemen auf wässriger Basis in Kombination mit Dyneon™ PTFE Dispersion. Dyneon PFA 6900G Z Fluorthermoplast Dispersion kann auch zum Imprägnieren und Versiegeln von porösen Materialien wie Keramik, Kohle, Metalle, Glasgeweben etc. verwendet werden.

Lieferform
Dyneon™ PFA 6900G Z Fluorthermoplast Dispersion wird in 30-Liter Gebinden sowie in Kubikmeter-Containern geliefert.

Lagerung und Handhabung
Dyneon™ PFA 6900G Z Fluorthermoplast Dispersion muss frostsicher gelagert werden (5 °C – 30 °C). Die Absetzneigung der Dispersion ist gering. Es empfiehlt sich jedoch, die Dyneon PFA 6900G Z Fluorthermoplast Dispersion ein bis zwei Mal pro Monat durch langsames Rollen oder Rühren zu homogenisieren. Falls sich trotz allem Bodensatz gebildet hat, kann dieser ebenfalls durch wie oben beschriebenes Homogenisieren wieder redispergiert werden.

Appendix D

AIRTECH
EUROPE S.A.

ZI Haneboesch
L-4562 Differdange
LUXEMBOURG

Phone: +352 58 22 82 1
Fax : +352 58 49 35

E-mail : sales@airtech.lu
Website: www.airtech.lu

DATA SHEET

Thermalimide

Ultra high temperature bagging film

DESCRIPTION

Thermalimide is a high performance bagging film for cure temperatures up to 426 °C.

TECHNICAL DATA

		Test method
Material type	Polyimide	
Elongation at break	95 %	ASTM D 882
Tensile strength	240 MPa	ASTM D 882
Maximum use temperature	426 °C	
Flammability (self extinguishing)	Yes	ATP-5034
Materials to avoid	None known	
Yield	27,7 m^2/Kg/25,4 µm	
Colour	Amber	

SIZES

Thickness	Width	Length	Weight / roll	Forms available*
0,002 inch (50,8 µm)	60 inch (1,52 m)	255 feet (77,7 m)	8,5 Kg	SHT

NOTES

> Maximum use temperature is dependant upon the duration at maximum temperature and is process specific. Airtech recommends testing prior to use.
> Minimum order quantity required.

* SHT = sheeting, CF = centerfold, LFT = lay-flat tubing, LFT-G = lay-flat tubing gusseted.

Catalogue position : **Bagging films**

Appendix E

Fontijne Hot-Press		
Model	TP 400	
Serial Nr	000.25.566-12.92	
Fontjine Ordrer Nr.	000.46.566	
Year of Manufacture	1992	
Plate Size	320 x 320	mm
Daylight	200	/mm
Electric load per plate	3.75	kW
Max. Temp	450	°C
Cylinder -diameter	160	mm
-stroke	200	mm
Hydraulic pressure	200	bar
Max. press force	400	kPa
Motorpump- rating	0.55	kW
Output - l.p.	15	dm^3/mm
-h.p.	0.46	dm^3/mm
Main supply voltage	3x380	V+N
Total Power consumption	10	kVA
Mass/weight	450	kg

Appendix F

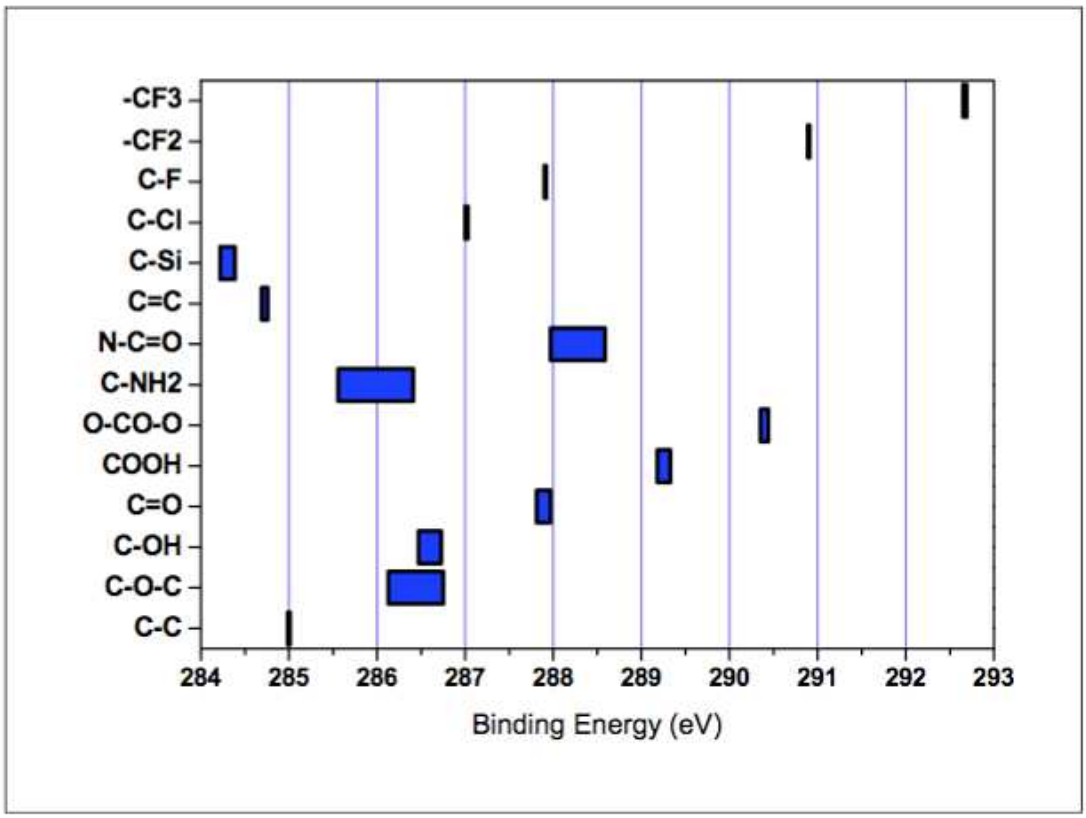
-CF3
-CF2
C-F
C-Cl
C-Si
C=C
N-C=O
C-NH2
O-CO-O
COOH
C=O
C-OH
C-O-C
C-C
284
285
286
287
288
289
290
291
292
293
Binding Energy (eV)

Appendix G

Auftraggeber/Telefon	**Datum**	**Auftragnehmer/Telefon**	**Verrechnung skonto**
CFK / 9862	**10.02.2010**	**/**	

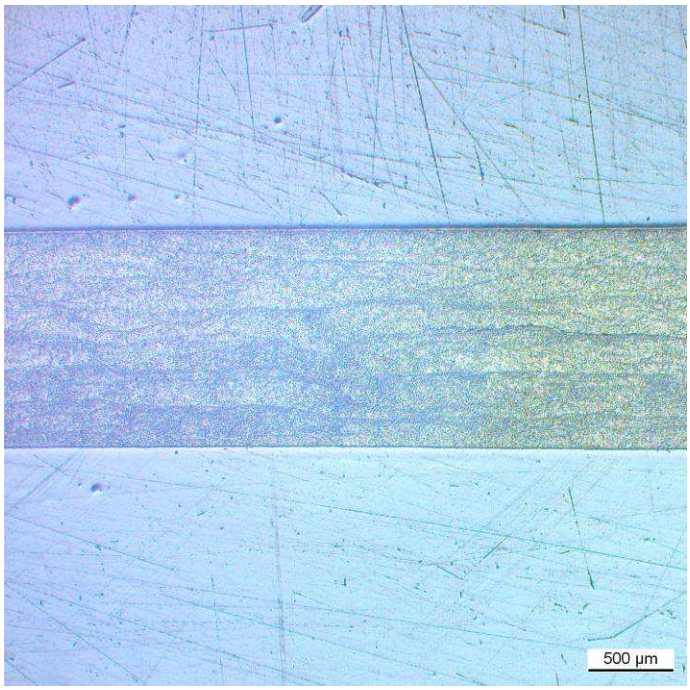

Bildname :	Bild_004946
Bearbeiter :	Robert Rudolf
Quelle :	1 Toho 1mm
Beschreibung:	
Aufnahme :	1.67*2.5
Präparation :	
Präparat :	1 Toho 1mm

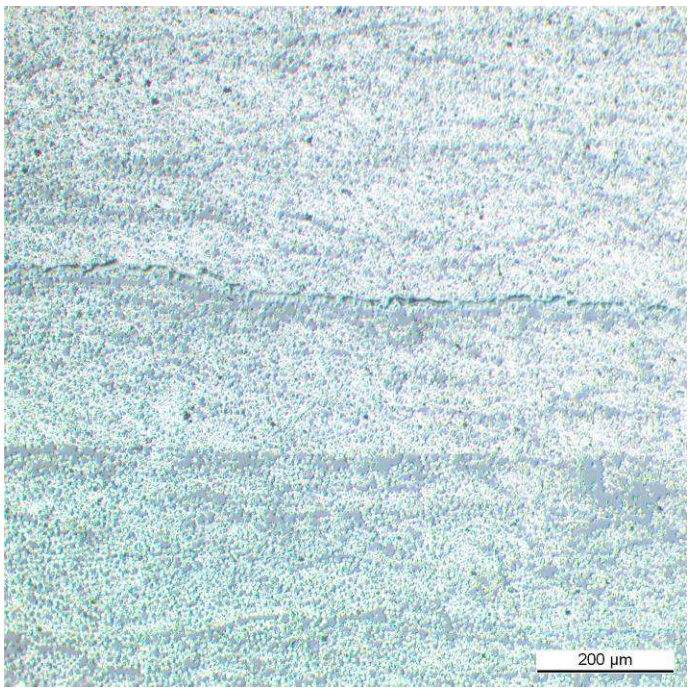

Bildname :	Bild_004948
Bearbeiter :	Robert Rudolf
Quelle :	1 Toho 1mm
Beschreibung:	
Aufnahme :	1.67*10
Präparation :	
Präparat :	1 Toho 1mm

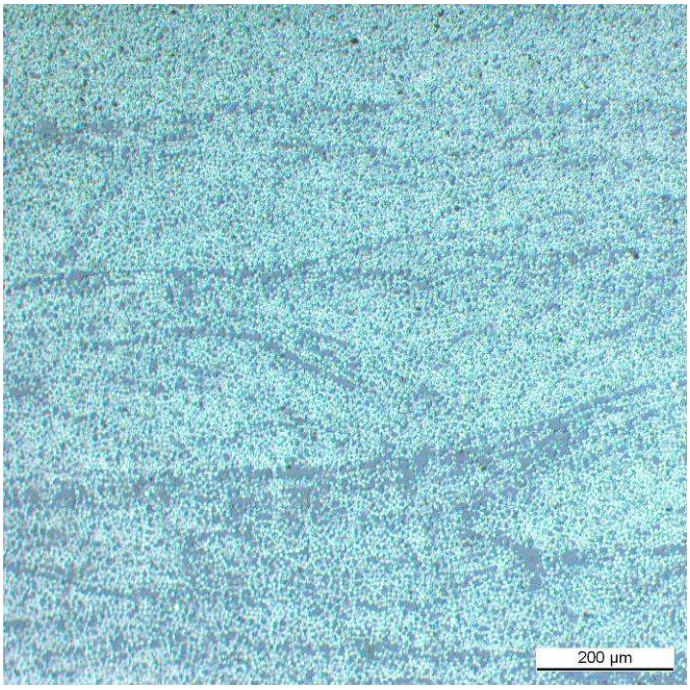

Bildname :	Bild_004957
Bearbeiter :	Robert Rudolf
Quelle :	1 Toho 1mm 3
Beschreibung:	
Aufnahme :	1.67*10
Präparation :	
Präparat :	1

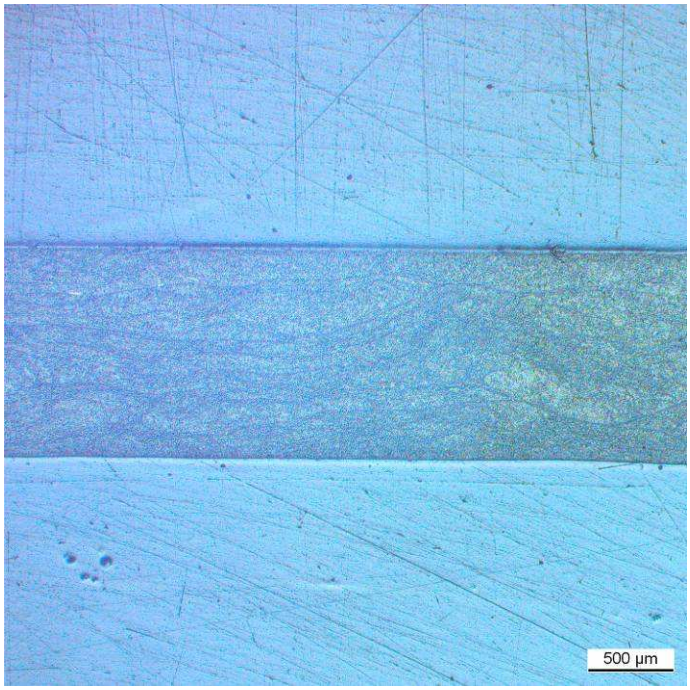

Bildname :	Bild_004960
Bearbeiter :	Robert Rudolf
Quelle :	1 Toho Flat 2
Beschreibung:	
Aufnahme :	1.67*2.5
Präparation :	
Präparat :	1 Toho flat 2

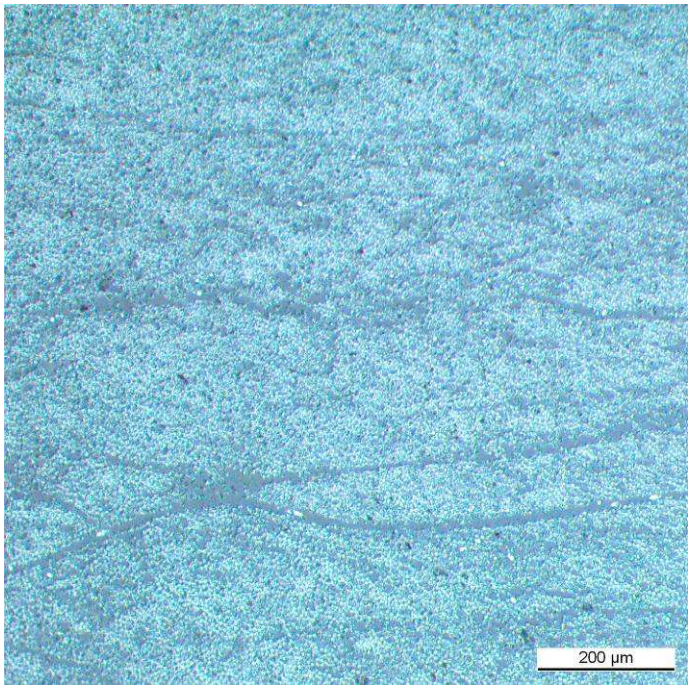

Bildname :	Bild_004962
Bearbeiter :	Robert Rudolf
Quelle :	1 Toho flat 2
Beschreibung:	
Aufnahme :	1.67*10
Präparation :	
Präparat :	1 Toho Flat 1

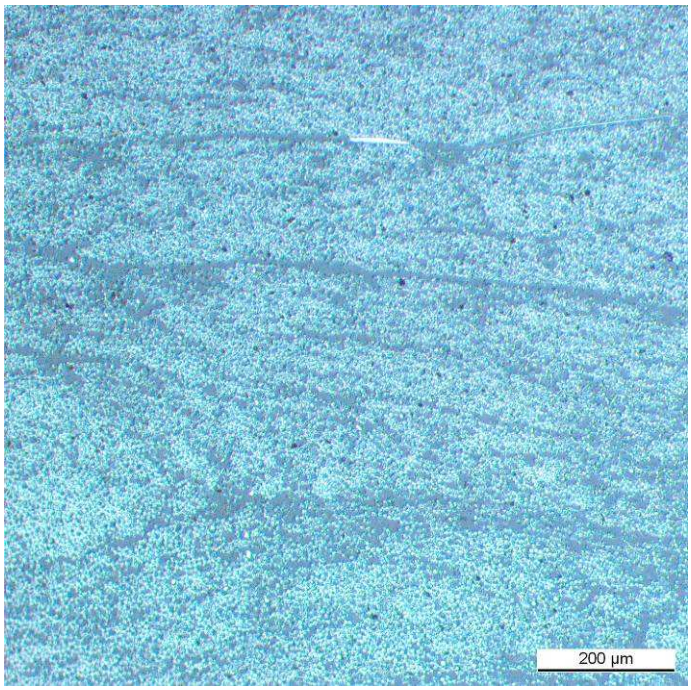

Bildname :	Bild_004965
Bearbeiter :	Robert Rudolf
Quelle :	1 Toho Flat 2
Beschreibung:	
Aufnahme :	1.67*2.5
Präparation :	
Präparat :	1 Toho flat 2

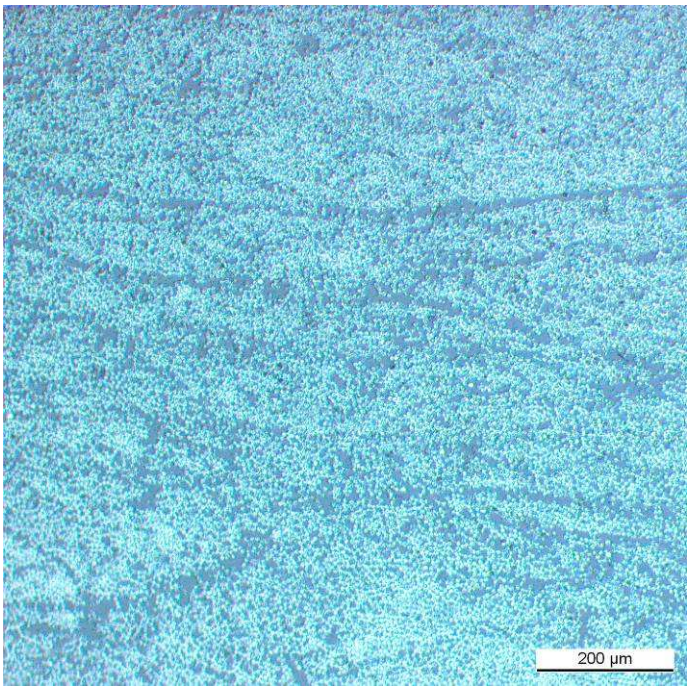

Bildname :	Bild_004967
Bearbeiter :	Robert rudolf
Quelle :	1 Toho flat 3
Beschreibung:	
Aufnahme :	1.67*10
Präparation :	
Präparat :	1 Toho flat 3

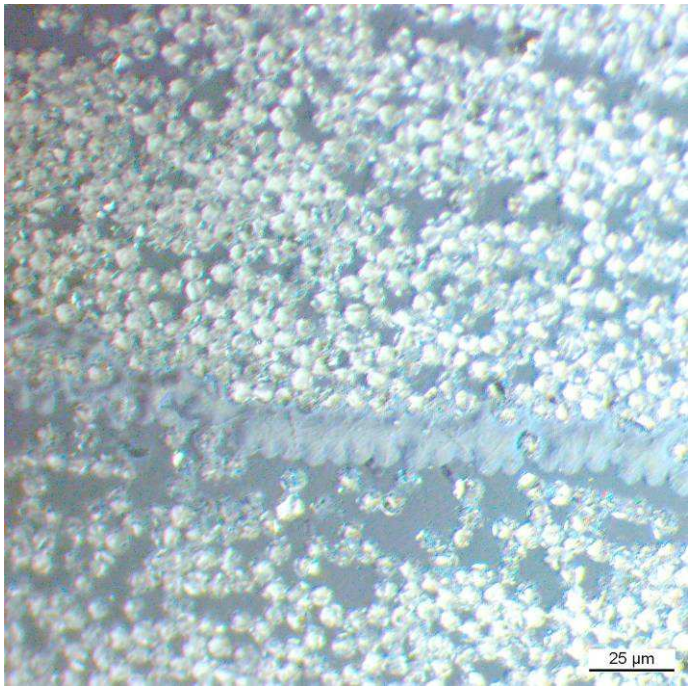

Bildname :	Bild_004950
Bearbeiter :	Robert Rudolf
Quelle :	1 Toho 1mm 1
Beschreibung:	50x Magnification of stripe
Aufnahme :	1.67*50
Präparation :	
Präparat :	1 Toho 1mm 1

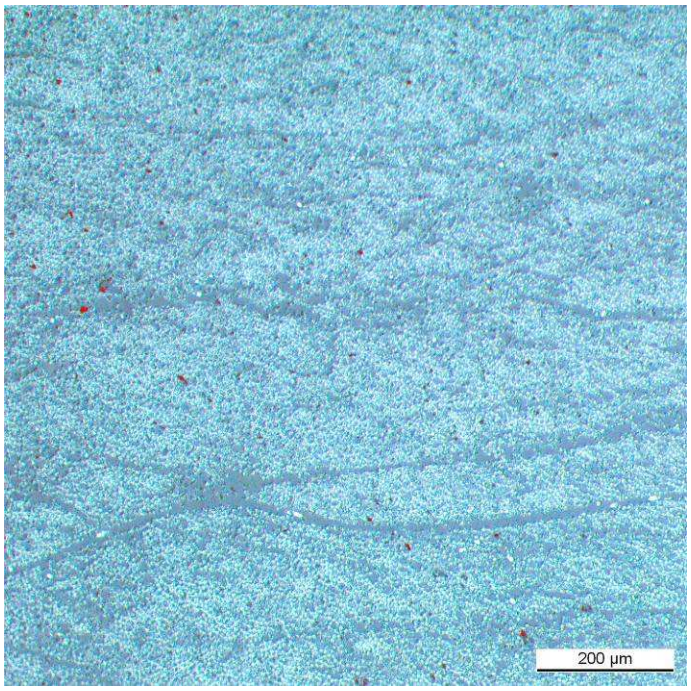

Bildname :	Bild_004963
Bearbeiter :	Robert Rudolf
Quelle :	1 Toho Flat 1 Binal
Beschreibung:	
Aufnahme :	1.67*10
Präparation :	
Präparat :	1 Toho Flat 0.185%

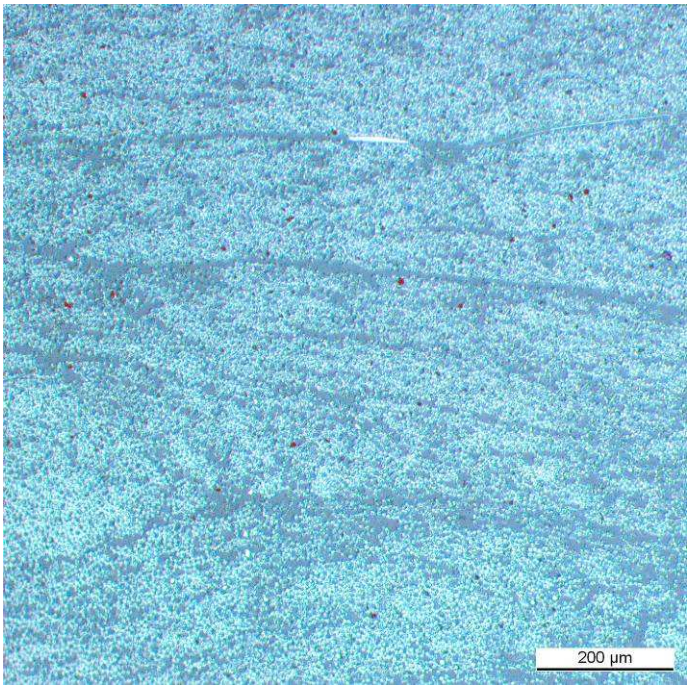

Bildname :	Bild_004966
Bearbeiter :	Robert rudolf
Quelle :	1 Toho flat 2 binal
Beschreibung:	
Aufnahme :	1.67*10
Präparation :	
Präparat :	1 Toho flat 2 0.128%

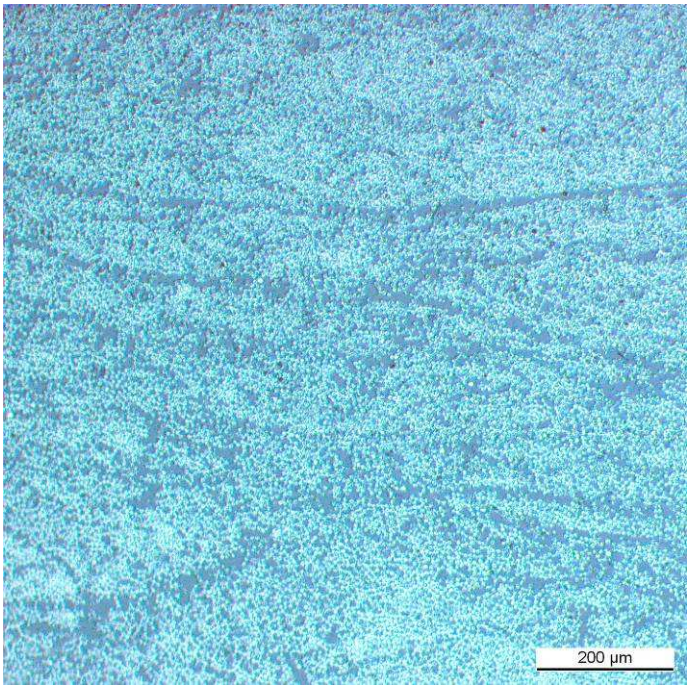

Bildname :	Bild_004968
Bearbeiter :	R:R
Quelle :	1 Toho Flat 3 binal
Beschreibung:	
Aufnahme :	1.67*10
Präparation :	
Präparat :	1 Toho Flat 3 0.129%

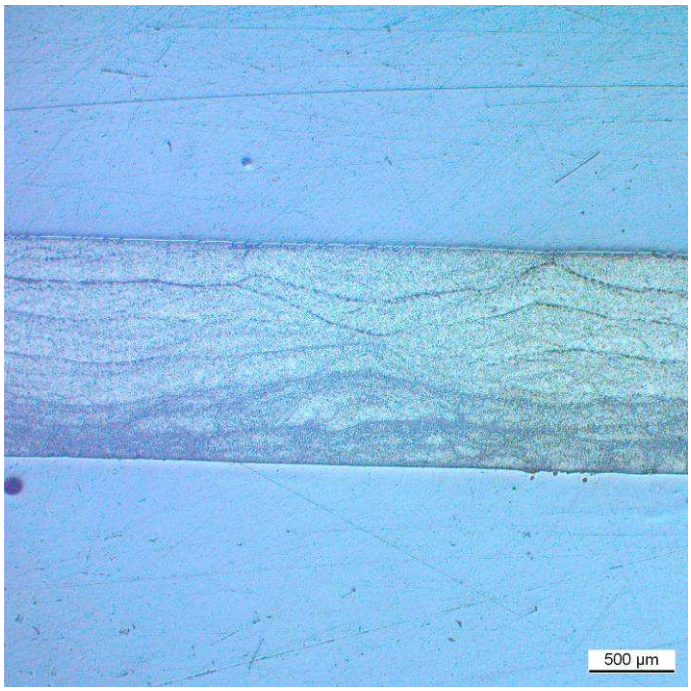

Bildname :	Bild_004969
Bearbeiter :	R:R
Quelle :	1 Hexcel 1mm
Beschreibung:	
Aufnahme :	1.67*2.5
Präparation :	
Präparat :	1 Hexcel 1mm

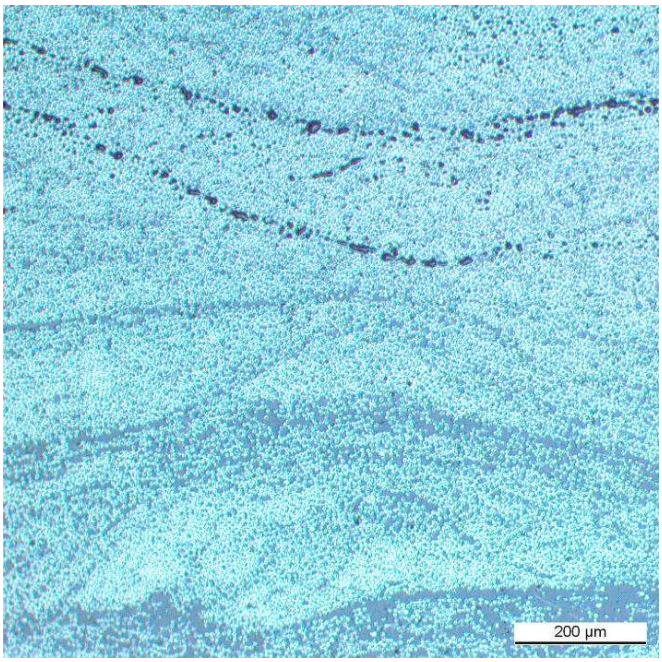

Bildname :	Bild_004970
Bearbeiter :	R:R
Quelle :	1 Hexcel 1mm 1
Beschreibung:	
Aufnahme :	1.67*10
Präparation :	
Präparat :	1 Hexcel 1mm 1

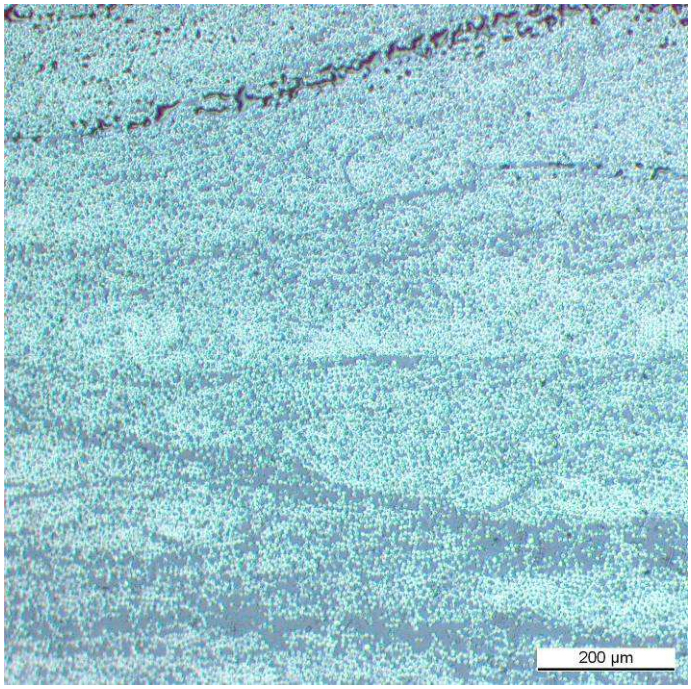

Bildname :	Bild_004972
Bearbeiter :	R:R
Quelle :	1 Hexcel 1mm 2
Beschreibung:	
Aufnahme :	1.67*10
Präparation :	
Präparat :	1 Hexcel 1mm 2

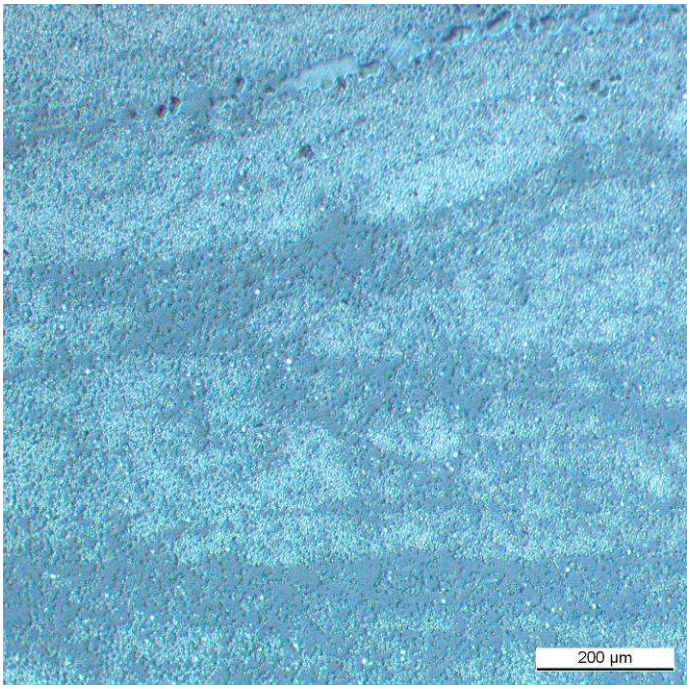

Bildname :	Bild_004974
Bearbeiter :	R:R
Quelle :	1 Hexcel 1mm 3
Beschreibung:	
Aufnahme :	1.67*10
Präparation :	
Präparat :	1 Hexcel 1mm 3

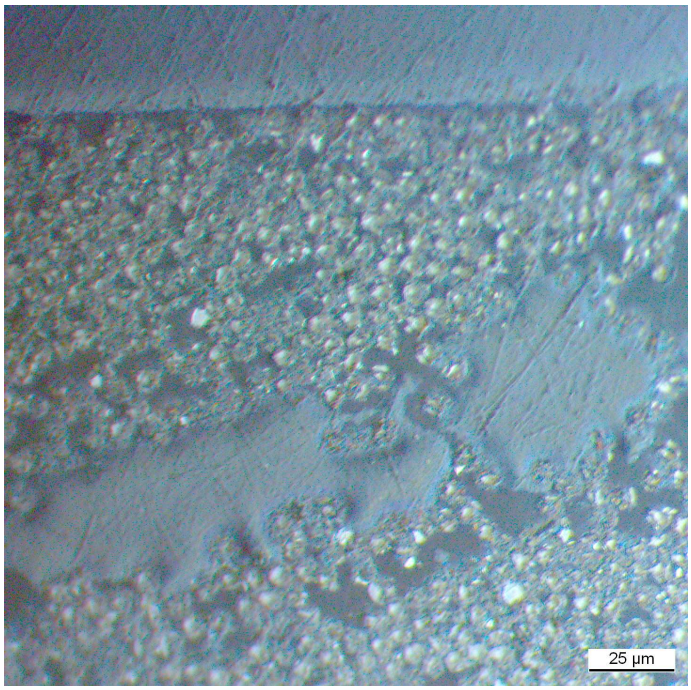

Bildname :	Bild_004976
Bearbeiter :	R:R
Quelle :	1 Hexcel 1mm 3
Beschreibung:	
Aufnahme :	1.67*50
Präparation :	
Präparat :	1 Hexcel 1mm 3 50x

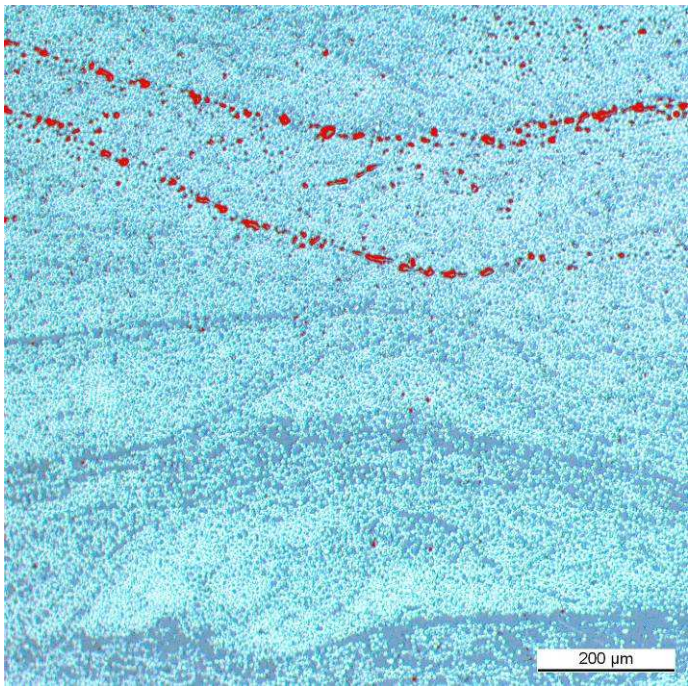

Bildname :	Bild_004971
Bearbeiter :	R.R
Quelle :	1 Hexcel 1mm 1 binal
Beschreibung:	
Aufnahme :	1.67*10
Präparation :	
Präparat :	1 Hexcel 1mm 1 1.16%

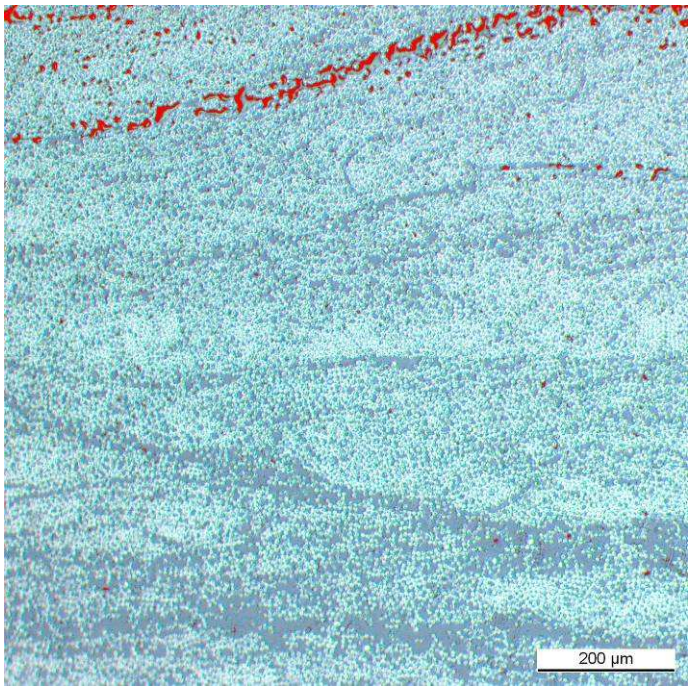

Bildname :	Bild_004973
Bearbeiter :	R:R
Quelle :	1 Hexcel 1 mm 2 Binal
Beschreibung:	
Aufnahme :	1.67*10
Präparation :	
Präparat :	1 Hexcel 1 mm 2 1.19%

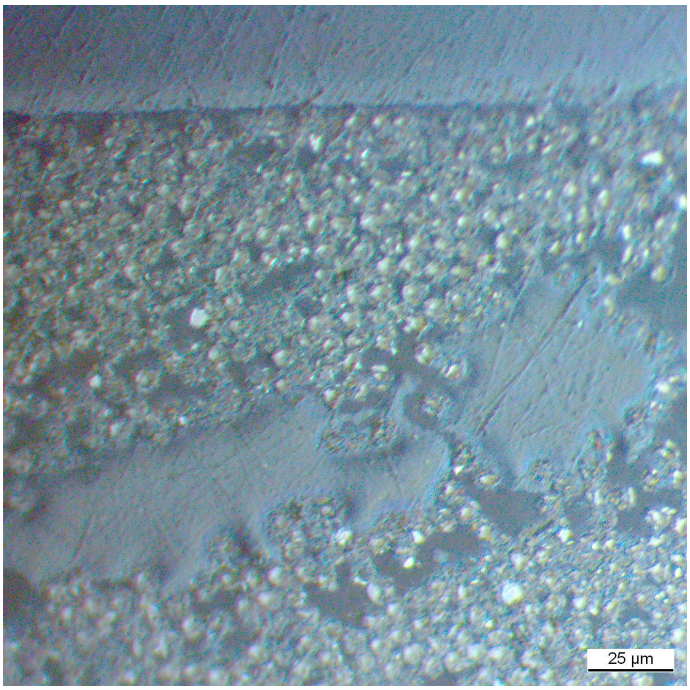

Bildname :	Bild_004976
Bearbeiter :	R:R
Quelle :	1 Hexcel 1mm 3
Beschreibung:	
Aufnahme :	1.67*50
Präparation :	
Präparat :	1 Hexcel 1mm 3 50x

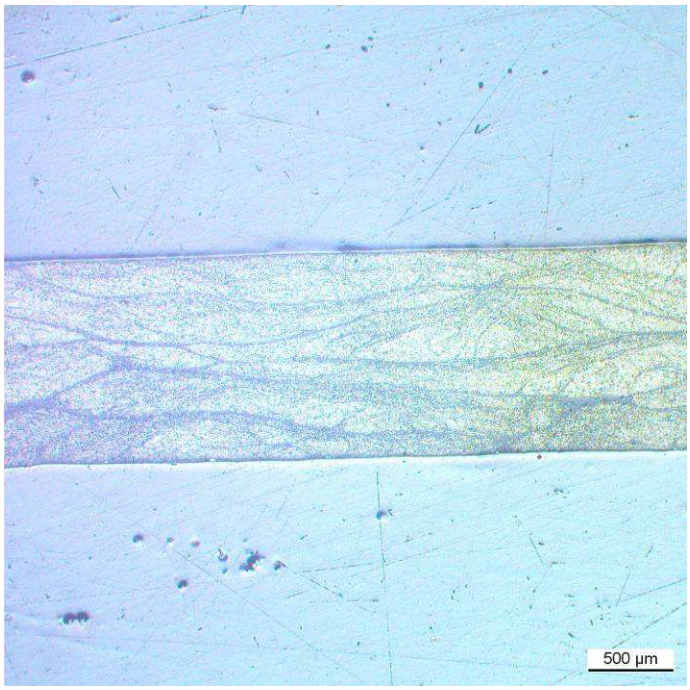

Bildname :	Bild_004977
Bearbeiter :	R:R
Quelle :	1 Hexcel flat
Beschreibung:	
Aufnahme :	1.67*2.5
Präparation :	
Präparat :	1 Hexcel flat

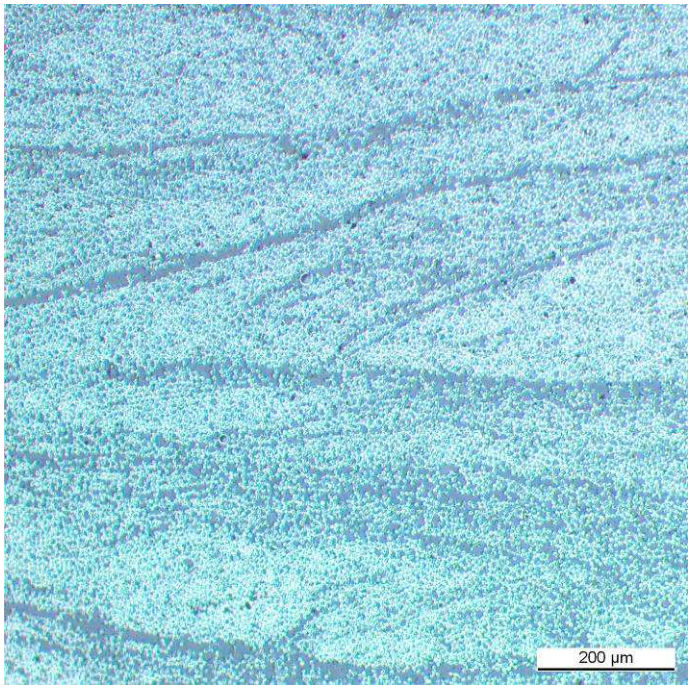

Bildname :	Bild_004979
Bearbeiter :	R:R
Quelle :	1 Hexcel flat 1
Beschreibung:	
Aufnahme :	1.67*10
Präparation :	
Präparat :	1 Hexcel flat 1

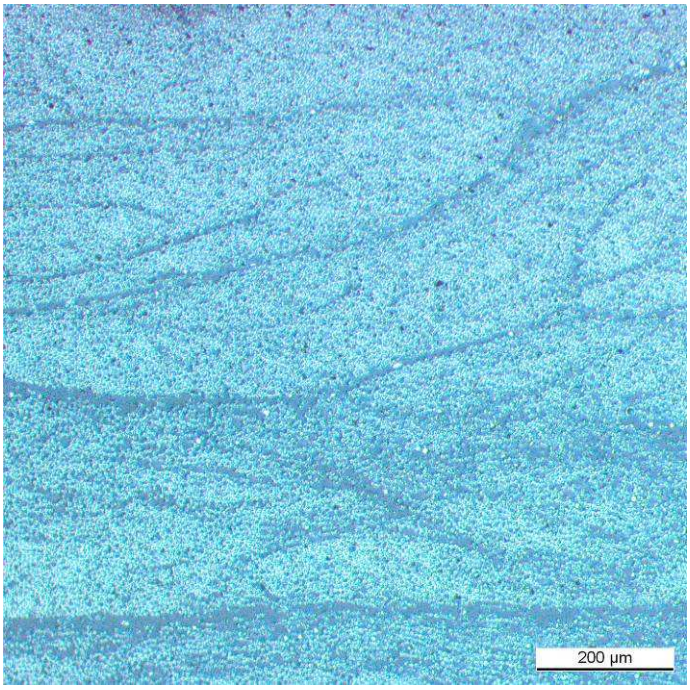

Bildname :	Bild_004981
Bearbeiter :	R:R
Quelle :	1 Hexcel flat 2
Beschreibung:	
Aufnahme :	1.67*10
Präparation :	
Präparat :	1 Hexcel flat 2

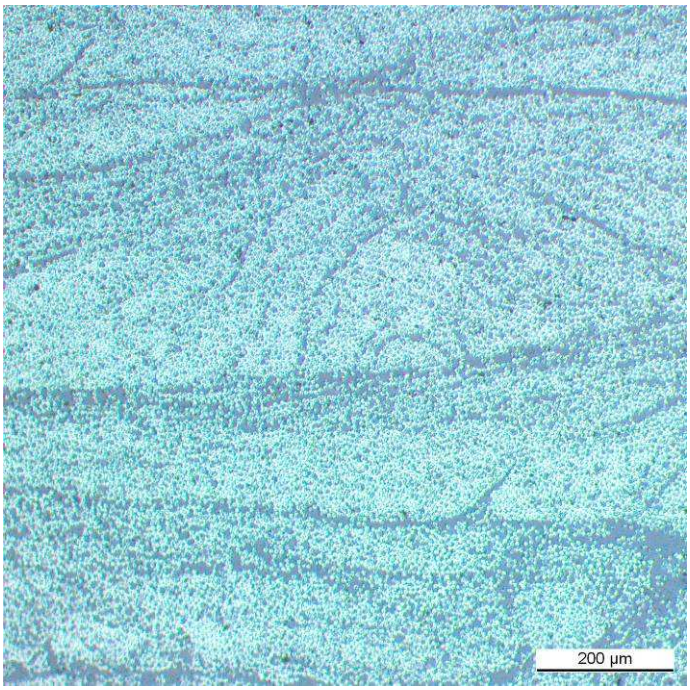

Bildname :	Bild_004983
Bearbeiter :	R:R
Quelle :	1 Hexcel flat 3
Beschreibung:	
Aufnahme :	1.67*10
Präparation :	
Präparat :	1 Hexcel flat 3

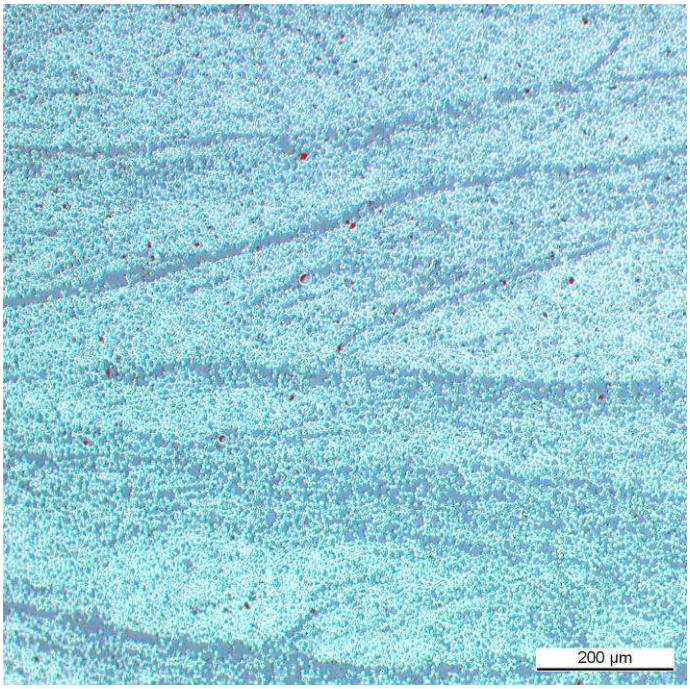

Bildname :	Bild_004980
Bearbeiter :	R:R
Quelle :	1 Hexcel flat 1 binal
Beschreibung:	
Aufnahme :	1.67*10
Präparation :	
Präparat :	1 Hexcel flat 1 0.478

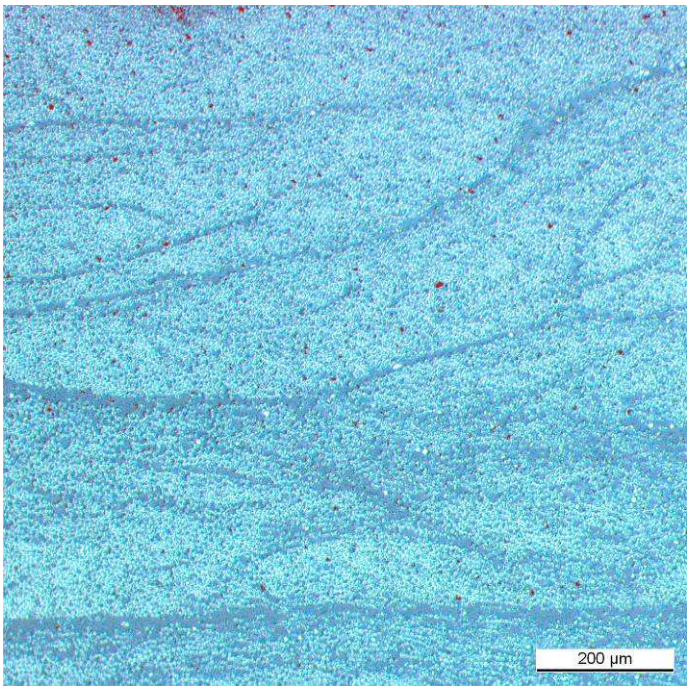

Bildname :	Bild_004982
Bearbeiter :	RR
Quelle :	1 Hexcel flat 2 binal
Beschreibung:	
Aufnahme :	1.67*10
Präparation :	
Präparat :	1 Hexcel flat 2 0.462%

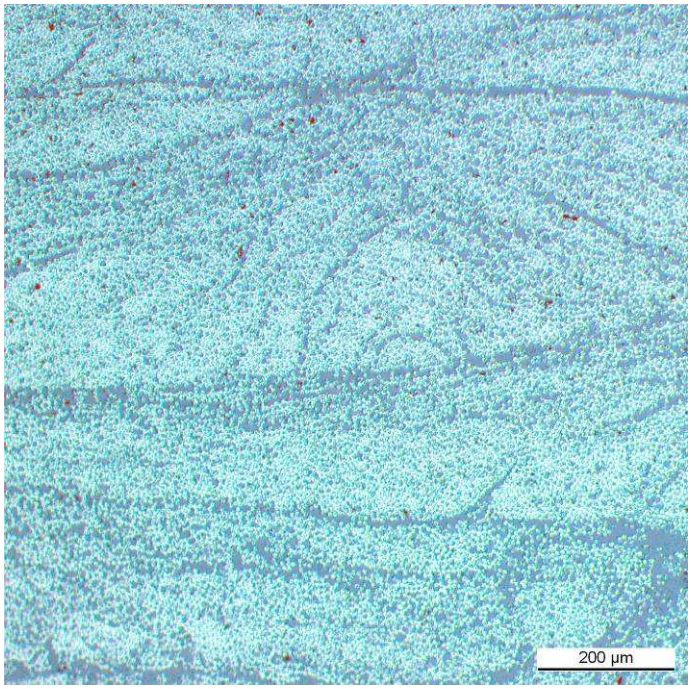

Bildname :	Bild_004984
Bearbeiter :	RR
Quelle :	1 Hexcel flat 3 binal
Beschreibung:	
Aufnahme :	1.67*10
Präparation :	
Präparat :	1 Hexcel flat 3 0.511

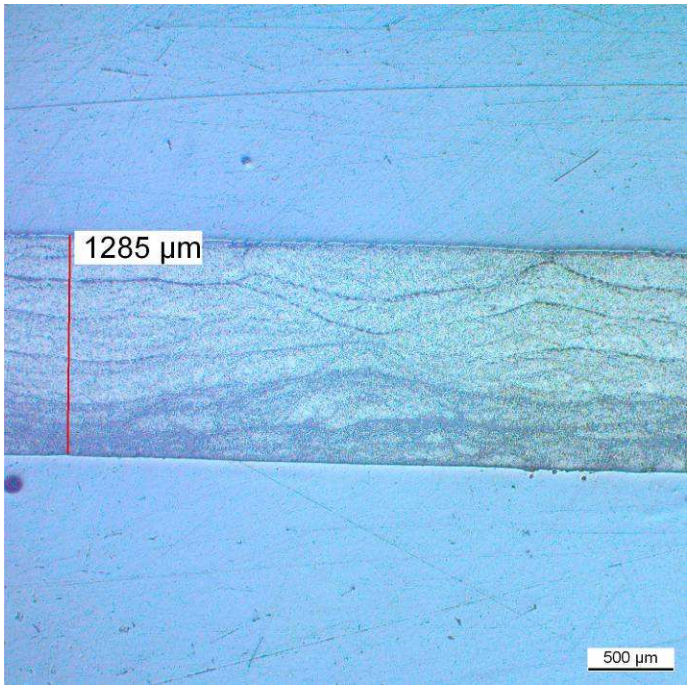

Bildname :	Bild_005076
Bearbeiter :	RR
Quelle :	1H1
Beschreibung:	
Aufnahme :	
Präparation :	
Präparat :	1H1

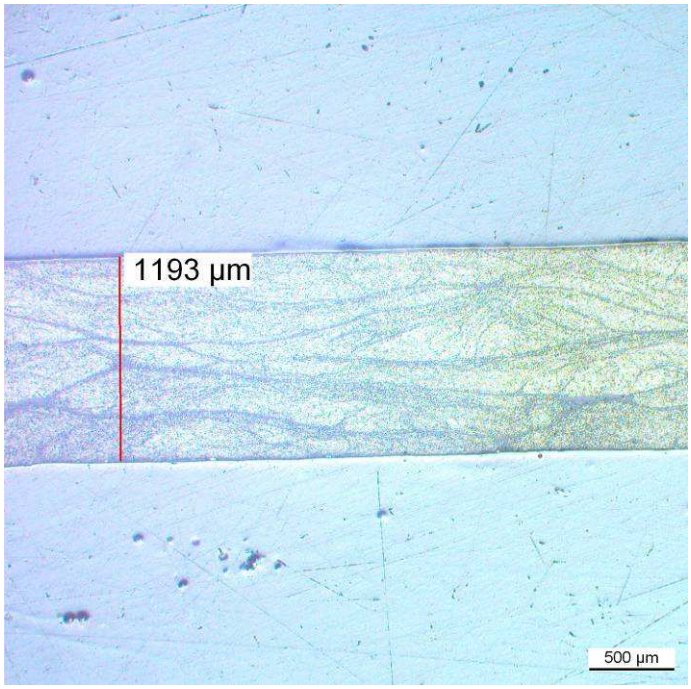

Bildname :	Bild_005077
Bearbeiter :	RR
Quelle :	1HF
Beschreibung:	
Aufnahme :	
Präparation :	
Präparat :	1HF

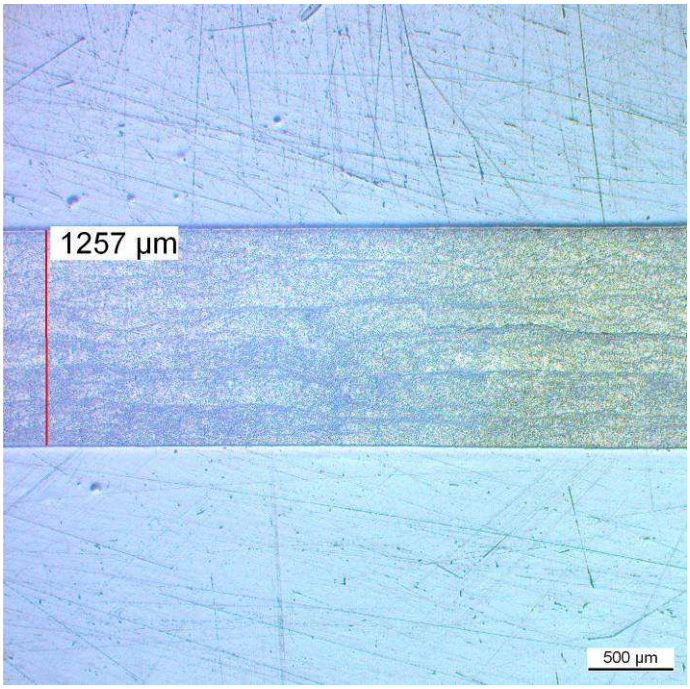

Bildname :	Bild_005078
Bearbeiter :	RR
Quelle :	1T1
Beschreibung:	
Aufnahme :	
Präparation :	
Präparat :	1T1

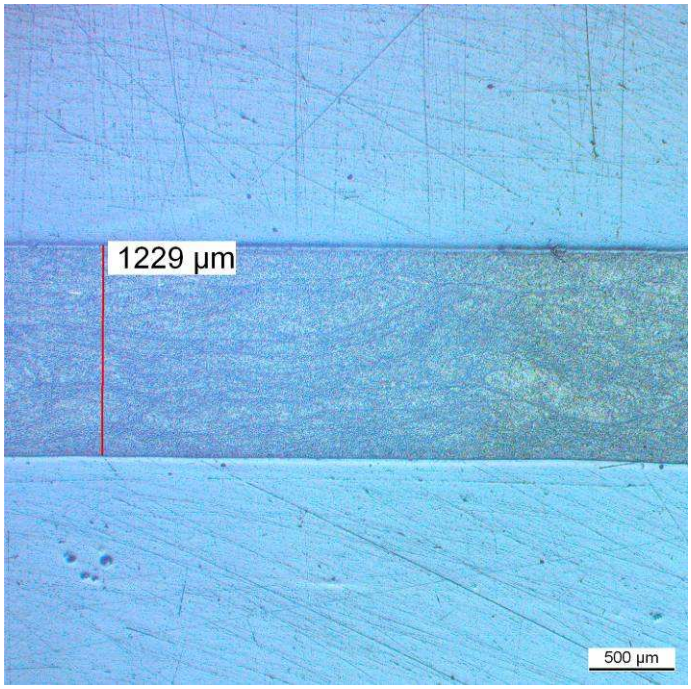

Bildname :	Bild_005079
Bearbeiter :	RR
Quelle :	1TF
Beschreibung:	
Aufnahme :	
Präparation :	
Präparat :	1TF

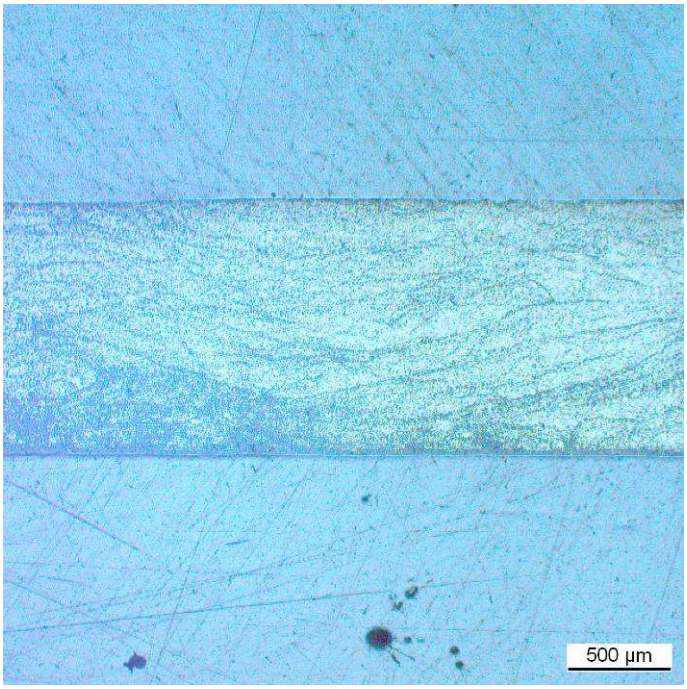

Bildname :	Bild_005003
Bearbeiter :	Robert Rudolf
Quelle :	2 Toho 1mm
Beschreibung:	
Aufnahme :	1.67*2.5
Präparation :	
Präparat :	2 Toho 1mm

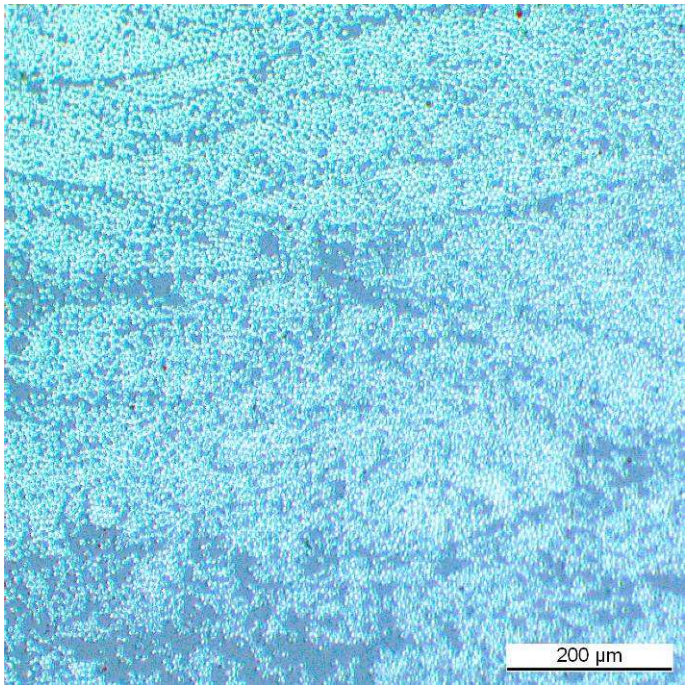

Bildname :	Bild_005004
Bearbeiter :	Robert Rudolf
Quelle :	2 Toho 1mm 1
Beschreibung:	
Aufnahme :	1.67*10
Präparation :	
Präparat :	2 Toho 1mm 1

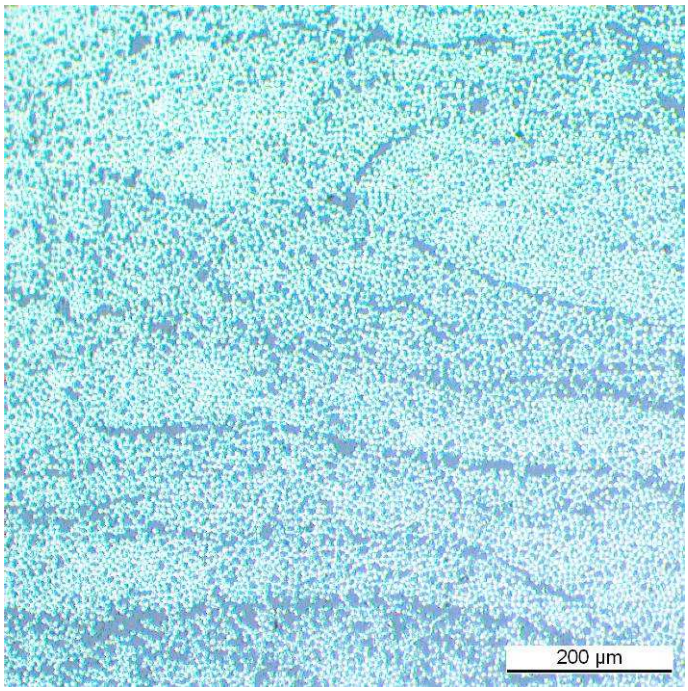

Bildname :	Bild_005005
Bearbeiter :	Robert Rudolf
Quelle :	2 Toho 1mm 2
Beschreibung:	
Aufnahme :	1.67*10
Präparation :	
Präparat :	2 Toho 1mm 2

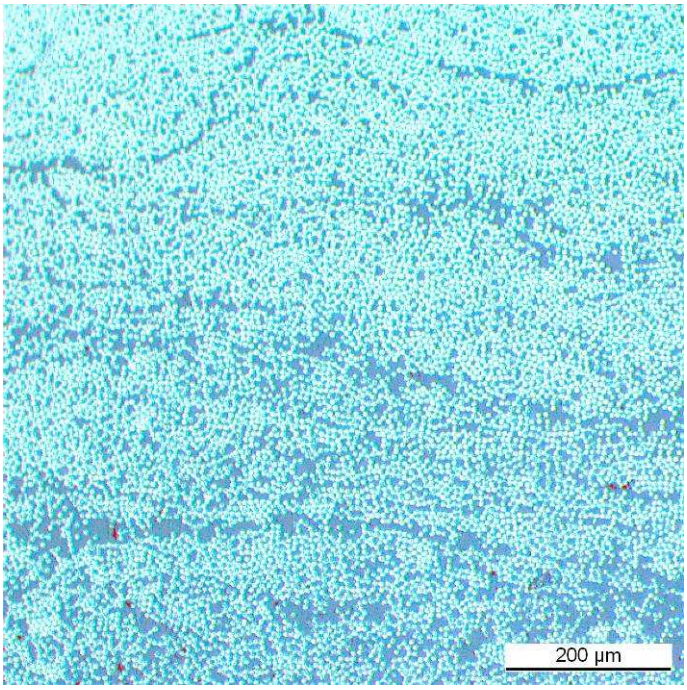

Bildname :	Bild_005007
Bearbeiter :	Robert Rudolf
Quelle :	2 Toho 1mm 3
Beschreibung:	
Aufnahme :	1.67*10
Präparation :	
Präparat :	2 Toho 1mm 3

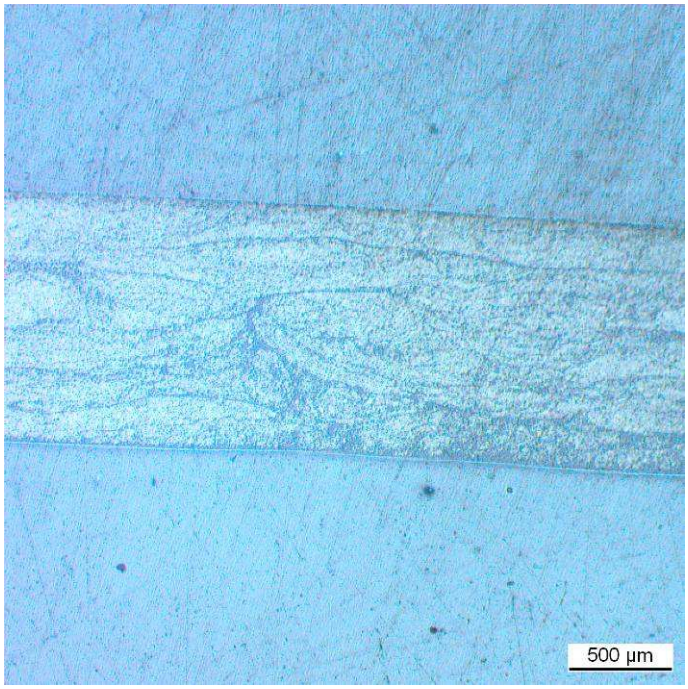

Bildname :	Bild_005008
Bearbeiter :	Robert Rudolf
Quelle :	2 Toho flat
Beschreibung:	
Aufnahme :	1.67*2.5
Präparation :	
Präparat :	2 Toho flat

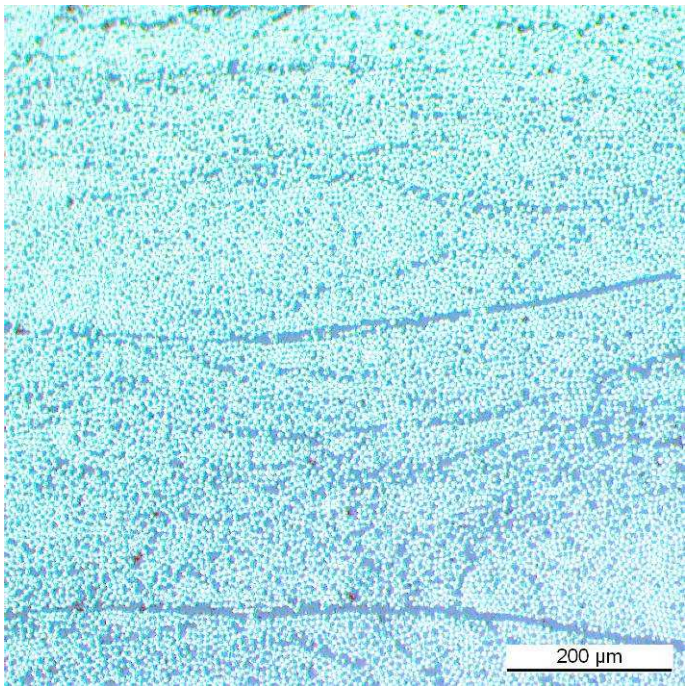

Bildname :	Bild_005009
Bearbeiter :	Robert Rudolf
Quelle :	2 Toho flat 1
Beschreibung:	
Aufnahme :	1.67*10
Präparation :	
Präparat :	2 Toho flat 1

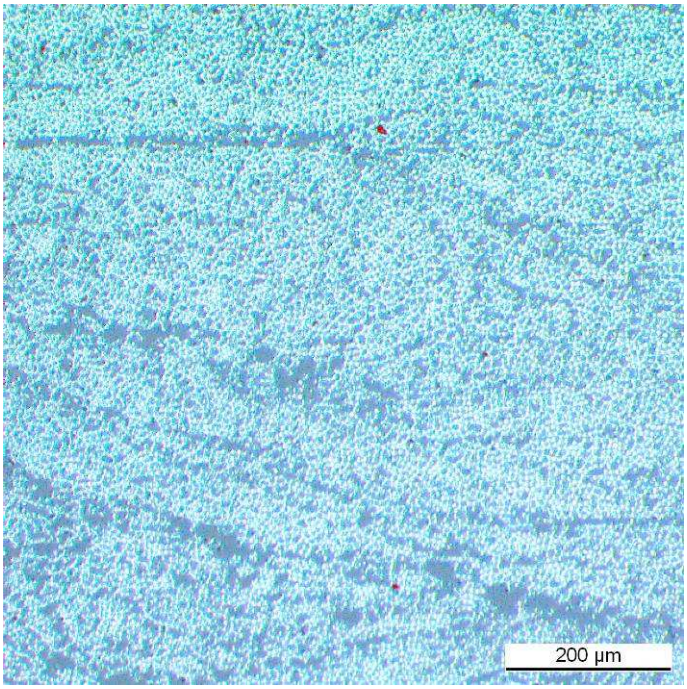

Bildname :	Bild_005010
Bearbeiter :	Robert Rudolf
Quelle :	2 Toho flat 2
Beschreibung:	
Aufnahme :	1.67*10
Präparation :	
Präparat :	2 Toho flat 2

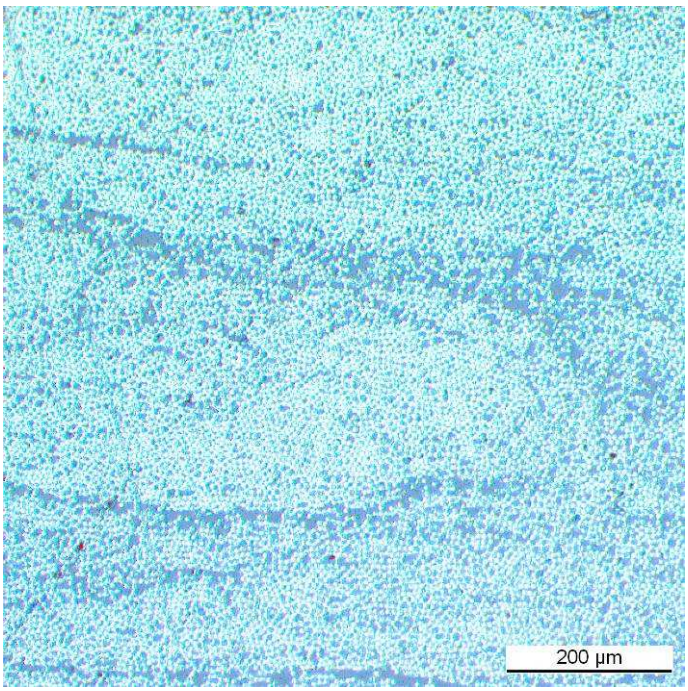

Bildname :	Bild_005011
Bearbeiter :	Robert Rudolf
Quelle :	2 Toho flat 3
Beschreibung:	
Aufnahme :	1.67*10
Präparation :	
Präparat :	2 Toho flat 3

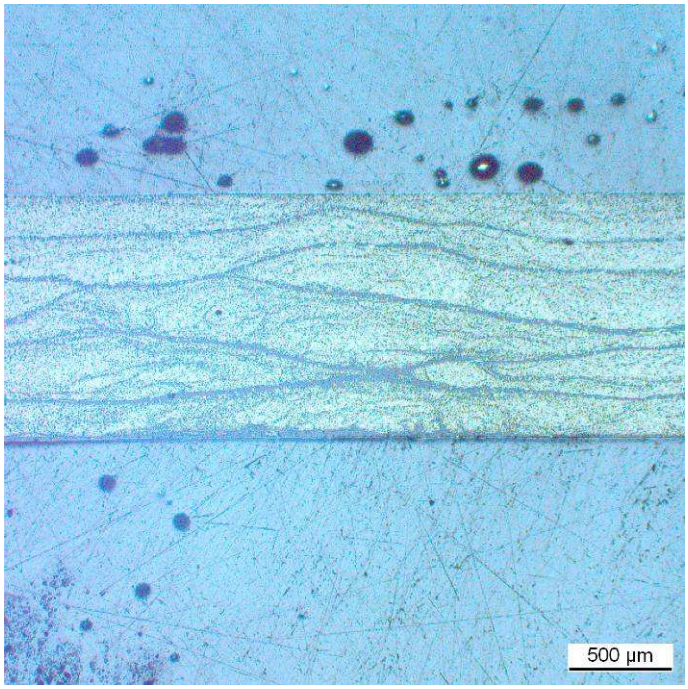

Bildname :	Bild_005012
Bearbeiter :	Robert Rudolf
Quelle :	2 Hexcel 1mm
Beschreibung:	
Aufnahme :	1.67*2.5
Präparation :	
Präparat :	2 Hexcel 1mm

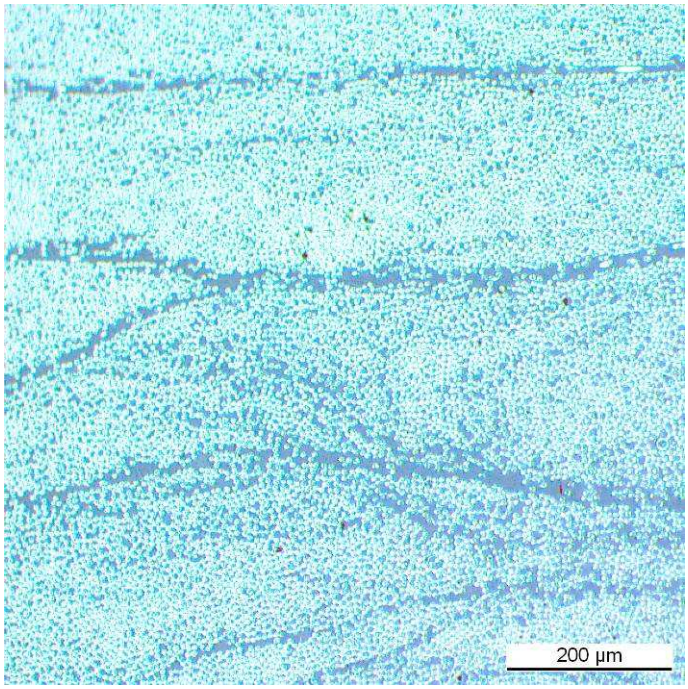

Bildname :	Bild_005013
Bearbeiter :	Robert Rudolf
Quelle :	2 Hexcel 1mm 1
Beschreibung:	
Aufnahme :	1.67*10
Präparation :	
Präparat :	2 Hexcel 1mm 1

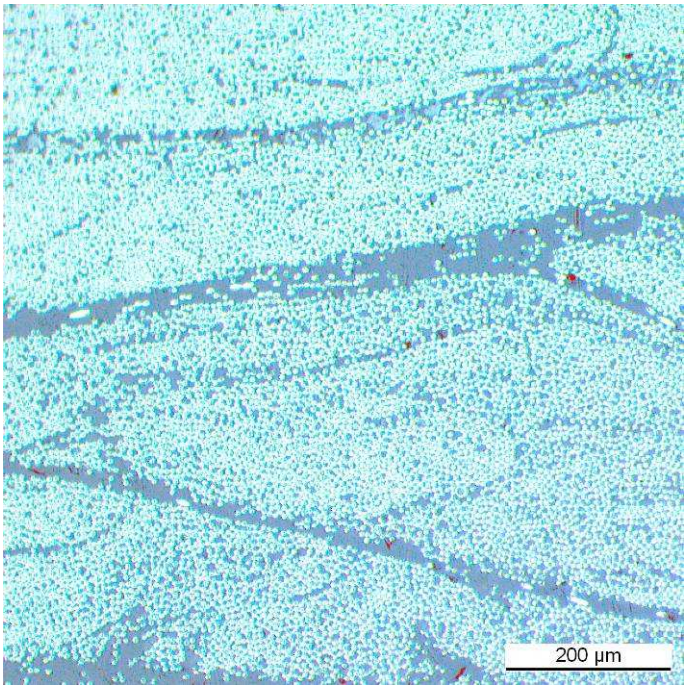

Bildname :	Bild_005014
Bearbeiter :	Robert Rudolf
Quelle :	2 Hexcel 1mm 2
Beschreibung:	
Aufnahme :	1.67*10
Präparation :	
Präparat :	2 Hexcel 1mm 2

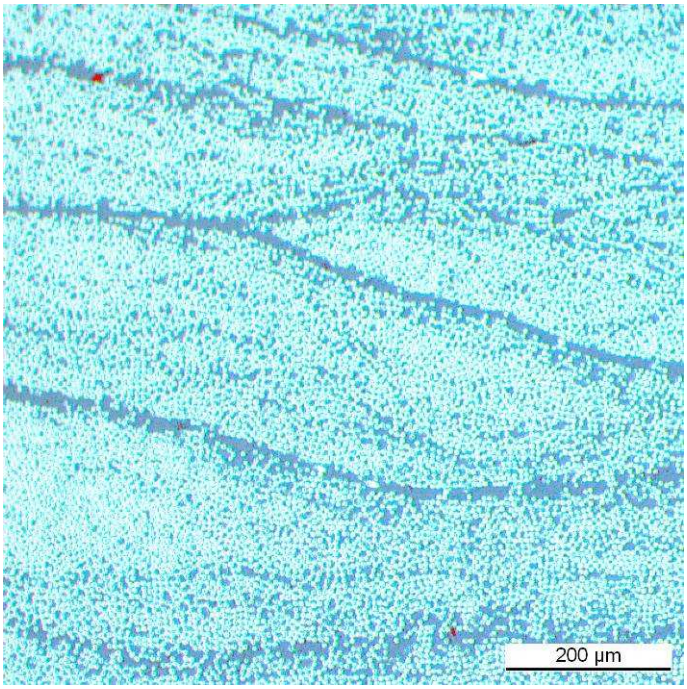

Bildname :	Bild_005015
Bearbeiter :	Robert Rudolf
Quelle :	2 Hexcel 1mm 3
Beschreibung:	
Aufnahme :	1.67*10
Präparation :	
Präparat :	2 Hexcel 1mm 3

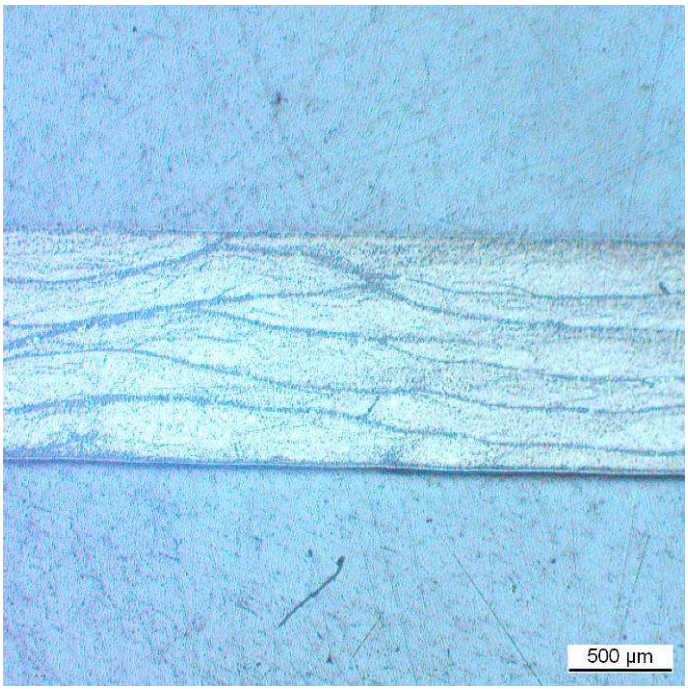

Bildname :	Bild_005016
Bearbeiter :	Robert Rudolf
Quelle :	2 Hexcel Flat
Beschreibung:	
Aufnahme :	1.67*2.5
Präparation :	
Präparat :	2 Hexcel flat

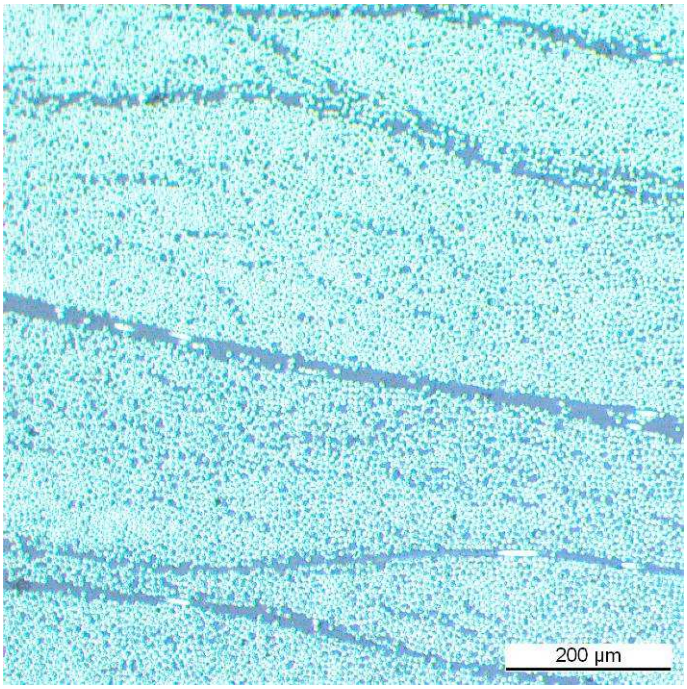

Bildname :	Bild_005017
Bearbeiter :	Robert Rudolf
Quelle :	2 Hexcel Flat 1
Beschreibung:	
Aufnahme :	1.67*10
Präparation :	
Präparat :	2 Hexcel flat 1

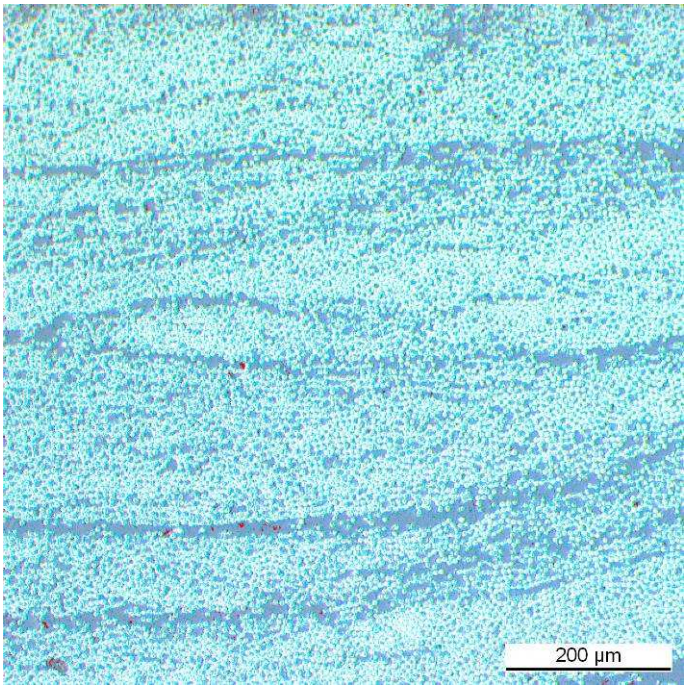

Bildname :	Bild_005018
Bearbeiter :	Robert Rudolf
Quelle :	2 Hexcel Flat 2
Beschreibung:	
Aufnahme :	1.67*10
Präparation :	
Präparat :	2 Hexcel flat 2

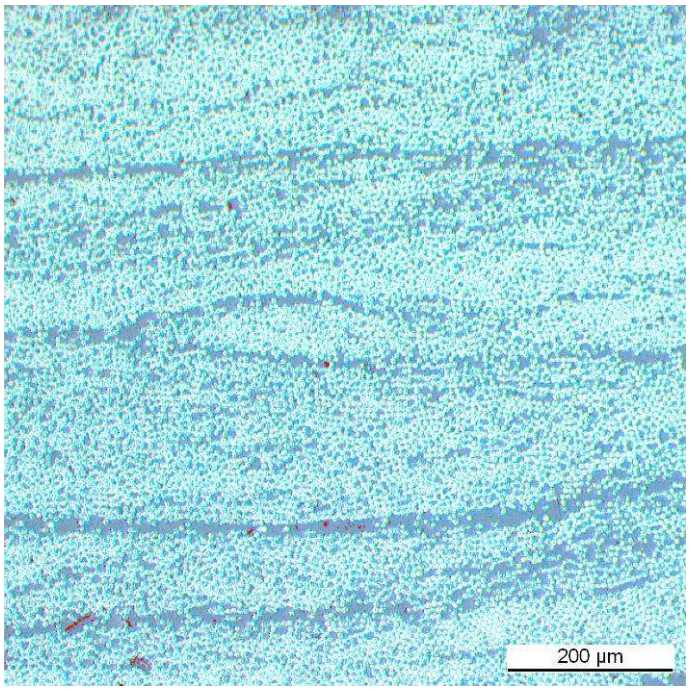

Bildname :	Bild_005020
Bearbeiter :	Robert Rudolf
Quelle :	2 Hexcel Flat 3
Beschreibung:	
Aufnahme :	1.67*10
Präparation :	
Präparat :	2 Hexcel flat 3

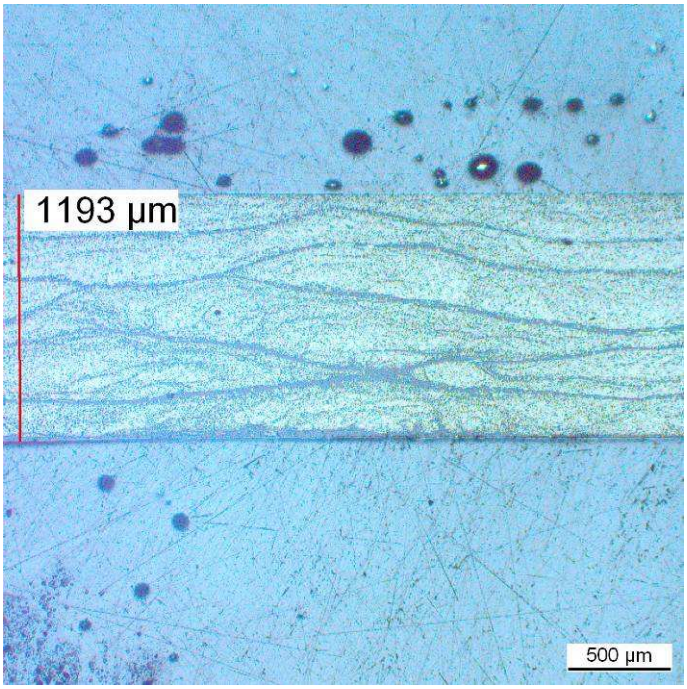

Bildname :	Bild_005080
Bearbeiter :	RR
Quelle :	2H1
Beschreibung:	
Aufnahme :	
Präparation :	
Präparat :	2H1

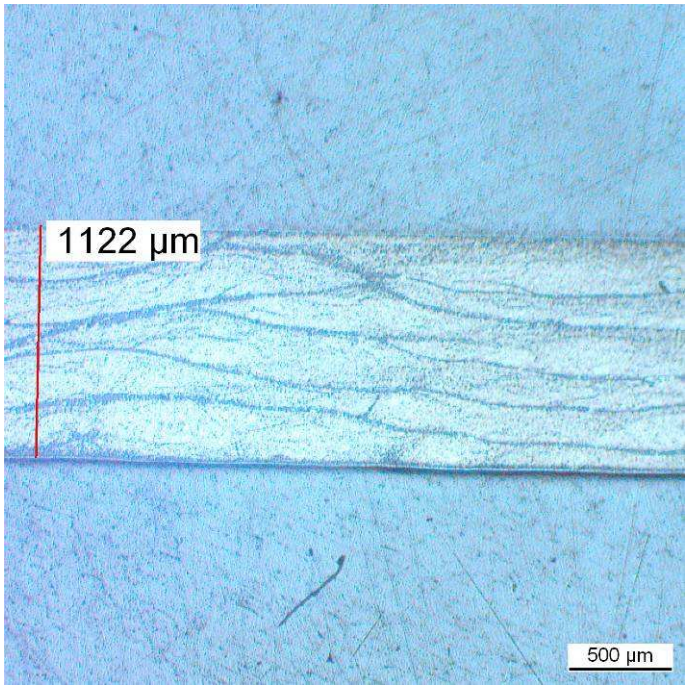

Bildname :	Bild_005081
Bearbeiter :	RR
Quelle :	2HF
Beschreibung:	
Aufnahme :	
Präparation :	
Präparat :	2HF

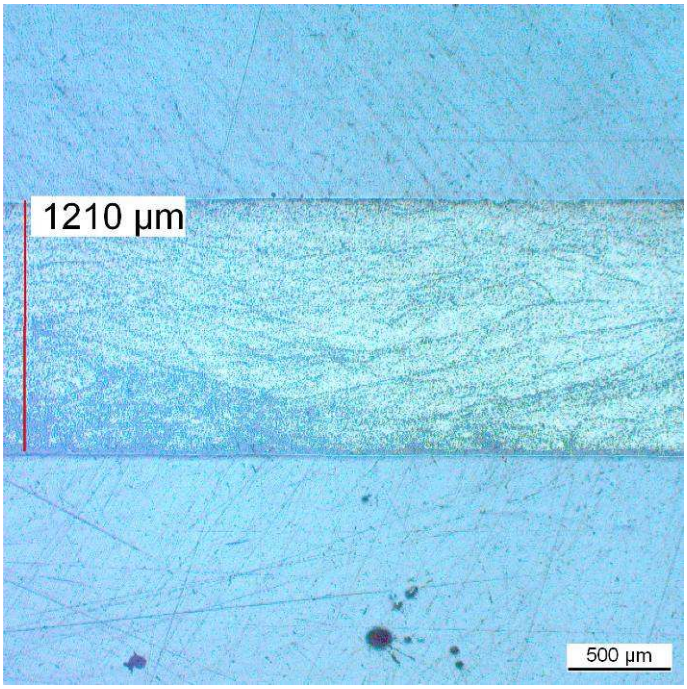

Bildname :	Bild_005082
Bearbeiter :	RR
Quelle :	2T1
Beschreibung:	
Aufnahme :	
Präparation :	
Präparat :	2T1

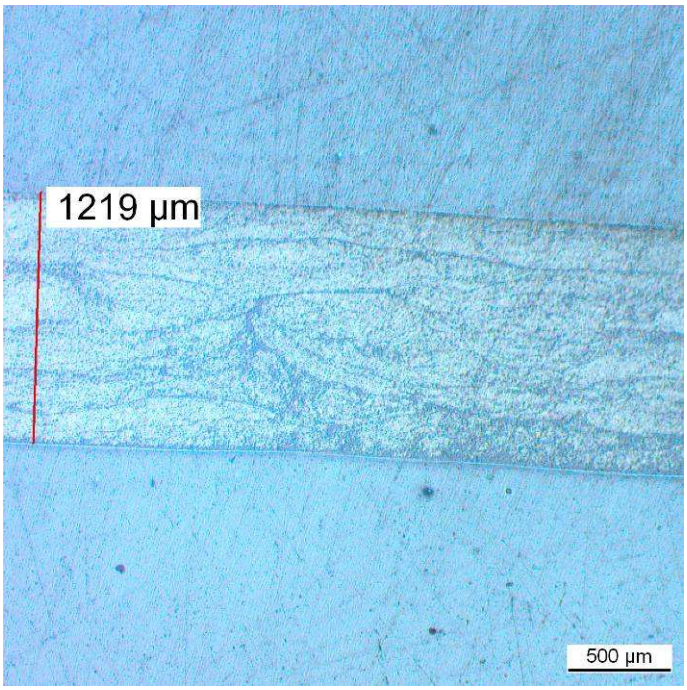

Bildname :	Bild_005083
Bearbeiter :	RR
Quelle :	2TF
Beschreibung:	
Aufnahme :	
Präparation :	
Präparat :	2TF

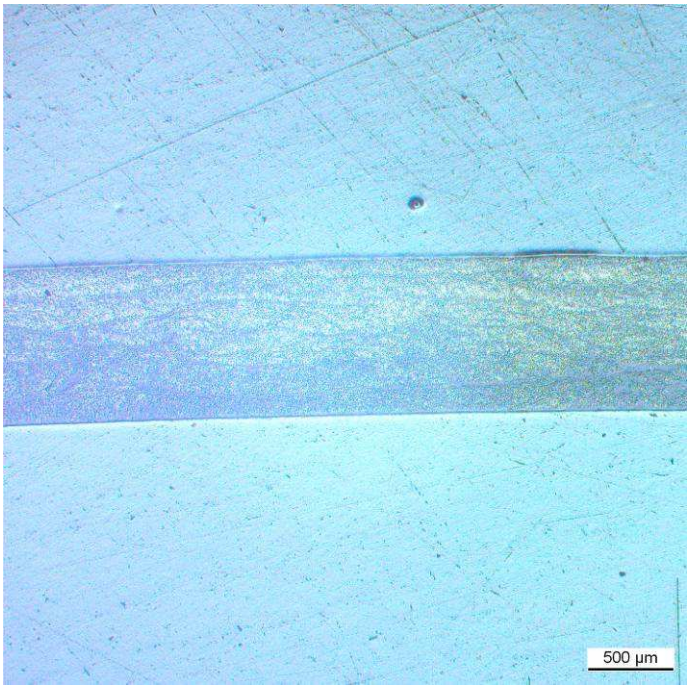

Bildname :	Bild_004985
Bearbeiter :	Robert Rudolf
Quelle :	3 Toho 1mm
Beschreibung:	
Aufnahme :	1.67*2.5
Präparation :	
Präparat :	3 Toho 1mm

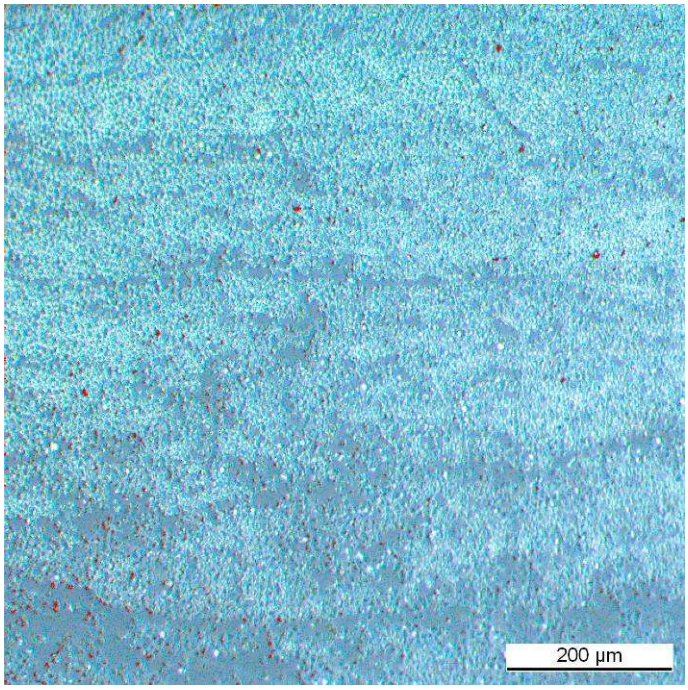

Bildname :	Bild_004986
Bearbeiter :	Robert Rudolf
Quelle :	3 Toho 1mm 1
Beschreibung:	
Aufnahme :	1.67*10
Präparation :	
Präparat :	3 Toho 1mm 1

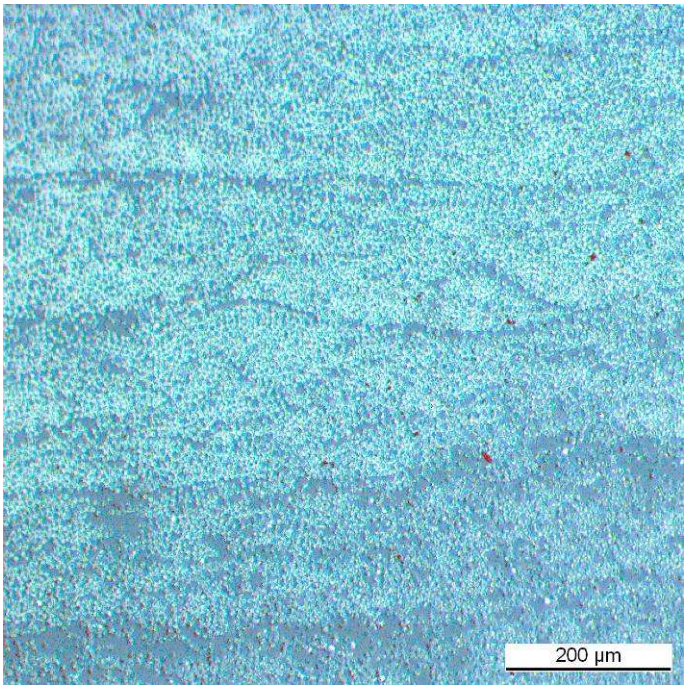

Bildname :	Bild_004987
Bearbeiter :	Robert Rudolf
Quelle :	3 Toho 1mm 2
Beschreibung:	
Aufnahme :	1.67*10
Präparation :	
Präparat :	3 Toho 1mm 2

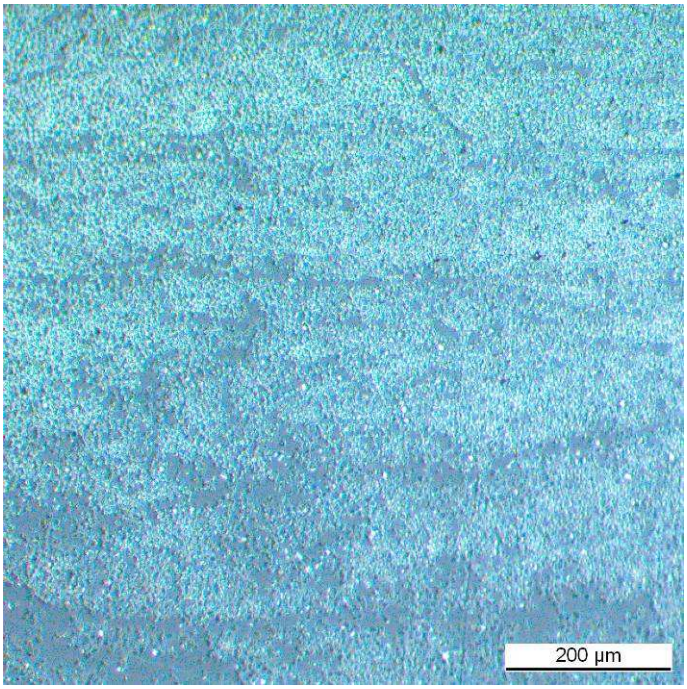

Bildname :	Bild_004988
Bearbeiter :	Robert Rudolf
Quelle :	3 Toho 1mm 3
Beschreibung:	
Aufnahme :	1.67*10
Präparation :	
Präparat :	3 Toho 1mm 3

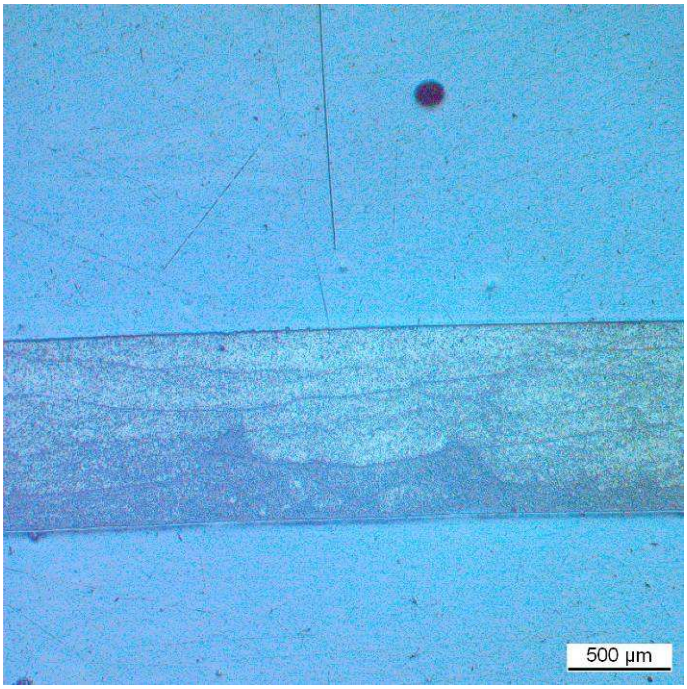

Bildname :	Bild_004990
Bearbeiter :	Robert Rudolf
Quelle :	3 Toho flat
Beschreibung:	
Aufnahme :	1.67*2.5
Präparation :	
Präparat :	3 Toho flat

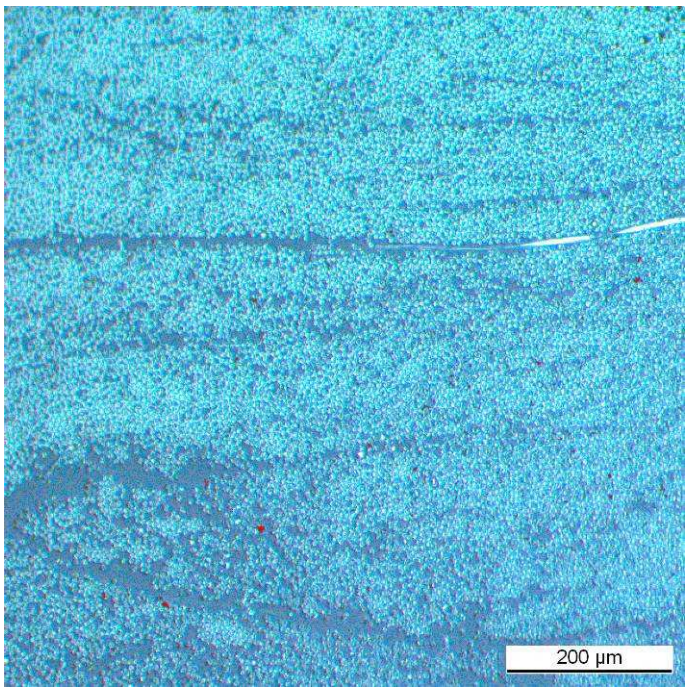

Bildname :	Bild_004991
Bearbeiter :	Robert Rudolf
Quelle :	3 Toho flat 1
Beschreibung:	
Aufnahme :	1.67*10
Präparation :	
Präparat :	3 Toho flat 1

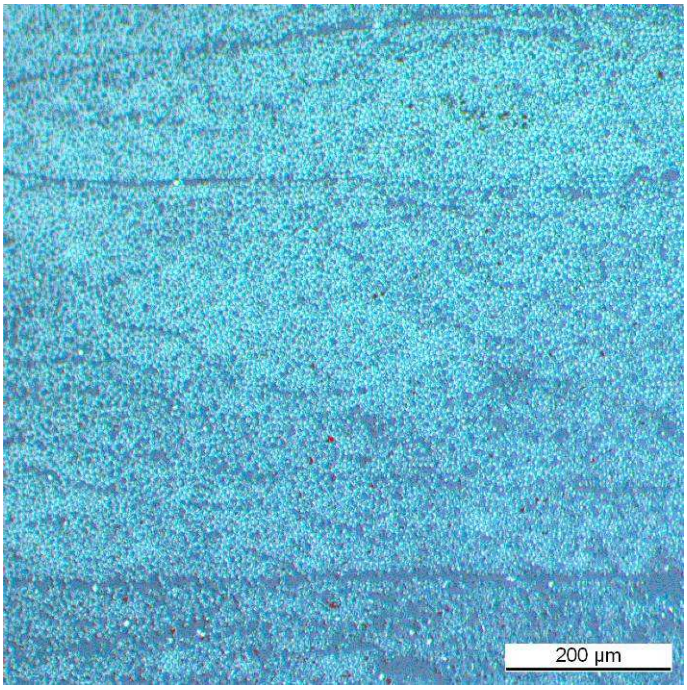

Bildname :	Bild_004992
Bearbeiter :	Robert Rudolf
Quelle :	3 Toho flat 2
Beschreibung:	
Aufnahme :	1.67*10
Präparation :	
Präparat :	3 Toho flat 2

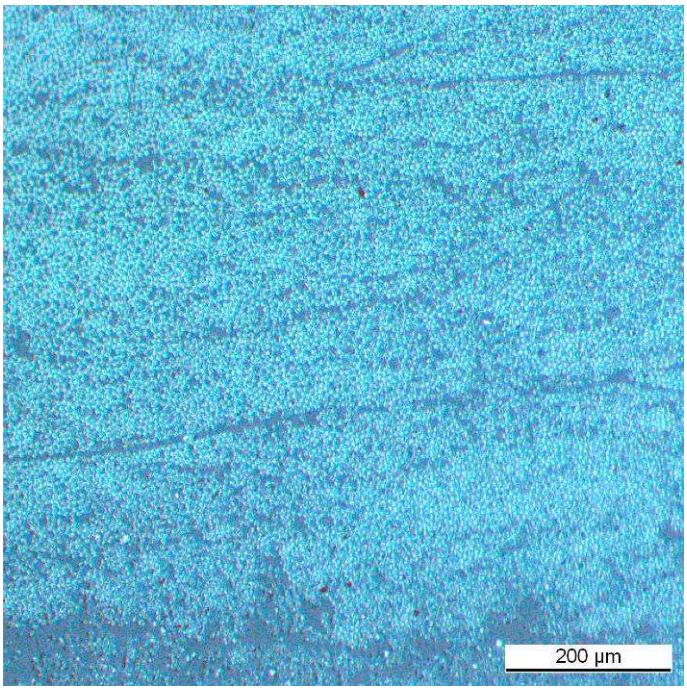

Bildname :	Bild_004993
Bearbeiter :	Robert Rudolf
Quelle :	3 Toho flat 3
Beschreibung:	
Aufnahme :	1.67*10
Präparation :	
Präparat :	3 Toho flat 3

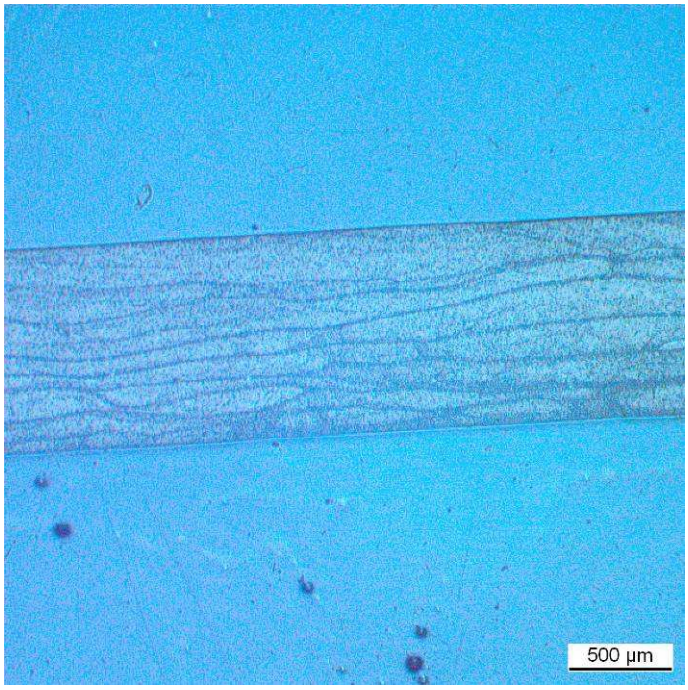

Bildname :	Bild_004994
Bearbeiter :	Robert Rudolf
Quelle :	3 Hexcel 1mm
Beschreibung:	
Aufnahme :	1.67*2.5
Präparation :	
Präparat :	3 Hexcel 1mm

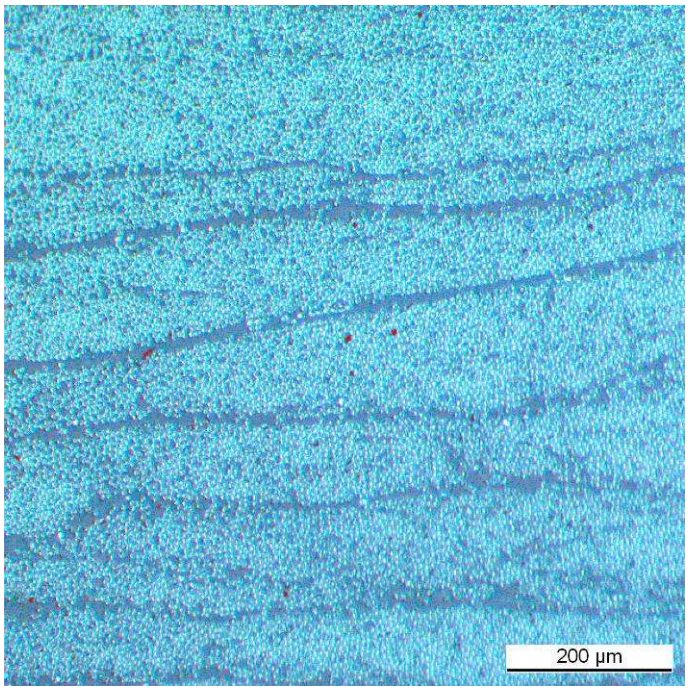

Bildname :	Bild_004995
Bearbeiter :	Robert Rudolf
Quelle :	3 Hexcel 1mm 1
Beschreibung:	
Aufnahme :	1.67*10
Präparation :	
Präparat :	3 Hexcel 1mm 1

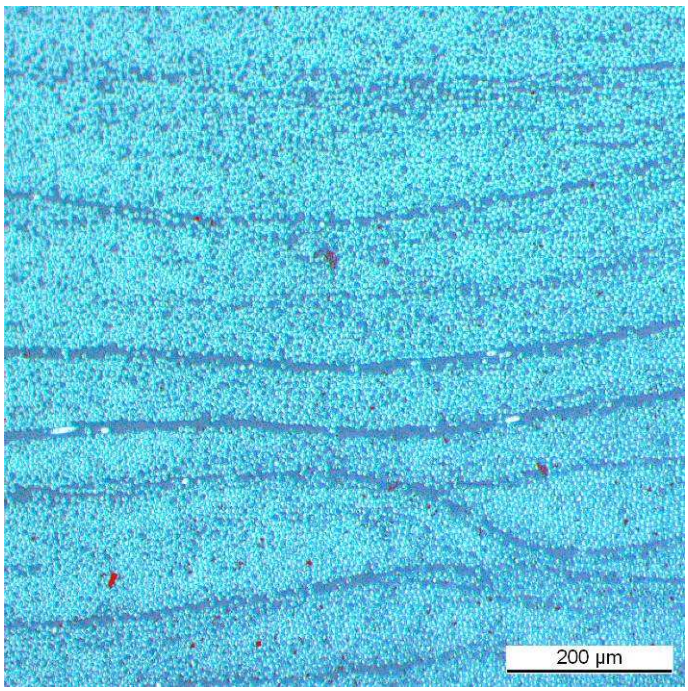

Bildname :	Bild_004996
Bearbeiter :	Robert Rudolf
Quelle :	3 Hexcel 1mm 2
Beschreibung:	
Aufnahme :	1.67*10
Präparation :	
Präparat :	3 Hexcel 1mm 2

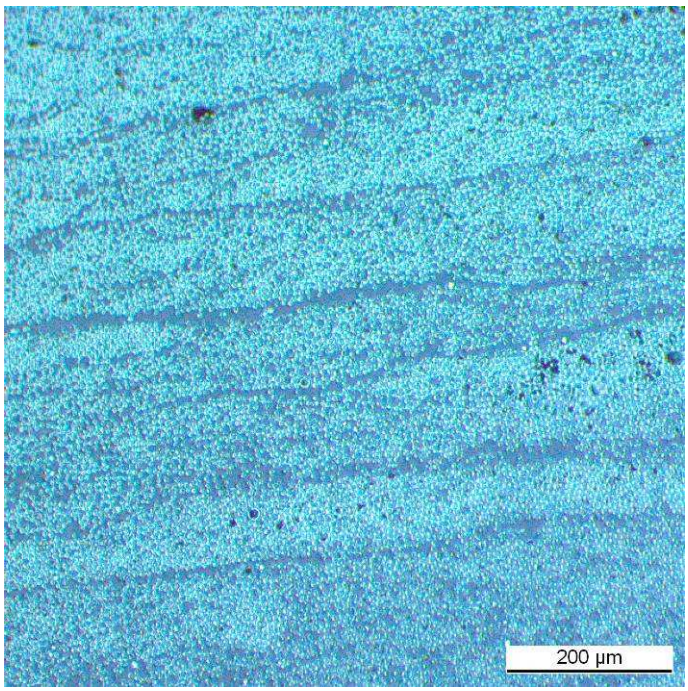

Bildname :	Bild_004997
Bearbeiter :	Robert Rudolf
Quelle :	3 Hexcel 1mm 3
Beschreibung:	
Aufnahme :	1.67*10
Präparation :	
Präparat :	3 Hexcel 1mm 3

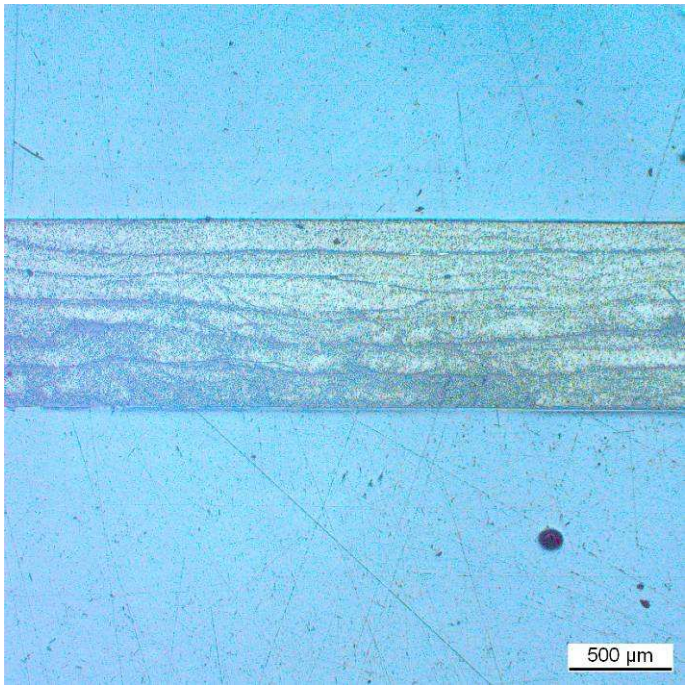

Bildname :	Bild_004999
Bearbeiter :	Robert Rudolf
Quelle :	3 Hexcel flat
Beschreibung:	
Aufnahme :	1.67*2.5
Präparation :	
Präparat :	3 Hexcel flat

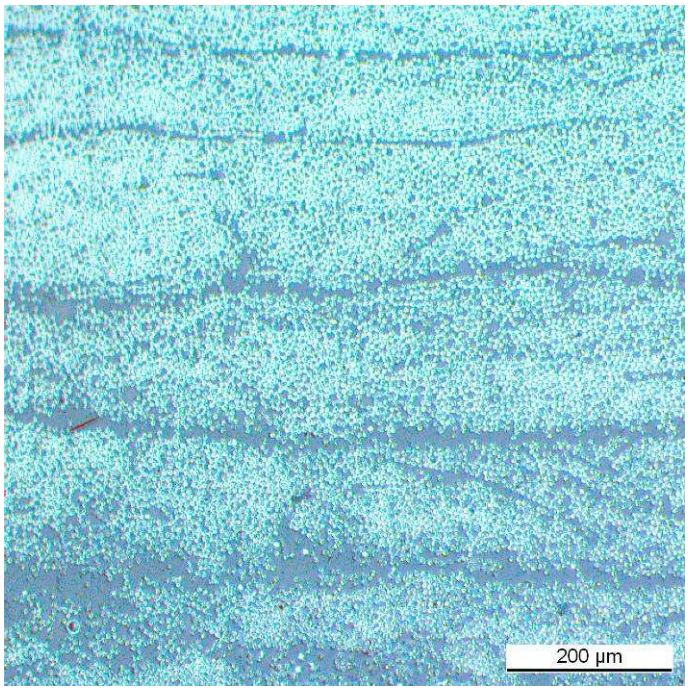

Bildname :	Bild_005000
Bearbeiter :	Robert Rudolf
Quelle :	3 Hexcel flat 1
Beschreibung:	
Aufnahme :	1.67*10
Präparation :	
Präparat :	3 Hexcel flat 1

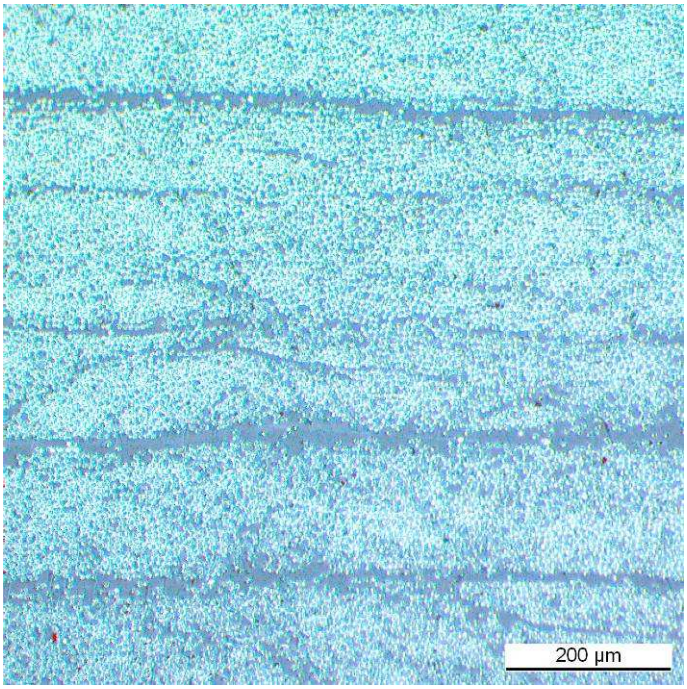

Bildname :	Bild_005001
Bearbeiter :	Robert Rudolf
Quelle :	3 Hexcel flat 2
Beschreibung:	
Aufnahme :	1.67*10
Präparation :	
Präparat :	3 Hexcel flat 2

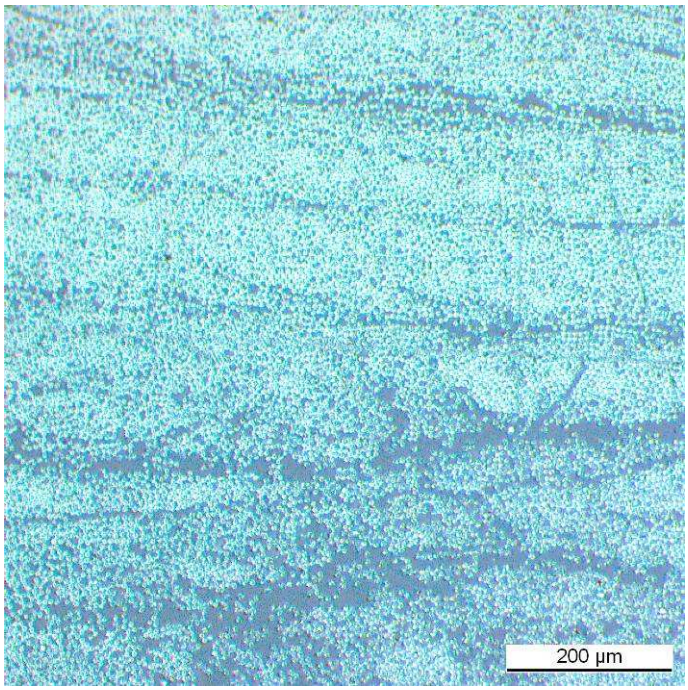

Bildname :	Bild_005002
Bearbeiter :	Robert Rudolf
Quelle :	3 Hexcel flat 3
Beschreibung:	
Aufnahme :	1.67*10
Präparation :	
Präparat :	3 Hexcel flat 3

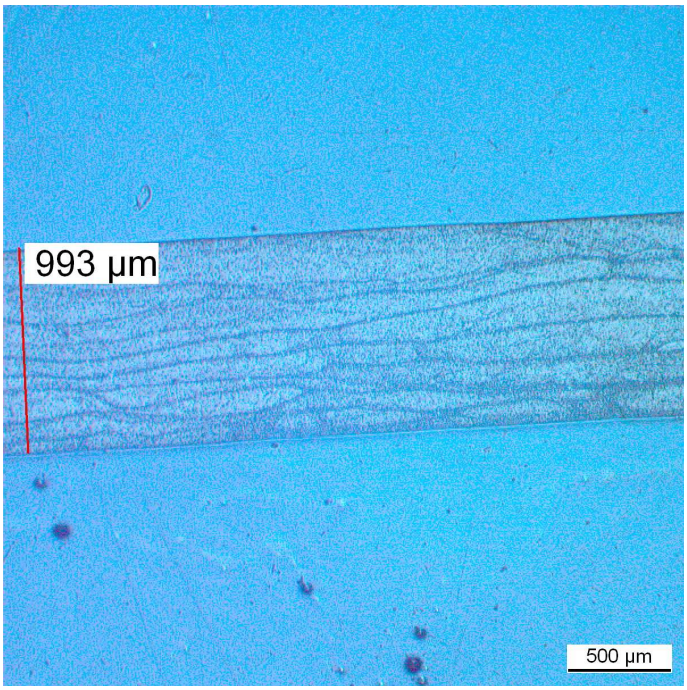

Bildname :	Bild_005084
Bearbeiter :	RR
Quelle :	3H1
Beschreibung:	
Aufnahme :	
Präparation :	
Präparat :	3H1

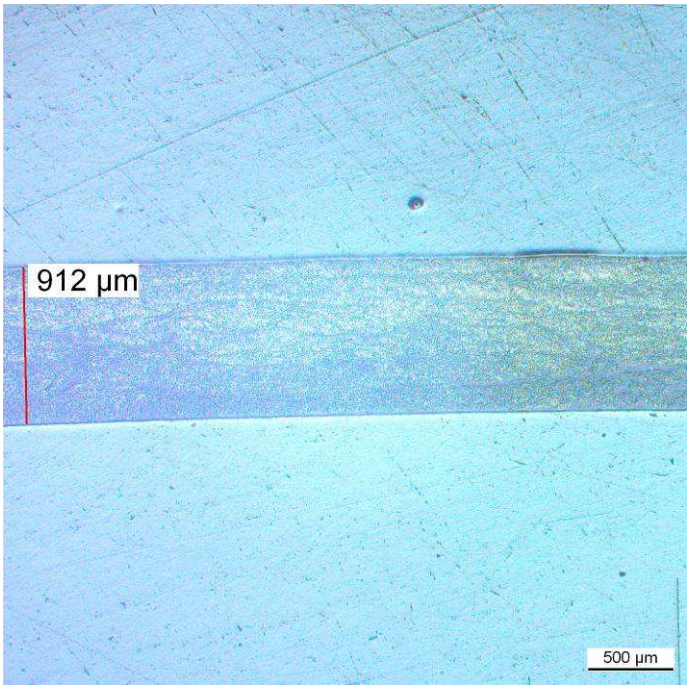

Bildname :	Bild_005086
Bearbeiter :	RR
Quelle :	3T1
Beschreibung:	
Aufnahme :	
Präparation :	
Präparat :	3T1

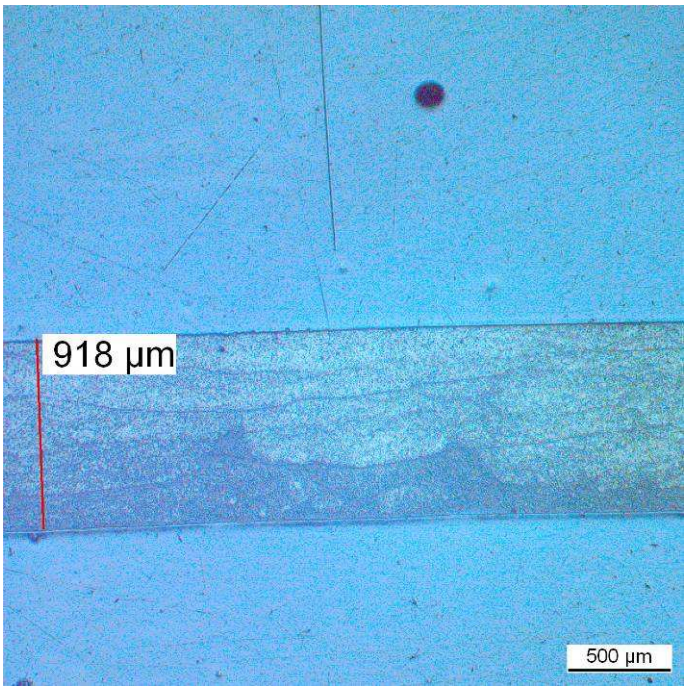

Bildname :	Bild_005087
Bearbeiter :	RR
Quelle :	3TF
Beschreibung:	
Aufnahme :	
Präparation :	
Präparat :	3TF

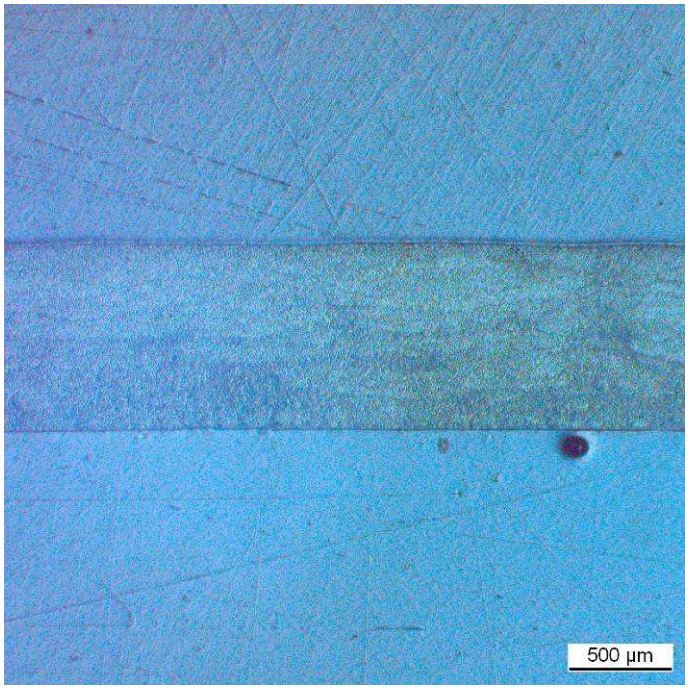

Bildname :	Bild_005022
Bearbeiter :	Robert Rudolf
Quelle :	4 Toho 1mm
Beschreibung:	
Aufnahme :	1.67*2.5
Präparation :	
Präparat :	4 Toho 1mm

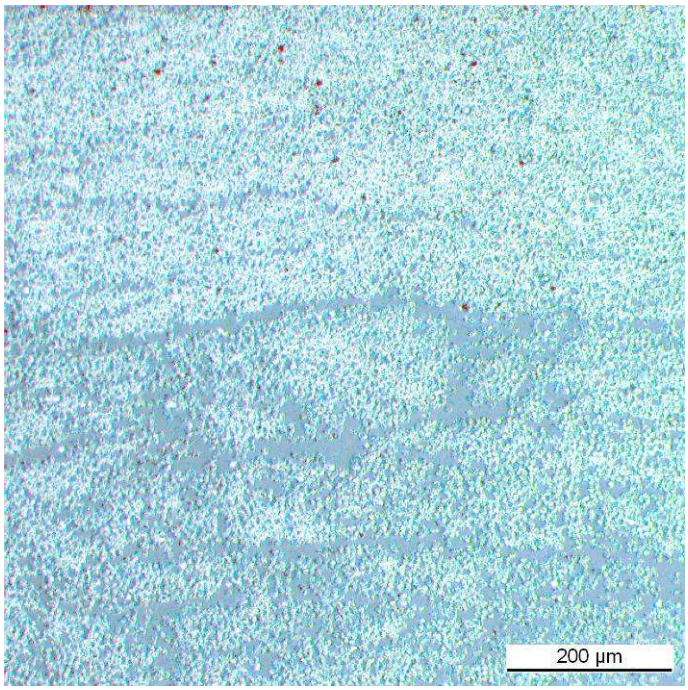

Bildname :	Bild_005024
Bearbeiter :	Robert Rudolf
Quelle :	4 Toho 1mm 1x
Beschreibung:	
Aufnahme :	1.67*10
Präparation :	
Präparat :	4 Toho 1mm 1x

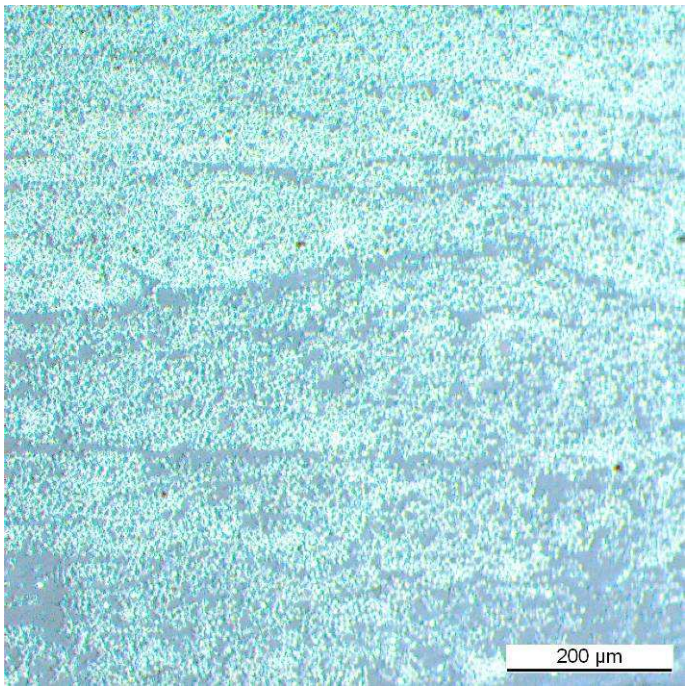

Bildname :	Bild_005025
Bearbeiter :	Robert Rudolf
Quelle :	4 Toho 1mm 2
Beschreibung:	
Aufnahme :	1.67*10
Präparation :	
Präparat :	4 Toho 1mm 2

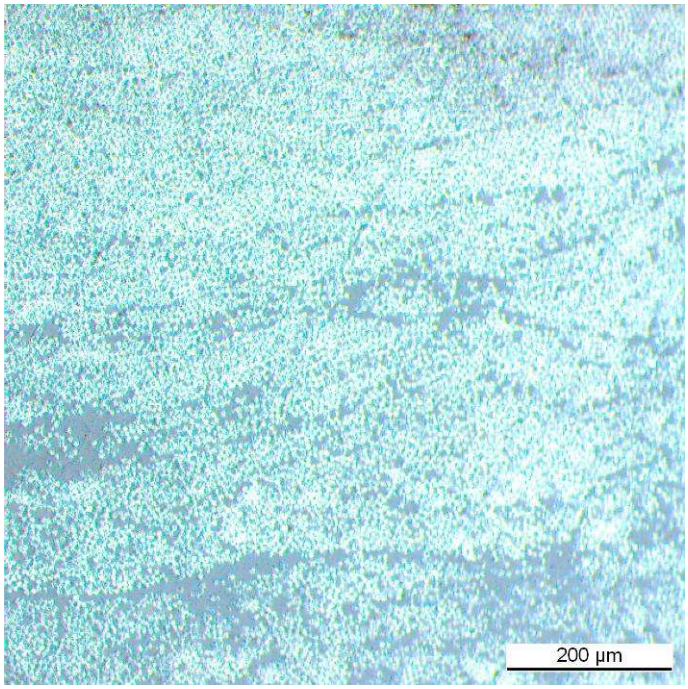

Bildname :	Bild_005026
Bearbeiter :	Robert Rudolf
Quelle :	4 Toho 1mm 3
Beschreibung:	
Aufnahme :	1.67*10
Präparation :	
Präparat :	4 Toho 1mm 3

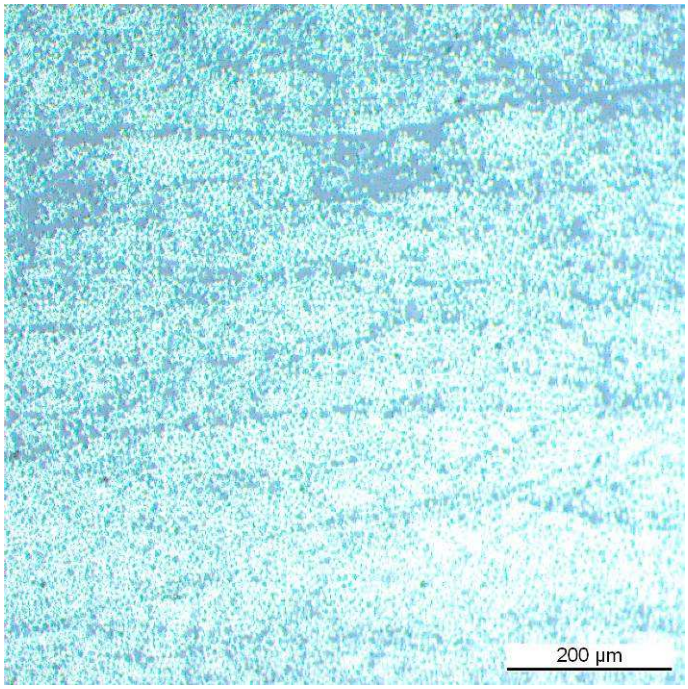

Bildname :	Bild_005028
Bearbeiter :	Robert Rudolf
Quelle :	4 Toho flat 1
Beschreibung:	
Aufnahme :	1.67*10
Präparation :	
Präparat :	4 Toho flat 1

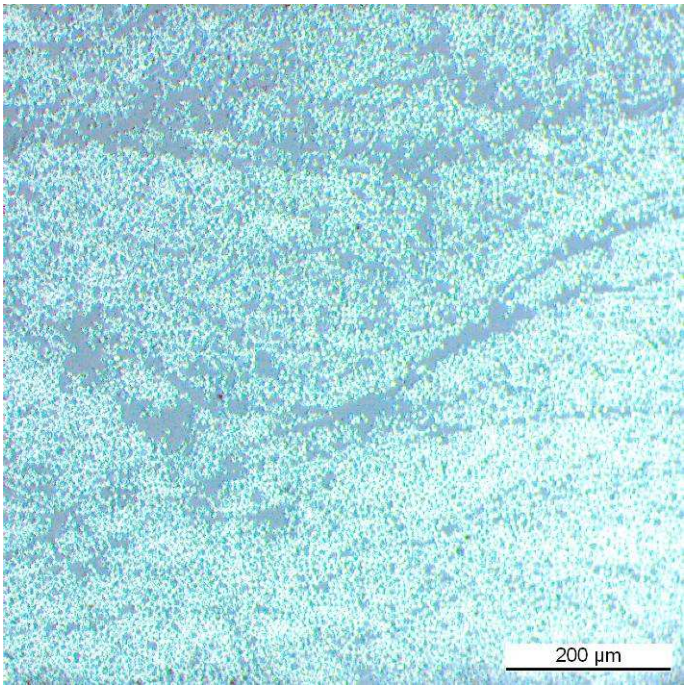

Bildname :	Bild_005029
Bearbeiter :	Robert Rudolf
Quelle :	4 Toho flat 2
Beschreibung:	
Aufnahme :	1.67*10
Präparation :	
Präparat :	4 Toho flat 2

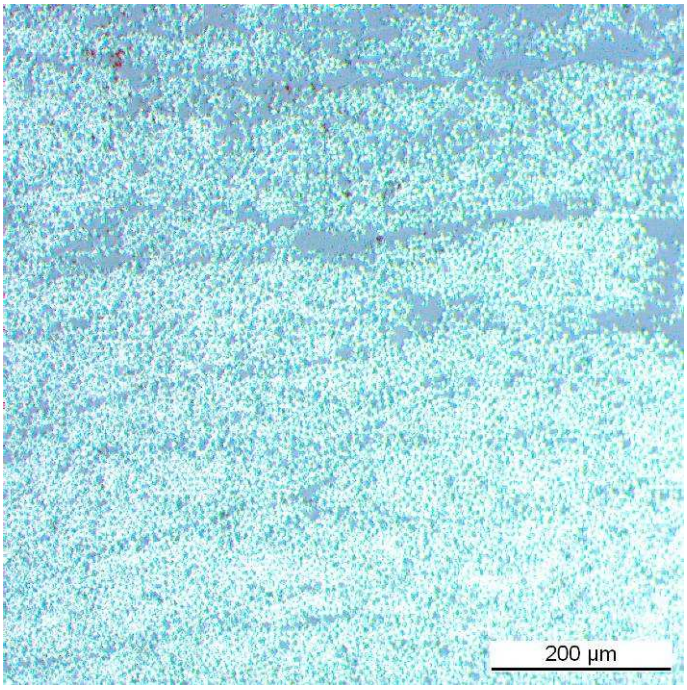

Bildname :	Bild_005030
Bearbeiter :	Robert Rudolf
Quelle :	4 Toho flat 3
Beschreibung:	
Aufnahme :	1.67*10
Präparation :	
Präparat :	4 Toho flat 3

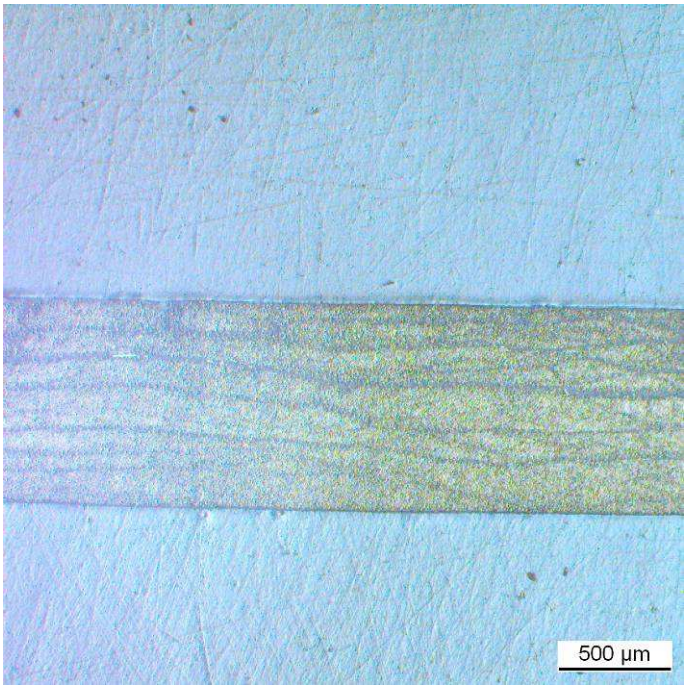

Bildname :	Bild_005031
Bearbeiter :	Robert Rudolf
Quelle :	4 Hexcel 1mm
Beschreibung:	
Aufnahme :	1.67*2.5
Präparation :	
Präparat :	4 Hexcel 1mm

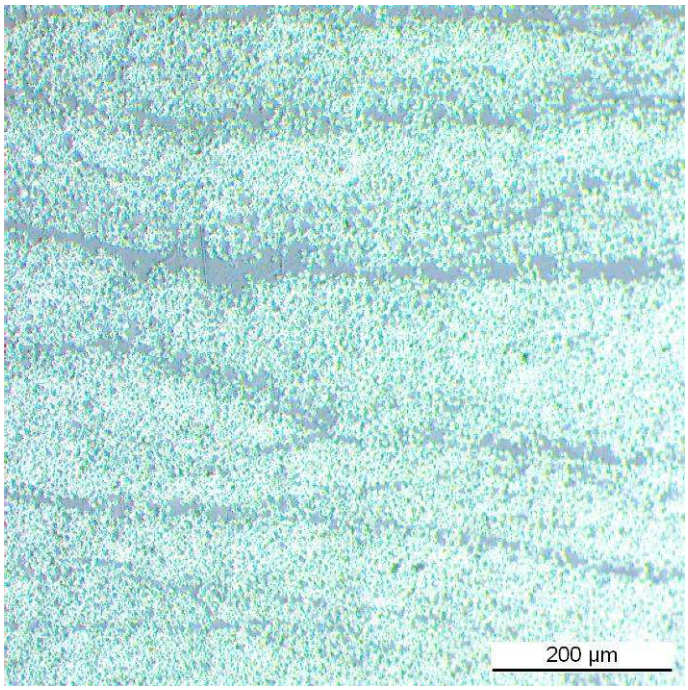

Bildname :	Bild_005032
Bearbeiter :	Robert Rudolf
Quelle :	4 Hexcel 1mm 1
Beschreibung:	
Aufnahme :	1.67*10
Präparation :	
Präparat :	4 Hexcel 1mm 1

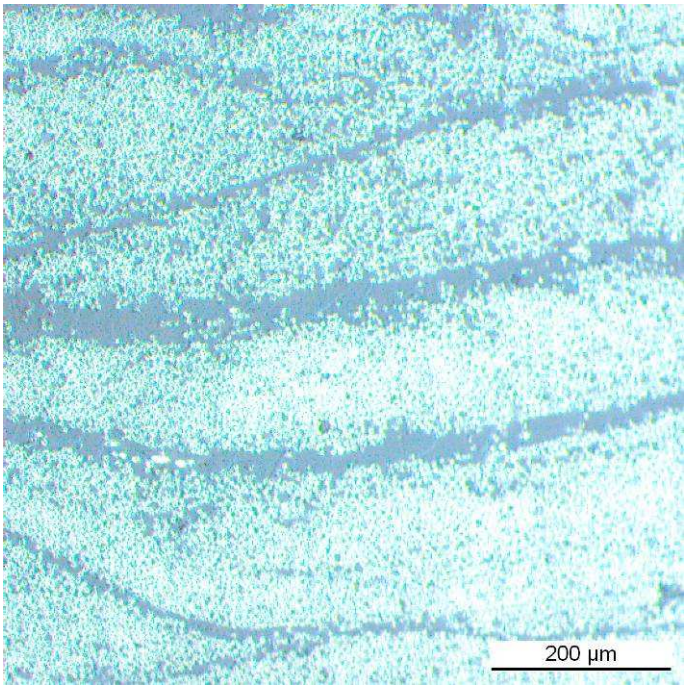

Bildname :	Bild_005033
Bearbeiter :	Robert Rudolf
Quelle :	4 Hexcel 1mm 2
Beschreibung:	
Aufnahme :	1.67*10
Präparation :	
Präparat :	4 Hexcel 1mm 2

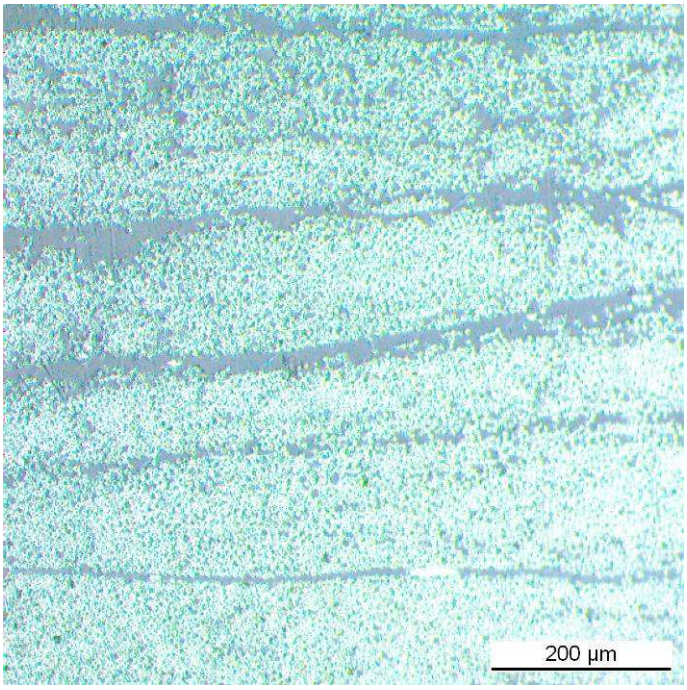

Bildname :	Bild_005034
Bearbeiter :	Robert Rudolf
Quelle :	4 Hexcel 1mm 3
Beschreibung:	
Aufnahme :	1.67*10
Präparation :	
Präparat :	4 Hexcel 1mm 3

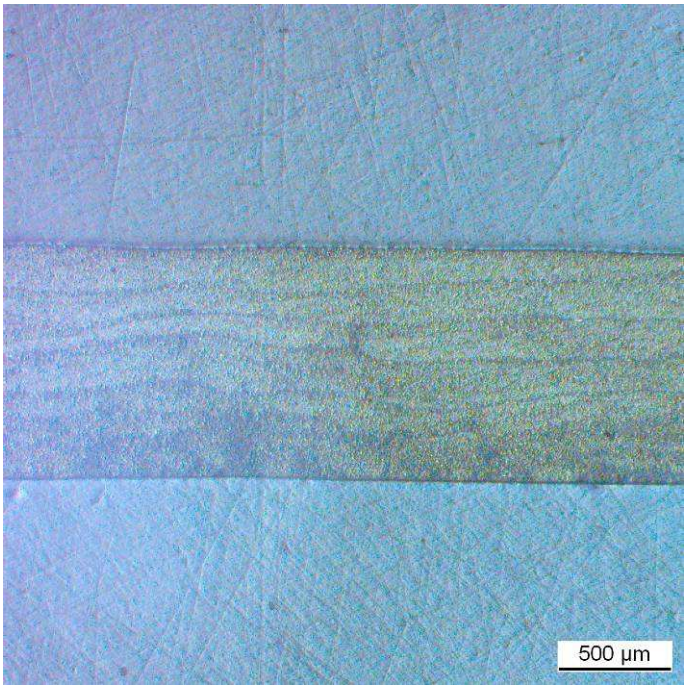

Bildname :	Bild_005035
Bearbeiter :	Robert Rudolf
Quelle :	4 Hexcel flat
Beschreibung:	
Aufnahme :	1.67*2.5
Präparation :	
Präparat :	4 Hexcel flat

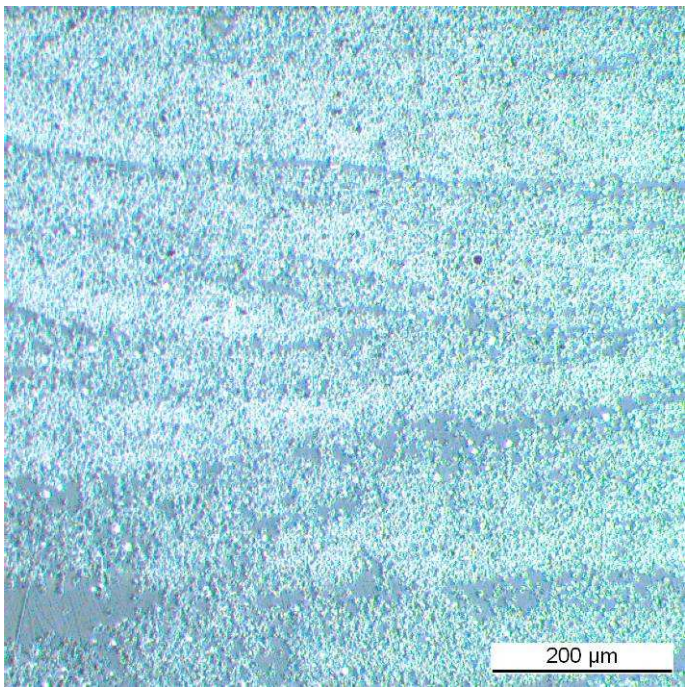

Bildname :	Bild_005036
Bearbeiter :	Robert Rudolf
Quelle :	4 Hexcel flat 1
Beschreibung:	
Aufnahme :	1.67*10
Präparation :	
Präparat :	4 Hexcel flat 1

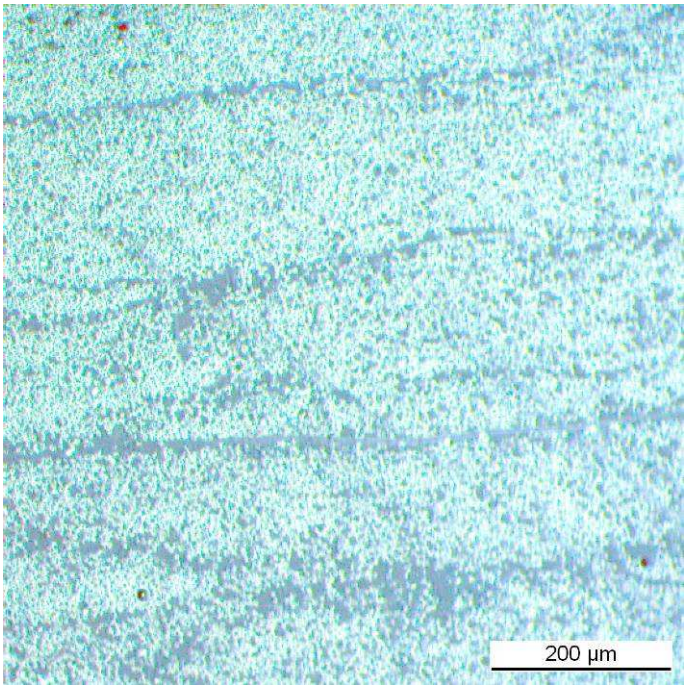

Bildname :	Bild_005037
Bearbeiter :	Robert Rudolf
Quelle :	4 Hexcel flat 2
Beschreibung:	
Aufnahme :	1.67*10
Präparation :	
Präparat :	4 Hexcel flat 2

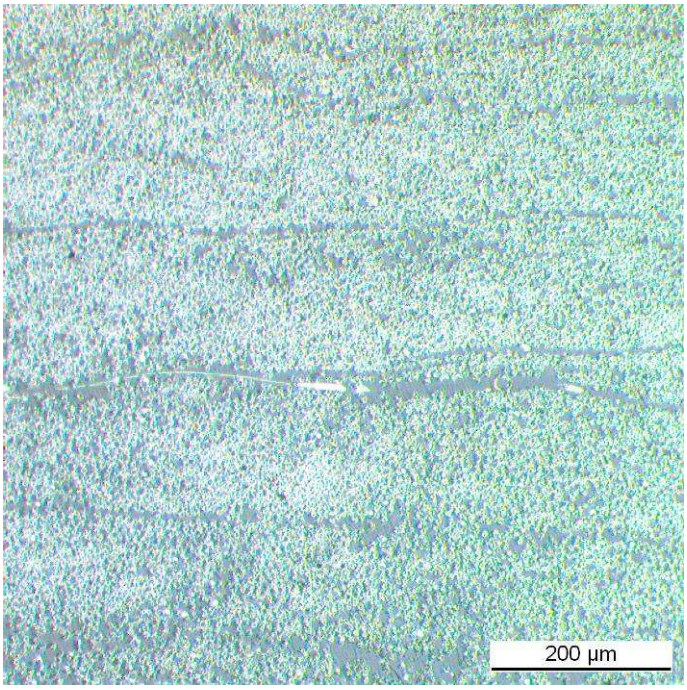

Bildname :	Bild_005039
Bearbeiter :	Robert Rudolf
Quelle :	4 Hexcel flat 3
Beschreibung:	
Aufnahme :	1.67*10
Präparation :	
Präparat :	4 Hexcel flat 3

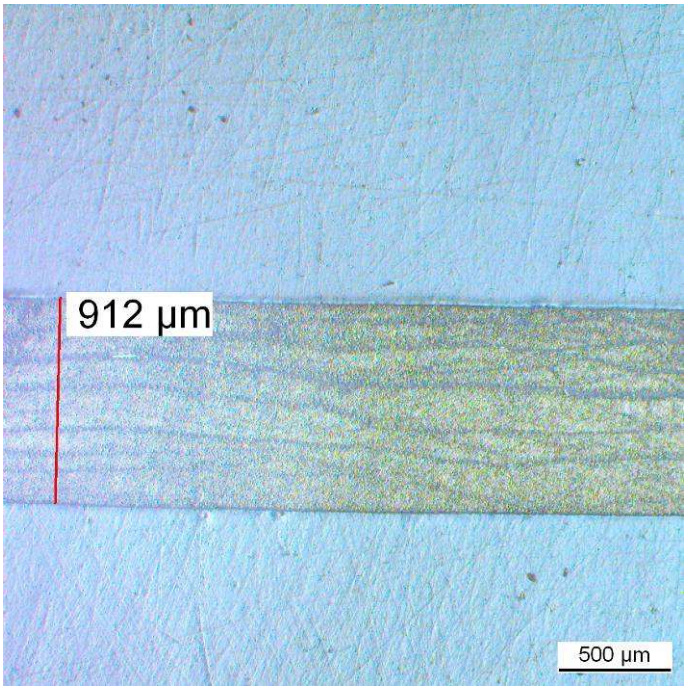

Bildname :	Bild_005088
Bearbeiter :	RR
Quelle :	4H1
Beschreibung:	
Aufnahme :	
Präparation :	
Präparat :	4H1

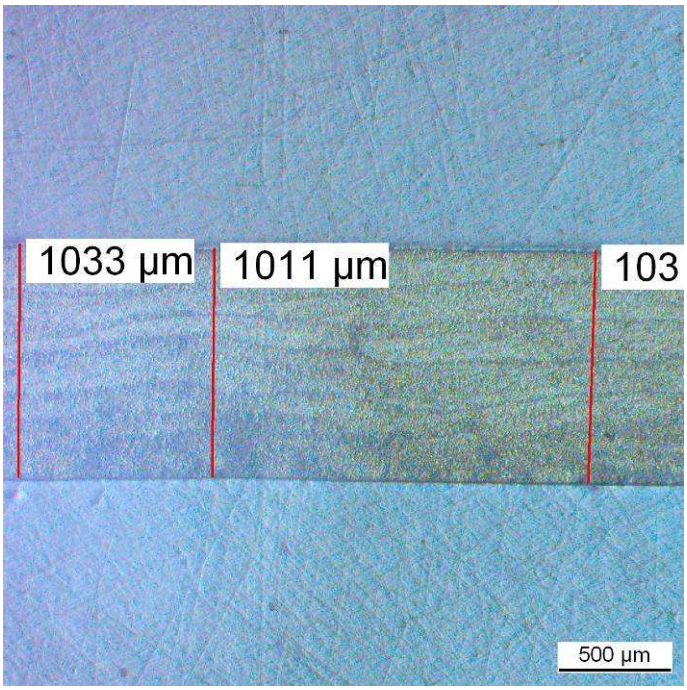

Bildname :	Bild_005089
Bearbeiter :	RR
Quelle :	4Hf
Beschreibung:	
Aufnahme :	
Präparation :	
Präparat :	4HF

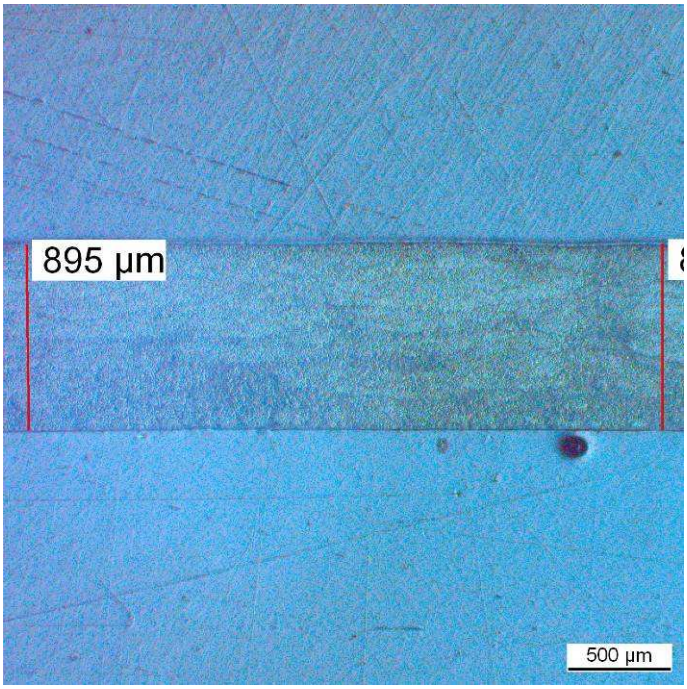

Bildname :	Bild_005090
Bearbeiter :	RR
Quelle :	4T1
Beschreibung:	
Aufnahme :	
Präparation :	
Präparat :	4T1

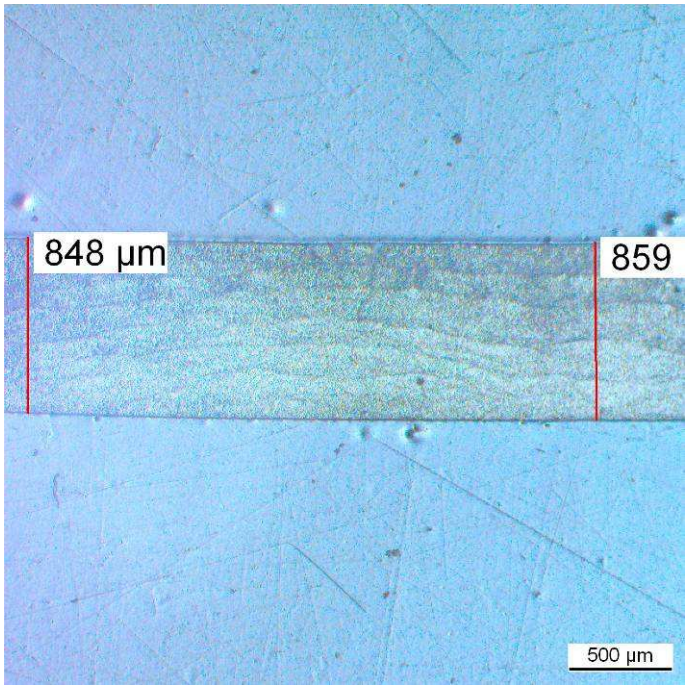

Bildname :	Bild_005091
Bearbeiter :	RR
Quelle :	4TF
Beschreibung:	
Aufnahme :	
Präparation :	
Präparat :	4TF

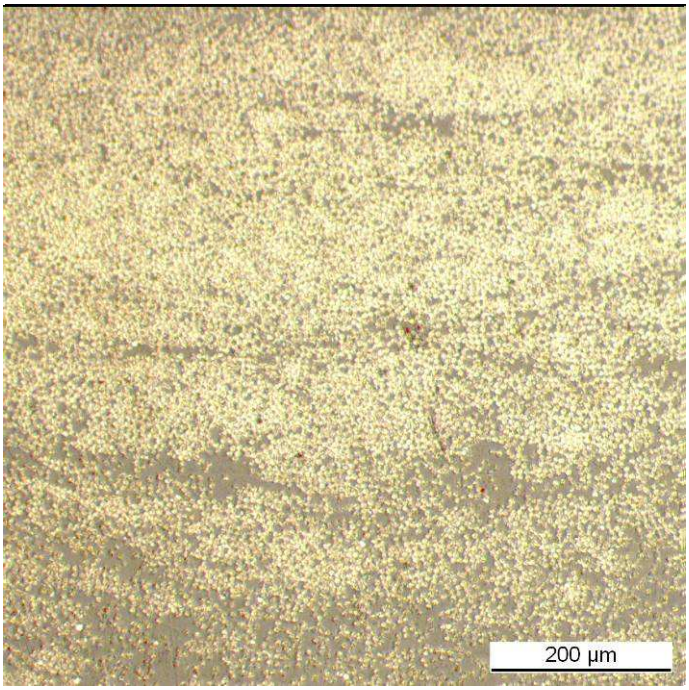

Bildname :	Bild_005058
Bearbeiter :	Robert Rudolf
Quelle :	5 Toho 1mm 1
Beschreibung:	
Aufnahme :	1.67*10
Präparation :	
Präparat :	5 Toho 1mm 1

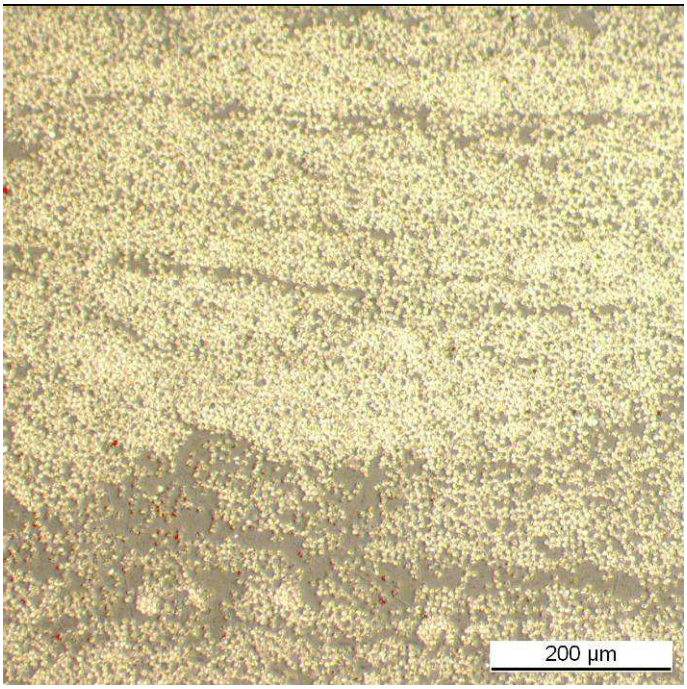

Bildname :	Bild_005059
Bearbeiter :	Robert Rudolf
Quelle :	5 Toho 1mm 2
Beschreibung:	
Aufnahme :	1.67*10
Präparation :	
Präparat :	5 Toho 1mm 2

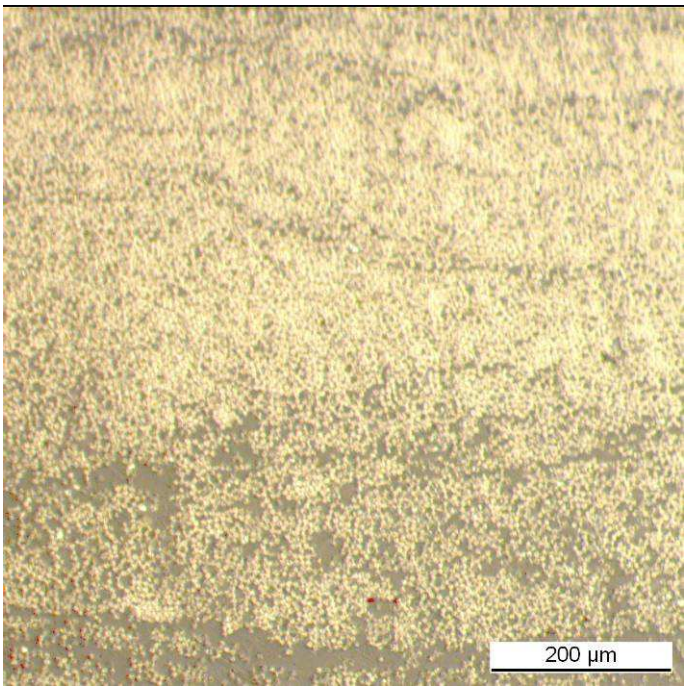

Bildname :	Bild_005060
Bearbeiter :	Robert Rudolf
Quelle :	5 Toho 1mm 3
Beschreibung:	
Aufnahme :	1.67*10
Präparation :	
Präparat :	5 Toho 1mm 3

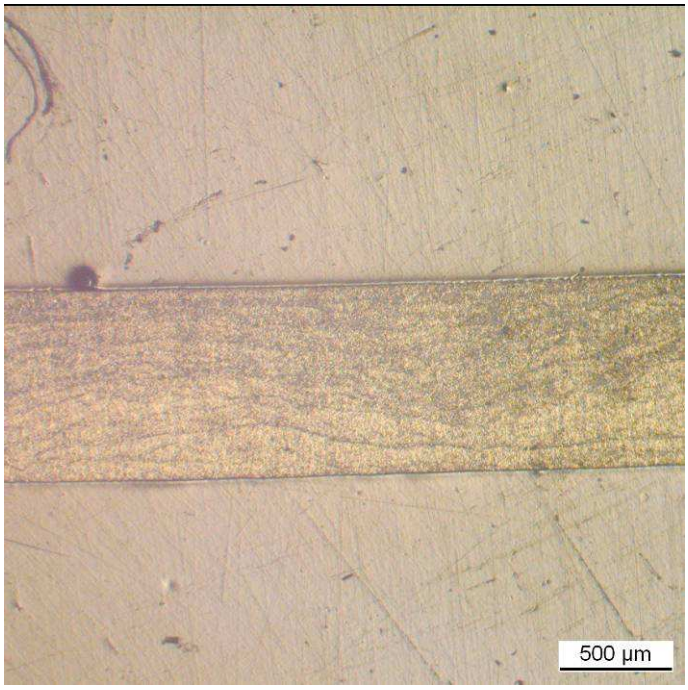

Bildname :	Bild_005061
Bearbeiter :	Robert Rudolf
Quelle :	5 Toho flat
Beschreibung:	
Aufnahme :	1.67*2.5
Präparation :	
Präparat :	5 Toho flat

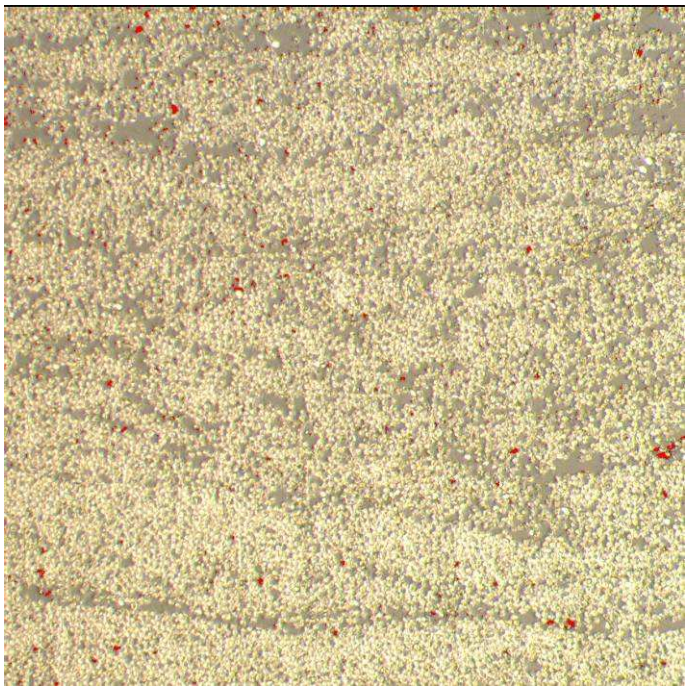

Bildname :	Bild_005062
Bearbeiter :	RR
Quelle :	5 Toho flat 1
Beschreibung:	
Aufnahme :	1.67*10
Präparation :	
Präparat :	5 Toho flat 1

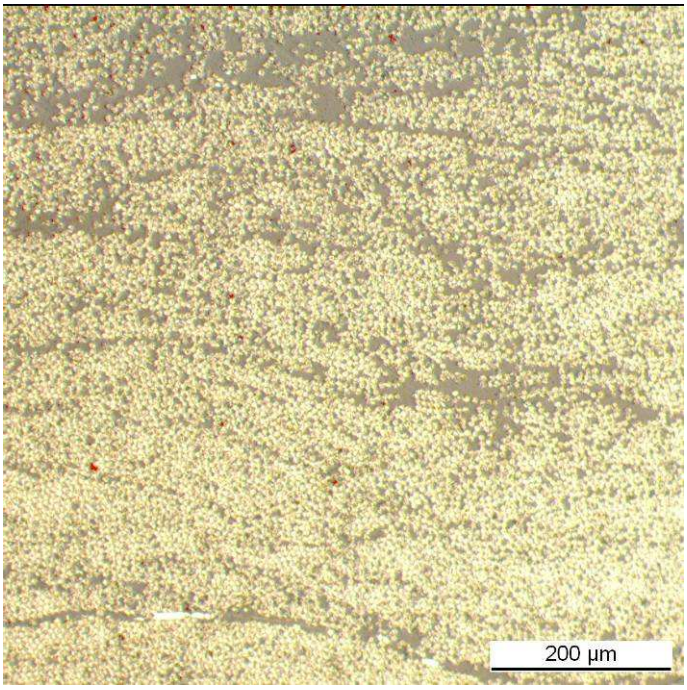

Bildname :	Bild_005063
Bearbeiter :	RR
Quelle :	5 Toho flat 2
Beschreibung:	
Aufnahme :	1.67*10
Präparation :	
Präparat :	5 Toho flat 2

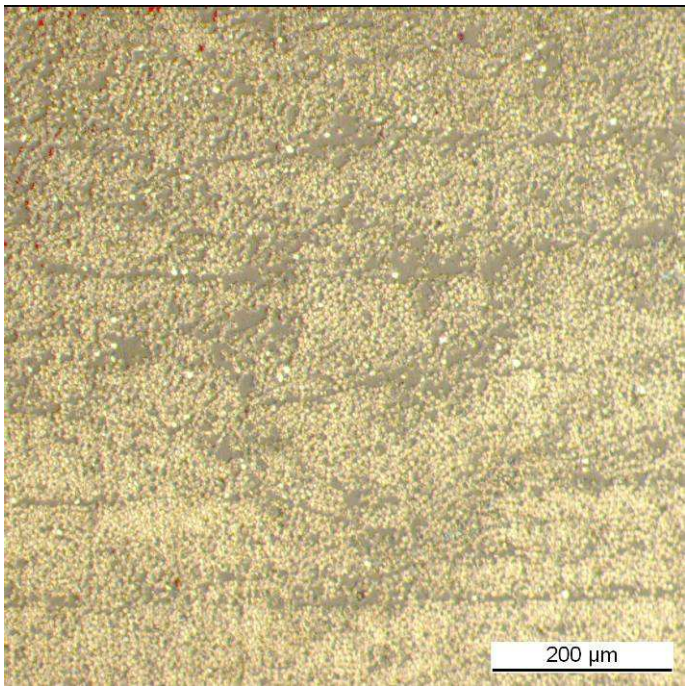

Bildname :	Bild_005064
Bearbeiter :	RR
Quelle :	5 Toho flat 3
Beschreibung:	
Aufnahme :	1.67*10
Präparation :	
Präparat :	5 Toho flat 3

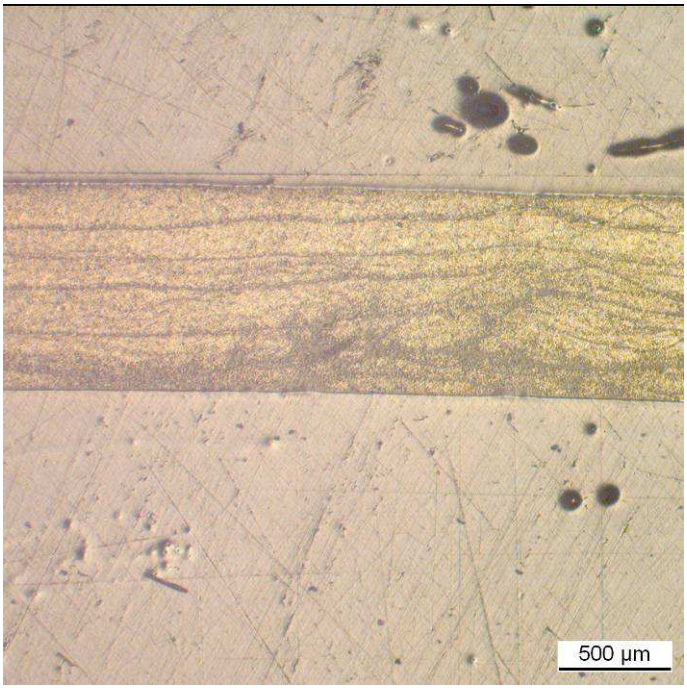

Bildname :	Bild_005065
Bearbeiter :	RR
Quelle :	5 Hexcel 1mm
Beschreibung:	
Aufnahme :	1.67*2.5
Präparation :	
Präparat :	5 Hexcel 1mm

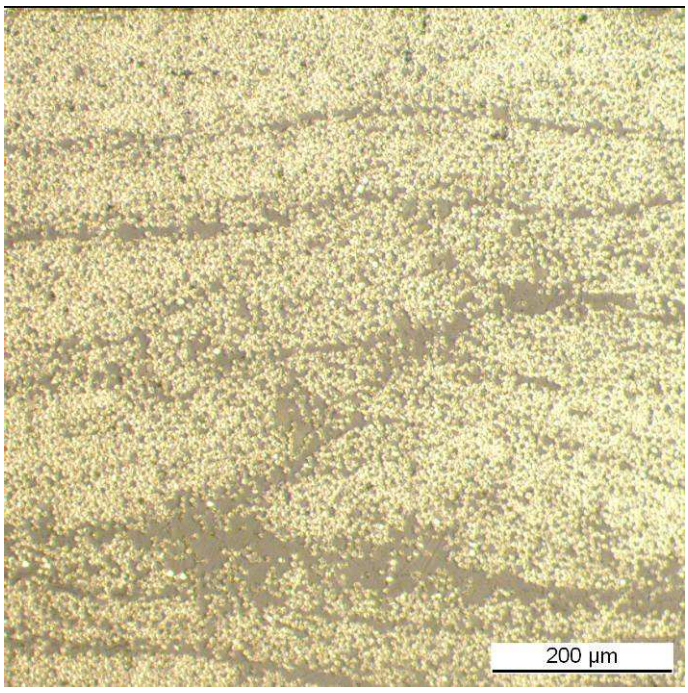

Bildname :	Bild_005066
Bearbeiter :	RR
Quelle :	5 Hexcel 1mm 1
Beschreibung:	
Aufnahme :	1.67*2.5
Präparation :	
Präparat :	5 Hexcel 1mm 1

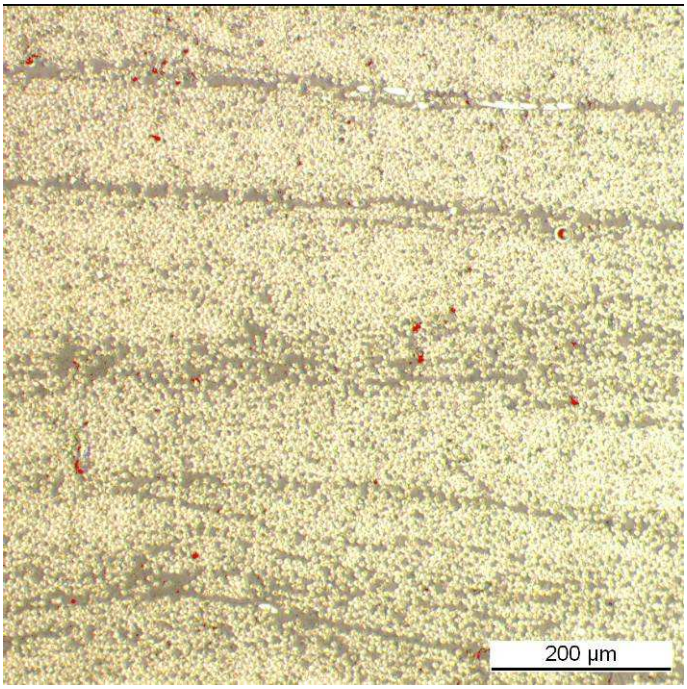

Bildname :	Bild_005067
Bearbeiter :	RR
Quelle :	5 Hexcel 1mm 2
Beschreibung:	
Aufnahme :	1.67*2.5
Präparation :	
Präparat :	5 Hexcel 1mm 2

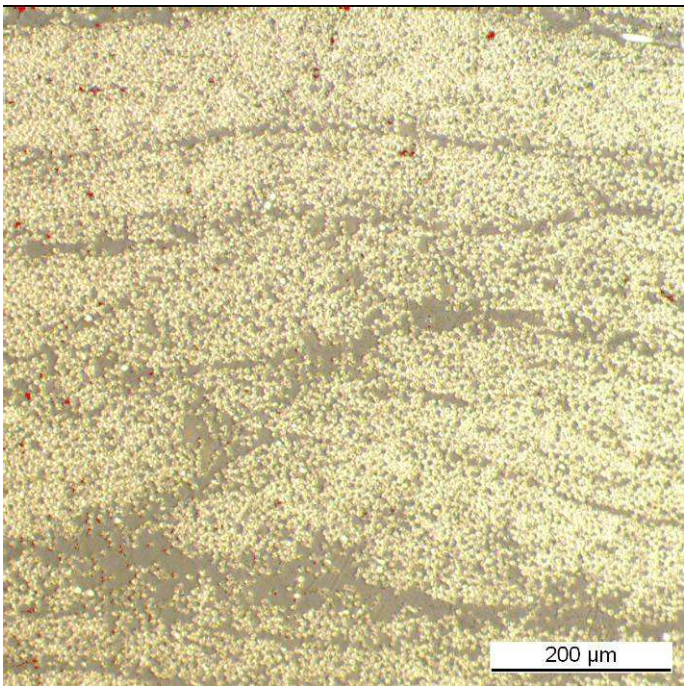

Bildname :	Bild_005068
Bearbeiter :	RR
Quelle :	5 Hexcel 1mm 3
Beschreibung:	
Aufnahme :	1.67*2.5
Präparation :	
Präparat :	5 Hexcel 1mm 3

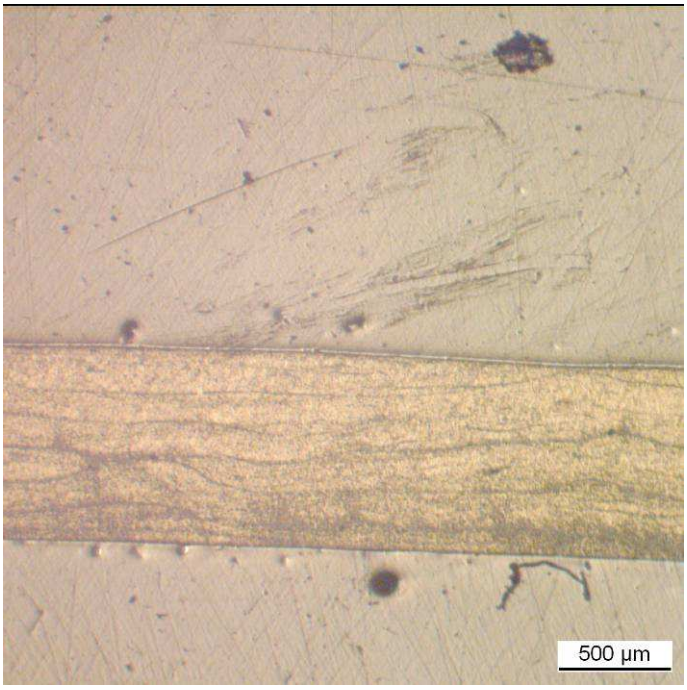

Bildname :	Bild_005069
Bearbeiter :	RR
Quelle :	5 Hexcel flat
Beschreibung:	
Aufnahme :	1.67*2.5
Präparation :	
Präparat :	5 Hexcel flat

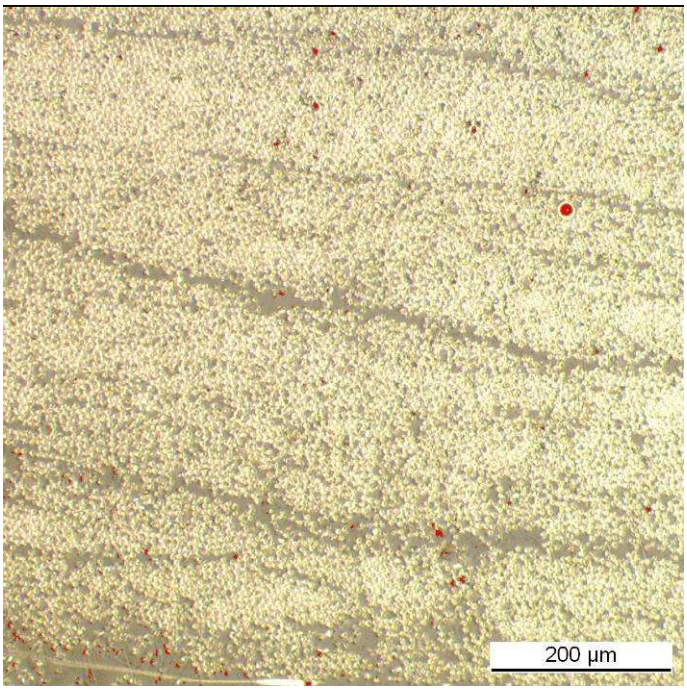

Bildname :	Bild_005070
Bearbeiter :	RR
Quelle :	5 Hexcel flat 1
Beschreibung:	
Aufnahme :	1.67*10
Präparation :	
Präparat :	5 Hexcel flat 1

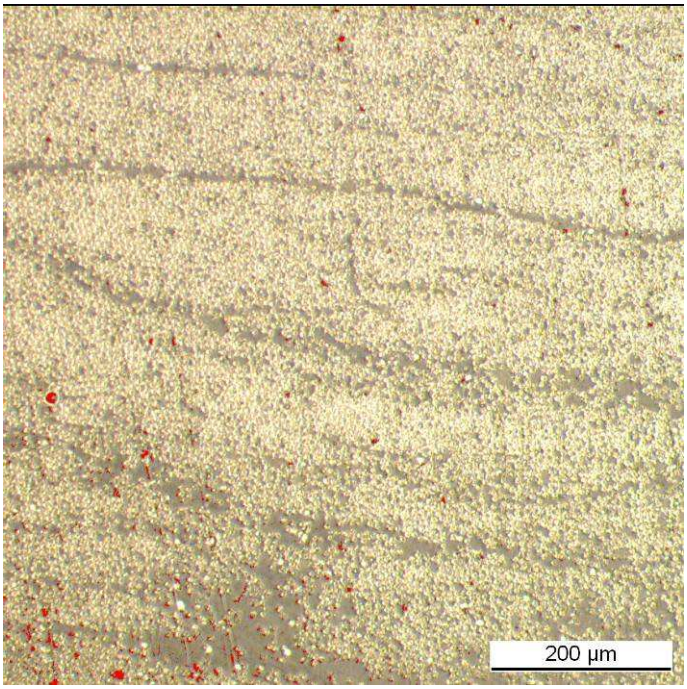

Bildname :	Bild_005071
Bearbeiter :	RR
Quelle :	5 Hexcel flat 2
Beschreibung:	
Aufnahme :	1.67*10
Präparation :	
Präparat :	5 Hexcel flat 2

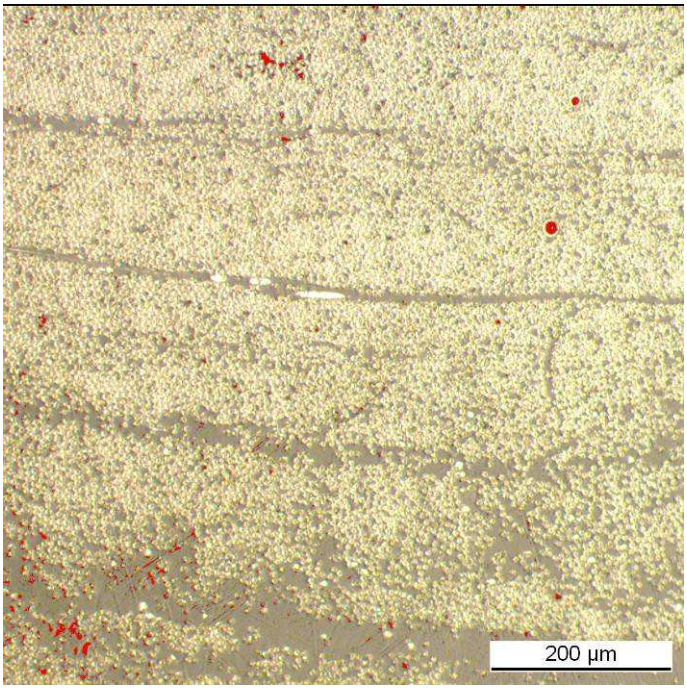

Bildname :	Bild_005072
Bearbeiter :	RR
Quelle :	5 Hexcel flat 3
Beschreibung:	
Aufnahme :	1.67*10
Präparation :	
Präparat :	5 Hexcel flat 3

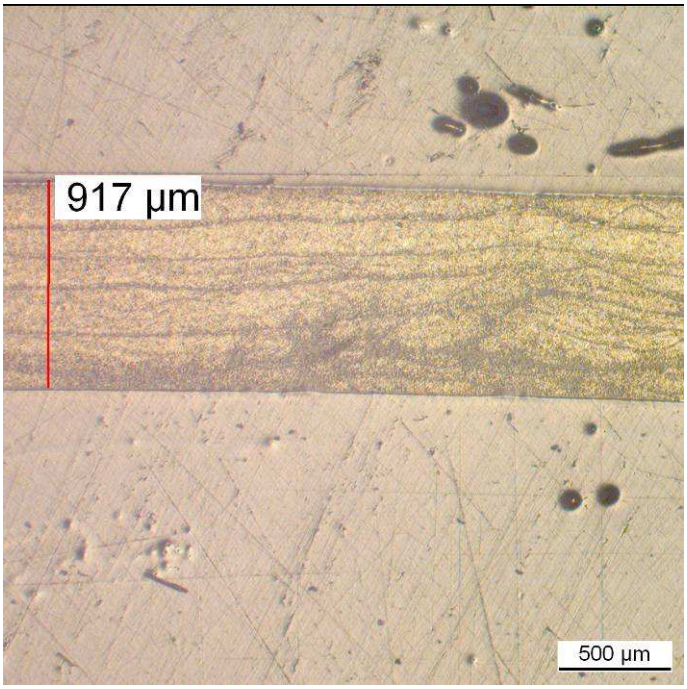

Bildname :	Bild_005092
Bearbeiter :	RR
Quelle :	5H1
Beschreibung:	
Aufnahme :	
Präparation :	
Präparat :	5H1

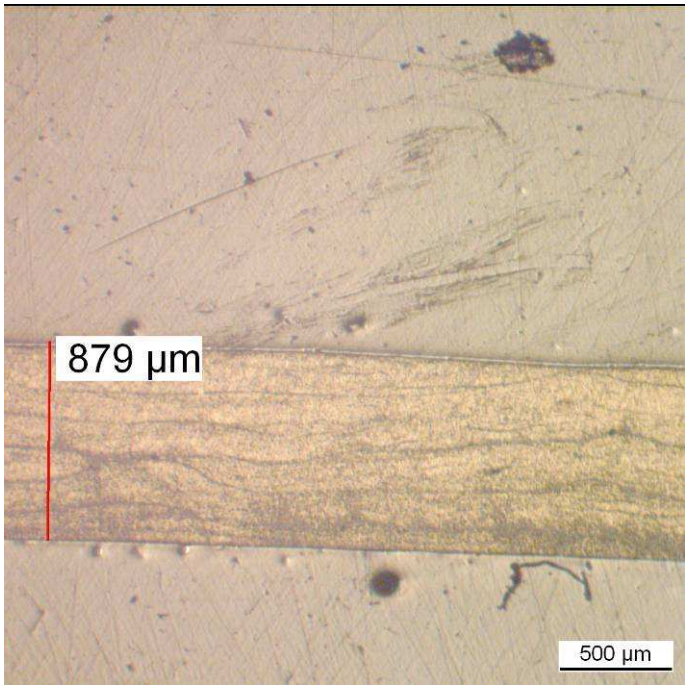

Bildname :	Bild_005093
Bearbeiter :	RR
Quelle :	5HF
Beschreibung:	
Aufnahme :	
Präparation :	
Präparat :	5HF

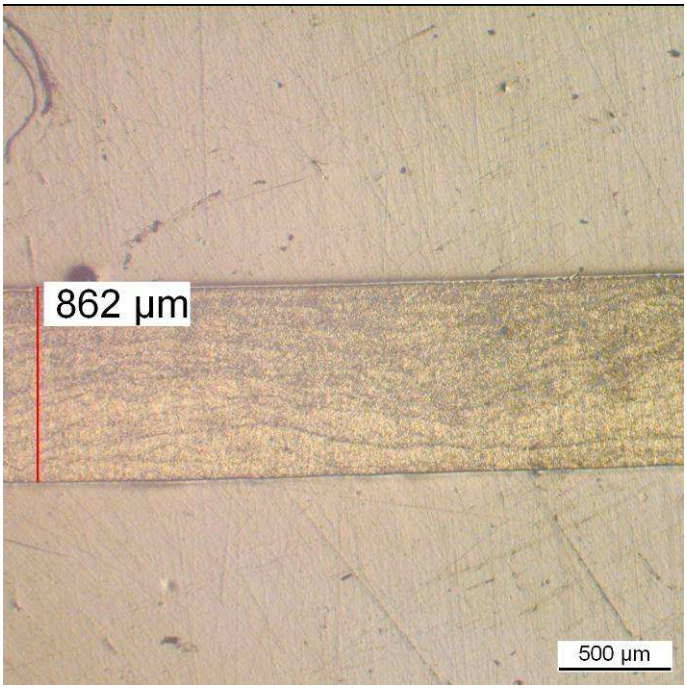

Bildname :	Bild_005094
Bearbeiter :	Robert Rudolf
Quelle :	5 Toho flat
Beschreibung:	
Aufnahme :	1.67*2.5
Präparation :	
Präparat :	5 Toho flat

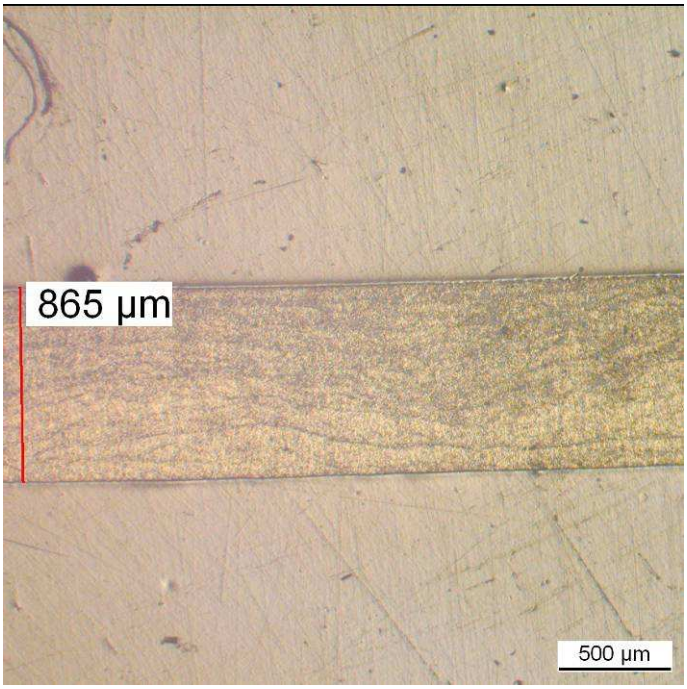

Bildname :	Bild_005075
Bearbeiter :	RR
Quelle :	5tf
Beschreibung:	
Aufnahme :	
Präparation :	
Präparat :	5tf

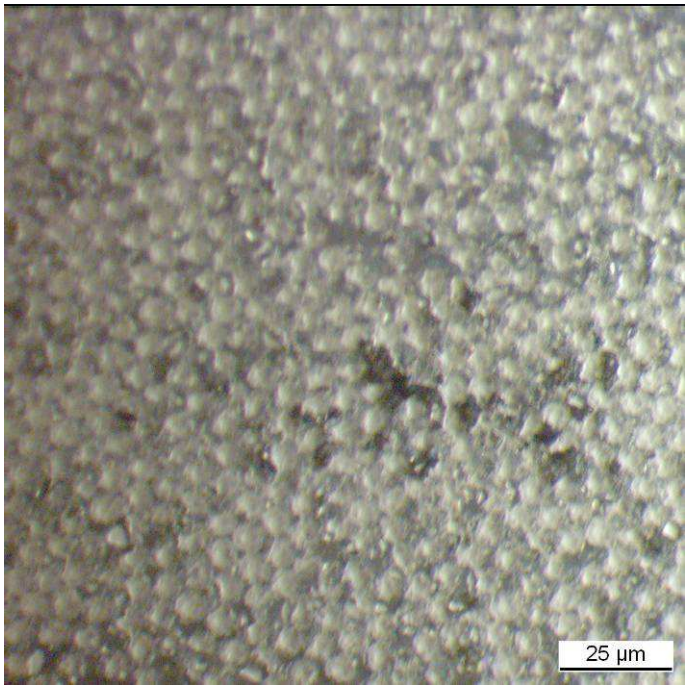

Bildname :	Bild_005073
Bearbeiter :	RR
Quelle :	holz 5tf
Beschreibung:	
Aufnahme :	1.67*50
Präparation :	
Präparat :	holz 5tf

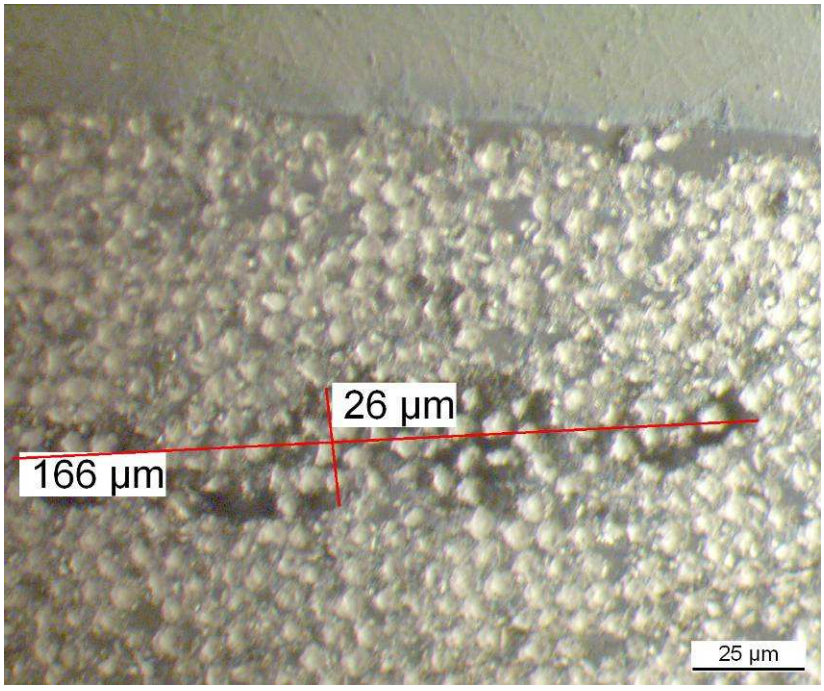

Bildname :	Bild_005074
Bearbeiter :	RR
Quelle :	holz 5tf
Beschreibung:	
Aufnahme :	1.67*50
Präparation :	
Präparat :	holz 5tf

Appendix H

HUBER+SUHNER
PHYSIKLABOR, CH-8330 PFÄFFIKON

09.02.10 11:26

Parametertabelle:

Prüfnorm	**: EN 20 178/ISO 178**
Material	**: Carbon PFA**
Prüfer	**: Robert Rudolf**
Beginn E-Modulermittlung	**: 0.05 %**
Ende E-Modulermittlung	**: 0.25 %**
Geschwindigkeit E-Modul	**: 2 mm/min**
Prüfgeschwindigkeit	**: 1 mm/min**
Stützweite L = (16 ±1) * h	**: 45 mm**
Maschinendaten	**: 144503 WN:103931**
	Traversenwegaufnehmer WN:103931
	Kraftsensor ID:1 WN:111937 500 N

Ergebnisse:

Nr	a0 mm	b0 mm	L = (16±1) * h mm	Biegemodul MPa	σfC MPa	σfM MPa	εfM %	σfB MPa	εfB %	ε-Bruch mm	ε-F max mm
1	1.03	15.25	45	80282.63	-	426.34	0.52	298.30	0.57	1.91	1.76
2	1.03	15.25	45	71165.46	-	434.38	0.62	424.54	0.62	2.05	2.04
3	1.01	14.93	45	78361.85	192.40	456.09	0.58	-	-	-	1.93
4	1.04	15.34	45	70625.26	190.01	439.37	0.60	-	-	-	1.96

Statistik:

Serie n = 4	a0 mm	b0 mm	L = (16±1) * h mm	Biegemodul MPa	σfC MPa	σfM MPa	εfM %	σfB MPa	εfB %	ε-Bruch mm	ε-F max mm
$\bar{x}$	1.03	15.19	45	75109.05	191.20	439.05	0.58	361.42	0.60	1.98	1.92
s	0.01	0.18	0.000	4932.67	1.69	12.57	0.04	89.27	0.04	0.10	0.12
v	1.22	1.19	0.00	6.57	0.88	2.86	7.61	24.70	6.93	4.84	6.17
med	1.03	15.25	45	74763.66	191.20	436.88	0.59	361.42	0.60	1.98	1.95

HUBER+SUHNER
PHYSIKLABOR, CH-8330 PFÄFFIKON

09.02.10 11:26

Prüfnorm	**: EN 20 178/ISO 178**
Material	**: Carbon PFA**
Prüfer	**: Robert Rudolf**
Beginn E-Modulermittlung	**: 0.05 %**
Ende E-Modulermittlung	**: 0.25 %**
Geschwindigkeit E-Modul	**: 2 mm/min**
Prüfgeschwindigkeit	**: 1 mm/min**
Stützweite L = (16 ±1) * h	**: 45 mm**
Maschinendaten	**: 144503 WN:103931**
	Traversenwegaufnehmer WN:103931
	Kraftsensor ID:1 WN:111937 500 N

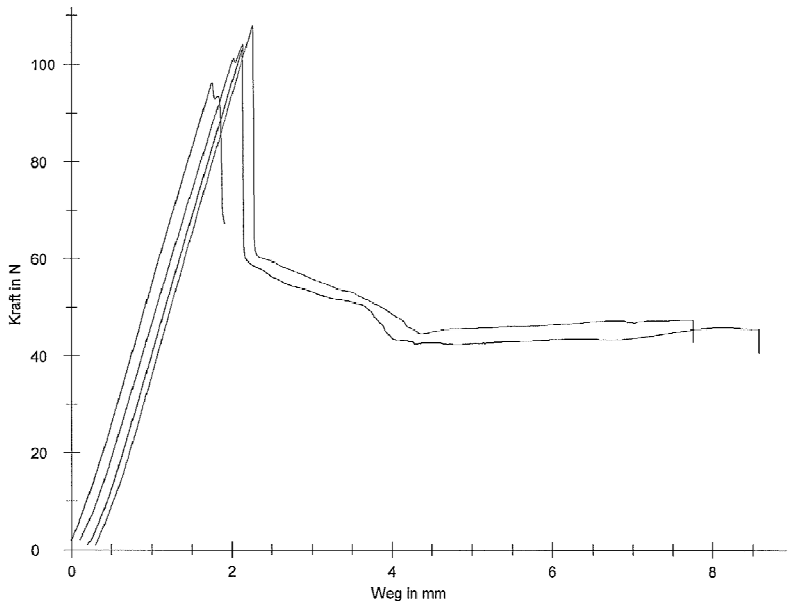

HUBER+SUHNER
PHYSIKLABOR, CH-8330 PFÄFFIKON

09.02.10 12:43

Parametertabelle:

Prüfnorm	**: EN 20 178/ISO 178**
Material	**: Carbon PFA**
Prüfer	**: Robert Rudolf**
Beginn E-Modulermittlung	**: 0.05 %**
Ende E-Modulermittlung	**: 0.25 %**
Geschwindigkeit E-Modul	**: 2 mm/min**
Prüfgeschwindigkeit	**: 1 mm/min**
Stützweite L = (16 ±1) * h	**: 45 mm**
Maschinendaten	**: 144503 WN:103931**
	Traversenwegaufnehmer WN:103931
	Kraftsensor ID:1 WN:111937 500 N

Ergebnisse:

Nr	a0 mm	b0 mm	L = (16±1) * h mm	Biegemodul MPa	σfC MPa	σfM MPa	εfM %	σfB MPa	εfB %	ε-Bruch mm	ε-F max mm
1	0.93	15.44	45	75907.05	-	594.90	0.75	-	-	-	2.73
2	0.93	15.30	45	71645.69	169.48	381.82	0.52	-	-	-	1.88
3	0.96	14.70	45	49133.25	162.38	255.05	0.74	-	-	-	2.59
4	0.96	15.12	45	77789.69	-	568.73	0.73	170.47	1.23	4.32	2.55

Statistik:

Serie n = 4	a0 mm	b0 mm	L = (16±1) * h mm	Biegemodul MPa	σfC MPa	σfM MPa	εfM %	σfB MPa	εfB %	ε-Bruch mm	ε-F max mm
$\bar{x}$	0.95	15.14	45	68618.92	165.93	450.12	0.68	170.47	1.23	4.32	2.44
s	0.02	0.32	0.000	13242.26	5.02	160.98	0.11	-	-	-	0.38
v	1.83	2.12	0.00	19.30	3.03	35.76	16.28	-	-	-	15.67
med	0.95	15.21	45	73776.37	165.93	475.28	0.73	170.47	1.23	4.32	2.57

HUBER+SUHNER
PHYSIKLABOR, CH-8330 PFÄFFIKON

09.02.10 12:43

Prüfnorm	**: EN 20 178/ISO 178**
Material	**: Carbon PFA**
Prüfer	**: Robert Rudolf**
Beginn E-Modulermittlung	**: 0.05 %**
Ende E-Modulermittlung	**: 0.25 %**
Geschwindigkeit E-Modul	**: 2 mm/min**
Prüfgeschwindigkeit	**: 1 mm/min**
Stützweite L = (16 ±1) * h	**: 45 mm**
Maschinendaten	**: 144503 WN:103931**
	Traversenwegaufnehmer WN:103931
	Kraftsensor ID:1 WN:111937 500 N

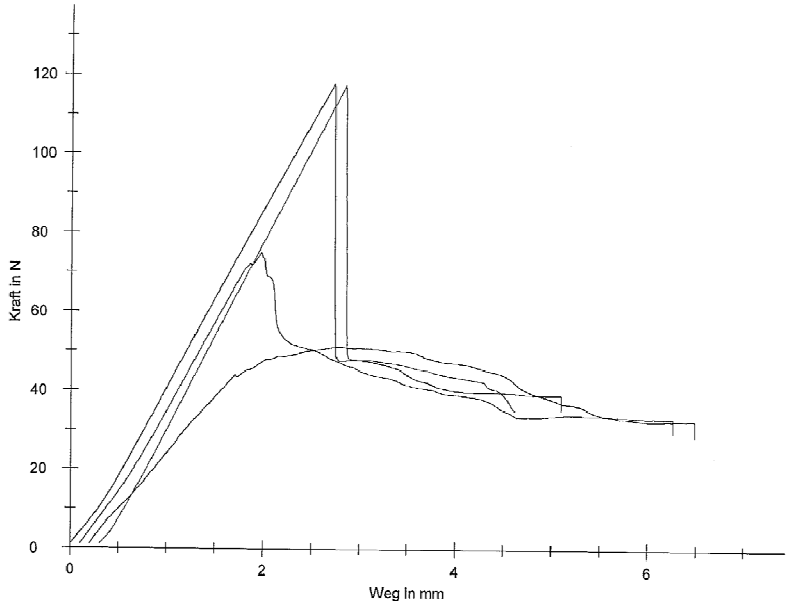

HUBER+SUHNER
PHYSIKLABOR, CH-8330 PFÄFFIKON

09.02.10 12:57

Parametertabelle:

Prüfnorm	**: EN 20 178/ISO 178**
Material	**: Carbon PFA**
Prüfer	**: Robert Rudolf**
Beginn E-Modulermittlung	**: 0.05 %**
Ende E-Modulermittlung	**: 0.25 %**
Geschwindigkeit E-Modul	**: 2 mm/min**
Prüfgeschwindigkeit	**: 1 mm/min**
Stützweite L = (16 ±1) * h	**: 45 mm**
Maschinendaten	**: 144503 WN:103931**
	Traversenwegaufnehmer WN:103931
	Kraftsensor ID:1 WN:111937 500 N

Ergebnisse:

Nr	a0 mm	b0 mm	L = (16±1) * h mm	Biegemodul MPa	σfC MPa	σfM MPa	εfM %	σfB MPa	εfB %	ε-Bruch mm	ε-F max mm
2	0.97	15.36	45	75964.91	-	373.15	0.51	-	-	-	1.78
3	0.97	15.42	45	49193.10	-	404.81	0.70	-	-	-	2.45
4	0.90	14.95	45	72706.51	-	539.63	0.72	-	-	-	2.70
5	0.97	15.01	45	68360.87	-	380.36	0.55	-	-	-	1.91

Statistik:

Serie n = 4	a0 mm	b0 mm	L = (16±1) * h mm	Biegemodul MPa	σfC MPa	σfM MPa	εfM %	σfB MPa	εfB %	ε-Bruch mm	ε-F max mm
$\bar{x}$	0.95	15.19	45	66556.35	-	424.49	0.62	-	-	-	2.21
s	0.04	0.24	0.000	11987.28	-	77.95	0.11	-	-	-	0.44
v	3.67	1.58	0.00	18.01	-	18.36	17.19	-	-	-	19.87
med	0.97	15.18	45	70533.69	-	392.59	0.63	-	-	-	2.18

HUBER+SUHNER
PHYSIKLABOR, CH-8330 PFÄFFIKON

09.02.10 12:57

Prüfnorm	**: EN 20 178/ISO 178**
Material	**: Carbon PFA**
Prüfer	**: Robert Rudolf**
Beginn E-Modulermittlung	**: 0.05 %**
Ende E-Modulermittlung	**: 0.25 %**
Geschwindigkeit E-Modul	**: 2 mm/min**
Prüfgeschwindigkeit	**: 1 mm/min**
Stützweite L = (16 ±1) * h	**: 45 mm**
Maschinendaten	**: 144503 WN:103931**
	Traversenwegaufnehmer WN:103931
	Kraftsensor ID:1 WN:111937 500 N

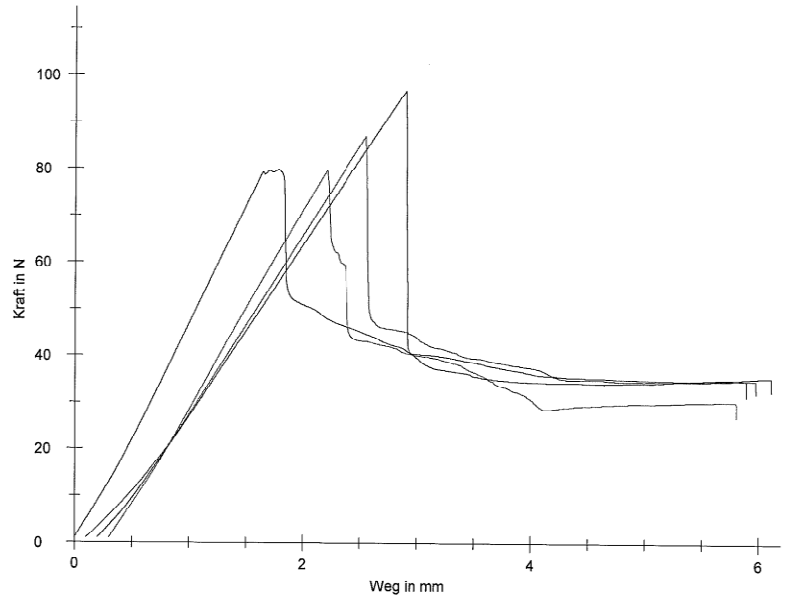

HUBER+SUHNER
PHYSIKLABOR, CH-8330 PFÄFFIKON

09.02.10 13:10

Parametertabelle:

Prüfnorm	**: EN 20 178/ISO 178**
Material	**: Carbon PFA**
Prüfer	**: Robert Rudolf**
Beginn E-Modulermittlung	**: 0.05 %**
Ende E-Modulermittlung	**: 0.25 %**
Geschwindigkeit E-Modul	**: 2 mm/min**
Prüfgeschwindigkeit	**: 1 mm/min**
Stützweite L = (16 ±1) * h	**: 45 mm**
Maschinendaten	**: 144503 WN:103931**
	Traversenwegaufnehmer WN:103931
	Kraftsensor ID:1 WN:111937 500 N

Ergebnisse:

Nr	a0 mm	b0 mm	L = (16±1) * h mm	Biegemodul MPa	σfC MPa	σfM MPa	εfM %	σfB MPa	εfB %	ε-Bruch mm	ε-F max mm
1	0.90	15.06	45	59673.67	-	344.04	0.53	-	-	-	1.98
2	0.95	15.35	45	45531.40	-	297.01	0.58	-	-	-	2.06
3	0.95	15.30	45	70535.60	-	373.39	0.52	-	-	-	1.83
4	0.95	14.68	45	67565.51	194.35	376.60	0.57	-	-	-	2.01

Statistik:

Serie n = 4	a0 mm	b0 mm	L = (16±1) * h mm	Biegemodul MPa	σfC MPa	σfM MPa	εfM %	σfB MPa	εfB %	ε-Bruch mm	ε-F max mm
x	0.94	15.10	45	60826.54	194.35	347.76	0.55	-	-	-	1.97
s	0.02	0.31	0.000	11179.60	-	36.87	0.03	-	-	-	0.10
v	2.67	2.03	0.00	18.38	-	10.60	5.54	-	-	-	4.99
med	0.95	15.18	45	63619.59	194.35	358.71	0.55	-	-	-	2.00

HUBER+SUHNER
PHYSIKLABOR, CH-8330 PFÄFFIKON

09.02.10 13:10

Prüfnorm	**: EN 20 178/ISO 178**
Material	**: Carbon PFA**
Prüfer	**: Robert Rudolf**
Beginn E-Modulermittlung	**: 0.05 %**
Ende E-Modulermittlung	**: 0.25 %**
Geschwindigkeit E-Modul	**: 2 mm/min**
Prüfgeschwindigkeit	**: 1 mm/min**
Stützweite L = (16 ±1) * h	**: 45 mm**
Maschinendaten	**: 144503 WN:103931**
	Traversenwegaufnehmer WN:103931
	Kraftsensor ID:1 WN:111937 500 N

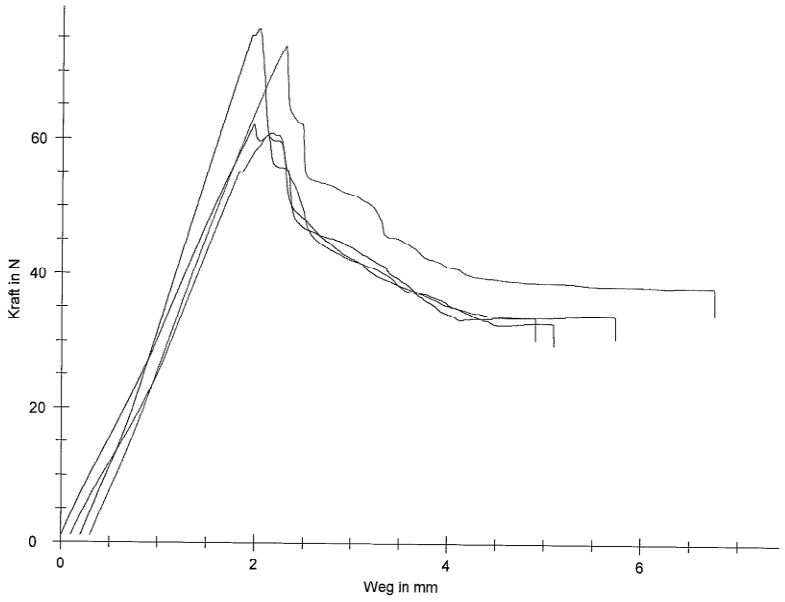

HUBER+SUHNER
PHYSIKLABOR, CH-8330 PFÄFFIKON

09.02.10 13:23

Parametertabelle:

Prüfnorm	:	**EN 20 178/ISO 178**
Material	:	**Carbon PFA**
Prüfer	:	**Robert Rudolf**
Beginn E-Modulermittlung	:	**0.05 %**
Ende E-Modulermittlung	:	**0.25 %**
Geschwindigkeit E-Modul	:	**2 mm/min**
Prüfgeschwindigkeit	:	**1 mm/min**
Stützweite L = (16 ±1) * h	:	**45 mm**
Maschinendaten	:	**144503 WN:103931**
		Traversenwegaufnehmer WN:103931
		Kraftsensor ID:1 WN:111937 500 N

Ergebnisse:

Nr	a0 mm	b0 mm	L = (16±1) * h mm	Biegemodul MPa	σfC MPa	σfM MPa	εfM %	σfB MPa	εfB %	ε-Bruch mm	ε-F max mm
1	1.01	14.88	45	69077.17	-	399.84	0.56	-	-	-	1.87
2	0.97	14.52	45	68231.83	-	455.30	0.64	-	-	-	2.21
3	0.95	14.64	45	79443.37	211.25	455.53	0.53	-	-	-	1.89
4	0.97	14.68	45	62399.08	190.26	605.30	0.90	-	-	-	3.11

Statistik:

Serie n = 4	a0 mm	b0 mm	L = (16±1) * h mm	Biegemodul MPa	σfC MPa	σfM MPa	εfM %	σfB MPa	εfB %	ε-Bruch mm	ε-F max mm
$\bar{x}$	0.97	14.68	45	69787.86	200.75	478.99	0.66	-	-	-	2.27
s	0.03	0.15	0.000	7088.70	14.84	88.19	0.17	-	-	-	0.58
v	2.58	1.02	0.00	10.16	7.39	18.41	25.23	-	-	-	25.66
med	0.97	14.66	45	68654.50	200.75	455.42	0.60	-	-	-	2.05

HUBER+SUHNER
PHYSIKLABOR, CH-8330 PFÄFFIKON

09.02.10 13:23

Prüfnorm	**: EN 20 178/ISO 178**
Material	**: Carbon PFA**
Prüfer	**: Robert Rudolf**
Beginn E-Modulermittlung	**: 0.05 %**
Ende E-Modulermittlung	**: 0.25 %**
Geschwindigkeit E-Modul	**: 2 mm/min**
Prüfgeschwindigkeit	**: 1 mm/min**
Stützweite L = (16 ±1) * h	**: 45 mm**
Maschinendaten	**: 144503 WN:103931**
	Traversenwegaufnehmer WN:103931
	Kraftsensor ID:1 WN:111937 500 N

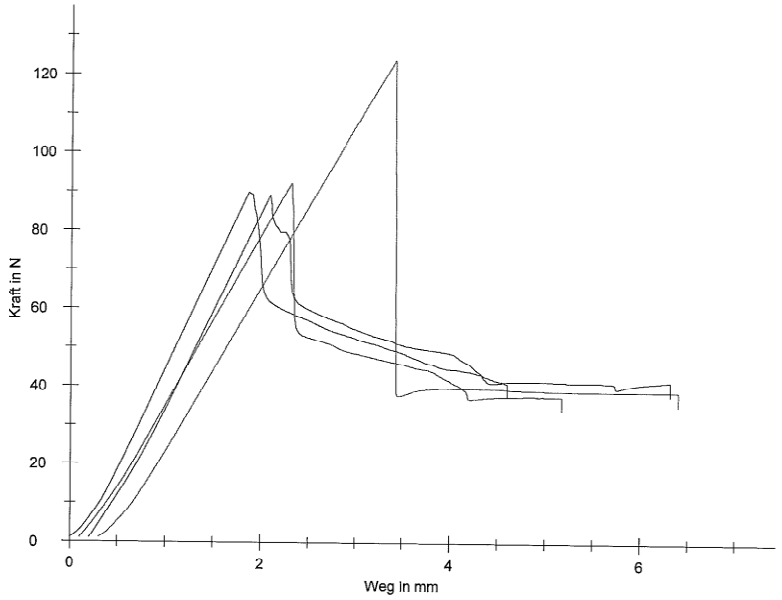

HUBER+SUHNER
PHYSIKLABOR, CH-8330 PFÄFFIKON

09.02.10 13:32

Parametertabelle:

Prüfnorm	**: EN 20 178/ISO 178**
Material	**: Carbon PFA**
Prüfer	**: Robert Rudolf**
Beginn E-Modulermittlung	**: 0.05 %**
Ende E-Modulermittlung	**: 0.25 %**
Geschwindigkeit E-Modul	**: 2 mm/min**
Prüfgeschwindigkeit	**: 1 mm/min**
Stützweite L = (16 ±1) * h	**: 45 mm**
Maschinendaten	**: 144503 WN:103931**
	Traversenwegaufnehmer WN:103931
	Kraftsensor ID:1 WN:111937 500 N

Ergebnisse:

Nr	a0 mm	b0 mm	L = (16±1) * h mm	Biegemodul MPa	σfC MPa	σfM MPa	εfM %	σfB MPa	εfB %	ε-Bruch mm	ε-F max mm
1	0.92	14.30	45	65158.60	-	423.73	0.61	-	-	-	2.25
2	0.93	14.44	45	74567.13	-	449.09	0.56	-	-	-	2.03
3	0.93	14.70	45	68135.58	205.67	376.83	0.53	-	-	-	1.93

Statistik:

Serie n = 3	a0 mm	b0 mm	L = (16±1) * h mm	Biegemodul MPa	σfC MPa	σfM MPa	εfM %	σfB MPa	εfB %	ε-Bruch mm	ε-F max mm
x̄	0.93	14.48	45	69287.10	205.67	416.55	0.57	-	-	-	2.07
s	0.01	0.20	0.000	4808.81	-	36.66	0.04	-	-	-	0.16
v	0.62	1.40	0.00	6.94	-	8.80	7.36	-	-	-	7.97
med	0.93	14.44	45	68135.58	205.67	423.73	0.56	-	-	-	2.03

HUBER+SUHNER
PHYSIKLABOR, CH-8330 PFÄFFIKON

09.02.10 13:32

Prüfnorm	:	**EN 20 178/ISO 178**
Material	:	**Carbon PFA**
Prüfer	:	**Robert Rudolf**
Beginn E-Modulermittlung	:	**0.05 %**
Ende E-Modulermittlung	:	**0.25 %**
Geschwindigkeit E-Modul	:	**2 mm/min**
Prüfgeschwindigkeit	:	**1 mm/min**
Stützweite L = (16 ±1) * h	:	**45 mm**
Maschinendaten	:	**144503 WN:103931**
		Traversenwegaufnehmer WN:103931
		Kraftsensor ID:1 WN:111937 500 N

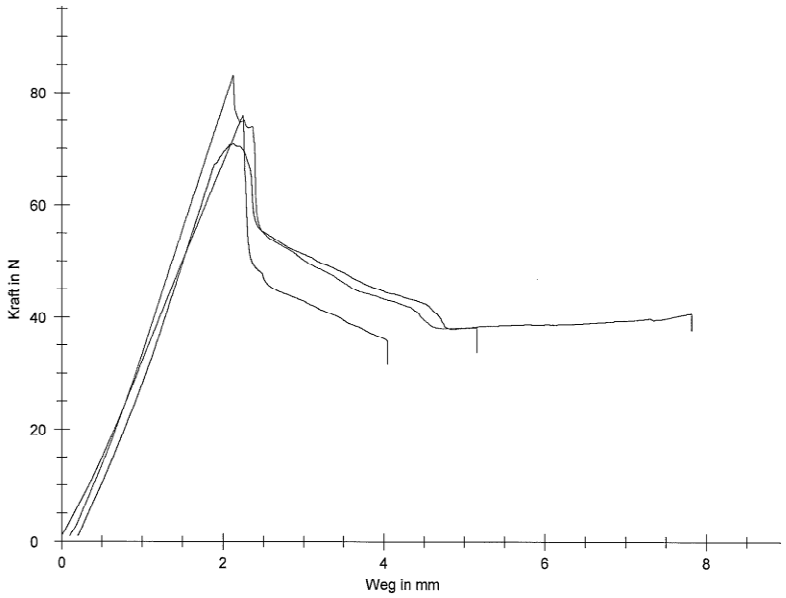

HUBER+SUHNER
PHYSIKLABOR, CH-8330 PFÄFFIKON

09.02.10 13:43

Parametertabelle:

Prüfnorm	**: EN 20 178/ISO 178**
Material	**: Carbon PFA**
Prüfer	**: Robert Rudolf**
Beginn E-Modulermittlung	**: 0.05 %**
Ende E-Modulermittlung	**: 0.25 %**
Geschwindigkeit E-Modul	**: 2 mm/min**
Prüfgeschwindigkeit	**: 1 mm/min**
Stützweite L = (16 ±1) * h	**: 45 mm**
Maschinendaten	**: 144503 WN:103931**
	Traversenwegaufnehmer WN:103931
	Kraftsensor ID:1 WN:111937 500 N

Ergebnisse:

Nr	a0 mm	b0 mm	L = (16±1) * h mm	Biegemodul MPa	σfC MPa	σfM MPa	εfM %	σfB MPa	εfB %	ε-Bruch mm	ε-F max mm
1	0.92	14.24	45	49517.12	-	305.95	0.68	-	-	-	2.51
2	0.90	15.01	45	69062.45	-	394.12	0.52	-	-	-	1.95
3	0.90	14.48	45	72368.71	-	506.26	0.63	-	-	-	2.37
4	0.89	14.13	45	73153.03	-	568.37	0.72	-	-	-	2.74

Statistik:

Serie n = 4	a0 mm	b0 mm	L = (16±1) * h mm	Biegemodul MPa	σfC MPa	σfM MPa	εfM %	σfB MPa	εfB %	ε-Bruch mm	ε-F max mm
x	0.90	14.47	45	66025.33	-	443.68	0.64	-	-	-	2.39
s	0.01	0.39	0.000	11147.31	-	116.75	0.09	-	-	-	0.33
v	1.39	2.71	0.00	16.88	-	26.31	13.86	-	-	-	13.99
med	0.90	14.36	45	70715.58	-	450.19	0.66	-	-	-	2.44

HUBER+SUHNER
PHYSIKLABOR, CH-8330 PFÄFFIKON

09.02.10 13:43

Prüfnorm	**: EN 20 178/ISO 178**
Material	**: Carbon PFA**
Prüfer	**: Robert Rudolf**
Beginn E-Modulermittlung	**: 0.05 %**
Ende E-Modulermittlung	**: 0.25 %**
Geschwindigkeit E-Modul	**: 2 mm/min**
Prüfgeschwindigkeit	**: 1 mm/min**
Stützweite L = (16 ±1) * h	**: 45 mm**
Maschinendaten	**: 144503 WN:103931**
	Traversenwegaufnehmer WN:103931
	Kraftsensor ID:1 WN:111937 500 N

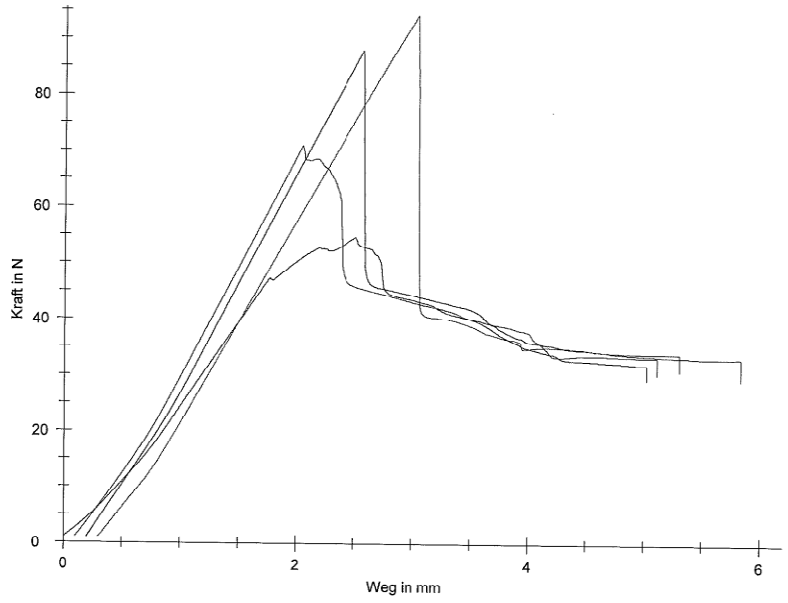

Appendix I (Source: Cardona et al., 2001)

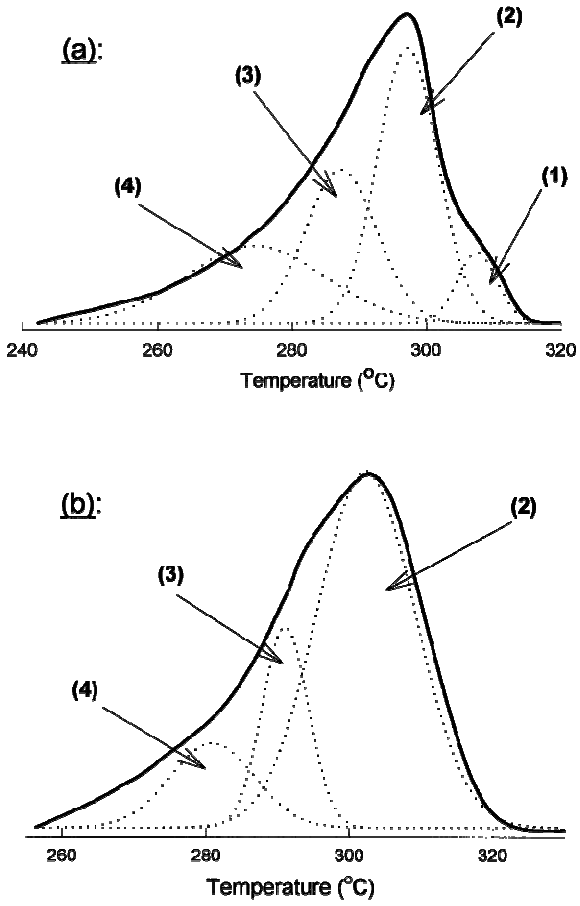

Fig. 5. DSC melting curves for PFA-A polymer showing the peaks corresponding to different crystalline fractions contributing: Ungrafted PFA sample (a) and after 50 kGy (b).

Appendix J

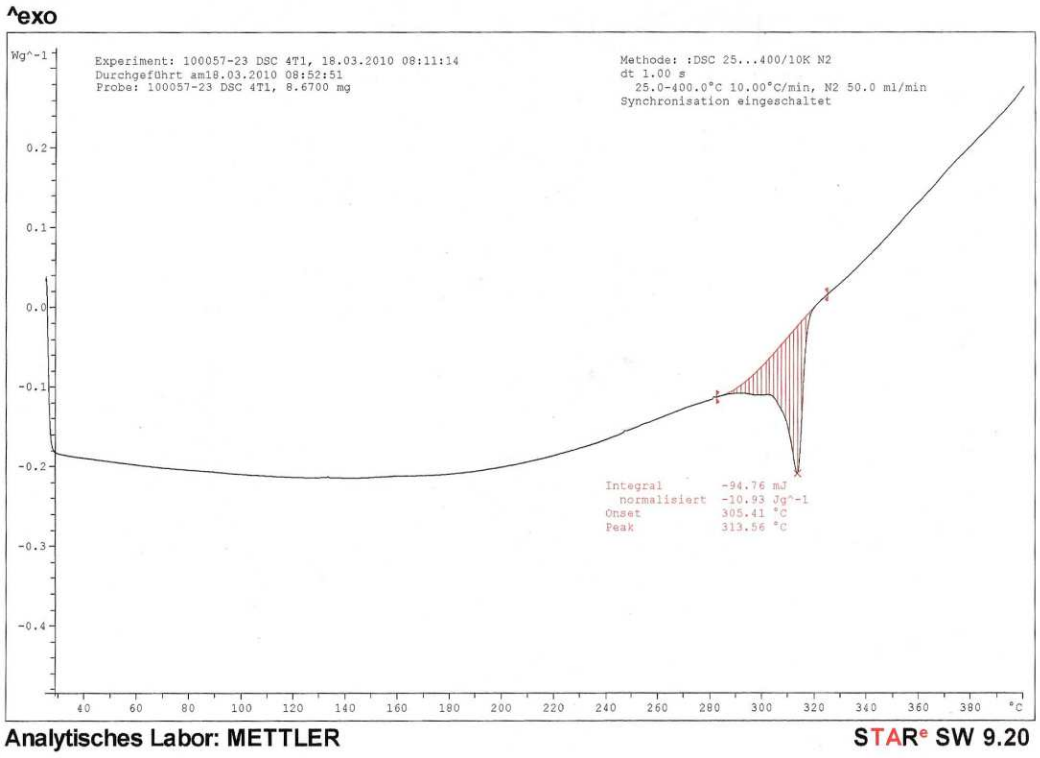
^exo
Wg^-1
Experiment: 100057-23 DSC 4T1, 18.03.2010 08:11:14
Durchgeführt am18.03.2010 08:52:51
Probe: 100057-23 DSC 4T1, 8.6700 mg
Methode: :DSC 25...400/10K N2
dt 1.00 s
25.0-400.0°C 10.00°C/min, N2 50.0 ml/min
Synchronisation eingeschaltet
Integral -94.76 mJ
normalisiert -10.93 Jg^-1
Onset 305.41 °C
Peak 313.56 °C
0.2
0.1
0.0
-0.1
-0.2
-0.3
-0.4
40 60 80 100 120 140 160 180 200 220 240 260 280 300 320 340 360 380 °C
Analytisches Labor: METTLER
STARe SW 9.20

Appendix K

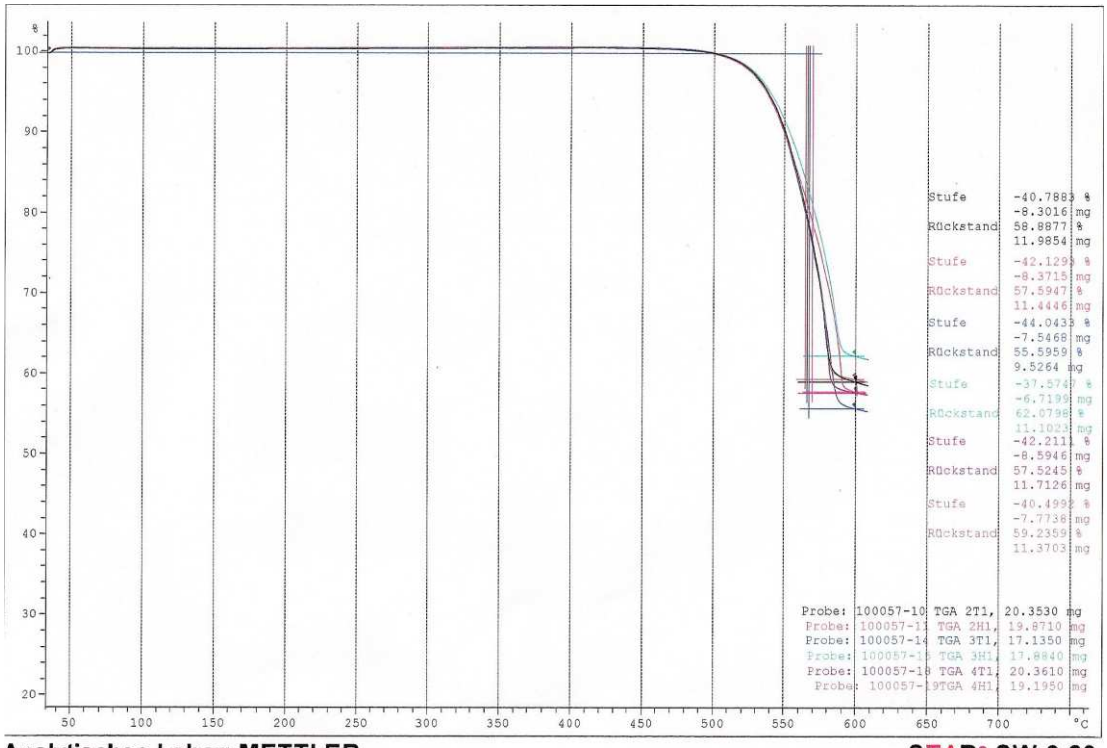
%
100
90
80
70
60
50
40
30
20
50 100 150 200 250 300 350 400 450 500 550 600 650 700 °C
Stufe -40.7883 %
-8.3016 mg
Rückstand 58.8877 %
11.9854 mg
Stufe -42.1295 %
-8.3715 mg
Rückstand 57.5947 %
11.4446 mg
Stufe -44.0433 %
-7.5468 mg
Rückstand 55.5959 %
9.5264 mg
Stufe -37.5748 %
-6.7199 mg
Rückstand 62.0798 %
11.1023 mg
Stufe -42.2111 %
-8.5946 mg
Rückstand 57.5245 %
11.7126 mg
Stufe -40.4992 %
-7.7738 mg
Rückstand 59.2359 %
11.3703 mg
Probe: 100057-10 TGA 2T1, 20.3530 mg
Probe: 100057-11 TGA 2H1, 19.8710 mg
Probe: 100057-14 TGA 3T1, 17.1350 mg
Probe: 100057-15 TGA 3H1, 17.8840 mg
Probe: 100057-18 TGA 4T1, 20.3610 mg
Probe: 100057-19TGA 4H1, 19.1950 mg
Analytisches Labor: METTLER
STARe SW 9.20

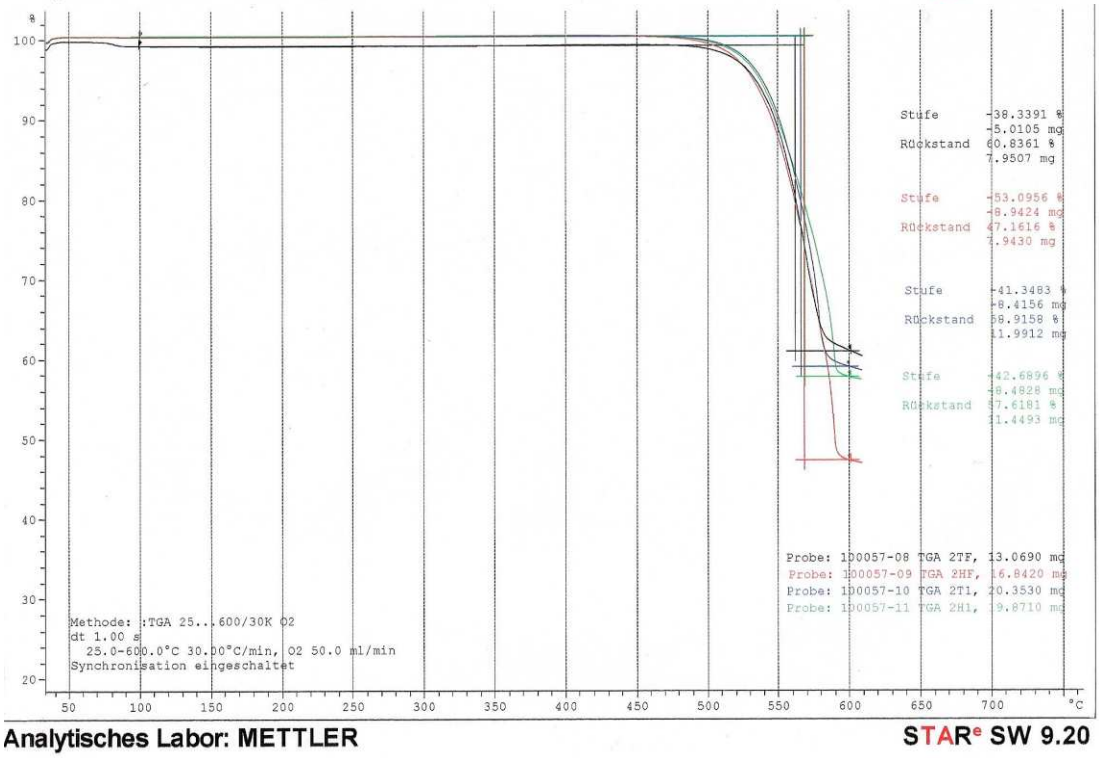
%
100
90
80
70
60
50
40
30
20
50 100 150 200 250 300 350 400 450 500 550 600 650 700 °C
Stufe -38.3391 %
-5.0105 mg
Rückstand 60.8361 %
7.9507 mg
Stufe -53.0956 %
-8.9424 mg
Rückstand 47.1616 %
7.9430 mg
Stufe -41.3483 %
-8.4156 mg
Rückstand 58.9158 %
11.9912 mg
Stufe -42.6896 %
-8.4828 mg
Rückstand 57.6181 %
11.4493 mg
Probe: 100057-08 TGA 2TF, 13.0690 mg
Probe: 100057-09 TGA 2HF, 16.8420 mg
Probe: 100057-10 TGA 2T1, 20.3530 mg
Probe: 100057-11 TGA 2H1, 19.8710 mg
Methode: :TGA 25...600/30K O2
dt 1.00 s
25.0-600.0°C 30.00°C/min, O2 50.0 ml/min
Synchronisation eingeschaltet
Analytisches Labor: METTLER
STARe SW 9.20

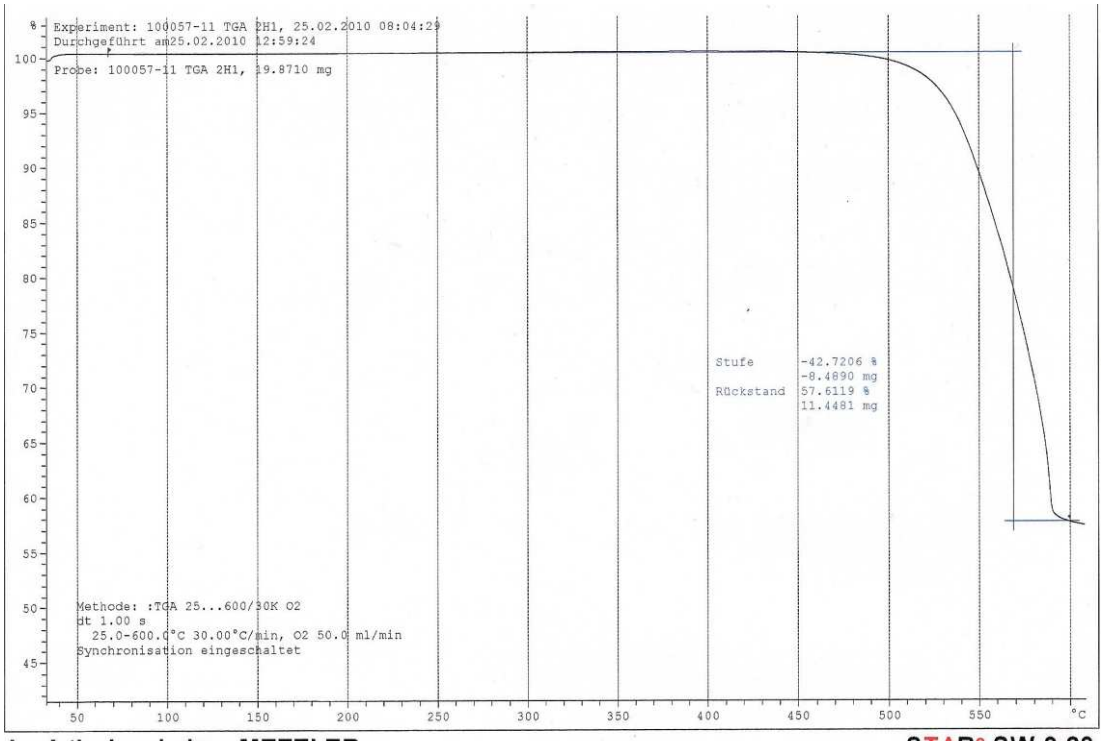
Experiment: 100057-11 TGA 2H1, 25.02.2010 08:04:29
Durchgeführt am 25.02.2010 12:59:24
Probe: 100057-11 TGA 2H1, 19.8710 mg
Stufe -42.7206 %
-8.4890 mg
Rückstand 57.6119 %
11.4481 mg
Methode: :TGA 25...600/30K O2
dt 1.00 s
25.0-600.0°C 30.00°C/min, O2 50.0 ml/min
Synchronisation eingeschaltet
Analytisches Labor: METTLER
STARe SW 9.20


Experiment: 100057-09 TGA 2HF, 25.02.2010 08:02:36
Durchgeführt am 25.02.2010 11:21:56
Probe: 100057-09 TGA 2HF, 16.8420 mg
Stufe -53.0540 %
-8.9354 mg
Rückstand 47.2023 %
7.9498 mg
Methode: :TGA 25...600/30K O2
dt 1.00 s
25.0-600.0°C 30.00°C/min, O2 50.0 ml/min
Synchronisation eingeschaltet
Analytisches Labor: METTLER
STARe SW 9.20

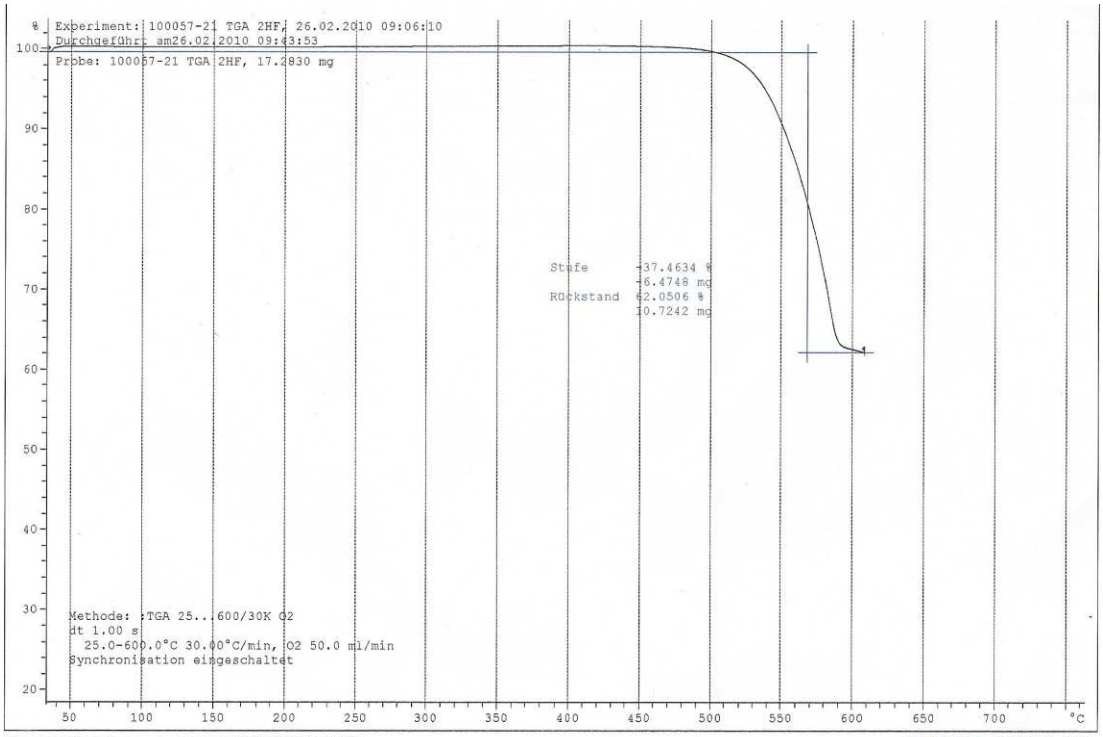
Experiment: 100057-21 TGA 2HF, 26.02.2010 09:06:10
Durchgeführt am26.02.2010 09:43:53
Probe: 100057-21 TGA 2HF, 17.2830 mg
Stufe -37.4634 %
-6.4748 mg
Rückstand 62.0506 %
10.7242 mg
Methode: :TGA 25...600/30K O2
dt 1.00 s
25.0-600.0°C 30.00°C/min, O2 50.0 ml/min
Synchronisation eingeschaltet
Analytisches Labor: METTLER
STARe SW 9.20

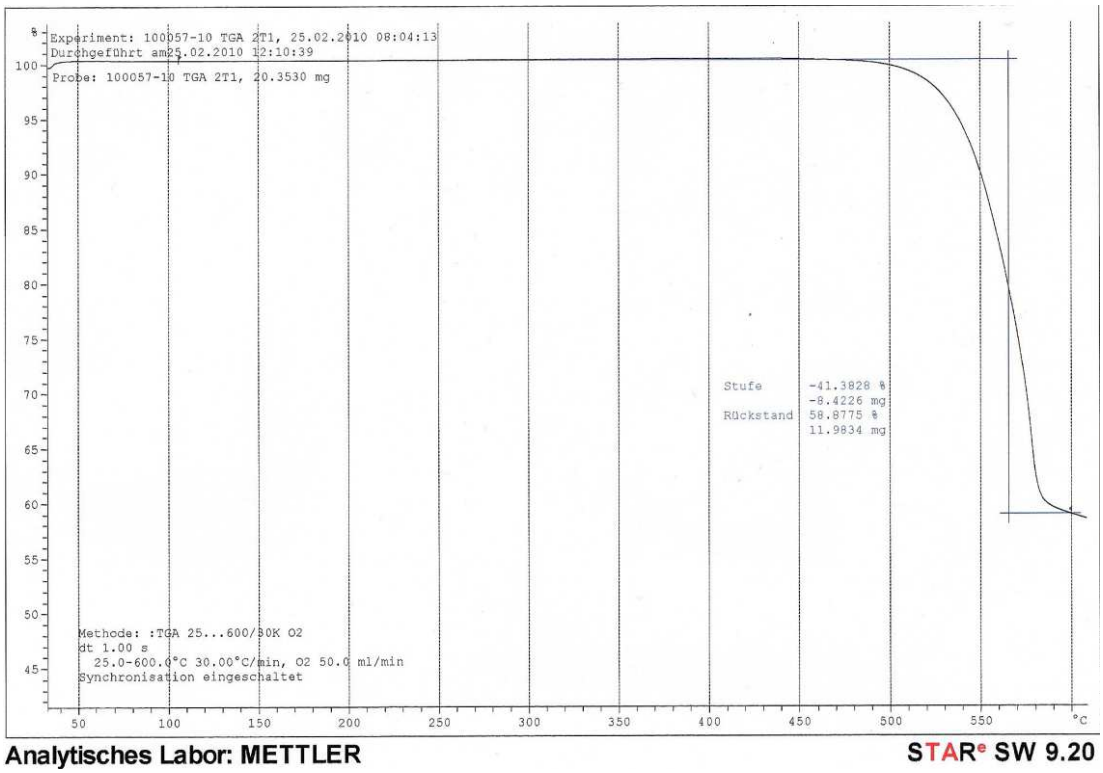
Experiment: 100057-10 TGA 2T1, 25.02.2010 08:04:13
Durchgeführt am25.02.2010 12:10:39
Probe: 100057-10 TGA 2T1, 20.3530 mg
Stufe -41.3828 %
-8.4226 mg
Rückstand 58.8775 %
11.9834 mg
Methode: :TGA 25...600/30K O2
dt 1.00 s
25.0-600.0°C 30.00°C/min, O2 50.0 ml/min
Synchronisation eingeschaltet
Analytisches Labor: METTLER
STARe SW 9.20

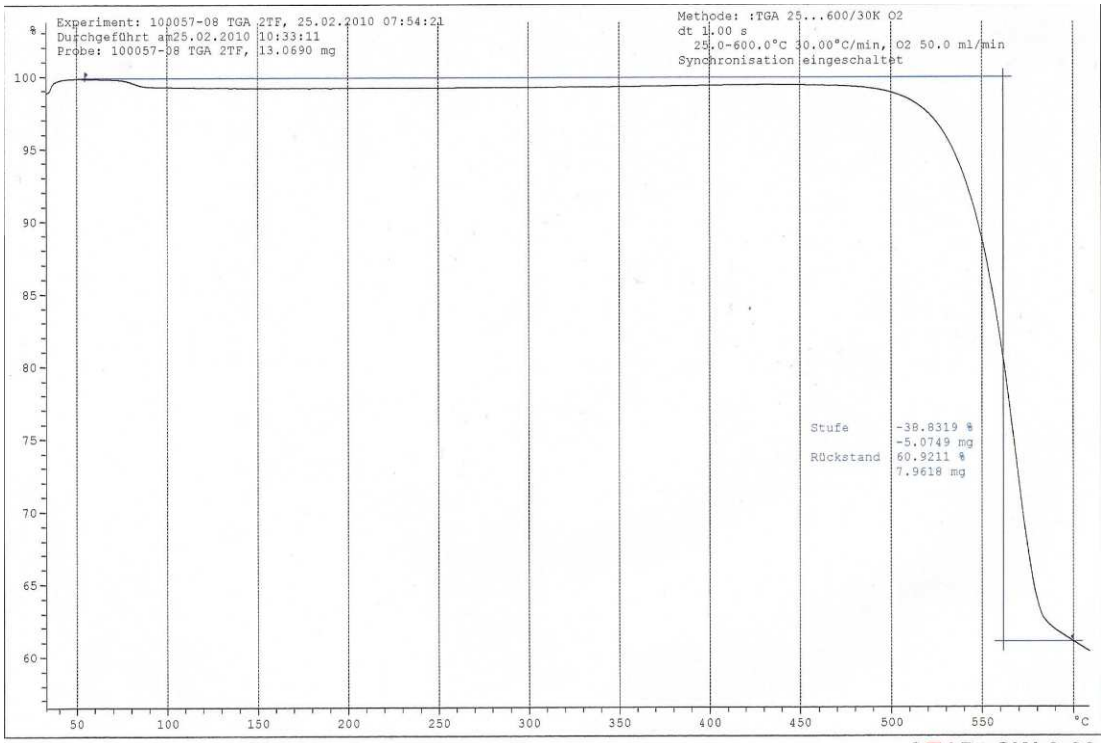

Analytisches Labor: METTLER **STARe SW 9.20**

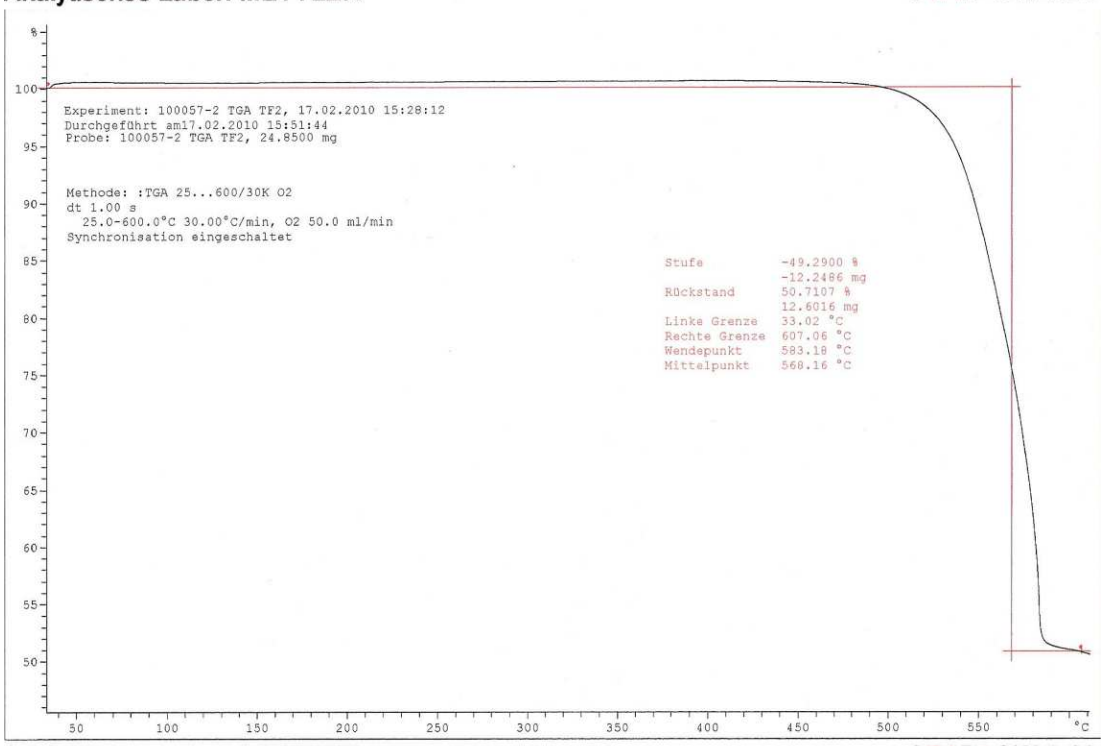

Analytisches Labor: METTLER k. 17557 **STARe SW 9.20**

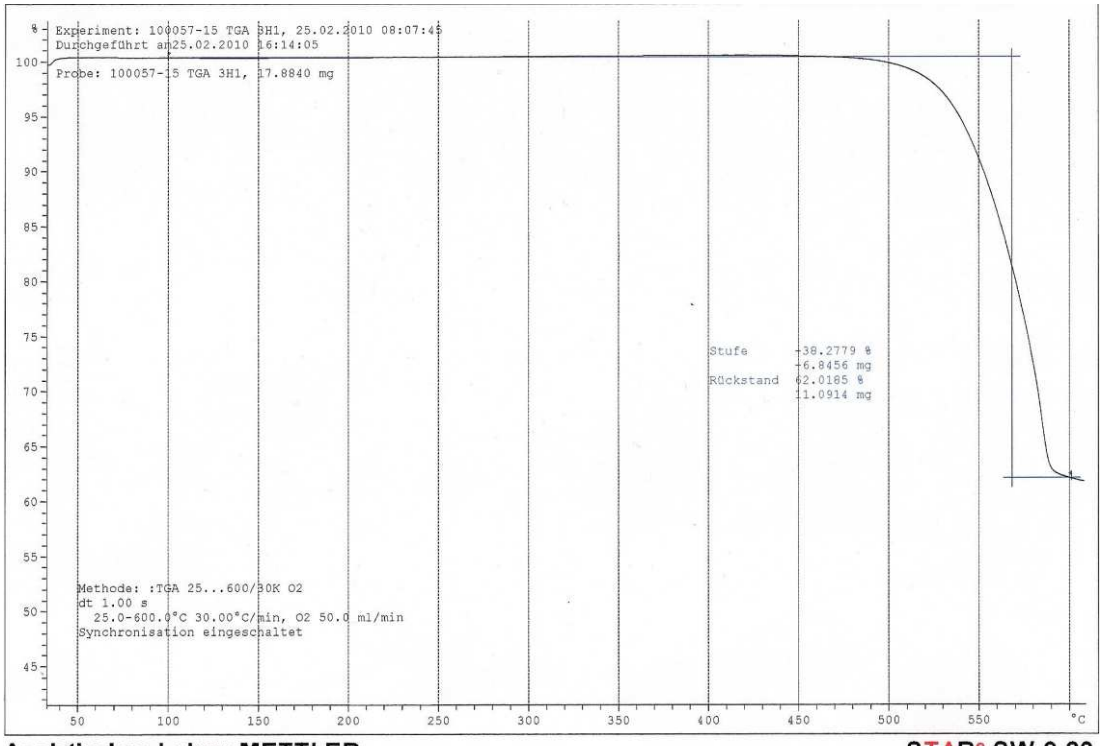
Experiment: 100057-15 TGA 3H1, 25.02.2010 08:07:45
Durchgeführt am 25.02.2010 16:14:05
Probe: 100057-15 TGA 3H1, 17.8840 mg
Stufe -38.2779 %
-6.8456 mg
Rückstand 62.0185 %
11.0914 mg
Methode: :TGA 25...600/30K O2
dt 1.00 s
25.0-600.0°C 30.00°C/min, O2 50.0 ml/min
Synchronisation eingeschaltet
Analytisches Labor: METTLER
STARe SW 9.20

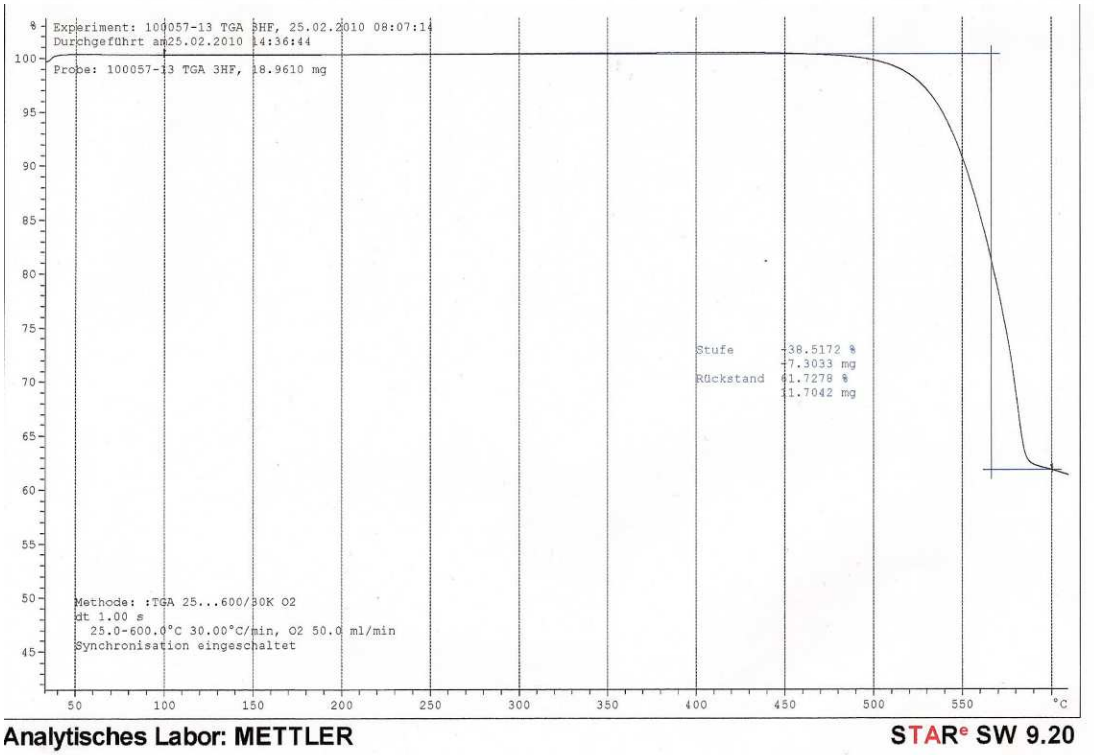
Experiment: 100057-13 TGA 3HF, 25.02.2010 08:07:14
Durchgeführt am 25.02.2010 14:36:44
Probe: 100057-13 TGA 3HF, 18.9610 mg
Stufe -38.5172 %
-7.3033 mg
Rückstand 61.7278 %
11.7042 mg
Methode: :TGA 25...600/30K O2
dt 1.00 s
25.0-600.0°C 30.00°C/min, O2 50.0 ml/min
Synchronisation eingeschaltet
Analytisches Labor: METTLER
STARe SW 9.20

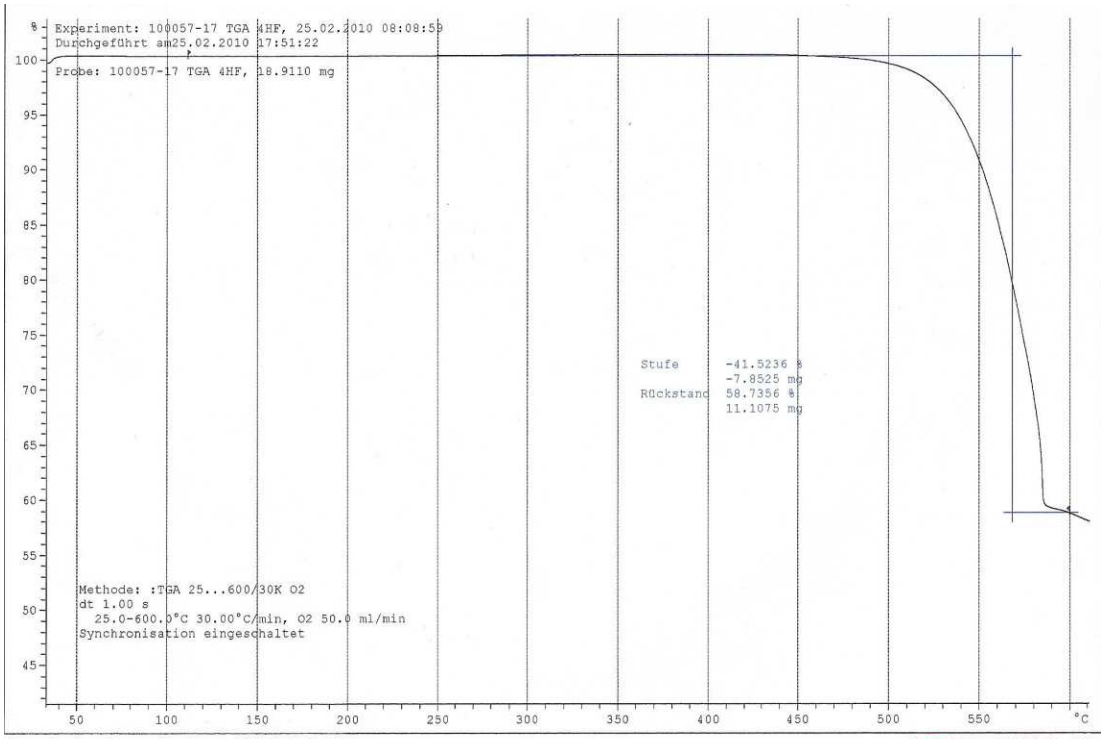
Experiment: 100057-17 TGA 4HF, 25.02.2010 08:08:59
Durchgeführt am25.02.2010 17:51:22
Probe: 100057-17 TGA 4HF, 18.9110 mg
Stufe -41.5236 %
-7.8525 mg
Rückstand 58.7356 %
11.1075 mg
Methode: :TGA 25...600/30K O2
dt 1.00 s
25.0-600.0°C 30.00°C/min, O2 50.0 ml/min
Synchronisation eingeschaltet
%
°C
Analytisches Labor: METTLER
STARe SW 9.20

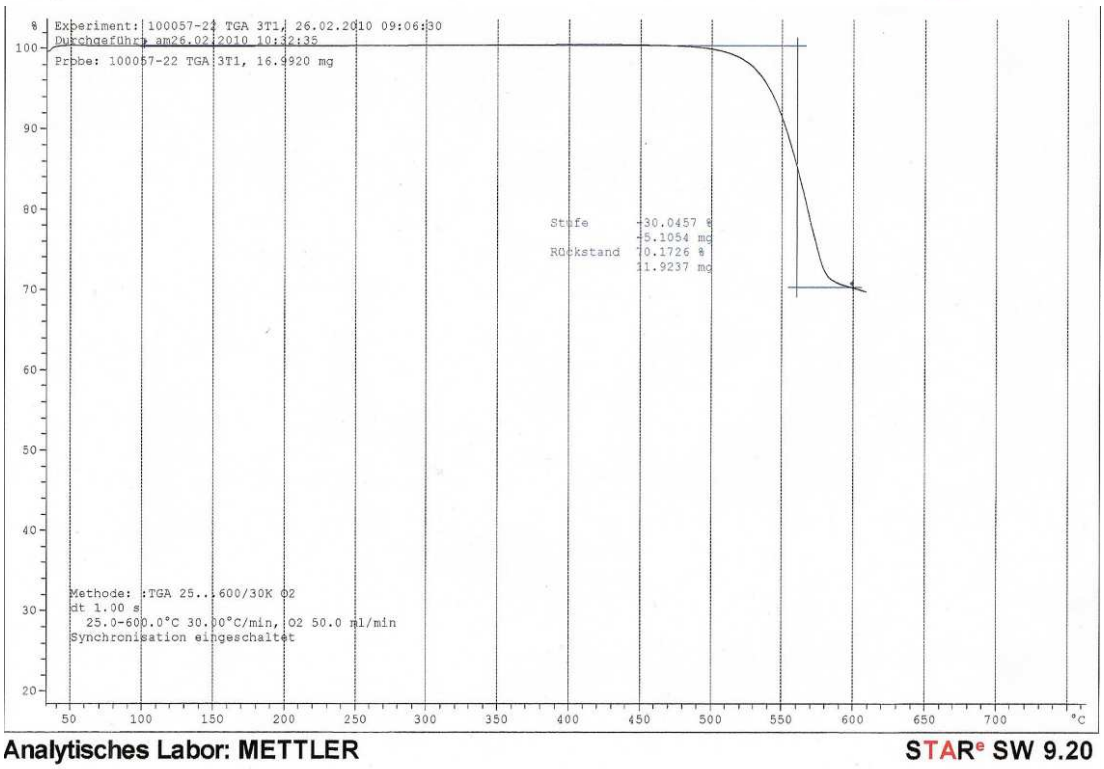
Experiment: 100057-22 TGA 3T1, 26.02.2010 09:06:30
Durchgeführt am26.02.2010 10:32:35
Probe: 100057-22 TGA 3T1, 16.9920 mg
Stufe -30.0457 %
-5.1054 mg
Rückstand 70.1726 %
11.9237 mg
Methode: :TGA 25...600/30K O2
dt 1.00 s
25.0-600.0°C 30.00°C/min, O2 50.0 ml/min
Synchronisation eingeschaltet
%
°C
Analytisches Labor: METTLER
STARe SW 9.20


Experiment: 100057-12 TGA 3TF, 25.02.2010 08:04:58
Durchgeführt am 25.02.2010 13:48:05
Probe: 100057-12 TGA 3TF, 17.7040 mg
Stufe +39.0824 %
+6.9191 mg
Rückstand 61.2060 %
10.8359 mg
Methode: :TGA 25...600/30K O2
dt 1.00 s
25.0-600.0°C 30.00°C/min, O2 50.0 ml/min
Synchronisation eingeschaltet
Analytisches Labor: METTLER
STARe SW 9.20

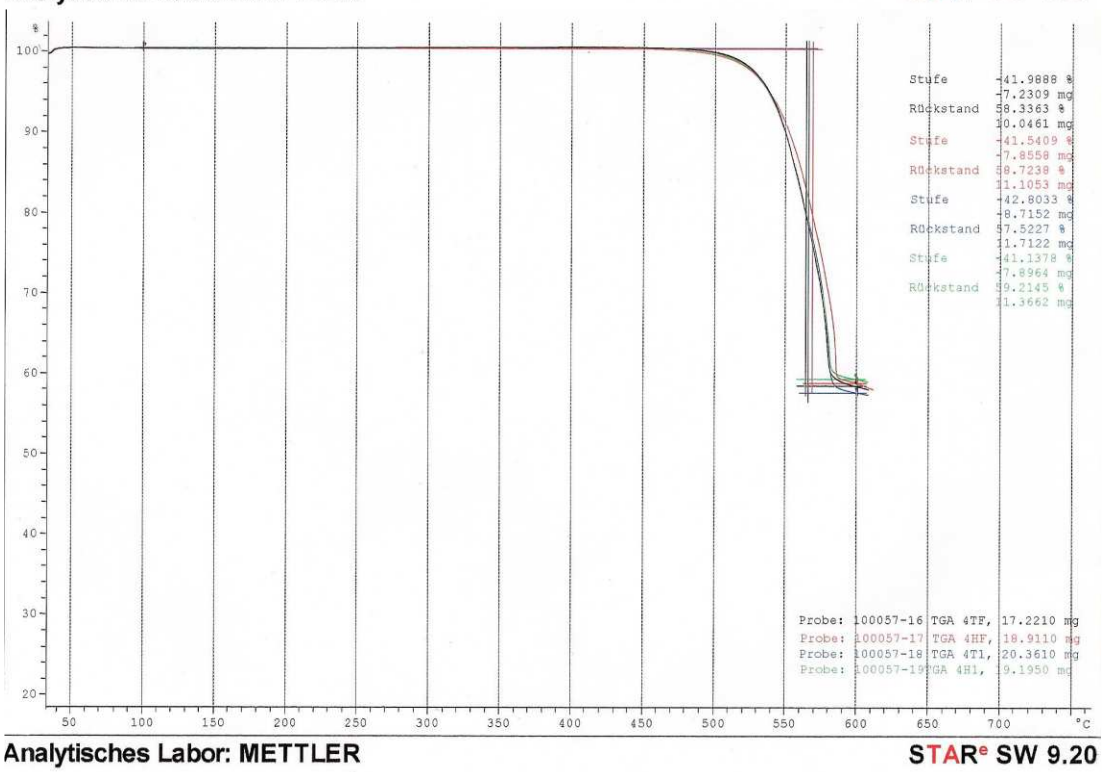
Stufe +41.9888 %
+7.2309 mg
Rückstand 58.3363 %
10.0461 mg
Stufe +41.5409 %
+7.8558 mg
Rückstand 58.7238 %
11.1053 mg
Stufe +42.8033 %
+8.7152 mg
Rückstand 57.5227 %
11.7122 mg
Stufe +41.1378 %
+7.8964 mg
Rückstand 59.2145 %
11.3662 mg
Probe: 100057-16 TGA 4TF, 17.2210 mg
Probe: 100057-17 TGA 4HF, 18.9110 mg
Probe: 100057-18 TGA 4T1, 20.3610 mg
Probe: 100057-19 TGA 4H1, 19.1950 mg
Analytisches Labor: METTLER
STARe SW 9.20

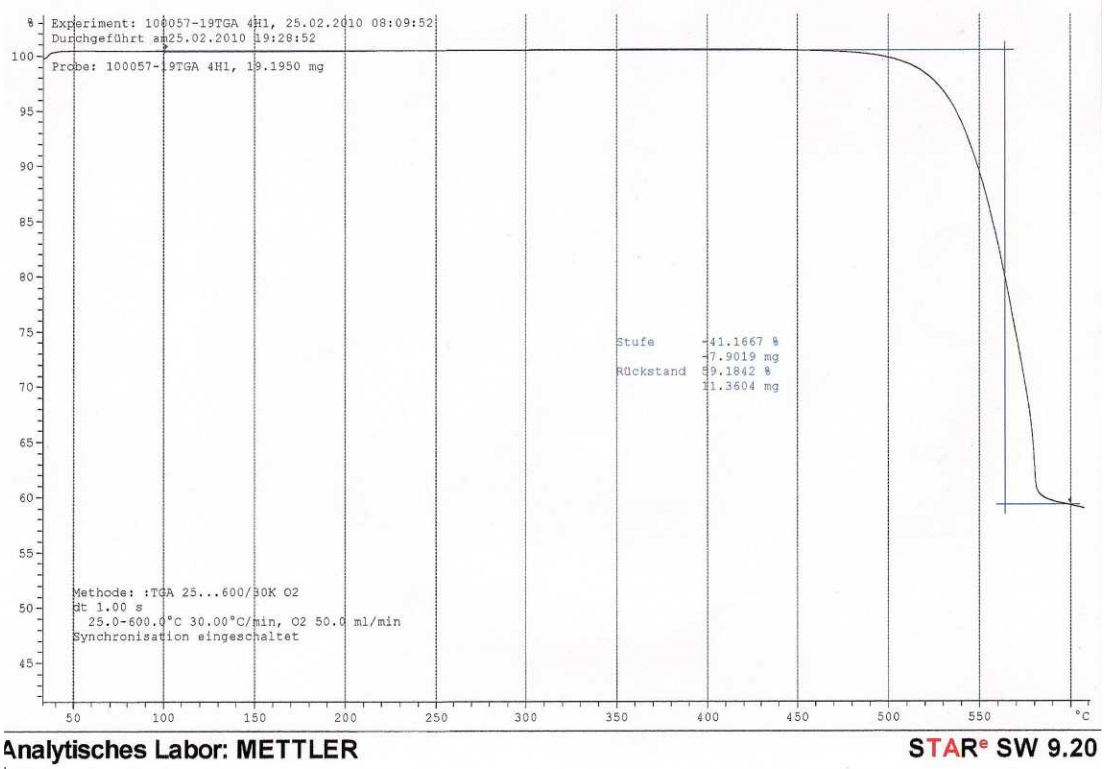
Experiment: 100057-19TGA 4H1, 25.02.2010 08:09:52
Durchgeführt am 25.02.2010 19:28:52
Probe: 100057-19TGA 4H1, 19.1950 mg
Stufe -41.1667 %
-7.9019 mg
Rückstand 59.1842 %
11.3604 mg
Methode: :TGA 25...600/30K O2
dt 1.00 s
25.0-600.0°C 30.00°C/min, O2 50.0 ml/min
Synchronisation eingeschaltet
Analytisches Labor: METTLER
STARe SW 9.20

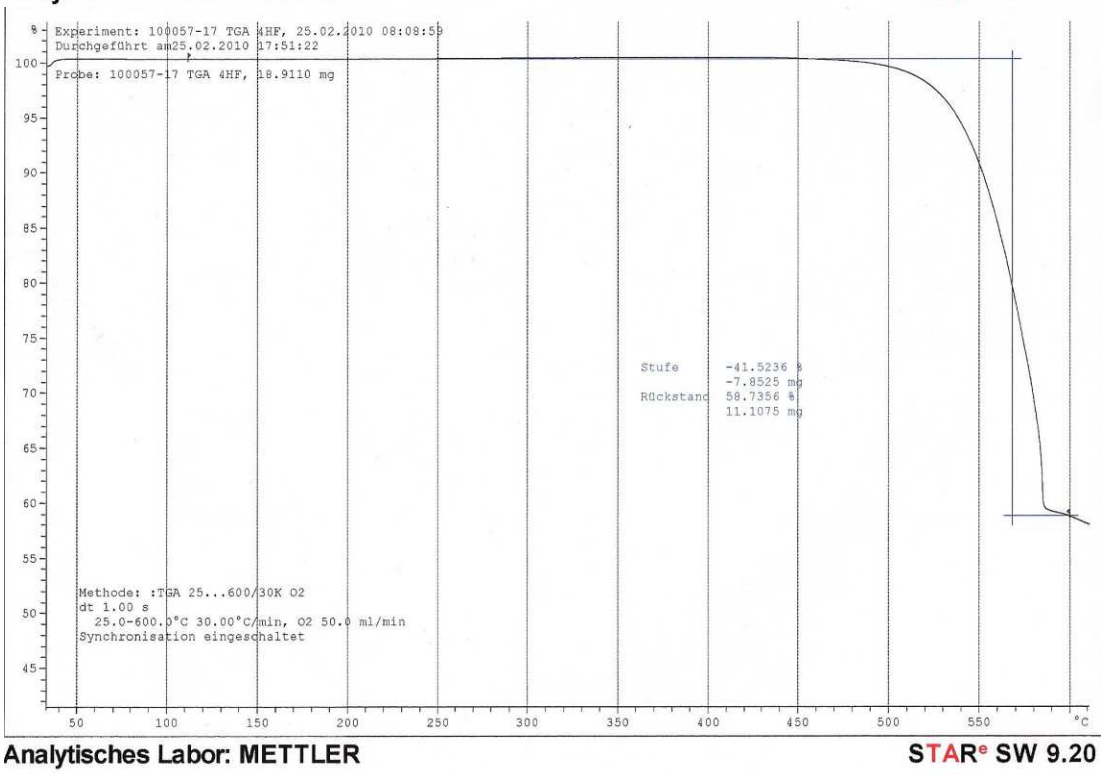
Experiment: 100057-17 TGA 4HF, 25.02.2010 08:08:59
Durchgeführt am 25.02.2010 17:51:22
Probe: 100057-17 TGA 4HF, 18.9110 mg
Stufe -41.5236 %
-7.8525 mg
Rückstand 58.7356 %
11.1075 mg
Methode: :TGA 25...600/30K O2
dt 1.00 s
25.0-600.0°C 30.00°C/min, O2 50.0 ml/min
Synchronisation eingeschaltet
Analytisches Labor: METTLER
STARe SW 9.20

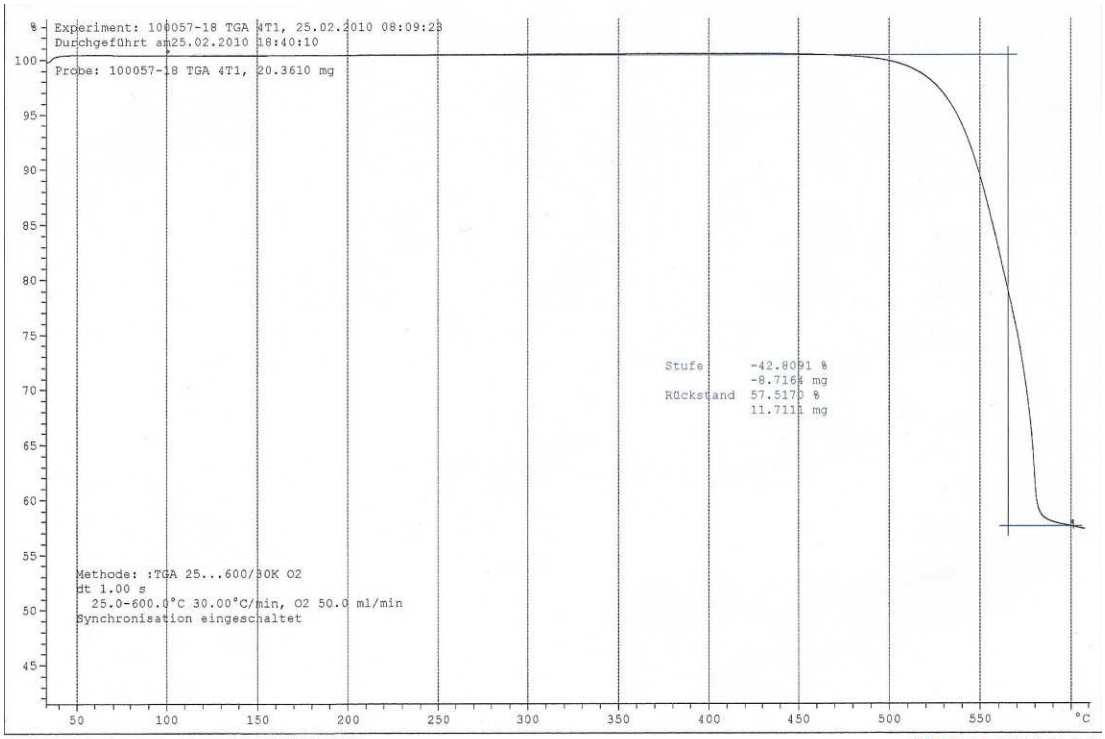
Experiment: 100057-18 TGA 4T1, 25.02.2010 08:09:23
Durchgeführt am 25.02.2010 18:40:10
Probe: 100057-18 TGA 4T1, 20.3610 mg
Stufe -42.8091 %
-8.7164 mg
Rückstand 57.5170 %
11.7111 mg
Methode: :TGA 25...600/30K O2
dt 1.00 s
25.0-600.0°C 30.00°C/min, O2 50.0 ml/min
Synchronisation eingeschaltet
Analytisches Labor: METTLER
STARe SW 9.20

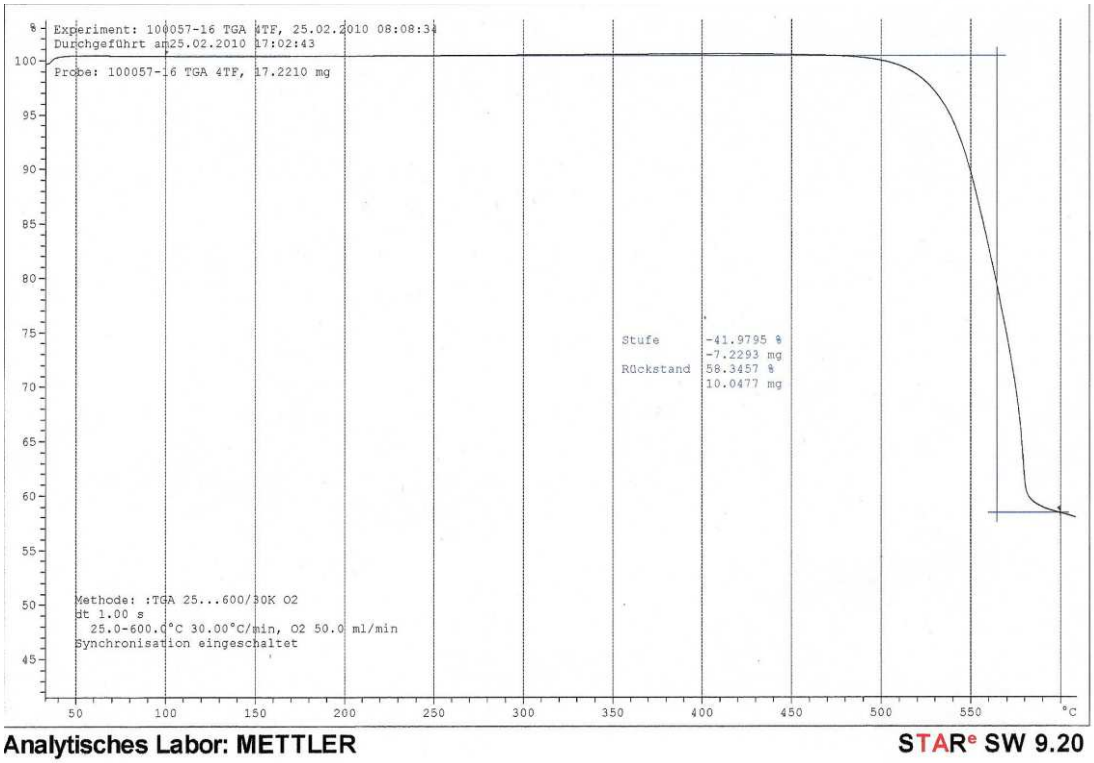
Experiment: 100057-16 TGA 4TF, 25.02.2010 08:08:34
Durchgeführt am 25.02.2010 17:02:43
Probe: 100057-16 TGA 4TF, 17.2210 mg
Stufe -41.9795 %
-7.2293 mg
Rückstand 58.3457 %
10.0477 mg
Methode: :TGA 25...600/30K O2
dt 1.00 s
25.0-600.0°C 30.00°C/min, O2 50.0 ml/min
Synchronisation eingeschaltet
Analytisches Labor: METTLER
STARe SW 9.20

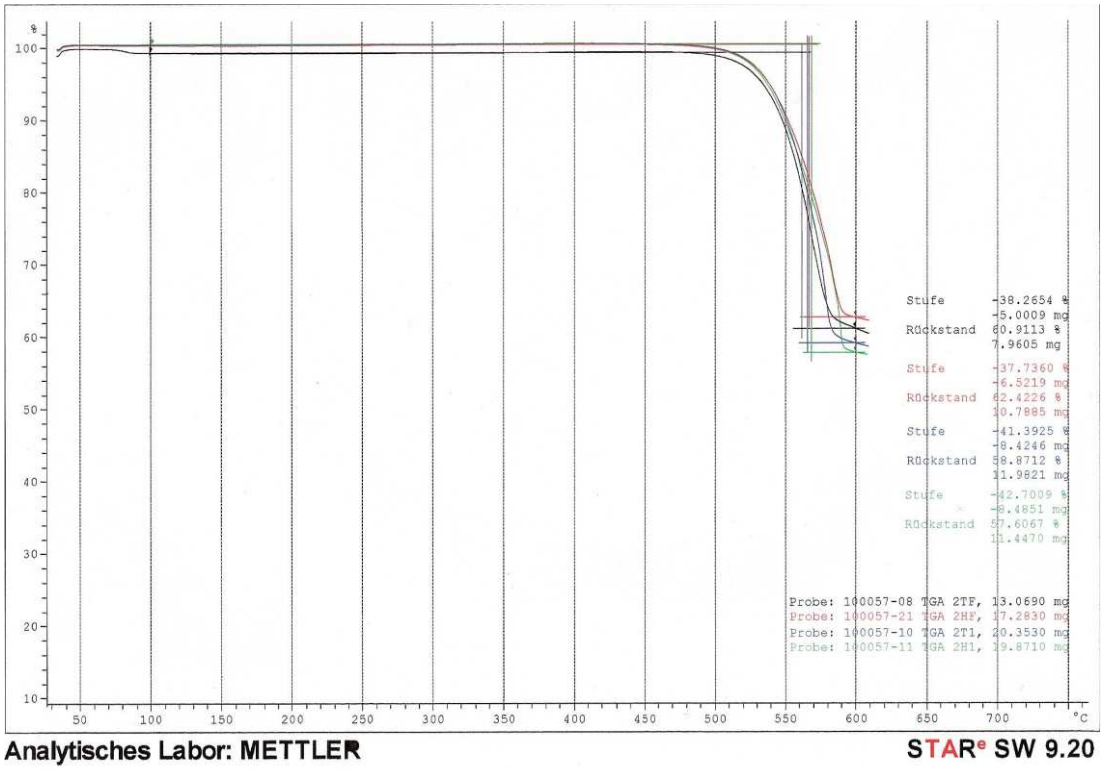
%
100
90
80
70
60
50
40
30
20
10
50
100
150
200
250
300
350
400
450
500
550
600
650
700
°C
Stufe -38.2654 %
-5.0009 mg
Rückstand 60.9113 %
7.9605 mg
Stufe -37.7360 %
-6.5219 mg
Rückstand 62.4226 %
10.7885 mg
Stufe -41.3925 %
-8.4246 mg
Rückstand 58.8712 %
11.9821 mg
Stufe -42.7009 %
-8.4851 mg
Rückstand 57.6067 %
11.4470 mg
Probe: 100057-08 TGA 2TF, 13.0690 mg
Probe: 100057-21 TGA 2HF, 17.2830 mg
Probe: 100057-10 TGA 2T1, 20.3530 mg
Probe: 100057-11 TGA 2H1, 19.8710 mg
Analytisches Labor: METTLER
STARe SW 9.20

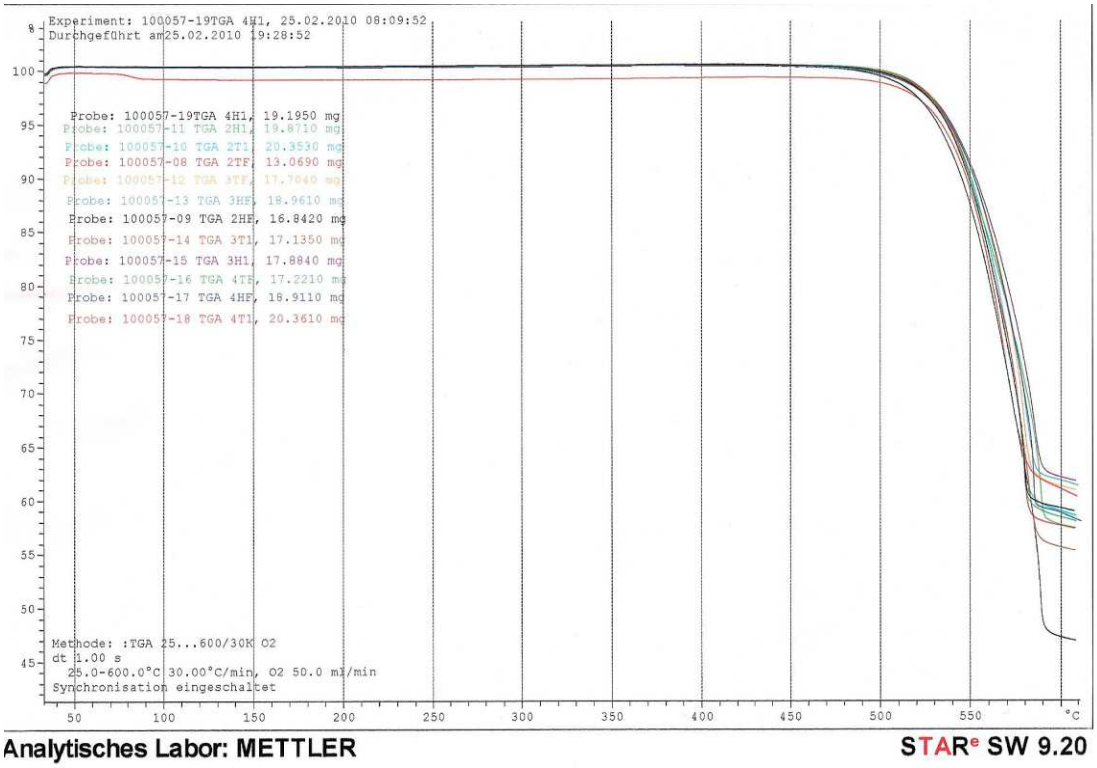
Experiment: 100057-19TGA 4H1, 25.02.2010 08:09:52
Durchgeführt am 25.02.2010 19:28:52
%
100
95
90
85
80
75
70
65
60
55
50
45
Probe: 100057-19TGA 4H1, 19.1950 mg
Probe: 100057-11 TGA 2H1, 19.8710 mg
Probe: 100057-10 TGA 2T1, 20.3530 mg
Probe: 100057-08 TGA 2TF, 13.0690 mg
Probe: 100057-12 TGA 3TF, 17.7040 mg
Probe: 100057-13 TGA 3HF, 18.9610 mg
Probe: 100057-09 TGA 2HF, 16.8420 mg
Probe: 100057-14 TGA 3T1, 17.1350 mg
Probe: 100057-15 TGA 3H1, 17.8840 mg
Probe: 100057-16 TGA 4TF, 17.2210 mg
Probe: 100057-17 TGA 4HF, 18.9110 mg
Probe: 100057-18 TGA 4T1, 20.3610 mg
Methode: :TGA 25...600/30K O2
dt 1.00 s
25.0-600.0°C 30.00°C/min, O2 50.0 ml/min
Synchronisation eingeschaltet
50
100
150
200
250
300
350
400
450
500
550
°C
Analytisches Labor: METTLER
STARe SW 9.20


Stufe -38.5483 %
-5.0379 mg
Rückstand 60.2586 %
7.8752 mg
Stufe -38.7573 %
-6.8616 mg
Rückstand 60.8782 %
10.7779 mg
Stufe -38.3680 %
-7.2750 mg
Rückstand 61.2900 %
11.6212 mg
Stufe -41.6851 %
-7.1786 mg
Rückstand 57.9560 %
9.9806 mg
Stufe -41.6998 %
-7.8858 mg
Rückstand 57.9681 %
10.9623 mg
Probe: 100057-08 TGA 2TF, 13.0690 mg
Probe: 100057-12 TGA 3TF, 17.7040 mg
Probe: 100057-13 TGA 3HF, 18.9610 mg
Probe: 100057-16 TGA 4TF, 17.2210 mg
Probe: 100057-17 TGA 4HF, 18.9110 mg
100
90
80
70
60
50
40
30
20
50
100
150
200
250
300
350
400
450
500
550
600
650
700
°C
Analytisches Labor: METTLER
STARe SW 9.20

Appendix L

Toho Tenax

	A time s	B G' Pa	C tan_delta	D Temp °C	E G" Pa
1	4	4.8529e+09	0.04374	-1.03	2.1226e+08
2	33	4.8894e+09	0.03946	0.27	1.9295e+08
3	63	4.9000e+09	0.03772	1.68	1.8482e+08
4	93	4.9017e+09	0.03647	2.54	1.8261e+08
5	123	4.8858e+09	0.03567	3.73	1.7681e+08
6	154	4.8662e+09	0.03504	4.97	1.7303e+08
7	183	4.8452e+09	0.03478	5.85	1.6850e+08
8	213	4.8031e+09	0.03438	7.14	1.6514e+08
9	244	4.7682e+09	0.03424	8.01	1.6328e+08
10	273	4.7289e+09	0.03371	8.84	1.5941e+08
11	303	4.7003e+09	0.03306	9.78	1.5538e+08
12	334	4.6579e+09	0.03245	10.86	1.5113e+08
13	363	4.6267e+09	0.03125	11.81	1.4460e+08
14	393	4.5921e+09	0.03000	13.04	1.3774e+08
15	423	4.5740e+09	0.02910	13.76	1.3312e+08
16	453	4.5491e+09	0.02776	15.07	1.2630e+08
17	483	4.5353e+09	0.02718	15.83	1.2327e+08
18	513	4.5190e+09	0.02649	17.06	1.1971e+08
19	543	4.5057e+09	0.02559	18.05	1.1770e+08
20	573	4.4956e+09	0.02559	18.84	1.1744e+08
21	603	4.4857e+09	0.02558	20.08	1.1474e+08
22	633	4.4739e+09	0.02533	21.05	1.1499e+08
23	663	4.4672e+09	0.02509	21.66	1.1447e+08
24	693	4.4598e+09	0.02555	23.01	1.1396e+08
25	723	4.4477e+09	0.02575	23.97	1.1451e+08
26	753	4.4371e+09	0.02627	24.94	1.1658e+08
27	783	4.4297e+09	0.02621	25.95	1.1609e+08
28	813	4.4205e+09	0.02645	26.91	1.1693e+08
29	843	4.4065e+09	0.02712	27.99	1.1951e+08
30	873	4.3951e+09	0.02721	30.12	1.2077e+08
31	903	4.4029e+09	0.02883	31.23	1.2457e+08
32	934	4.3604e+09	0.02863	32.23	1.2641e+08
33	963	4.3323e+09	0.03044	33.00	1.2903e+08
34	993	4.3216e+09	0.03044	33.32	1.2966e+08
35	1024	4.3123e+09	0.03062	34.44	1.3067e+08
36	1053	4.2994e+09	0.03095	35.35	1.3169e+08
37	1083	4.2861e+09	0.03118	36.27	1.3365e+08
38	1114	4.2726e+09	0.03185	37.26	1.3607e+08
39	1143	4.2571e+09	0.03243	38.20	1.3805e+08
40	1173	4.2413e+09	0.03287	39.19	1.3942e+08
41	1204	4.2268e+09	0.03338	40.14	1.4111e+08
42	1233	4.2107e+09	0.03400	41.14	1.4317e+08
43	1263	4.1968e+09	0.03442	42.12	1.4447e+08
44	1294	4.1806e+09	0.03507	43.12	1.4660e+08
45	1323	4.1654e+09	0.03561	44.10	1.4832e+08

	A time s	B G' Pa	C tan_delta	D Temp °C	E G" Pa
46	1353	4.1522e+09	0.03622	45.08	1.5038e+08
47	1384	4.1385e+09	0.03701	46.07	1.5317e+08
48	1413	4.1227e+09	0.03739	47.07	1.5415e+08
49	1443	4.1104e+09	0.03780	48.06	1.5536e+08
50	1474	4.0981e+09	0.03840	49.04	1.5736e+08
51	1503	4.0815e+09	0.03903	50.04	1.5932e+08
52	1533	4.0678e+09	0.03911	51.04	1.5909e+08
53	1563	4.0543e+09	0.03975	52.02	1.6117e+08
54	1593	4.0408e+09	0.04075	53.00	1.6466e+08
55	1623	4.0256e+09	0.04155	54.03	1.6725e+08
56	1653	4.0136e+09	0.04194	54.99	1.6831e+08
57	1683	3.9983e+09	0.04246	56.01	1.6977e+08
58	1713	3.9841e+09	0.04317	57.01	1.7198e+08
59	1744	3.9684e+09	0.04407	58.01	1.7488e+08
60	1773	3.9509e+09	0.04435	59.00	1.7523e+08
61	1803	3.9358e+09	0.04563	60.00	1.7960e+08
62	1834	3.9177e+09	0.04598	61.00	1.8013e+08
63	1863	3.9023e+09	0.04688	61.99	1.8296e+08
64	1893	3.8831e+09	0.04738	63.00	1.8397e+08
65	1923	3.8656e+09	0.04798	64.00	1.8546e+08
66	1953	3.8467e+09	0.04857	64.98	1.8685e+08
67	1983	3.8273e+09	0.04925	66.01	1.8850e+08
68	2013	3.8076e+09	0.04995	67.00	1.9020e+08
69	2043	3.7867e+09	0.05119	67.97	1.9383e+08
70	2073	3.7685e+09	0.05144	68.98	1.9384e+08
71	2103	3.7473e+09	0.05217	70.01	1.9550e+08
72	2133	3.7253e+09	0.05252	70.96	1.9566e+08
73	2163	3.7046e+09	0.05280	71.98	1.9559e+08
74	2193	3.6829e+09	0.05387	72.99	1.9838e+08
75	2223	3.6632e+09	0.05439	73.95	1.9926e+08
76	2253	3.6372e+09	0.05447	74.97	1.9813e+08
77	2283	3.6173e+09	0.05570	75.97	2.0150e+08
78	2314	3.5941e+09	0.05632	76.98	2.0242e+08
79	2343	3.5725e+09	0.05602	77.98	2.0012e+08
80	2373	3.5494e+09	0.05685	78.99	2.0178e+08
81	2404	3.5277e+09	0.05765	80.00	2.0338e+08
82	2433	3.5062e+09	0.05826	80.97	2.0428e+08
83	2463	3.4853e+09	0.05849	81.99	2.0387e+08
84	2493	3.4633e+09	0.05898	82.98	2.0425e+08
85	2523	3.4411e+09	0.05914	83.98	2.0351e+08
86	2553	3.4200e+09	0.05946	85.00	2.0337e+08
87	2583	3.3976e+09	0.05944	85.98	2.0196e+08
88	2613	3.3763e+09	0.05976	86.97	2.0175e+08
89	2643	3.3552e+09	0.05988	87.97	2.0091e+08
90	2673	3.3364e+09	0.05949	89.00	1.9849e+08

	A time s	B G' Pa	C tan_delta	D Temp °C	E G" Pa
91	2703	3.3164e+09	0.05957	89.94	1.9757e+08
92	2733	3.2986e+09	0.06003	90.97	1.9803e+08
93	2763	3.2794e+09	0.05972	91.98	1.9586e+08
94	2794	3.2616e+09	0.05979	92.98	1.9503e+08
95	2823	3.2427e+09	0.05946	93.97	1.9282e+08
96	2853	3.2231e+09	0.05948	94.98	1.9171e+08
97	2884	3.2067e+09	0.05934	95.97	1.9027e+08
98	2913	3.1881e+09	0.05918	96.99	1.8868e+08
99	2943	3.1705e+09	0.05923	98.03	1.8779e+08
100	2973	3.1539e+09	0.05924	98.98	1.8682e+08
101	3003	3.1408e+09	0.05940	99.95	1.8655e+08
102	3033	3.1237e+09	0.05898	100.97	1.8425e+08
103	3063	3.1067e+09	0.05886	102.00	1.8287e+08
104	3093	3.0919e+09	0.05873	102.96	1.8159e+08
105	3123	3.0747e+09	0.05820	103.97	1.7895e+08
106	3153	3.0605e+09	0.05888	105.00	1.8020e+08
107	3183	3.0491e+09	0.05919	105.96	1.8049e+08
108	3213	3.0330e+09	0.05841	106.98	1.7716e+08
109	3243	3.0184e+09	0.05833	107.98	1.7606e+08
110	3274	3.0049e+09	0.05820	108.99	1.7488e+08
111	3303	2.9894e+09	0.05806	109.97	1.7356e+08
112	3333	2.9768e+09	0.05789	110.96	1.7233e+08
113	3364	2.9641e+09	0.05796	111.99	1.7179e+08
114	3393	2.9512e+09	0.05836	113.00	1.7224e+08
115	3423	2.9390e+09	0.05826	113.98	1.7122e+08
116	3454	2.9253e+09	0.05835	115.00	1.7068e+08
117	3483	2.9162e+09	0.05813	115.98	1.6953e+08
118	3513	2.9047e+09	0.05839	116.98	1.6959e+08
119	3543	2.8917e+09	0.05776	117.97	1.6703e+08
120	3573	2.8800e+09	0.05796	118.98	1.6692e+08
121	3603	2.8696e+09	0.05812	119.95	1.6677e+08
122	3633	2.8589e+09	0.05830	120.99	1.6666e+08
123	3663	2.8460e+09	0.05837	121.95	1.6613e+08
124	3693	2.8359e+09	0.05839	122.99	1.6558e+08
125	3723	2.8263e+09	0.05822	123.95	1.6455e+08
126	3753	2.8162e+09	0.05888	124.94	1.6582e+08
127	3783	2.8057e+09	0.05878	125.98	1.6491e+08
128	3813	2.7947e+09	0.05886	126.98	1.6450e+08
129	3843	2.7839e+09	0.05823	127.95	1.6210e+08
130	3873	2.7708e+09	0.05797	128.97	1.6062e+08
131	3903	2.7599e+09	0.05862	129.97	1.6180e+08
132	3934	2.7509e+09	0.05816	130.99	1.5999e+08
133	3963	2.7418e+09	0.05820	131.99	1.5956e+08
134	3993	2.7318e+09	0.05840	132.95	1.5953e+08
135	4024	2.7206e+09	0.05865	133.98	1.5957e+08

	A time s	B G' Pa	C tan_delta	D Temp °C	E G" Pa
136	4053	2.7113e+09	0.05861	134.98	1.5890e+08
137	4083	2.7039e+09	0.05866	135.97	1.5860e+08
138	4113	2.6941e+09	0.05892	137.00	1.5874e+08
139	4143	2.6854e+09	0.05910	137.95	1.5872e+08
140	4173	2.6770e+09	0.05942	139.00	1.5906e+08
141	4203	2.6659e+09	0.05936	139.98	1.5826e+08
142	4233	2.6585e+09	0.06024	140.95	1.6014e+08
143	4263	2.6476e+09	0.05985	141.98	1.5846e+08
144	4293	2.6394e+09	0.06018	142.97	1.5884e+08
145	4323	2.6281e+09	0.06025	143.97	1.5833e+08
146	4353	2.6194e+09	0.06030	144.97	1.5794e+08
147	4383	2.6101e+09	0.06016	145.95	1.5702e+08
148	4414	2.6043e+09	0.06060	147.00	1.5782e+08
149	4443	2.5935e+09	0.06050	147.97	1.5692e+08
150	4473	2.5863e+09	0.06135	148.96	1.5866e+08
151	4504	2.5779e+09	0.06142	149.99	1.5832e+08
152	4533	2.5682e+09	0.06129	150.99	1.5740e+08
153	4563	2.5584e+09	0.06150	151.96	1.5735e+08
154	4593	2.5511e+09	0.06228	152.99	1.5889e+08
155	4623	2.5420e+09	0.06270	153.98	1.5938e+08
156	4653	2.5335e+09	0.06229	154.99	1.5781e+08
157	4683	2.5248e+09	0.06267	155.96	1.5823e+08
158	4713	2.5150e+09	0.06296	156.95	1.5835e+08
159	4743	2.5078e+09	0.06306	158.00	1.5814e+08
160	4773	2.4994e+09	0.06396	158.97	1.5987e+08
161	4803	2.4906e+09	0.06352	159.97	1.5819e+08
162	4833	2.4820e+09	0.06405	160.96	1.5897e+08
163	4863	2.4751e+09	0.06460	161.99	1.5988e+08
164	4893	2.4660e+09	0.06399	162.94	1.5781e+08
165	4923	2.4575e+09	0.06501	163.97	1.5977e+08
166	4953	2.4487e+09	0.06544	164.99	1.6023e+08
167	4984	2.4398e+09	0.06570	165.99	1.6029e+08
168	5013	2.4297e+09	0.06540	166.95	1.5891e+08
169	5043	2.4191e+09	0.06534	168.01	1.6037e+08
170	5074	2.4110e+09	0.06589	169.01	1.6119e+08
171	5103	2.4025e+09	0.06624	169.97	1.6149e+08
172	5133	2.3953e+09	0.06691	170.97	1.6235e+08
173	5163	2.3904e+09	0.06745	171.98	1.6332e+08
174	5193	2.3800e+09	0.06789	172.98	1.6365e+08
175	5223	2.3698e+09	0.06793	173.97	1.6304e+08
176	5253	2.3626e+09	0.06960	174.99	1.6444e+08
177	5283	2.3552e+09	0.06943	175.94	1.6566e+08
178	5313	2.3465e+09	0.06946	176.97	1.6512e+08
179	5343	2.3410e+09	0.07114	178.00	1.6867e+08
180	5373	2.3294e+09	0.07098	178.94	1.6746e+08

	A time s	B G' Pa	C tan_delta	D Temp °C	E G" Pa
181	5403	2.3231e+09	0.07191	179.98	1.6917e+08
182	5433	2.3124e+09	0.07167	180.98	1.6784e+08
183	5464	2.3027e+09	0.07211	181.98	1.6813e+08
184	5493	2.2952e+09	0.07319	182.95	1.7007e+08
185	5523	2.2856e+09	0.07325	183.98	1.6949e+08
186	5554	2.2783e+09	0.07373	184.99	1.6797e+08
187	5583	2.2686e+09	0.07406	185.97	1.6800e+08
188	5613	2.2610e+09	0.07610	186.94	1.7207e+08
189	5643	2.2512e+09	0.07601	188.01	1.7112e+08
190	5673	2.2404e+09	0.07679	188.96	1.7204e+08
191	5703	2.2316e+09	0.07702	189.93	1.7187e+08
192	5733	2.2216e+09	0.07810	190.98	1.7351e+08
193	5763	2.2150e+09	0.08039	191.96	1.7807e+08
194	5793	2.2058e+09	0.07928	192.98	1.7489e+08
195	5823	2.1965e+09	0.07972	193.99	1.7511e+08
196	5853	2.1870e+09	0.08141	194.96	1.7804e+08
197	5883	2.1762e+09	0.08113	195.98	1.7656e+08
198	5913	2.1665e+09	0.08210	196.99	1.7787e+08
199	5943	2.1554e+09	0.08307	197.94	1.7905e+08
200	5973	2.1484e+09	0.08399	198.97	1.8045e+08
201	6003	2.1395e+09	0.08545	199.98	1.8281e+08
202	6034	2.1304e+09	0.08617	201.00	1.8358e+08
203	6063	2.1256e+09	0.08857	201.95	1.8827e+08
204	6093	2.1124e+09	0.08720	202.98	1.8815e+08
205	6124	2.1051e+09	0.09003	203.98	1.8952e+08
206	6153	2.0953e+09	0.09218	205.00	1.9314e+08
207	6183	2.0881e+09	0.09179	205.98	1.9652e+08
208	6214	2.0767e+09	0.09328	206.97	1.9856e+08
209	6243	2.0612e+09	0.09290	207.97	1.9629e+08
210	6273	2.0528e+09	0.09581	208.97	2.0145e+08
211	6303	2.0334e+09	0.09620	209.97	2.0034e+08
212	6333	2.0204e+09	0.09918	210.99	2.0214e+08
213	6363	2.0045e+09	0.09906	211.97	2.0030e+08
214	6393	1.9890e+09	0.10007	213.01	2.0507e+08
215	6423	1.9757e+09	0.10086	213.95	2.0530e+08
216	6453	1.9645e+09	0.10309	214.94	2.0609e+08
217	6483	1.9473e+09	0.10317	215.98	2.0276e+08
218	6514	1.9376e+09	0.10501	216.95	2.0529e+08
219	6543	1.9245e+09	0.10494	218.00	2.0634e+08
220	6573	1.9223e+09	0.10566	218.98	2.0740e+08
221	6604	1.8985e+09	0.10806	219.99	2.0515e+08
222	6633	1.8881e+09	0.10840	220.97	2.0467e+08
223	6663	1.8726e+09	0.10977	221.98	2.0555e+08
224	6694	1.8639e+09	0.11117	222.98	2.0703e+08
225	6723	1.8543e+09	0.11139	223.94	2.0800e+08

	A time s	B G' Pa	C tan_delta	D Temp °C	E G" Pa
226	6753	1.8396e+09	0.11351	224.97	2.0691e+08
227	6783	1.8292e+09	0.11292	225.99	2.0631e+08
228	6813	1.8153e+09	0.11424	226.94	2.0978e+08
229	6843	1.8048e+09	0.11462	228.00	2.0686e+08
230	6873	1.7920e+09	0.11629	228.97	2.0838e+08
231	6903	1.7859e+09	0.11676	229.94	2.1098e+08
232	6933	1.7794e+09	0.11833	230.98	2.0842e+08
233	6963	1.7695e+09	0.11928	231.98	2.0764e+08
234	6993	1.7485e+09	0.11885	232.94	2.1194e+08
235	7023	1.7360e+09	0.11983	233.97	2.0984e+08
236	7053	1.7298e+09	0.12094	234.98	2.0845e+08
237	7084	1.7204e+09	0.12145	235.96	2.0819e+08
238	7113	1.7045e+09	0.12305	236.97	2.0696e+08
239	7143	1.6899e+09	0.12190	237.97	2.0876e+08
240	7174	1.6799e+09	0.12442	238.97	2.0901e+08
241	7203	1.6767e+09	0.12594	240.00	2.1262e+08
242	7233	1.6652e+09	0.12575	240.96	2.1085e+08
243	7263	1.6499e+09	0.12782	242.01	2.0704e+08
244	7293	1.6350e+09	0.12793	242.96	2.1116e+08
245	7323	1.6253e+09	0.12916	244.03	2.0613e+08
246	7353	1.6185e+09	0.13083	244.94	2.1175e+08
247	7383	1.6033e+09	0.13029	245.99	2.0888e+08
248	7413	1.5929e+09	0.13156	246.96	2.0881e+08
249	7443	1.5774e+09	0.13300	247.98	2.1047e+08
250	7473	1.5659e+09	0.13254	248.94	2.1341e+08
251	7503	1.5543e+09	0.13439	249.95	2.1113e+08
252	7533	1.5420e+09	0.13460	251.00	2.0979e+08
253	7564	1.5239e+09	0.13571	251.98	2.0907e+08
254	7593	1.5158e+09	0.13778	252.97	2.0886e+08
255	7623	1.5101e+09	0.14019	254.00	2.1515e+08
256	7654	1.4948e+09	0.13969	254.98	2.0881e+08
257	7683	1.4829e+09	0.14201	255.95	2.1059e+08
258	7713	1.4706e+09	0.14448	256.95	2.1450e+08
259	7743	1.4642e+09	0.14510	257.98	2.1246e+08
260	7773	1.4484e+09	0.14644	258.96	2.1211e+08
261	7803	1.4372e+09	0.14766	259.96	2.1358e+08
262	7833	1.4196e+09	0.15016	260.99	2.1451e+08
263	7864	1.4088e+09	0.15022	261.94	2.1296e+08
264	7893	1.3991e+09	0.15272	262.96	2.1483e+08
265	7923	1.3856e+09	0.15385	263.98	2.1431e+08
266	7953	1.3696e+09	0.15505	264.98	2.1081e+08
267	7983	1.3555e+09	0.15763	265.97	2.1522e+08
268	8013	1.3411e+09	0.15931	266.99	2.1265e+08
269	8043	1.3191e+09	0.16156	267.97	2.1551e+08
270	8074	1.3074e+09	0.16479	268.96	2.1637e+08

	A time s	B G' Pa	C tan_delta	D Temp °C	E G" Pa
271	8103	1.2891e+09	0.16735	269.95	2.1573e+08
272	8133	1.2847e+09	0.16805	270.98	2.1589e+08
273	8163	1.2742e+09	0.17347	272.00	2.2105e+08
274	8193	1.2496e+09	0.17509	272.95	2.1929e+08
275	8223	1.2417e+09	0.17842	273.96	2.1983e+08
276	8253	1.2179e+09	0.18033	274.97	2.1963e+08
277	8284	1.2132e+09	0.18549	276.02	2.2314e+08
278	8313	1.1915e+09	0.18835	276.95	2.2206e+08
279	8343	1.1755e+09	0.19058	277.99	2.2403e+08
280	8373	1.1574e+09	0.19644	278.97	2.2736e+08
281	8403	1.1448e+09	0.20006	279.94	2.2611e+08
282	8433	1.1236e+09	0.20449	280.98	2.2977e+08
283	8463	1.0995e+09	0.20611	282.00	2.2457e+08
284	8493	1.0910e+09	0.21305	282.96	2.2742e+08
285	8523	1.0662e+09	0.22017	283.95	2.2818e+08
286	8553	1.0651e+09	0.21949	284.98	2.2748e+08
287	8584	1.0298e+09	0.23428	286.00	2.2446e+08
288	8613	1.0187e+09	0.23635	286.98	2.2785e+08
289	8643	9.8054e+08	0.24833	287.98	2.2428e+08
290	8673	9.5767e+08	0.25737	288.99	2.2297e+08
291	8703	9.2011e+08	0.26570	289.96	2.1934e+08
292	8733	8.7753e+08	0.28089	290.98	2.1507e+08
293	8763	8.3171e+08	0.29543	291.96	2.1754e+08
294	8794	7.6994e+08	0.31160	292.94	2.1003e+08
295	8823	7.1607e+08	0.32768	293.98	2.0623e+08
296	8853	6.3895e+08	0.34151	294.95	2.0168e+08
297	8883	5.5263e+08	0.37900	295.99	1.9358e+08
298	8913	4.9530e+08	0.40144	296.96	1.8783e+08
299	8943	4.3971e+08	0.44582	297.95	1.7919e+08
300	8973	3.8113e+08	0.46353	299.00	1.7667e+08
301	9004	3.3666e+08	0.52609	299.97	1.6489e+08
302	9033	2.8460e+08	0.57061	300.96	1.6239e+08
303	9063	2.4006e+08	0.64326	302.01	1.5773e+08
304	9094	2.0869e+08	0.70826	302.97	1.5751e+08
305	9123	1.9583e+08	0.77118	303.93	1.5766e+08
306	9153	1.9224e+08	0.81803	304.93	1.6072e+08
307	9183	1.9088e+08	0.84393	305.99	1.6465e+08
308	9213	1.9234e+08	0.87147	306.94	1.7383e+08
309	9243	1.9407e+08	0.89986	307.96	1.7881e+08
310	9273	1.9612e+08	0.93826	308.99	1.8401e+08
311	9304	1.9455e+08	0.95707	309.96	1.8648e+08
312	9333	1.9282e+08	0.97867	310.95	1.8871e+08
313	9363	1.8752e+08	1.01505	311.99	1.9034e+08
314	9393	1.8699e+08	1.03774	312.97	1.9127e+08
315	9423	1.7582e+08	1.08368	313.95	1.9053e+08

	A time s	B G' Pa	C tan_delta	D Temp °C	E G" Pa
316	9453	1.6718e+08	1.12522	314.97	1.9138e+08
317	9483	1.6456e+08	1.16567	315.98	1.8831e+08
318	9514	1.5848e+08	1.19915	316.98	1.9004e+08
319	9543	1.4801e+08	1.26353	317.96	1.8701e+08
320	9573	1.4659e+08	1.26055	319.03	1.8478e+08
321	9603	1.3593e+08	1.34925	319.96	1.8341e+08
322	9633	1.3207e+08	1.36053	320.94	1.7969e+08
323	9663	1.2713e+08	1.42084	322.00	1.8062e+08
324	9693	1.2863e+08	1.43340	322.94	1.8160e+08
325	9724	1.1759e+08	1.48098	324.01	1.7817e+08
326	9753	1.1916e+08	1.51569	324.95	1.7769e+08
327	9783	1.1281e+08	1.55532	325.95	1.7409e+08
328	9813	1.1494e+08	1.56931	326.99	1.7898e+08
329	9843	1.0694e+08	1.63035	327.95	1.7601e+08
330	9873	1.0316e+08	1.64252	328.99	1.6945e+08
331	9903	1.0507e+08	1.67542	330.01	1.7411e+08
332	9934	9.7778e+07	1.72590	330.97	1.7058e+08
333	9963	9.6426e+07	1.74276	331.97	1.6921e+08
334	9993	9.8935e+07	1.76669	332.94	1.7479e+08
335	10023	9.5292e+07	1.83443	333.93	1.7100e+08
336	10053	9.1823e+07	1.85082	334.95	1.6921e+08
337	10083	8.8962e+07	1.88076	335.99	1.6665e+08
338	10113	8.3733e+07	1.90572	336.96	1.6170e+08
339	10144	8.5553e+07	1.94675	337.99	1.6304e+08
340	10173	7.8570e+07	1.98000	338.98	1.6060e+08
341	10203	7.8554e+07	2.04166	339.96	1.6038e+08
342	10233	8.0057e+07	2.04572	341.01	1.6377e+08
343	10263	7.7884e+07	2.07932	341.95	1.6195e+08
344	10293	7.3499e+07	2.14272	342.95	1.5498e+08
345	10323	7.9380e+07	2.19677	343.99	1.5768e+08
346	10354	6.9503e+07	2.25016	344.95	1.5237e+08
347	10383	7.3522e+07	2.26851	345.12	1.5484e+08

Hexcel

	A time s	B G' Pa	C tan_delta	D Temp °C	E G" Pa
1	4	5.0492e+09	0.04065	23.01	2.0524e+08
2	33	5.0519e+09	0.03734	24.16	1.8862e+08
3	63	5.0342e+09	0.03661	26.94	1.8429e+08
4	93	5.0154e+09	0.03640	28.93	1.8254e+08
5	123	4.9909e+09	0.03726	30.88	1.8598e+08
6	153	4.9652e+09	0.03793	32.92	1.8833e+08
7	183	4.9346e+09	0.03882	34.94	1.9158e+08
8	213	4.9011e+09	0.04005	36.89	1.9631e+08
9	243	4.8676e+09	0.04172	38.94	2.0308e+08
10	273	4.8320e+09	0.04280	40.95	2.0682e+08
11	303	4.7960e+09	0.04419	42.89	2.1192e+08
12	333	4.7581e+09	0.04581	44.93	2.1796e+08
13	363	4.7220e+09	0.04693	46.97	2.2159e+08
14	393	4.6892e+09	0.04791	48.91	2.2468e+08
15	423	4.6562e+09	0.04904	50.94	2.2833e+08
16	453	4.6219e+09	0.05043	52.96	2.3307e+08
17	483	4.5892e+09	0.05136	54.88	2.3571e+08
18	513	4.5530e+09	0.05250	56.96	2.3903e+08
19	543	4.5186e+09	0.05333	58.95	2.4099e+08
20	573	4.4789e+09	0.05477	60.88	2.4533e+08
21	603	4.4411e+09	0.05602	62.95	2.4877e+08
22	633	4.3994e+09	0.05733	64.96	2.5223e+08
23	663	4.3599e+09	0.05796	66.90	2.5272e+08
24	693	4.3144e+09	0.05982	68.93	2.5809e+08
25	723	4.2658e+09	0.06147	70.96	2.6223e+08
26	753	4.2259e+09	0.06164	72.90	2.6050e+08
27	783	4.1760e+09	0.06312	74.94	2.6361e+08
28	813	4.1277e+09	0.06393	76.95	2.6389e+08
29	843	4.0818e+09	0.06470	78.91	2.6408e+08
30	873	4.0356e+09	0.06524	80.91	2.6330e+08
31	903	3.9862e+09	0.06590	82.97	2.6267e+08
32	933	3.9425e+09	0.06622	84.90	2.6107e+08
33	963	3.8975e+09	0.06659	86.95	2.5955e+08
34	993	3.8518e+09	0.06706	88.95	2.5831e+08
35	1023	3.8110e+09	0.06716	90.89	2.5595e+08
36	1053	3.7650e+09	0.06807	92.93	2.5626e+08
37	1083	3.7281e+09	0.06706	94.98	2.5001e+08
38	1114	3.6876e+09	0.06787	96.96	2.5026e+08
39	1143	3.6546e+09	0.06674	98.93	2.4389e+08
40	1173	3.6178e+09	0.06668	100.97	2.4122e+08
41	1204	3.5831e+09	0.06683	102.95	2.3945e+08
42	1233	3.5479e+09	0.06701	104.95	2.3776e+08
43	1263	3.5174e+09	0.06626	106.98	2.3305e+08
44	1294	3.4901e+09	0.06658	108.93	2.3238e+08
45	1323	3.4595e+09	0.06623	110.97	2.2911e+08

H

	A time s	B G' Pa	C tan_delta	D Temp °C	E G" Pa
46	1353	3.4313e+09	0.06613	112.92	2.2692e+08
47	1384	3.4029e+09	0.06592	114.98	2.2431e+08
48	1413	3.3739e+09	0.06611	116.92	2.2304e+08
49	1443	3.3444e+09	0.06587	118.94	2.2030e+08
50	1473	3.3179e+09	0.06585	120.97	2.1847e+08
51	1503	3.2920e+09	0.06574	122.92	2.1642e+08
52	1533	3.2661e+09	0.06590	124.96	2.1525e+08
53	1563	3.2424e+09	0.06592	126.94	2.1374e+08
54	1593	3.2147e+09	0.06627	128.91	2.1304e+08
55	1623	3.1890e+09	0.06656	130.95	2.1225e+08
56	1653	3.1665e+09	0.06692	132.95	2.1190e+08
57	1683	3.1433e+09	0.06667	134.91	2.0956e+08
58	1713	3.1193e+09	0.06640	136.95	2.0712e+08
59	1743	3.0950e+09	0.06703	138.95	2.0746e+08
60	1774	3.0706e+09	0.06703	140.95	2.0581e+08
61	1803	3.0483e+09	0.06693	142.94	2.0402e+08
62	1833	3.0236e+09	0.06797	144.93	2.0551e+08
63	1863	3.0009e+09	0.06765	146.97	2.0301e+08
64	1893	2.9785e+09	0.06751	148.93	2.0108e+08
65	1923	2.9542e+09	0.06858	150.94	2.0261e+08
66	1953	2.9300e+09	0.06904	152.95	2.0228e+08
67	1983	2.9081e+09	0.06856	154.87	1.9939e+08
68	2013	2.8846e+09	0.06950	156.97	2.0049e+08
69	2043	2.8652e+09	0.06913	158.97	1.9807e+08
70	2073	2.8416e+09	0.06936	160.87	1.9710e+08
71	2103	2.8188e+09	0.07003	162.97	1.9740e+08
72	2133	2.7963e+09	0.07031	164.98	1.9662e+08
73	2164	2.7743e+09	0.07087	166.95	1.9661e+08
74	2193	2.7525e+09	0.07108	168.95	1.9564e+08
75	2223	2.7298e+09	0.07133	170.96	1.9473e+08
76	2253	2.7078e+09	0.07173	172.96	1.9422e+08
77	2283	2.6846e+09	0.07224	174.91	1.9394e+08
78	2313	2.6626e+09	0.07304	176.96	1.9448e+08
79	2343	2.6402e+09	0.07332	178.95	1.9358e+08
80	2373	2.6154e+09	0.07385	180.95	1.9314e+08
81	2403	2.5916e+09	0.07426	182.94	1.9244e+08
82	2433	2.5684e+09	0.07488	184.97	1.9233e+08
83	2464	2.5437e+09	0.07529	186.97	1.9152e+08
84	2493	2.5224e+09	0.07629	188.94	1.9243e+08
85	2523	2.4974e+09	0.07684	190.95	1.9189e+08
86	2554	2.4741e+09	0.07681	192.94	1.9004e+08
87	2583	2.4506e+09	0.07750	194.94	1.8991e+08
88	2613	2.4261e+09	0.07853	196.93	1.9053e+08
89	2643	2.4015e+09	0.07911	198.98	1.8999e+08
90	2673	2.3794e+09	0.07915	200.90	1.8834e+08

	A time s	B G' Pa	C tan_delta	D Temp °C	E G" Pa
91	2703	2.3556e+09	0.08003	202.97	1.8851e+08
92	2733	2.3320e+09	0.08032	204.97	1.8731e+08
93	2763	2.3097e+09	0.08115	206.91	1.8744e+08
94	2793	2.2856e+09	0.08196	208.93	1.8733e+08
95	2823	2.2606e+09	0.08257	210.97	1.8665e+08
96	2853	2.2376e+09	0.08331	212.88	1.8642e+08
97	2883	2.2126e+09	0.08382	214.96	1.8546e+08
98	2913	2.1867e+09	0.08425	216.94	1.8422e+08
99	2944	2.1673e+09	0.08575	218.96	1.8585e+08
100	2973	2.1413e+09	0.08598	220.95	1.8410e+08
101	3003	2.1142e+09	0.08724	222.99	1.8445e+08
102	3033	2.0893e+09	0.08754	224.98	1.8289e+08
103	3063	2.0634e+09	0.08895	226.91	1.8354e+08
104	3093	2.0363e+09	0.08892	228.92	1.8107e+08
105	3123	2.0074e+09	0.09067	230.99	1.8202e+08
106	3153	1.9811e+09	0.09144	232.95	1.8115e+08
107	3183	1.9584e+09	0.09170	234.97	1.7959e+08
108	3213	1.9328e+09	0.09286	236.94	1.7949e+08
109	3243	1.9050e+09	0.09419	238.93	1.7944e+08
110	3273	1.8775e+09	0.09475	240.92	1.7790e+08
111	3303	1.8493e+09	0.09579	242.99	1.7714e+08
112	3334	1.8201e+09	0.09655	244.92	1.7574e+08
113	3363	1.7899e+09	0.09824	246.90	1.7584e+08
114	3393	1.7609e+09	0.09970	248.99	1.7556e+08
115	3423	1.7317e+09	0.09997	250.95	1.7311e+08
116	3453	1.7026e+09	0.10182	252.93	1.7337e+08
117	3483	1.6687e+09	0.10272	254.90	1.7142e+08
118	3513	1.6381e+09	0.10417	256.96	1.7063e+08
119	3543	1.6079e+09	0.10472	258.93	1.6838e+08
120	3573	1.5730e+09	0.10692	260.98	1.6819e+08
121	3603	1.5404e+09	0.10839	262.94	1.6696e+08
122	3633	1.5045e+09	0.11103	264.94	1.6705e+08
123	3663	1.4683e+09	0.11320	266.96	1.6622e+08
124	3693	1.4280e+09	0.11529	268.97	1.6463e+08
125	3724	1.3872e+09	0.11713	270.99	1.6248e+08
126	3753	1.3515e+09	0.11919	272.90	1.6108e+08
127	3783	1.3006e+09	0.12355	274.93	1.6070e+08
128	3814	1.2613e+09	0.12639	276.94	1.5941e+08
129	3843	1.2122e+09	0.13014	278.92	1.5776e+08
130	3873	1.1645e+09	0.13464	280.97	1.5679e+08
131	3903	1.1072e+09	0.14028	282.97	1.5531e+08
132	3933	1.0466e+09	0.14542	284.91	1.5219e+08
133	3963	9.8749e+08	0.14864	286.94	1.4678e+08
134	3993	9.1043e+08	0.15549	288.95	1.4156e+08
135	4023	8.2809e+08	0.16690	290.91	1.3821e+08

	A time s	B G' Pa	C tan_delta	D Temp °C	E G" Pa
136	4053	7.3866e+08	0.17961	292.92	1.3267e+08
137	4083	6.4398e+08	0.19529	294.94	1.2576e+08
138	4114	5.3351e+08	0.21760	296.98	1.1609e+08
139	4143	4.2178e+08	0.24822	298.93	1.0469e+08
140	4173	3.3006e+08	0.28284	300.95	9.3355e+07
141	4204	2.6001e+08	0.32836	302.98	8.5377e+07
142	4233	2.2915e+08	0.35503	304.87	8.1353e+07
143	4263	2.0573e+08	0.40207	306.95	8.2716e+07
144	4293	1.9110e+08	0.43776	308.96	8.3657e+07
145	4323	1.8068e+08	0.47624	310.90	8.6049e+07
146	4353	1.7482e+08	0.49914	312.92	8.7261e+07
147	4383	1.7226e+08	0.52826	314.94	9.0995e+07
148	4414	1.6265e+08	0.57086	316.95	9.2852e+07
149	4443	1.6161e+08	0.62445	318.93	9.4694e+07
150	4473	1.4748e+08	0.67140	320.95	9.6107e+07
151	4503	1.4087e+08	0.68805	322.96	9.6015e+07
152	4533	1.3556e+08	0.70847	324.88	9.6038e+07
153	4563	1.3157e+08	0.73856	326.96	9.7170e+07
154	4593	1.2924e+08	0.75258	328.95	9.7260e+07
155	4624	1.2689e+08	0.77719	330.98	9.8618e+07
156	4653	1.2483e+08	0.79461	332.90	9.9194e+07
157	4683	1.2104e+08	0.81060	334.91	9.8120e+07
158	4714	1.1892e+08	0.82522	336.98	9.8139e+07
159	4743	1.1888e+08	0.82451	338.88	9.8014e+07
160	4773	1.1760e+08	0.84626	340.95	9.9517e+07
161	4803	1.1623e+08	0.85045	342.91	9.8851e+07
162	4833	1.1356e+08	0.86114	344.95	9.7788e+07
163	4863	1.1130e+08	0.87999	346.97	9.7942e+07
164	4893	1.1075e+08	0.88216	348.91	9.7698e+07
165	4923	1.0558e+08	0.90398	350.88	9.7719e+07
166	4953	1.0512e+08	0.91279	352.94	9.5956e+07
167	4983	1.0389e+08	0.91695	354.98	9.5261e+07
168	5014	1.0281e+08	0.92529	356.93	9.5126e+07
169	5043	1.0178e+08	0.93715	358.94	9.5379e+07
170	5073	9.8983e+07	0.95611	360.95	9.4638e+07
171	5104	9.7860e+07	0.96681	362.93	9.4612e+07
172	5133	9.7357e+07	0.96381	364.93	9.3834e+07
173	5163	9.5351e+07	0.97743	366.99	9.3199e+07
174	5193	9.3887e+07	0.98491	368.91	9.2470e+07
175	5223	9.2576e+07	1.00005	370.93	9.2580e+07
176	5253	9.0695e+07	1.01458	372.90	9.2017e+07
177	5283	8.9810e+07	1.01116	374.99	9.0812e+07
178	5313	8.7312e+07	1.03588	376.85	9.0445e+07
179	5343	8.6638e+07	1.04364	378.97	9.0419e+07
180	5373	8.6622e+07	1.03760	380.96	8.9880e+07

	A time s	B G' Pa	C tan_delta	D Temp °C	E G" Pa
181	5404	8.3780e+07	1.05437	382.96	8.9075e+07
182	5433	8.0995e+07	1.07091	384.89	8.7454e+07
183	5463	8.1004e+07	1.08396	386.95	8.7805e+07
184	5494	7.9713e+07	1.08305	388.96	8.6333e+07
185	5523	7.7624e+07	1.10431	390.87	8.5720e+07
186	5553	7.5167e+07	1.11577	392.96	8.4521e+07
187	5583	7.5748e+07	1.12564	395.00	8.5921e+07
188	5613	7.4414e+07	1.13898	396.89	8.5401e+07
189	5643	7.4442e+07	1.14906	398.92	8.4401e+07
190	5673	7.3791e+07	1.15119	400.94	8.3819e+07
191	5703	7.2761e+07	1.16323	402.89	8.3525e+07
192	5733	6.9362e+07	1.18884	404.90	8.2461e+07
193	5763	7.0681e+07	1.17877	406.96	8.1507e+07
194	5793	6.7773e+07	1.20153	408.86	8.1432e+07
195	5823	6.8762e+07	1.19526	410.90	8.0567e+07
196	5853	6.8314e+07	1.21025	412.94	8.1331e+07
197	5884	6.3835e+07	1.23501	414.94	7.7579e+07
198	5913	6.2763e+07	1.22618	416.92	7.6150e+07
199	5943	6.0484e+07	1.25113	418.91	7.5673e+07